Louisiana State University

LSU Digital Commons

1993

Pollutant Transport in Buoyancy Driven Atmospheric Flows.

Youn-seo Koo
Louisiana State University and Agricultural & Mechanical College

Follow this and additional works at: https://digitalcommons.lsu.edu/gradschool_disstheses

INFORMATION TO USERS

This manuscript has been reproduced from the microfilm master. UMI films the text directly from the original or copy submitted. Thus, some thesis and dissertation copies are in typewriter face, while others may be from any type of computer printer.

The quality of this reproduction is dependent upon the quality of the copy submitted. Broken or indistinct print, colored or poor quality illustrations and photographs, print bleedthrough, substandard margins, and improper alignment can adversely affect reproduction.

In the unlikely event that the author did not send UMI a complete manuscript and there are missing pages, these will be noted. Also, if unauthorized copyright material had to be removed, a note will indicate the deletion.

Oversize materials (e.g., maps, drawings, charts) are reproduced by sectioning the original, beginning at the upper left-hand corner and continuing from left to right in equal sections with small overlaps. Each original is also photographed in one exposure and is included in reduced form at the back of the book.

Photographs included in the original manuscript have been reproduced xerographically in this copy. Higher quality 6" x 9" black and white photographic prints are available for any photographs or illustrations appearing in this copy for an additional charge. Contact UMI directly to order.

Pollutant transport in buoyancy driven atmospheric flows

Koo, Youn-Seo, Ph.D.

The Louisiana State University and Agricultural and Mechanical Col., 1993

POLLUTANT TRANSPORT IN BUOYANCY DRIVEN ATMOSPHERIC FLOWS

A Dissertation

Submitted to the Graduate Faculty of the
Louisiana State University and
Agricultural and Mechanical College
in partial fulfillment of the
requirements for the degree of
Doctor of Philosophy

in

The Department of Chemical Engineering

by
Youn-Seo Koo
B.S., Seoul City University, 1982
M.S., Seoul National University, 1984
December, 1993

Acknowledgements

I will forever be indebted to my advisor, Dr. Danny D. Reible. His guidance, encouragement, and sincere support have helped me throughout this study. In particular, his unique way of research activities and his thorough review of this work are greatly appreciated.

I would also like to thank all my committee members: Dr. John R. Collier, Dr. Louis J. Thibodeaux, Dr. Ralph W. Pike, Dr. Sumanta P. Acharya and Dr. Juhan Frank.

I also thank the financial support from Department of Chemical Engineering and Energy Center.

Special thanks are to my father, mother, father-in-law, mother-in law, brothers and sisters for their understandings and supports. Finally, I deeply thank my wife Ilsook and my lovely son, Jiseok for their supports and patience.

Table of Contents

List of Tables

List of Figures

Nomenclature

a : drag coefficient

A(s), B(s) : functions of parameter s

c' : turbulent concentration

C : mean concentration

$c's$: constants in turbulence model

c_ϵ : Kolmogorov constant

c_h : proportionality constant for eddy diffusivity

c_m : proportionality constant for eddy viscosity

c_p : specific heat at constant pressure

E : turbulent kinetic energy

f : Coriolis parameter or a wall function

F_h, F_m : functions for heat and momentum transfer in surface layer

g : gravitational acceleration

h, H : boundary layer height in the neutral and stable conditions

k : turbulent kinetic energy

K_h^j, K_h^j : eddy diffusivity in j-direction

K_m^j, K_m^j : eddy viscosity in j-direction

L : Obukhov length

P : pressure

Q_s : surface heat flux

R : gas constant

R_f : flux Richardson number

R_{iB} : bulk Richardson number

t : time

T_* : convective temperature scale

u' : turbulent velocity in the x-direction

U : mean velocity in the x-direction

u_i' : turbulent velocity in the i-direction

u_* : friction velocity

U_g : geostrophic wind speed in the x-direction

v_i' : turbulent velocity in the i-direction

V : mean velocity in the y-direction

V_g : geostrophic wind speed in the y-direction

w' : turbulent velocity in the z-direction

W : mean velocity in the z-direction

w_* : convective velocity scale

x : horizontal direction (main flow direction)

x_i : Cartesian coordinates in tensor notation

y : horizontal direction perpendicular to the x-direction or lateral direction

z : vertical direction

z_i : inversion layer height in the convective boundary layer

z_o : roughness length

Greek symbols

α : isobaric angle between longitudinal and lateral surface winds

β : volumetric expansion coefficient

δ_{ij} : Knonecker delta

σ_E : turbulent Prandtl number for kinetic energy

σ_t : turbulent Prandtl number for temperature

σ_ϵ : turbulent Prandtl number for dissipation rate

ϵ : dissipation rate of turbulent kinetic energy

ϵ_{ijk} : alternating unit tensor

θ': turbulent fluctuating potential temperature

Θ : mean potential temperature

θ_* : temperature scale in the surface layer

κ : von Karman constant

ν : kinematic molecular viscosity

ρ : mean density

ϕ_h and ϕ_m : dimensionless functions for heat and momentum transfer

ζ : Obukhov stability parameter(z/L)

Ω : angular velocity of earth rotation

Ψ_h and Ψ_m : surface layer stability correction terms for heat and momentum transfer.

Subscripts

i,j,k,l : components of i,j,k, and l directions

o : reference state

p : grid point above the surface

s : surface

t : turbulent property

Superscripts

' : fluctuating variable or a deviation from the background value

x,z : viscosity/diffusivity directions

Abstract

Due to the complexity of some buoyancy driven atmospheric flows, it is sometimes not possible to accurately predict pollutant transport on the basis of sparse wind field measurements. A possible solution is mathematical modelling of both the flow and pollutant transport.

In order to overcome shortcomings of the conventional E-ϵ model such as defining proportionality coefficients (c_m, c_h) and to develop a more general model of stratified environmental flows, a modified E-ϵ model was proposed through use of the algebraic stress model including wall proximity effects. The resulting model was compared herein to data and higher order simulations in stable, neutral and convective atmospheric boundary layers (ABL). The modified E-ϵ model reproduced well the observed behaviors.

The modified E-ϵ model with full nonhydrostatic equations was applied to a sea breeze circulation. The key characteristics of the sea breeze, such as development of a daytime onshore flow, deep inland penetration of the breeze in late afternoon, frontal development in late evening, thermal internal boundary layer (TIBL) and fumigation in the TIBL were reproduced. The residual plume over the sea showed great impacts on the ground level concentration during the following day sea breeze and it should be considered in the estimation of pollutants near the coastal

region. All the plume emitted from an elevated line source during the nighttime offshore flow also returned back to the land with the subsequent afternoon sea breeze.

The modified E-ϵ model was also used to estimate the dispersion of pollutants by a "thermal fence" under neutral and stable conditions. A line of heaters or a thermal fence has been proposed as a means of reducing ground level concentrations near area source such as a landfill under nighttime stable condition. It was proved that the thermal fence with the relatively small heating rate enhanced the dispersion of the pollutants behind it by increasing the vertical mixing under the neutral and stable conditions.

Chapter 1. Introduction

The flow in the atmospheric boundary layer (ABL) is naturally buoyancy driven anisotropic turbulent flow with stratification. The stratification often has a strong influence on the flow as well as on the dispersion of pollutants. Of primary concern here is the prediction of the concentration and the temperature fields which are convected by the mean fluid motion and are dispersed by the turbulent motion. Due to the complexity of atmospheric flows and the inability to adequately define that flow on the basis of routinely available measurements, a mathematical model must be capable of describing correctly both the velocity field and the turbulent dispersion characteristics. In order to calculate the turbulent flows and their effect on the transport of pollutants in the ABL, the time-dependent turbulent flow equations for momentum, energy, and pollutant must be solved simultaneously. These equations cannot be exactly solved for practical problems with present knowledge. At present the only economically feasible method is to solve the mean flow equations which govern the distribution of quantities averaged over a time which is long compared with the time scale of the turbulence but short compared with that of the mean flow. The mean flow equations contain turbulent transport terms which must be approximated by a turbulence model in order to close the equations.

The turbulence models which represent approximate methods range from the first order closure model which is based on Prandtl's mixing length hypothesis to the second order closure model that involves prognostic transport equations for the Reynolds stresses and turbulent fluxes. The simple first order model lacks universality because it assumes that the turbulence is determined by the local mean flow and neglects transport history effects. As it is difficult to prescribe the mixing length distribution in situations other than simple shear-layer flow, the first order model is not suitable for flows with a complex structure. Further, entirely empirical modifications to the model are necessary to make it applicable to buoyancy driven flows. Unfortunately, these modifications have not proven to be of general applicability.

Another alternative is the second order closure model for turbulence which employs transport equations for the individual Reynolds stresses and turbulent fluxes. Since they are derived from the Navier-Stokes equations and the corresponding temperature and concentration equations, they contain terms explicitly accounting for the influence of buoyancy forces on the Reynolds stresses and turbulent fluxes. Even though the exact forms of these equations cannot be accessed directly but require the introduction of model approximations, they form a more realistic basis for taking into account the effects of buoyancy on the Reynolds

stresses and turbulent fluxes. The resulting model is however rather complex which makes it less suitable for solving practical problems.

An intermediate second order closure model, the so-called E-ϵ turbulence model (often called the k-ϵ turbulence model, k or E referring to the turbulent kinetic energy), provides only prognostic equations for the velocity, the turbulent kinetic energy and the dissipation rate(ϵ) of the turbulent kinetic energy. The E-ϵ model has been found to be a fairly successful compromise between capability and simplicity. The E-ϵ model has been shown to work quite well in the engineering field for many different flows not controlled by buoyancy force (Rodi, 1985). This popularity in the engineering field raises the question whether it could be also used for modelling atmospheric flows, especially for flows in which the length scale or mixing length scale cannot be prescribed in advance. There are numerous examples of applications of the E-ϵ model to atmospheric flows from a simple atmospheric boundary layer to complex recirculating flows such as a sea breeze, pollutant dispersion near irregular terrain, and three dimensional plume downwash. A detailed description of these applications will be discussed in Section 2.1.

According to these studies, the turbulent flow in the ABL can be predicted by an E-ϵ model if the constants used in the E-ϵ model are modified. Those modifications are mainly

due to the buoyancy and stratification. Constants used in the conventional E-ϵ model have been tuned by comparing model results with observations from neutral turbulent boundary layers, such as wall or channel flows. Hence, one cannot expect that buoyant turbulent flows in the ABL can be modelled appropriately with the conventional E-ϵ model.

Although the conventional E-ϵ model can be applied to atmospheric flows by the adjustment of the constants, the model does not fully account for the anisotropic influence of stratification on the Reynolds stresses and turbulent fluxes. In addition, if conditions change from stable to unstable, the application of this model is quite questionable because the constants were only adjusted for a specific stability condition.

In summary, the conventional model has two main drawbacks. One is that the model coefficients (c_m and c_h) are not constant but strongly dependent on the flow structure and buoyancy. The other problem is that the dissipation rate equation is not an exact prognostic equation. There are numerous suggestions for its formulation and the constant values that arise in the dissipation equation. None of them have the universal and general applicability under various stability conditions.

To account for the anisotropic effects on the model coefficients due to stratification and buoyancy forces, a modified version of the E-ϵ model is proposed by simplifying

the more complex prognostic transport equations of the second order closure. The simplification results in algebraic relations for the individual Reynolds stresses and fluxes. The proportionality coefficients required to estimate the vertical eddy viscosity and diffusivity will then become functions of the buoyancy and flow dynamics.

The objectives of this studies are 1)to test this model formulation against the data and other models of the atmospheric boundary layer and 2)to apply this model to describe flow and pollutant transport in buoyancy driven atmospheric flows. Specific flows of interest include the sea breeze circulation and ABL manipulation by a thermal fence.

In order to achieve the objectives, the modified $E-\epsilon$ model will be proposed in Chapter 2. In Chapter 3, the modification will be compared to literature data and higher order turbulence model in neutral, stable and convective atmospheric boundary layers. After checking the validity of this modification, the modified $E-\epsilon$ model will be applied to the modeling of the sea breeze circulation in Chapter 4 and to atmospheric boundary layer manipulation by a line source of heat, a "thermal fence" in Chapter 5. The general character of contaminant transport in both flows will be investigated with the model.

Chapter 2. Theoretical Background

In this chapter a modified E-ϵ turbulence model will be proposed for describing flow and pollutant transport in the atmospheric boundary layer based on the algebraic stress model of Gibson and Launder (1978).

2.1. Governing Equations for Atmospheric Flows

For an atmospheric flow assuming incompressibility, the governing equations for mean velocities, potential temperature and pollutant concentration are (Stull,1988; Nieuwstadt and Dop,1982; Pielke,1984):

Continuity Equation

$$\frac{\partial U_j}{\partial x_j} = 0 \tag{2.1}$$

Momentum Equations

$$\frac{\partial U_i}{\partial t} + \frac{\partial (U_i U_j)}{\partial x_j} = -\frac{1}{\rho}\frac{\partial P}{\partial x_i} + \frac{\partial}{\partial x_j}(-\overline{u_i' u_j'}) + g_i - 2\epsilon_{ijk}\Omega_j U_k \tag{2.2}$$

Energy Conservation Equation

$$\frac{\partial \Theta}{\partial t} + U_j \frac{\partial \Theta}{\partial x_j} = \frac{\partial}{\partial x_j}(-\overline{u_j' \theta'}) \tag{2.3}$$

Conservation Equation of a Scalar Quantity

$$\frac{\partial C}{\partial t} + U_j \frac{\partial C}{\partial x_j} = \frac{\partial}{\partial x_j}(-\overline{u_j' c'}) \tag{2.4}$$

The capital letters represent the mean variables and the small letters with a prime imply the fluctuating variables, respectively. U_i and U_j are mean velocities in the i and j directions. Θ is potential temperature and C is concentration. The Einstein summation convention is used for repeated indices.

The governing equations for the mean flow are not a closed set of equations because there are unknown turbulent fluxes due to the Reynolds stress, turbulent heat and mass fluxes ($-\overline{u_i'u_j'}$, $-\overline{u_j'\theta'}$, $-\overline{u_j'c'}$). These unknown terms should be expressed in terms of the mean variables to close the governing equations. This problem is referred to as the closure problem of turbulence.

Most of the turbulence models of practical use today are based on the eddy viscosity / diffusivity concept, Boussinesq's eddy viscosity concept, relating the Reynolds stresses to the mean velocity gradients. This may be expressed as

$$-\overline{u_i'u_j'} = K_m^j(\frac{\partial U_i}{\partial x_j} + \frac{\partial U_j}{\partial x_i}) - \frac{2}{3}E\delta_{ij} \qquad (2.5)$$

E is a turbulent kinetic energy and parameter K_m^j is a turbulent eddy viscosity in the j-direction. It is not a fluid property but depends strongly on the state of turbulence. The introduction of this concept alone does not therefore constitute a turbulence model but only provides a

framework for constructing such a model. The main problem is to determine the K^j_m.

In direct analogy to the turbulent momentum transport, the eddy diffusivity concept assumes the turbulent heat or mass fluxes to be related to the gradient of the transported quantity:

$$-\overline{u_j'\theta'} = K^j_h \frac{\partial \Theta}{\partial x_j} \tag{2.6}$$

$$-\overline{u_j'c'} = K^j_c \frac{\partial C}{\partial x_j} \tag{2.7}$$

K^j_h and K^j_c are turbulent eddy diffusivities of heat and mass in the j-direction, respectively.

According to the E-ϵ turbulence model, the turbulent eddy viscosity and eddy diffusivities can be expressed as a function of the turbulent kinetic energy(E) and dissipation rate(ϵ) (Launder and Spalding, 1974).

$$K^j_m = c_m \frac{E^2}{\epsilon} \tag{2.8}$$

$$K^j_h = K^j_c = c_h \frac{E^2}{\epsilon} \tag{2.9}$$

where $E = \frac{1}{2}\overline{u_i'^2}$, $\epsilon = \nu \overline{\frac{\partial u_i'}{\partial x_j} \frac{\partial u_i'}{\partial x_j}}$. c_m and c_h are proportionality coefficients for eddy viscosity and diffusivity, respectively.

Using an E-ϵ model, additional prognostic equations for the turbulent kinetic energy and dissipation rate are required for closure. The turbulent kinetic energy transport equation is;

$$\frac{\partial E}{\partial t} + U_j \frac{\partial E}{\partial x_j} = \frac{\partial}{\partial x_j}(\frac{K_m^j}{\sigma_E}\frac{\partial E}{\partial x_j}) - \overline{u_i'u_j'}\frac{\partial U_i}{\partial x_j} - \beta g_j\overline{u_j'\theta'} - \epsilon \qquad (2.10)$$

and the dissipation rate equation for the turbulent energy is;

$$\frac{\partial \epsilon}{\partial t} + U_j \frac{\partial \epsilon}{\partial x_j} = \frac{\partial}{\partial x_j}(\frac{K_m^j}{\sigma_\epsilon}\frac{\partial \epsilon}{\partial x_j}) - c_1\frac{\epsilon}{E}\overline{u_i'u_j'}\frac{\partial U_i}{\partial x_j} - c_2\frac{\epsilon^2}{E} - c_3\beta g_j\overline{u_j'\theta'} \quad (2.11)$$

where the constants c_1, c_2 and c_3 are defined by comparison to experiment. Different dissipation rate equations have been defined by selecting different values of these constants.

The use of E-ϵ model in engineering turbulent flow is now quite standard (Launder and Spalding, 1974; Rodi, 1985) and the constants of this model are listed in Table 2.1. In this study, the ϵ-equation with the constants of Launder and Spalding (1974) is referred to as the standard E-ϵ model. The standard E-ϵ model can be used for isotropic turbulent flow without modification. But the values of these constants in anisotropic turbulent flows, such as buoyancy influenced flows and rotational flows, are quite controversial. The standard constants have been tuned by comparing model results with observations from non-rotating and neutral

turbulent flows. Hence one cannot expect that the atmospheric boundary layer flows can be modelled appropriately with the standard E-ϵ model. As indicated in Chapter one, there are two main problems to applying the E-ϵ turbulence model in the atmospheric flow, the values and constancy of the proportionality coefficients and the formulation of the dissipation rate equation.

Table 2.1. Constants values used in the conventional E-ϵ turbulence model.

turbulence model	c_m	c_1	c_2	c_3	σ_E	σ_ϵ
standard	0.09	1.44	1.92	1.44	1.0	1.3
Duynkerke, 1988	0.033	1.46	1.83	1.46	1.0	2.38
Detering and Etling, 1987	0.026	*	1.90	*	0.74	1.3

* : 48.2 f $E^{1.5}/\epsilon$

Although the transport equation of the dissipation rate (ϵ) is not an exact equation (Launder and Spalding, 1974; Mellor and Yamada, 1982; Stull, 1988), it has been used for the simulation of the ABL (Wyngaard et al., 1974; Zeman and Lumley, 1979; André et al., 1979; Detering and Etling, 1985; Duynkerke,1988; Huang and Raman, 1991a, 1991b; Andrén, 1991). The challenge of applying the E-ϵ model to the atmospheric flow is to redefine the values of constants used in the model equations and to appropriately define the ϵ-equation. Below are several examples of such applications.

Detering and Etling (1985) compared their model results for the neutral ABL with the "Leipzig Wind Profile" and concluded that both the eddy viscosity and the boundary layer height calculated by the standard E-ϵ model were much too large. In order to meet the real situation, they modified the ϵ-equation by making one of the constants (c_1) as a function of lf/u_*, the ratio of a turbulent length scale (l) and the depth of the neutral ABL (u_*/f). u_* is a friction velocity and f is a Coriolis parameter. As pointed out by Duynkerke (1988), this is analogous to a length scale formulation in which l is proportional to u_*/f (Blackadar, 1962) and there is no inherent advantage in using the ϵ-equation above the well-known length scale formulation by Blackadar (1962). The application of the model may also be limited to the neutral "Leipzig Wind Profile". The length scale mentioned here is corresponding to the Prandtl's mixing length which is a characteristic traveling length of turbulent eddies (Schlichting, 1979).

Duynkerke (1988) modified the constant values on the basis of atmospheric data and considered the diffusion term in the turbulent kinetic energy equation as an additional production term in the ϵ-equation only when its value was positive. With this modification, a good agreement between the model results and the available data in the neutral and stable ABL were obtained. The constants by Detering and Etling (1985) and Duynkerke (1988) are listed in Table 2.1.

Huang and Raman (1991a) used Duynkerke constants and a background dissipation rate instead of only the positive contributions of the diffusion term of turbulent kinetic energy to the ϵ-equation. This approach is essentially similar in concept to Duynkerke's (1988) in that the background dissipation rate limits the length scale near the top of the boundary layer. The applications of these approaches are limited, however, in the neutral boundary layer. Under convective conditions, Duynkerke's modifications show no effect because the diffusion term of the kinetic energy equation is negative in a large portion of the calculation domain. The Huang and Raman's approach predicts unrealistic profiles under both stable and unstable conditions. The background dissipation rate value is so large to change the surface layer profile dramatically.

Andrén(1991) compared several existing ϵ-equations and defined the constants in the ϵ-equation as a function of the second invariant of an anisotropy tensor. He neglected the buoyancy term in the ϵ-equation of the standard E-ϵ model in his comparisons with other models. He also used a level 2.5 model (Mellor and Yamada, 1982) with wall effects which does not predict appropriate physics according to our realization analysis. This will be discussed further in Section 2.2. The proposed ϵ-equation also required the calculation of the second invariant of the anisotropy tensor every time and

iteration step. As a result of these problem, the ϵ-equation of Andrén is not considered here.

Although specification of the ϵ-equation and the constants remains uncertain, the E-ϵ model has been used frequently in atmospheric flow situations, especially when a length scale is difficult to define. Kitada (1987), Ly (1991) and Sha et al. (1991, 1993) used the standard model and Huang and Raman (1991b, 1992) used the Duynkerke model for the sea/land breeze. Mouzakis and Bergels (1991) and Suttan et al. (1986) also used the standard model for pollutant dispersion near solid obstacles. Stubley and Rooney (1986) and Riopell and Stubley (1989) applied the standard model for neutral and stable boundary layers. Guenther et al. (1990) used the Detering and Etling model for the three dimensional simulation of plume downwash.

A comprehensive comparison of standard, Duynkerke, and Detering and Etling constants used in the dissipation rate equation for various stability conditions such as the neutral, stable, and convective ABL is rarely found. Their performance is also likely to be dependent on the turbulence closure.

In order to understand and compare their performances with the following modified E-ϵ turbulence model, the standard, Duynkerke, and Detering and Etling constants of the ϵ-equation will be tested in the neutral, stable and convective ABL.

2.2. Modified E-ϵ Turbulence Model

To account for the anisotropic effects on the proportionality coefficients, c_m and c_h, a modified E-ϵ model has been proposed by simplifying the more complex, but still approximate prognostic equations of Reynolds stresses and turbulent fluxes. One simplification, neglect of differential terms in these prognostic transport equations, results in algebraic relations for the individual Reynolds stress and turbulent flux. It is often referred to as the algebraic stress model (ASM). The detailed equations and derivations of the ASM with wall effects proposed by Gibson and Launder (1978) are in Appendix A.

The proportionality coefficients can be defined by functions of flow structure and buoyancy from ASM.

$$c_m = \frac{2}{3} \ \frac{(c_1 - 1) \ (E_7 - A \ G_H)}{E_4 + \dfrac{E_4 \ E_8}{C_{1T}} G_H - E_5 \ E_7 \ G_M + E_5 \ A \ G_H \ G_M} \tag{2.12}$$

$$c_h = \frac{\dfrac{2}{3} \ (C_1 - 1) + E_5 \ G_M \ c_m}{(c_{1T} + c_{1T}' \ f) \ E_4 + (\dfrac{2 \ E_4 \ E_9}{E_{10}} + E_6) \ G_H} \tag{2.13}$$

The derivations of c_m and c_h from the ASM are also shown in Appendix A. f is the wall function which reflects the effect of the ground proximity on the Reynolds stress and turbulent heat flux. The definition of f is Equation (A-21) in

Appendix A. The c_m and c_h are functions of G_M, the production of turbulent kinetic energy by mean velocity shear, and G_H, the production / loss of turbulent kinetic energy by buoyancy.

$$G_M = (\frac{E}{\epsilon})^2 \left[(\frac{\partial \overline{U}}{\partial z})^2 + (\frac{\partial \overline{V}}{\partial z})^2 \right] \qquad (2.14)$$

$$G_H = \beta \, g \, (\frac{E}{\epsilon})^2 \, \frac{\partial \Theta}{\partial z} \qquad (2.15)$$

β is the volumetric thermal expansion coefficient. This approach is called the modified E-ϵ turbulence model.

A similar modification has been proposed by Rodi(1985) and he called it an extended E-ϵ turbulence model. He applied his extended model to two-dimensional heated surface jets discharged into stagnant ambient, stably stratified wall jets, stably stratified open channel flow and a plane wake in stratified environment in the two dimensional case without Coriolis force. Rodi's approach has been applied to the stable boundary layer by Uno et al. (1989). The applications of Rodi's extended model are limited to stable conditions because of an approximation employed for the diffusion terms. Under unstable conditions, physically unrealistic predictions are possible such as negative velocity variances. The detailed expressions for the approximate diffusion terms are Equations (A-22) and (A-23)

in Appendix A. Further details of Rodi's extended model will be discussed later in this section.

Dutta and Acharya (1993) proposed a modified E-ϵ turbulence model for the turbulent separated flow situation such as flow past a backstep by using same procedures. Their modification however was motivated by the streamline curvature effects on proportionality coefficients. Since our modification is mainly due to buoyancy effects, the expressions of the proportionality coefficients in this study are different from those by Dutta and Acharya (1993).

Similar approaches to the modified E-ϵ model also have been studied by Mellor and Yamada (1974,1982). They proposed various level closure models based on systematic simplifications resulting from an order analysis of the anisotropy of prognostic equations for Reynolds stresses and turbulent heat fluxes. Their level 2.5 model is similar to the modified model but the local equilibrium assumption of production balancing dissipation of kinetic energy was implicitly incorporated. The algebraic equations for Mellor and Yamada's level 2.5 model are in Appendix B. Andrén (1990, 1991) extended Mellor and Yamada's level 2.5 model to include the wall function suggested by Gibson and Launder(1978). The c_m and c_h of Andrén approach based on the level 2.5 model are Equations (B-15) and (B-16) in Appendix B.

Even if the modified E-ε model and the 2.5 level model with wall effects are closely related, there are significant differences in respect to their behaviors as a function of atmospheric stability. Figure 2.1 shows the effect of the wall function on the c_m and c_h as functions of G_M and G_H with the modified model. In this case, the approximate diffusion terms described in Appendix A are not included. f is set to zero in Figure 2.1(a) and f is 1 in Figure 2.1(b). The thin dotted lines in Figure 2.1 are for E two times of the vertical velocity variance, i.e., maximum available value of the vertical velocity variance with zero values of horizontal and lateral velocity variances. Figure 2.2 is as Figure 2.1 except for Mellor and Yamada's level 2.5 model. Figure 2.3 shows the ratio of vertical velocity variance to kinetic energy as a function of G_M and G_H for the modified model and level 2.5 model. The thin dotted lines in Figure 2.2 correspond to values of the vertical velocity variance of 0.24E. According to Mellor and Yamada(1982), Rotta's hypothesis (1951) on the energy redistribution might not be satisfied if the vertical variance is less than 0.24 E. Thus the application of the modified model is limited to the shaded regions in Figure 2.1 where the vertical velocity variance is greater than 0.24E and less than 2E. This constraint is similar to the realization condition used by Hassid and Galperin (1983). This realization condition is necessary to avoid unphysical behavior of the model such as
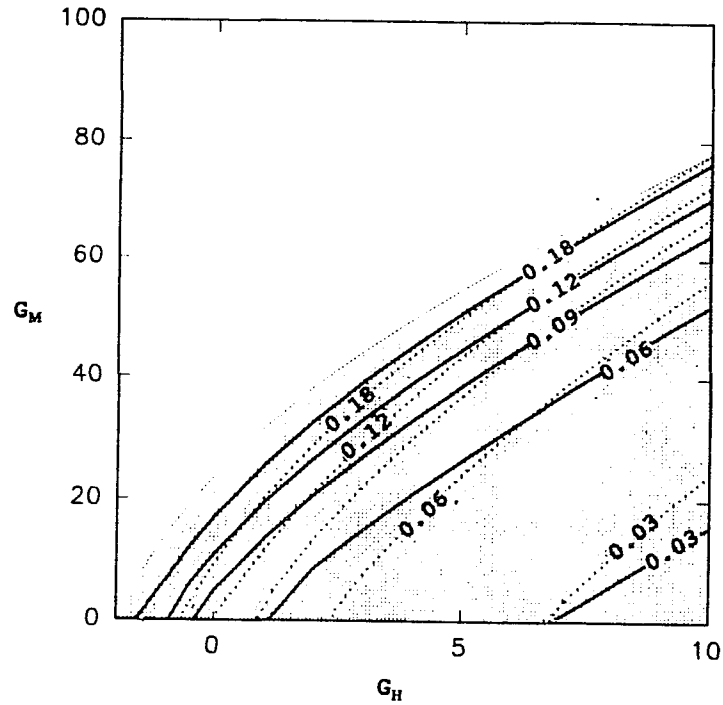
(a) f = 0
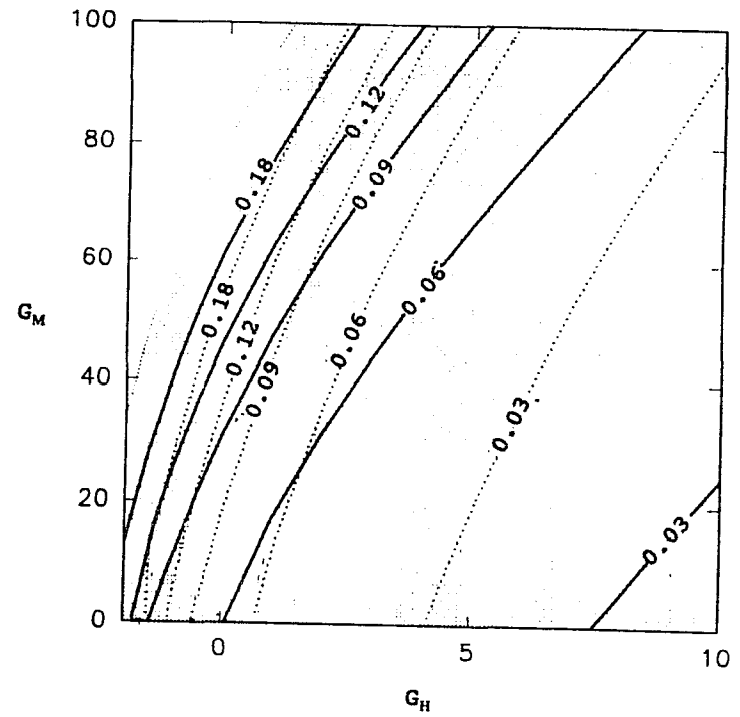
(b) f = 1

Fig.2.1. Effects of wall function on c_m and c_h as functions of G_M and G_{II} for the modified E-ϵ turbulence model without inclusion of additional diffusion terms in Equation (A-22) and (A-23). Shaded areas represent realization regions. Solid lines are c_m, dotted lines c_h and the thin dashed lines for $\overline{w'^2} = 2E$
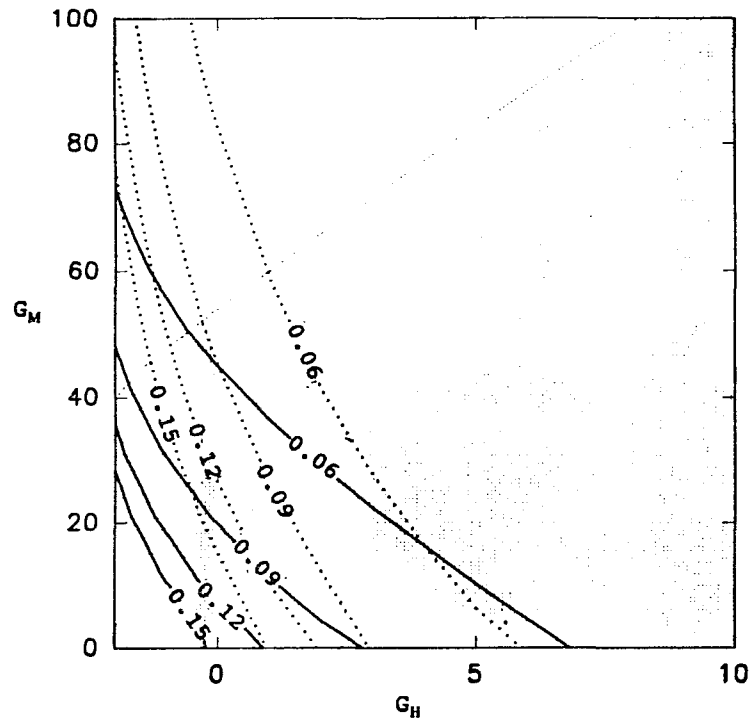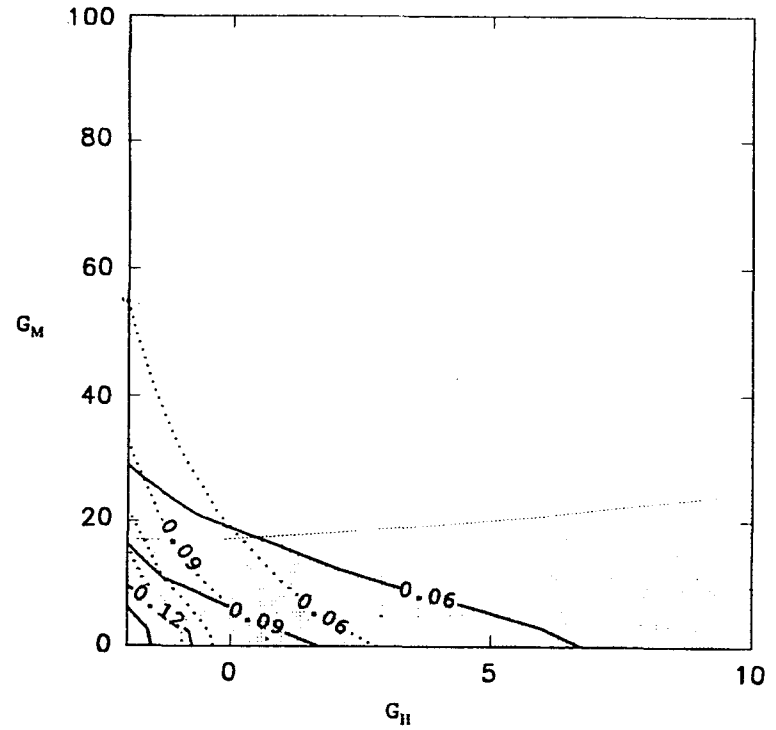
Fig.2.2. Effects of wall function on c_m and c_h as functions of G_M and G_H for the level 2.5 model. Shaded region, solid lines and dotted lines as in Figure 2.1 except thin dashed lines for $\overline{w'^2} = 0.24E$

(a) f = 0

(b) f = 1
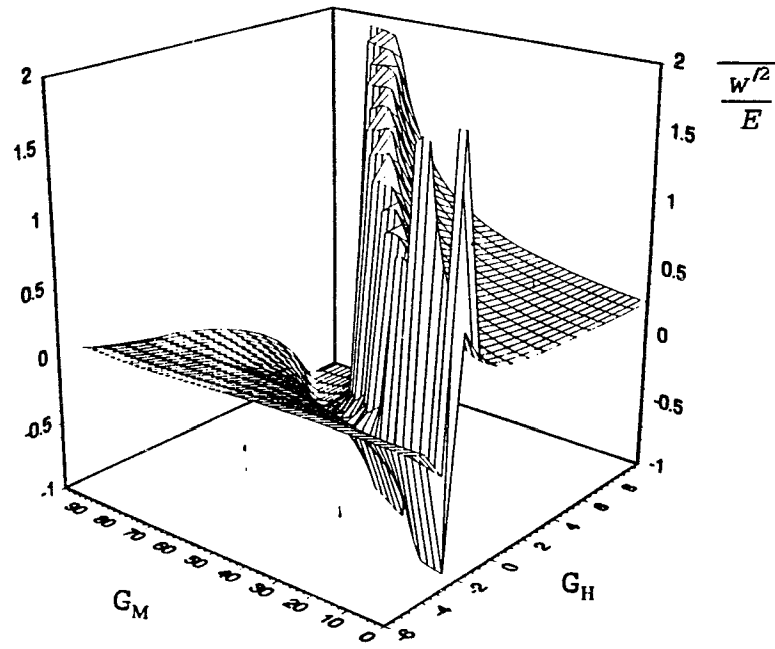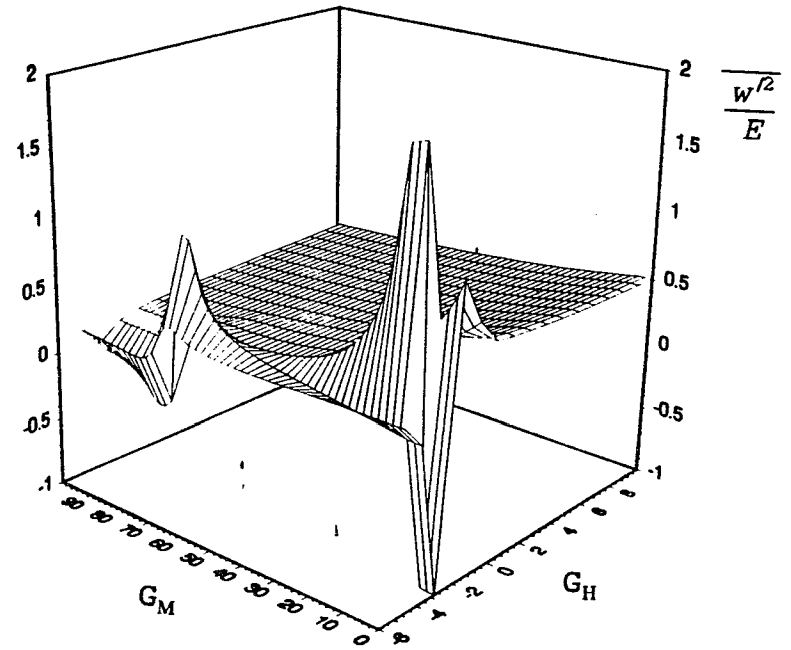
(a)modified model   (b)level 2.5 model

Fig.2.3.The $\overline{w'^2}/E$ as function of G_M and G_H with the modified model and level 2.5 model.

negative velocity variances and negative values of c_m and c_h especially in unstable condition. The shaded regions in Figure 2.1 and 2.2 are called a realization region.

As shown by the figures, there are notable differences between the modified model and the level 2.5 model. First, the c_m, c_h and vertical velocity variance with the modified model increase as G_M increases but those calculated from the level 2.5 model show exactly opposite trends. Second, the modified model shown in Figure 2.1 shows the expansion of the realization region with f=1.0 but the level 2.5 model in Figure 2.2 displays the opposite trend. The level 2.5 model with f=1 shown in Figure 2.2 displays a very narrow realization region in unstable condition (negative G_H). The application of the level 2.5 model with the wall effects in the unstable convective boundary layer is quite limited. This probably resulted in Andrén's use of a lower level model in the convective boundary layer.

Figure 2.4 shows that Rodi's extended model has no realization region under the unstable condition with $\dfrac{(P + G - \epsilon)}{\epsilon} = -1$ as a result of the approximate diffusion terms in the Equations (A-22) and (A-23). The value of $\dfrac{(P + G - \epsilon)}{\epsilon} = -1$ is often obtained near the inversion layer where the divergences of temperature and velocity change abruptly. This pathological behavior makes the application of Rodi's extended model with the additional diffusion terms
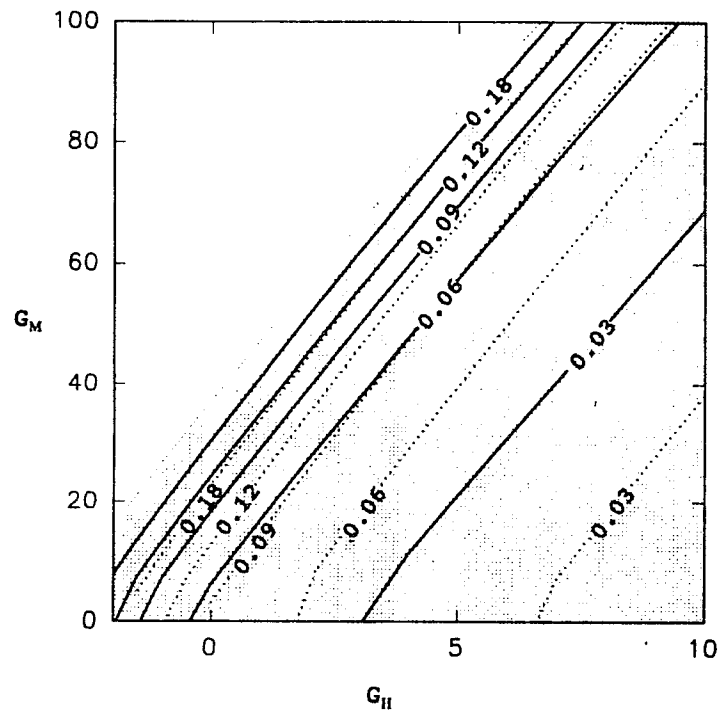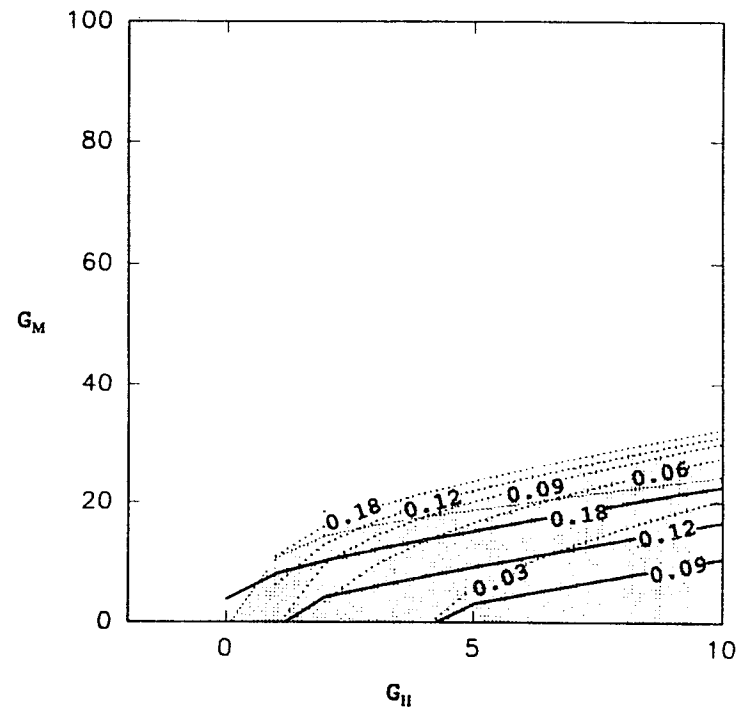
Fig.2.4.Effects of additional diffusion terms of Equations (A-22) and (A-23) on c_m and c_h as functions of G_M and G_H for the modified model. Shaded regions and lines as in Figure 2.1.

impossible in the convective boundary layer. In fact, the additional diffusion terms have little effect in the neutral and stable ABLs because the transport term in the turbulent kinetic energy budget is relatively small. The modified $E-\epsilon$ model, therefore, does not include the approximate diffusion terms suggested by Rodi(1985) and set the realization range of G_M and G_H for c_m and c_h based on the realization analysis.

In summary, Rodi's extended model and Andrén's level 2.5 model with wall effects have problems in applying their models to the unstable condition due to limited realization region. The modified model, developed herein, overcomes the drawbacks of their models.

Chapter 3. Comparison of Modified E-ϵ Turbulence Model to Observations

3.1. Introduction

In this chapter, the modified E-ϵ model will be tested in the neutral, stable and convective ABLs by comparison to available data. The comparisons of the standard, Duynkerke, and Detering and Etling dissipation rate equations are also included. The model is evaluated for a horizontal flow.

The governing equations will be discussed and the detailed structure for various ABLs will be compared with measurements by Caughey and Palmer (1979), Caughey et al. (1979), Nieuwstadt (1984), calculations of higher order closure by Brost and Wyngaard (1978), and large eddy simulation by Moeng and Wyngaard (1989). Simulations under neutral conditions will be compared with measurements by Brost et al. (1982), Grant (1986, 1992) for the turbulence statistics and with large eddy simulation of Mason and Thomson (1987).

3.2. Model Formulation

3.2.1. Governing Equations

The governing equations for a horizontal flow in a homogeneous boundary layer are.

$$\frac{\partial U}{\partial t} = -\frac{\partial \overline{u'w'}}{\partial z} + f\,(V - V_g) \qquad (3.1)$$

$$\frac{\partial V}{\partial t} = -\frac{\overline{\partial v'w'}}{\partial z} - f\ (U - U_g) \qquad (3.2)$$

$$\frac{\partial \Theta}{\partial t} = -\frac{\overline{\partial w'\theta'}}{\partial z} \qquad (3.3)$$

We consider a horizontal flow with the mean velocities (U, V) in the x(longitudinal) and y(lateral) directions. U_g and V_g are the geostrophic winds in the x and y directions. w' is the fluctuating vertical (z-) direction velocity. f ($=10^{-4}$ sec^{-1}) is the Coriolis parameter.

3.2.2. Boundary Conditions and Numerical Method

In order to calculate the turbulent fluxes near the surface, Monin-Obukhov similarity is used to relate the turbulent fluxes to the vertical gradients in the surface layer.

$$\phi_m = \frac{\kappa\ z}{u_*}\frac{\partial V_a}{\partial z}$$

$$\qquad (3.4)$$

$$\phi_h = \frac{\kappa\ z}{\theta_*}\frac{\partial \Theta}{\partial z}$$

κ is von Karman constant (0.4), θ_* is the temperature scale and V_a is the horizontal resultant wind speed.

$$\theta_* = -\frac{\overline{(w'\theta')}_s}{u_*} \qquad (3.5)$$

$$V_a = (U^2 + V^2)^{\frac{1}{2}}$$

The subscript s stands for the surface value. Based on field data, Businger et al. (1971) estimated the dimensionless functional forms for the momentum transfer(ϕ_m) and the heat transfer(ϕ_h) for neutral and stable conditions,

$$\phi_m = 1 + 4.7 \, \zeta$$

$$\phi_h = 0.74 + 4.7 \, \zeta$$

(3.6)

and for unstable condition.

$$\phi_m = (1 - 15 \, \zeta)^{-\frac{1}{4}}$$

$$\phi_h = 0.74 \, (1 - 9 \, \zeta)^{-\frac{1}{2}}$$

(3.7)

where $\zeta(=z/L)$ is a stability parameter, and L is the Monin-Obukhov length defined as:

$$L = - \frac{u_*^2}{\beta \, \kappa \, g \, \theta_*}$$

(3.8)

The fluxes for momentum and heat to the surface then obey the relations:

$$u_* = \frac{\kappa \, V_a}{[\ln(\frac{z}{z_o}) - \psi_m]}$$

$$\theta_* = \frac{\kappa \, (\Theta - \Theta_{zo})}{[\, 0.74 \, (\ln(\frac{z}{z_o}) - \psi_h)]}$$

(3.9)

Ψ_m and Ψ_h are for stable condition:

$$\psi_m = -4.7\ \zeta$$

$$\psi_h = -6.35\ \zeta \tag{3.10}$$

and for unstable condition:

$$\psi_m = 2\ \ln[(1 + \phi_m^{-1})/2] + \ln[(1 + \phi_m^{-2})/2] - 2\ \tan^{-1}(\phi_m^{-1}) + \frac{\pi}{2} \tag{3.11}$$

$$\psi_h = 2\ \ln[(1 + 0.74\ \phi_h^{-1})/2]$$

The friction velocity(u_*) and temperature scale(θ_*) in Equation (3.9) are nonlinearly coupled with the Monin-Obukhov length through the dimensionless functions (Ψ_m, Ψ_h). Therefore, iterations are required to obtain the momentum flux(ρu_*^2) and heat flux($u_*\theta_*$) from the model variables V_a and ($\Theta - \Theta_{z0}$). z_o is roughness length.

To solve the turbulent kinetic energy and dissipation rate equations, E and ϵ are specified at the first grid point above ground level. The values of E and ϵ are prescribed at the first grid level above the surface as:

$$\epsilon_p = \frac{u_*^3}{\kappa}\ (\frac{\phi_m}{z} - \frac{1}{L}) \tag{3.12}$$

$$E_p = c_{mp}^{\frac{1}{2}}\ u_*^2$$

The subscript p means the grid point above the ground and the value of ϵ_p was determined from viscous dissipation in the surface layer being in balance with buoyancy production.

At the top of the calculation domain, the boundary conditions are

$$\frac{\partial U}{\partial z} = \frac{\partial V}{\partial z} = \frac{\partial E}{\partial z} = \frac{\partial \epsilon}{\partial z} = 0, \quad \frac{\partial \Theta}{\partial z} = const. \tag{3.13}$$

In order to solve the governing equations with boundary conditions, the finite difference method with a control volume formulation in space (Patankar, 1980) was used. A staggered grid was employed as shown in Figure 3.1. The vertical grids for variables were spatially staggered with the mean velocities and the turbulence properties such as the kinetic energy and dissipation rate. The fully implicit method was used in time. 80 grids with a log-linear scale along the height were used for the neutral and convective runs and 60 grids for the stable run.

3.3. General Characteristics of ABL

The lowest 1-2km layer of the atmosphere is called the atmospheric boundary layer (ABL). This is the region in which the atmosphere is influenced by the surface effects through vertical exchange of momentum, heat, and moisture. The structure of the ABL over the land is strongly influenced by a diurnal cycle of surface heating and cooling. Figure 3.2 shows a well defined structure that evolves with a diurnal cycle. The three major components of this structure are the convectively mixed layer during a day, the residual layer, and the stable boundary layer at
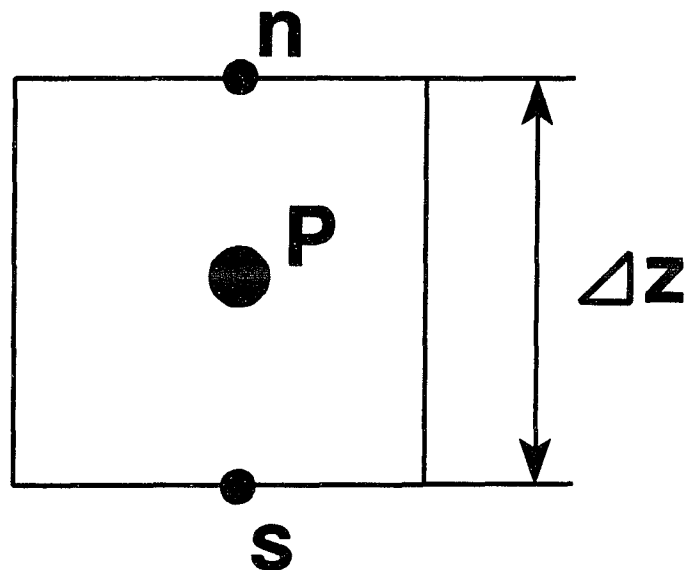
Fig.3.1. A control volume for one dimensional simulation. P is a grid point for turbulent properties(E, ϵ, and K^z_m). n and s are interfaces between control volumes for horizontal velocities(U,V) and temperature(Θ).
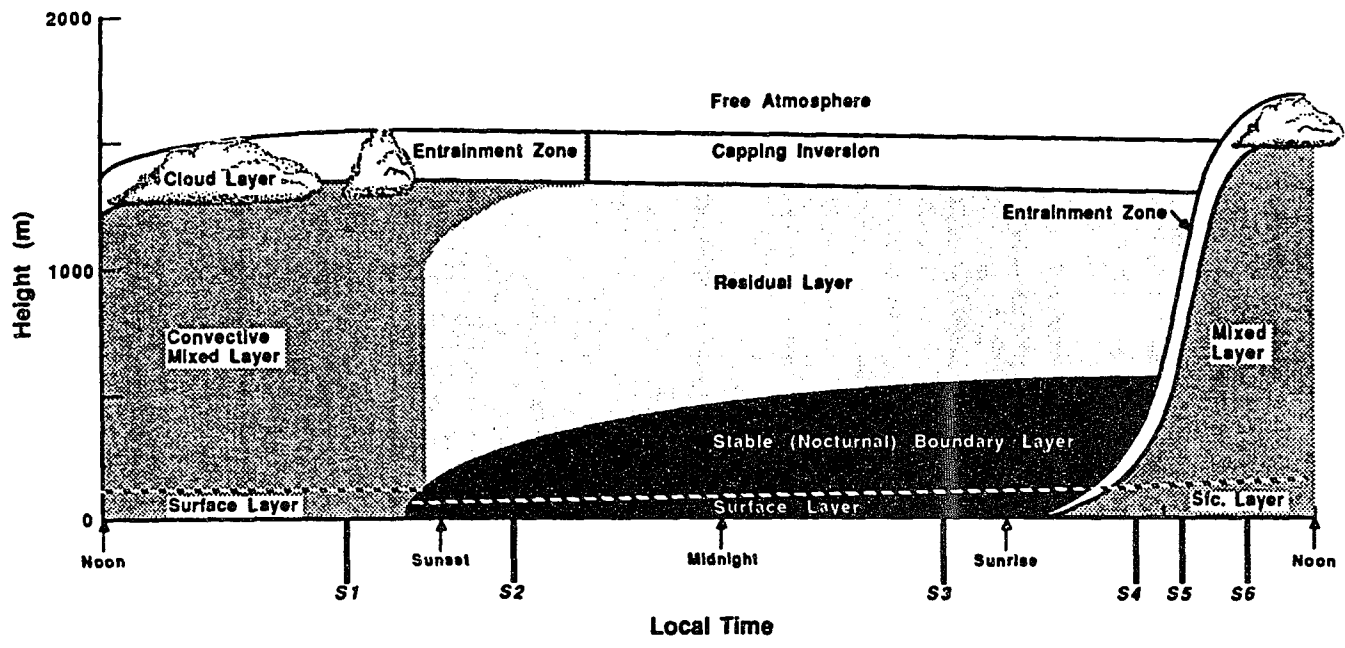
Fig.3.2.The atmospheric boundary layer over land with diurnal cycle (Stull, 1988). Time markers indicated by S1-S6 will be used in Fig.3.3.

night (Stull, 1988). The surface layer is the region at the bottom of the ABL where turbulent fluxes and stress vary by less than 10% from their maximum values. Figure 3.3 shows profiles of potential temperature variations during a diurnal cycle. The potential temperature will be defined and the characteristics of convective, stable, and neutral ABL will be discussed in the following.

Potential Temperature

Buoyancy is the major driving force for turbulence in the ABL. Thermals of warm air rises because they are less dense than the surrounding air. In order to relate the true buoyancy to temperature, the pressure variation with height has to be considered in the calculation of temperature. If a parcel of dry air is moved vertically without exchanging heat with its surroundings, the first law of thermodynamics becomes

$$c_p \, dT - \frac{1}{\rho} \, dP = 0 \qquad (3.14)$$

where c_p is a specific heat of air at constant pressure and T is an absolute temperature. Substituting from the hydrostatic equation ($\frac{\partial P}{\partial z} = - \rho g$), the adiabatic temperature gradient (or an adiabatic lapse rate) is:

$$(\frac{dT}{dz})_{ad} = - \frac{g}{c_p} = - \frac{0.98°C}{100m} \qquad (3.15)$$
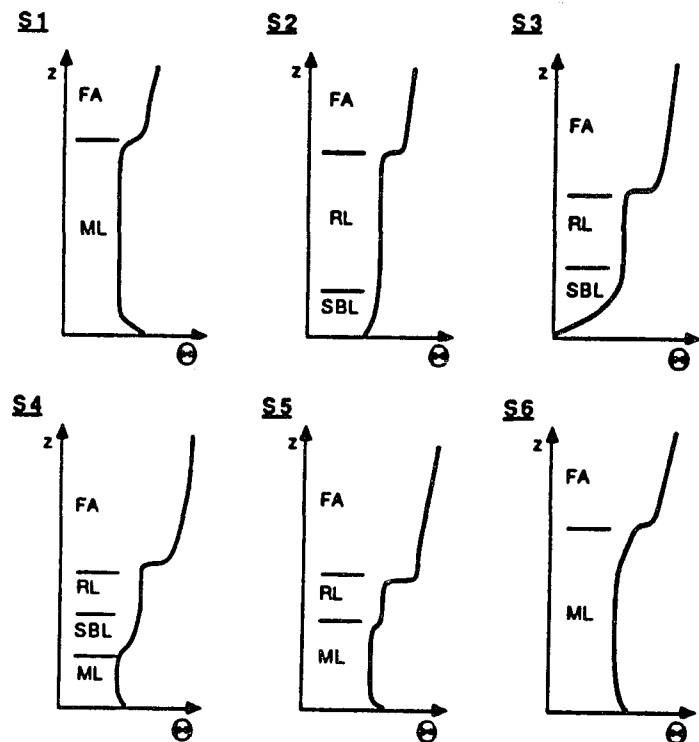
Fig.3.3. Profiles of potential temperature showing the evolution of the atmospheric boundary layer with diurnal cycle. FA is free atmosphere, ML is mixed layer, RL is residual layer, and SBL is stable boundary layer

This means that the absolute temperature decreases about 1 C for each elevation increase of 100m. A potential temperature (Θ) can be obtained from equation (3.14) by substituting for $(1/\rho)$ with the use of the ideal gas equation of state and by integrating from sea level pressure(P_o) to the pressure P at certain elevation.

$$\Theta = T \, (\frac{P_o}{P})^{\frac{R}{c_p}} \qquad (3.16)$$

where R is a gas constant and R/c_p is 0.286. In other words, the potential temperature of a parcel of air at temperature(T) and pressure(P) is the temperature that would result in if the parcel was brought down adiabatically from a pressure P to a sea level pressure P_o. The relationship between the potential temperature (Θ) and the absolute temperature (T) can be obtained by eliminating P in Equations (3.14) and (3.16).

$$\frac{d\Theta}{dz} = \frac{dT}{dz} + \frac{g}{c_p} \qquad (3.17)$$

and

$$\Theta = T + \frac{g}{c_p} z \qquad (3.18)$$

The potential temperature gradient defines the static stability of the atmosphere. Potential and absolute temperature profiles during neutral, stable and unstable

conditions are shown in Figure 3.4. Under neutral conditions, the absolute temperature gradient (dT/dz) is equal to the adiabatic lapse rate and the potential temperature gradient (dΘ/dz) is zero. It means that there is no buoyancy force to drive the vertical motion. If dT/dz is greater than the adiabatic lapse rate or dΘ/dz is negative, a superadiabatic lapse rate is said to apply and unstable conditions occur. The density of the parcel of an air at low elevation is less than that of its surroundings. The parcel is accelerated upward and buoyancy causes turbulence and mixing in the unstable condition. If dT/dz is less than the adiabatic lapse rate or dΘ/dz is positive, a subadiabatic lapse rate is said to apply and stable conditions occur. Under stable conditions, a parcel of air always tends to return to its original position, i.e., damping turbulence and mixing.

Convective ABL

The convective ABL consists of the mixed layer and surface layer as shown in Figures 3.2 and 3.3. In the daytime, thermal turbulence dominates the mechanical turbulence. The turbulence of the mixed layer is convectively driven. Convective sources include heat transfer from a warm ground surface and radiative cooling from the top of the ABL. Time S6 in Figure 3.3 shows typical daytime profiles of potential temperature in the convective ABL. Potential temperature is nearly adiabatic in
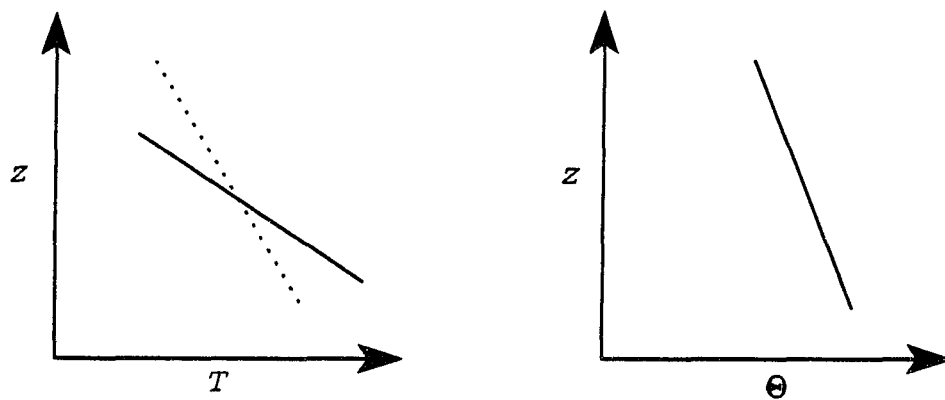
(a)unstable condition
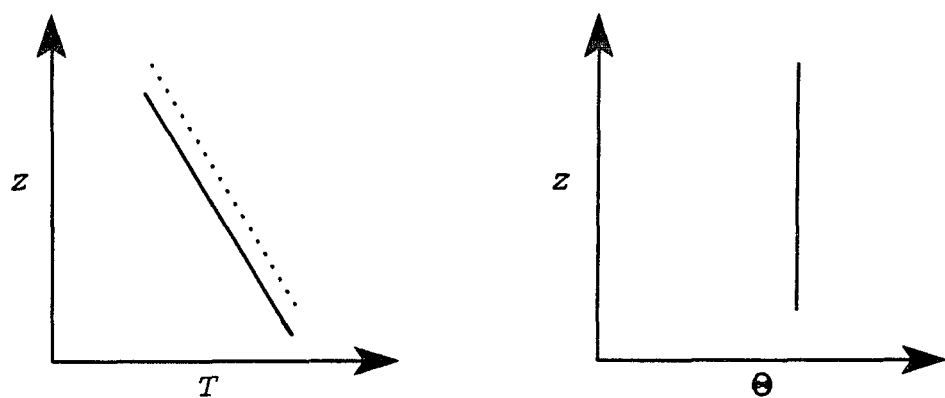
(b)neutral condition
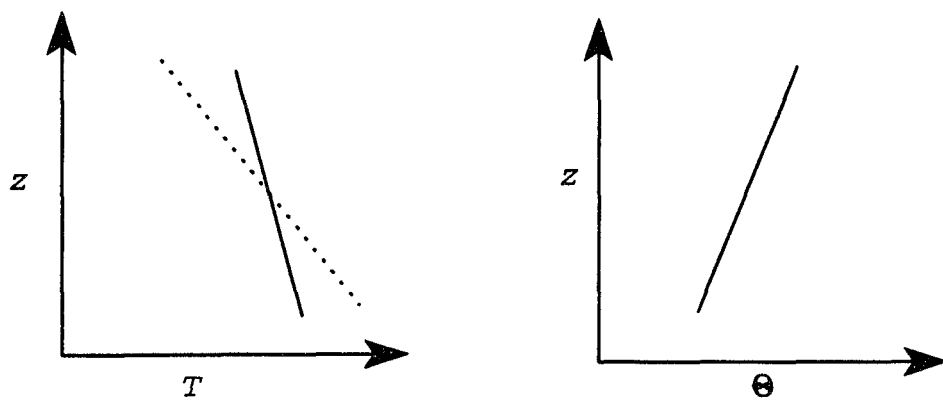
(c)stable condition

Fig.3.4. Absolute(T) and potential(Θ) temperature profiles with a height for various static stability conditions. Dotted line is an adiabatic lapse rate (-0.98 C/100m).

the middle portion of the convective ABL and superadiabatic in the surface layer. A stable layer at the top of the mixed layer acts as a lid to the rising thermal, thus restraining the domain of turbulence within the boundary layer. It is called the entrainment zone because entrainment into the mixed layer occurs there.

<u>Stable ABL</u>

At night, stable air with weaker, sporadic turbulence is formed due to the radiative cooling of the ground. The typical profiles of the potential temperature are shown in Figure 3.3. at time S3. The potential temperature increases with height. The statically stable air tends to suppress turbulence, while the developing nocturnal jet aloft enhances wind shear.

<u>Neutral ABL</u>

It often occurs at early morning and late afternoon with strong wind speed or little surface heating or cooling resulting in statically neutral conditions. Truly neutral ABL is , however, rarely found in the real atmosphere and the simulation suggests that the prevailing stability aloft can significantly influence the surface layer behavior.

3.4. Neutral ABL

The neutral ABL implies no heat flux at the surface and no background stratification, which is hardly observed. The available observations are typically influenced by a weak heat flux at the surface and stable stratification above the

boundary layer. The prognostic ϵ-equations often fail to describe the neutral ABL. They overpredict the eddy viscosity and give a deep boundary layer. Detering and Etling (1985) and Duynkerke (1988) modified the ϵ-equation to fit the observed data in the nearly neutral ABL. Unfortunately the modification of the ϵ-equation based on the neutral ABL cannot be applied to the stable and convective ABL (Andrén,1990).

There are examples showing that weak background stratification changes the dynamics of the neutral ABL. That is because the neutral boundary layer in the atmosphere does not exist except as a nearly neutral boundary layer influenced by the stratification aloft. Duynkerke (1988) set a background stratification for the simulation of the neutral ABL and he showed that the general flow characteristics were close to those observed. Riopelle and Stubley (1989) showed that a weak background stratification and surface heat flux were essential to describe the 'Leipzig' boundary layer structure. In this study, a neutral ABL with weak surface heat flux and background stratification will be tested with the available data.

In order to understand the influence of the background stratification and surface heat flux, several case studies have been carried out. Table 3.1 shows the numerical conditions and the calculated key parameters. In the calculation, $U_g = 10$ m/s, $V_g = 0$. and $z_0 = 0.01$m were used.

Table 3.1. Examples of case study in the nearly neutral ABL.

Case	$-(d\Theta/dt)_s$ $K\text{-hr}^{-1}$	$(d\Theta/dz)_b$ $K\text{-m}^{-1}$	h,m	d	$u_*,$ $m\text{-s}^{-1}$	L,m	θ_*	α
C1	0.	0.	2996	0.85	0.353	∞	0.	10.9
C2	0.001	10^{-6}	1929	0.55	0.351	12540	0.0007	12.5
C3	0.003	10^{-6}	1461	0.42	0.350	4753	0.0019	13.7
C4	0.005	10^{-6}	1241	0.36	0.349	3066	0.0028	15.5
C5	0.01	10^{-6}	989	0.28	0.346	1725	0.0052	16.1
C6	0.003	10^{-5}	1380	0.40	0.349	4472	0.0020	13.9
C7	0.003	10^{-4}	1058	0.30	0.350	3438	0.0027	14.6
C8	0.003	10^{-3}	638	0.18	0.352	1768	0.0051	16.7

$-(d\Theta/dt)_s$: surface heat flux(cooling rate).,
$(d\Theta/dz)_b$: background stratification.

Upper boundary of the model was 3500m. The normalized profiles for vertical eddy viscosity, turbulent kinetic energy, longitudinal and lateral stress with various background stratifications are shown in Figure 3.5. In this calculation, the standard ϵ-equation was used. The eddy viscosity and turbulent kinetic energy without stratification and surface heat flux (C1 in Figure 3.5) show large values and the boundary layer height (h) reaches up to the top of the calculation domain of the model. h is taken as the height at which the stress is 5% of its surface value. As the background stratification increases, boundary layer height decreases and the normalized profiles shown in Figure 3.5 are limited within the boundary layer. The effects of the surface heat fluxes on the normalized flow characteristics are shown in Figure 3.6. As the surface heat flux increases, the boundary layer height and the normalized profiles show similar behaviors to those shown for varying background stratifications. The turbulence structure as a function of the surface heat flux is shown in Figure 3.7. According to the observations of Grant (1992), the ratios of the selected turbulence variables as shown in Figure 3.7 show constant values in the lower half of the boundary layer. The calculated turbulence variables also indicate constancy as the surface heat flux increases. From the large eddy simulations (Deardorff 1972; Mason and Thomson 1987), the value of d(=h f/u$_*$) is in the range 0.4-0.5 and
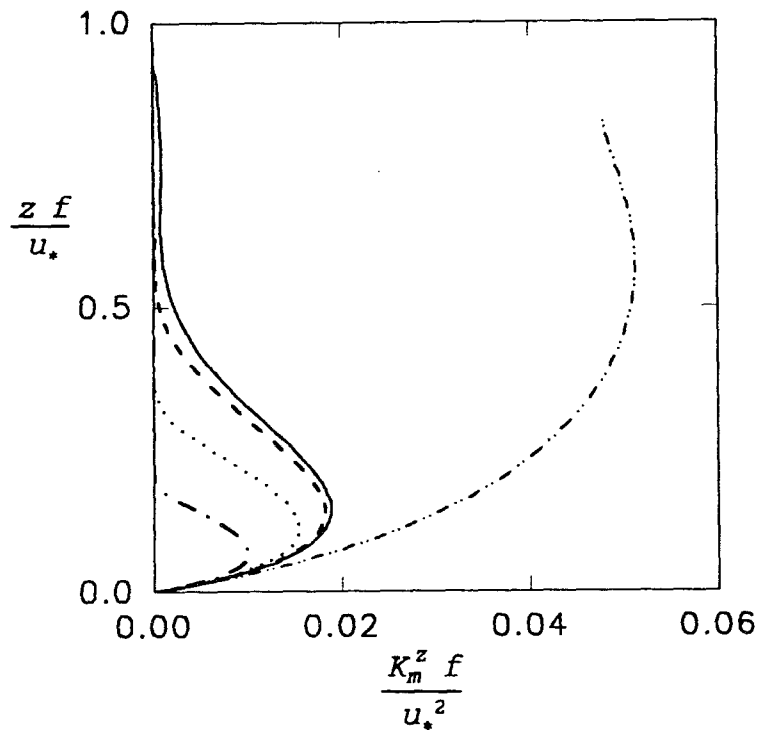
(a)vertical eddy viscosity
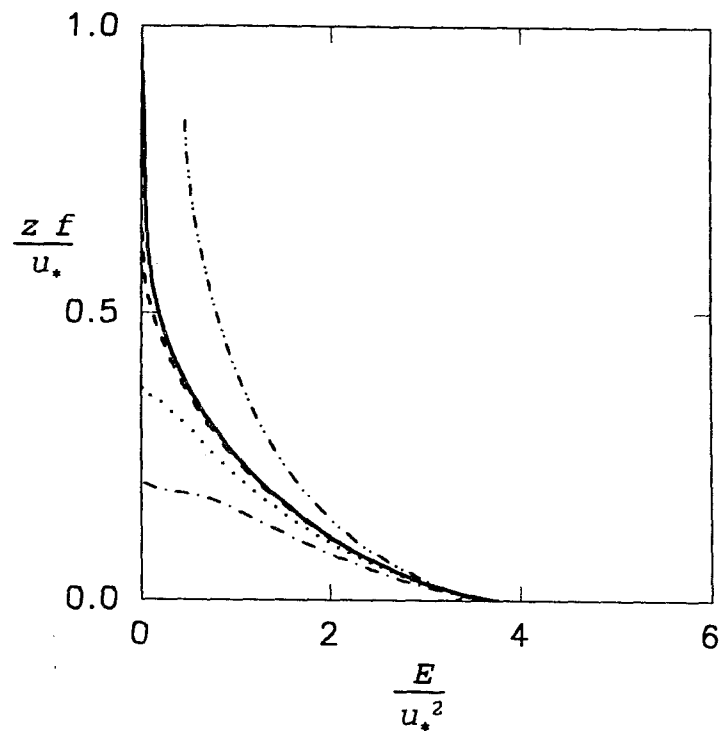
(b)turbulent kinetic energy

Fig.3.5. Effects of background stratification on normalized profiles in the neutral ABL. Double dot-dashed lines are for case C1 in Table 3.1, solid lines for C3, dashed lines for C6, dotted line for C7, and dot-dashed lines for C8. Fig. continued.
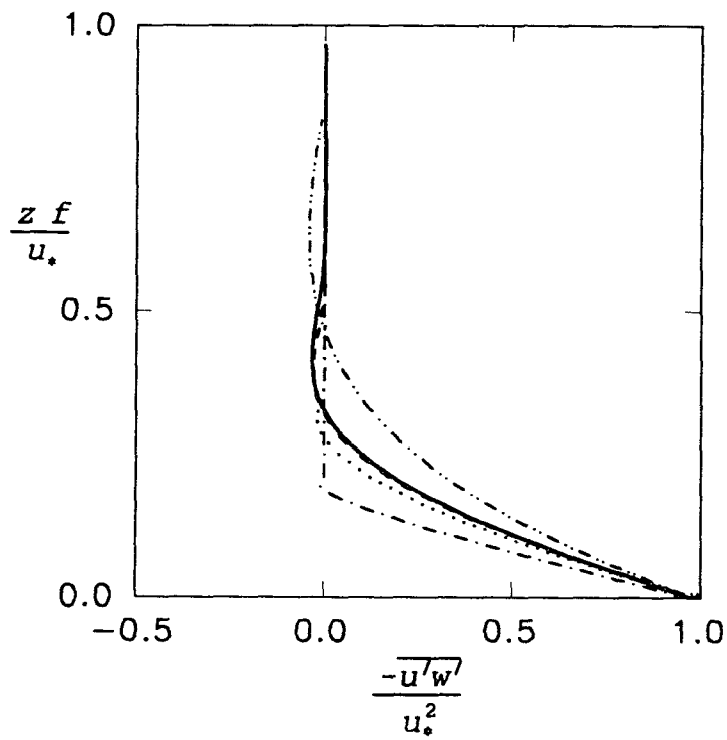
(c)longitudinal stress
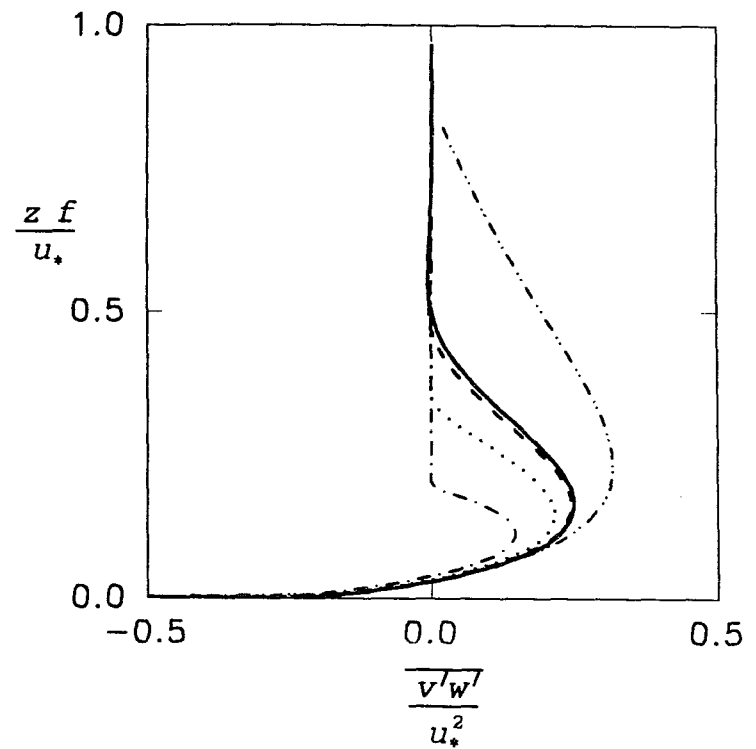
(d)lateral stress
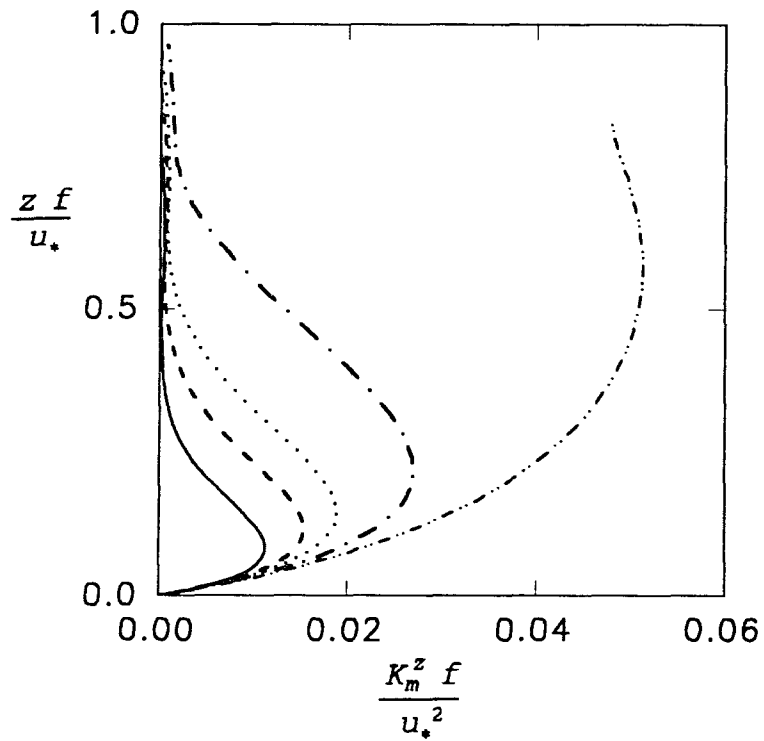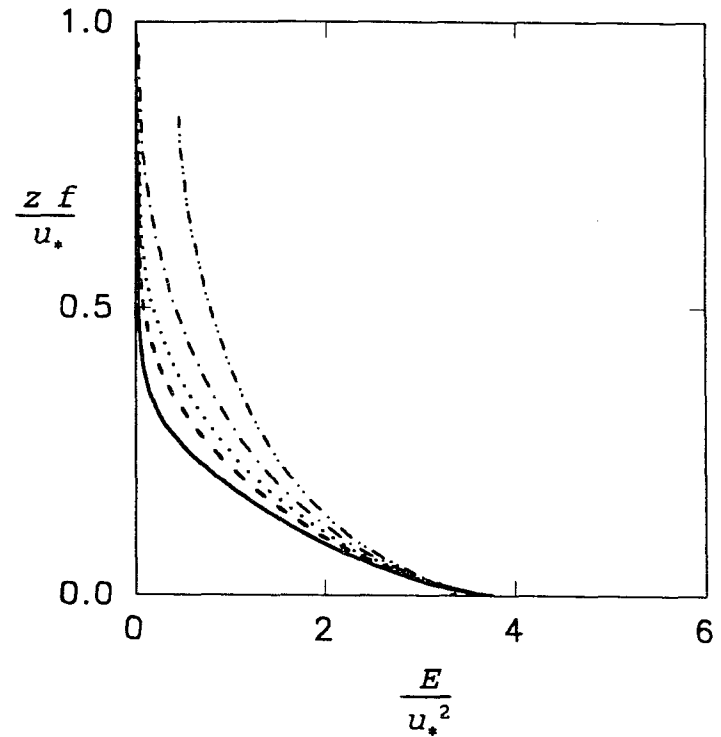
(a)vertical eddy viscosity   (b)turbulent kinetic energy

Fig.3.6. Effects of surface heat flux on normalized profiles in the neutral ABL. Double dot-dashed lines are for case C1 in Table 2.1, solid lines for C5, dashed lines for C4, dotted line for C3, and dot-dashed lines for C2. Fig. continued.
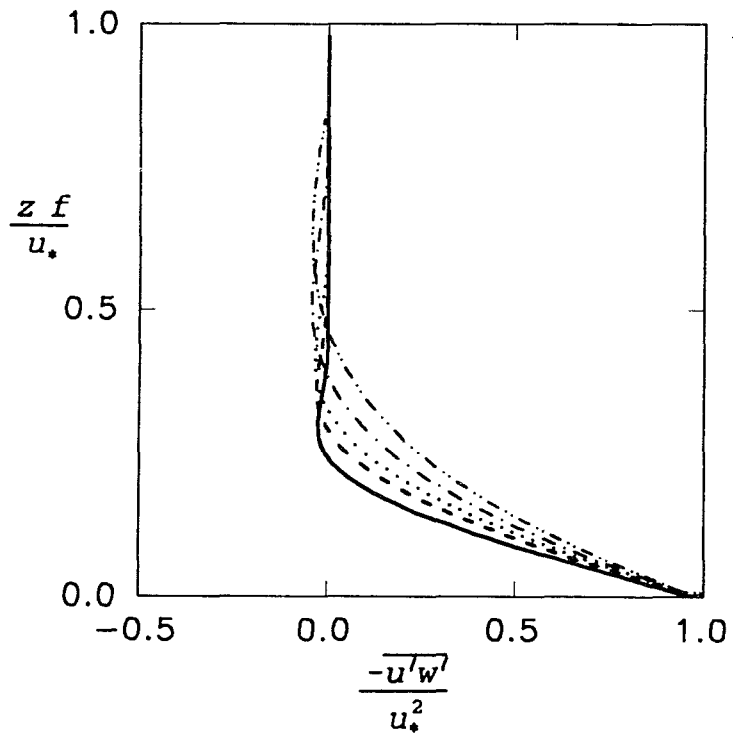
(c)longitudinal stress
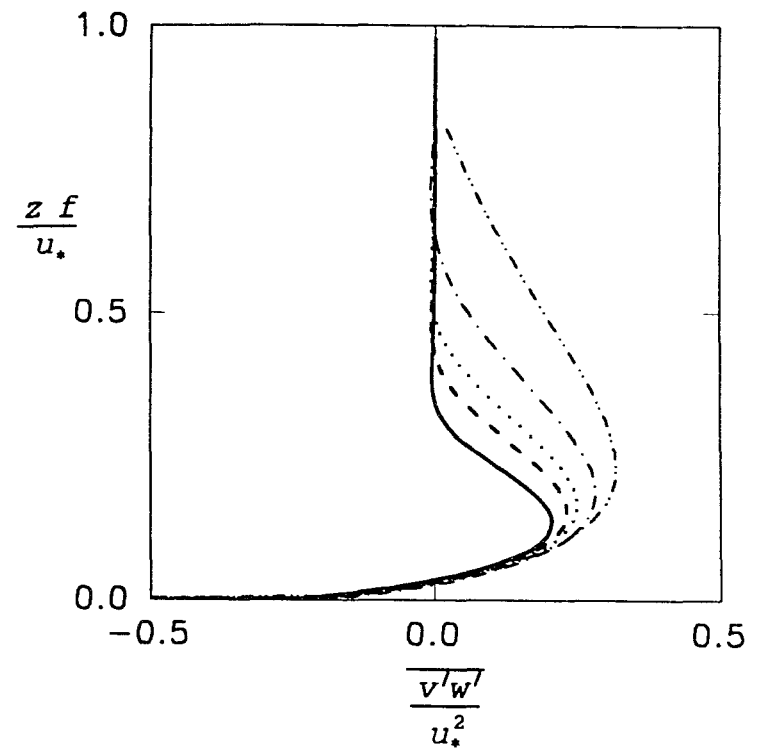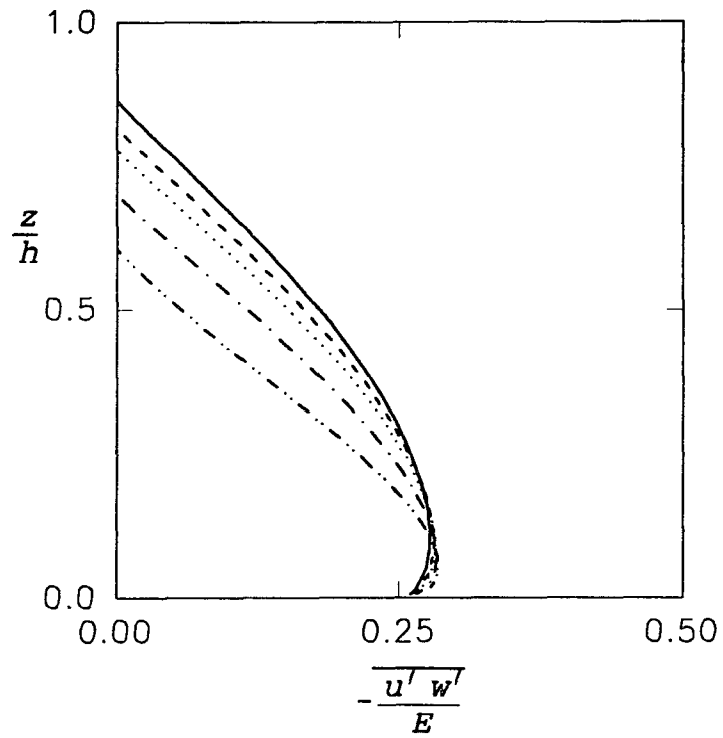
(d)lateral stress

(a)ratio of the shear stress
kinetic energy

(b)ratio of the lateral and
longitudinal velocity variances

Fig.3.7. Effects of surface heat flux on turbulence structure in
the neutral ABL. Lines as in Figure 3.6. Fig. continued.

(c)ratio of the vertical and
lateral velocity variances
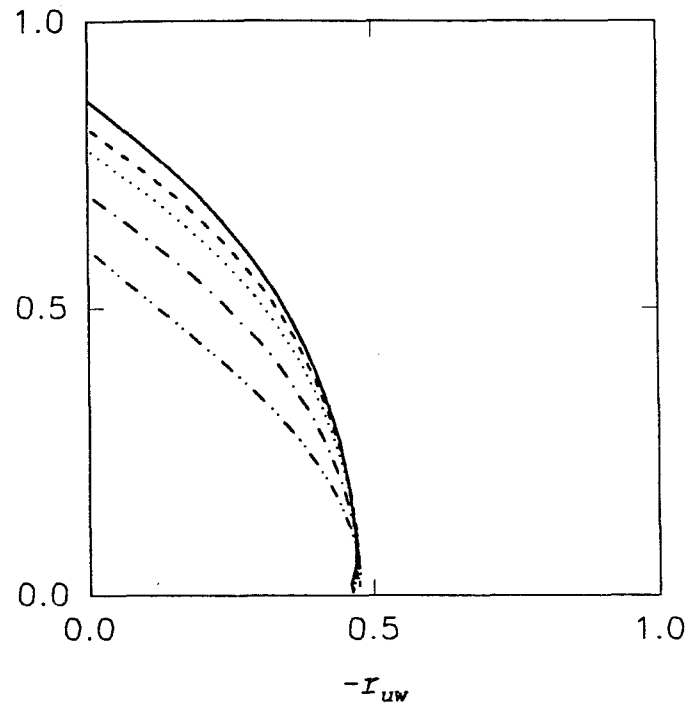
(d)stress correlation coefficient

α(isobaric angle of surface winds) is about 14 degree. The simulations of case C3 and C6 in Table 3.1 show a similar range of d and α values. Case C3 most nearly corresponds to the expected behavior in a nearly neutral atmosphere and was used in subsequent simulation of the neutral boundary layer. It remains unclear if the actual nearly neutral atmosphere is as sensitive to the background stratification as is the numerical model.

Table 3.2. Calculated surface layer parameters with modified E-ϵ model in the neural ABL.

ϵ-equation	h,m	d	u_*,ms^{-1}	L,m	θ_*	α
standard	1461	0.42	0.350	4753	0.0019	13.7
Duynkerke	1704	0.47	0.364	4924	0.0020	12.8
Detering & Etling	1134	0.383	0.383	6274	0.0017	16.6

Table 3.2 shows the calculated surface layer parameters in the neutral ABL. Figure 3.8 shows the normalized profiles for eddy viscosity, turbulent kinetic energy, longitudinal and lateral stresses. The modified E-ϵ model with Duynkerke ϵ-equation shows an energetic boundary layer, i.e., large eddy viscosity, high turbulent kinetic energy level and a deep boundary layer. The model with standard ϵ-equation shows a similar profile. The modified model with Detering and Etling ϵ-equation shows lower estimates of eddy viscosity as shown in Figure 3.8(a). The estimates of the kinetic energy and the boundary layer height also show lower
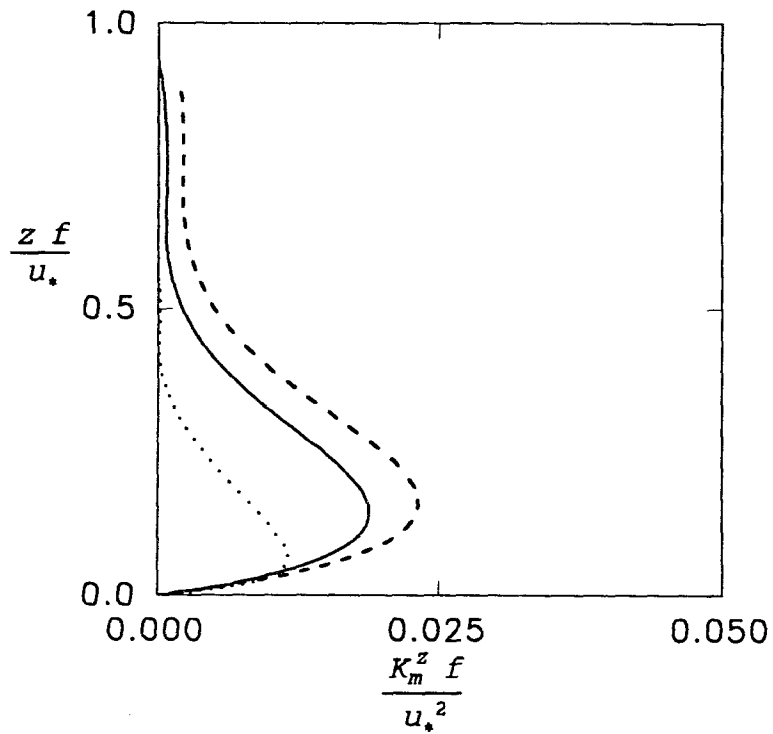
(a)vertical eddy viscosity
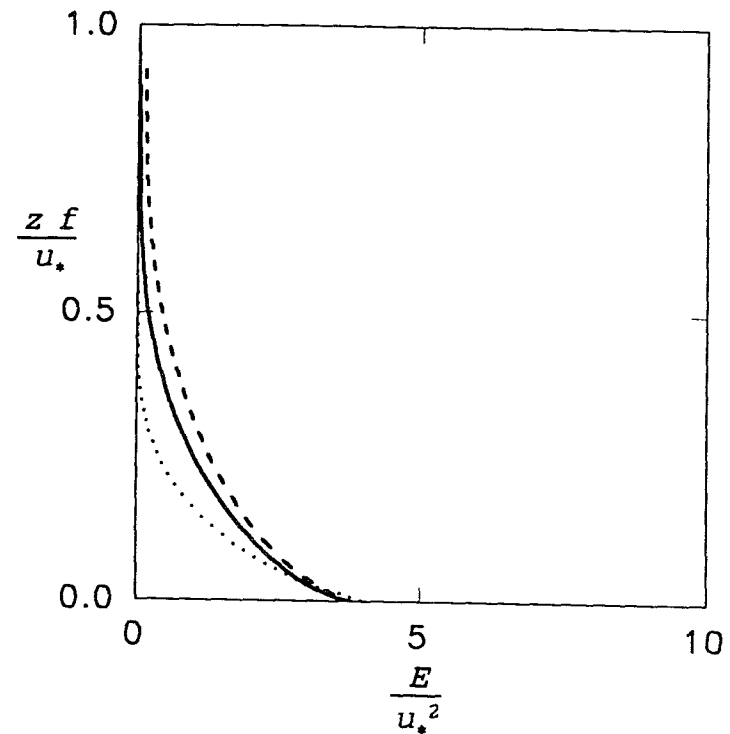
(b)turbulent kinetic energy

Fig.3.8. Normalized profiles in the neutral ABL. Solid lines are standard ϵ-equation, dashed lines Duynkerke ϵ-equation, and dotted lines Detering and Etling ϵ-equation. Fig. continued.
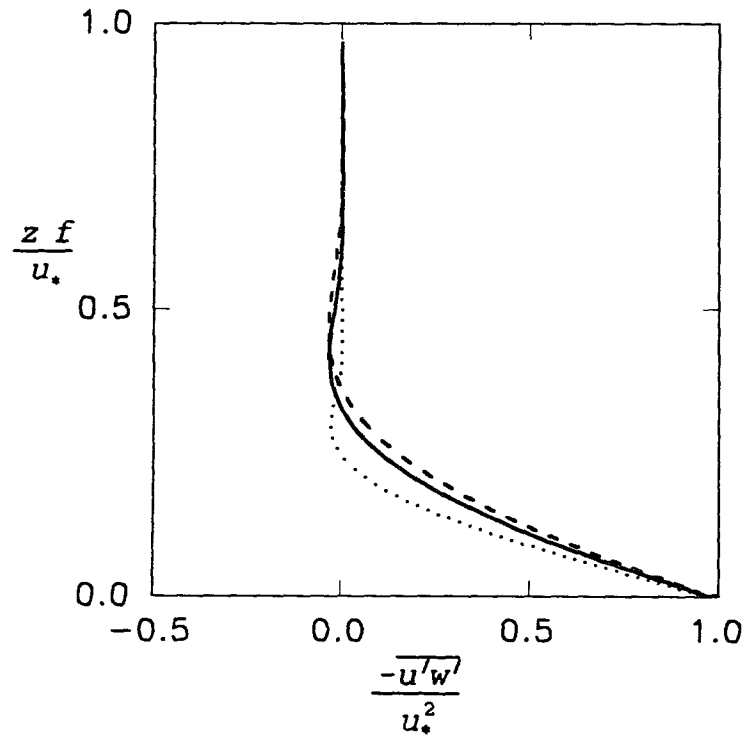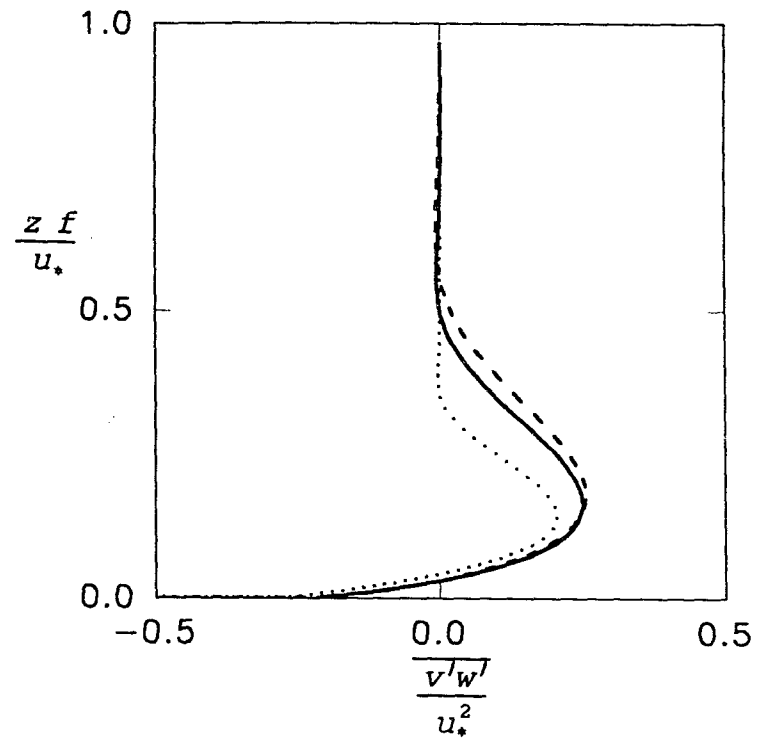
(c)longitudinal stress   (d)lateral stress

values. The stresses in Figure 3.8(c) and (d) of the standard and Duynkerke ϵ-equations show typical neutral boundary layer profiles compared with the estimates of Deardorff (1972) and Wyngaard et al. (1974) (not shown in Figure 3.8). The velocity variances of the modified E-ϵ model in Figure 3.9 show good agreement with measurements regardless of the ϵ-equation used.

According to local similarity, selected ratios of the turbulence statistics as shown in Figure 3.10 should be constant in the lower half of the boundary layer (Grant 1992). This is because the dissipation balances the production in the turbulent kinetic energy budgets and the turbulent transport term is not significant. The comparisons of the turbulence structure with the model calculations are shown in Figure 3.10. The calculated profiles show good agreement with measurements but the range of constant values is limited to the lower third of the boundary layer. Grant (1992) approximated the boundary layer height by the height of the zero stress. The observed value of h based on the data (Grant, 1992) is relatively low compared with the model prediction. Good agreement is found between predicted and observed profile shapes. The results of large eddy simulations (Mason and Thomson, 1987) show similar patterns although the ratios of lateral and longitudinal velocity variances differ as shown in Figure 3.10(b). According to Grant (1992), this difference may be
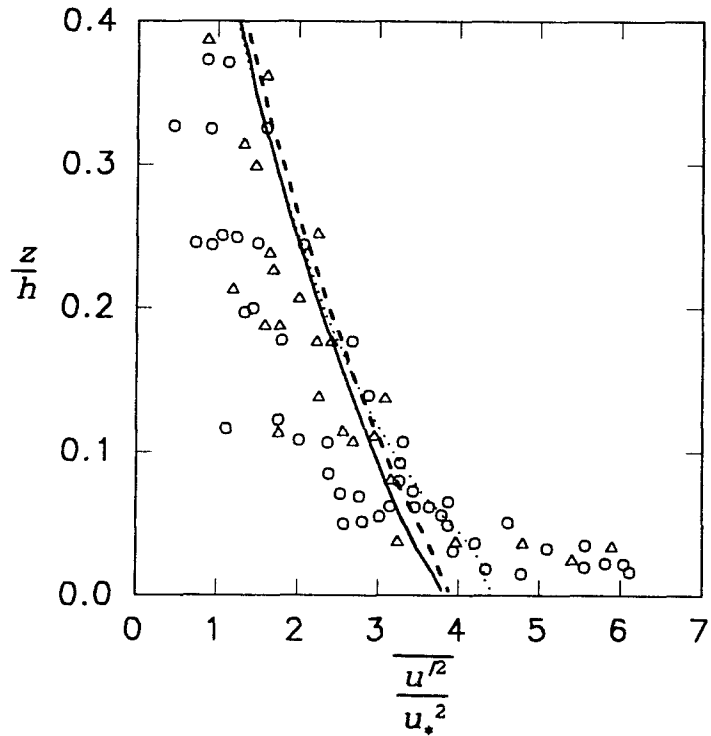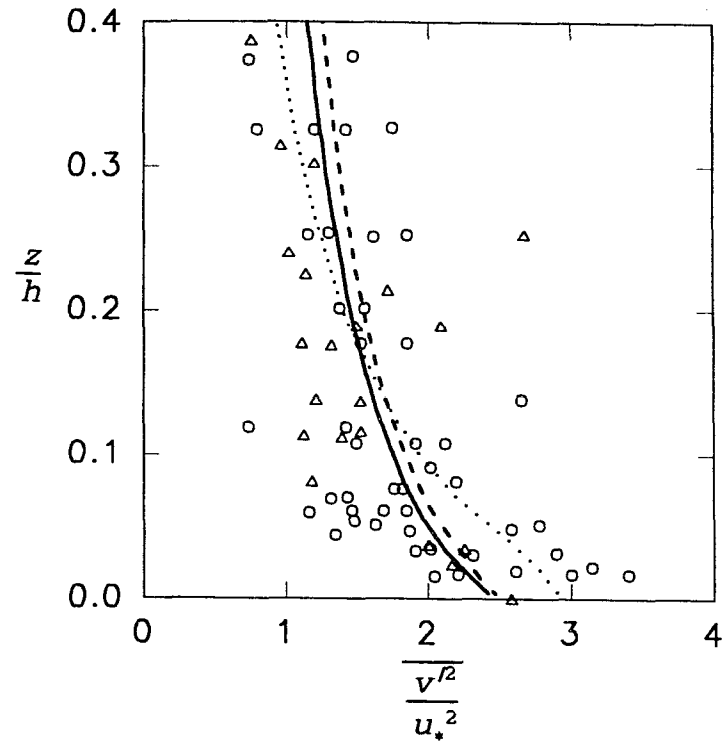
(a)longitudinal velocity variance   (b)lateral velocity variance

Fig.3.9. Normalized velocity variances in the neutral ABL. Lines as in Figure 3.8. Circles are data from Grant (1986) and Triangles from Brost et al.(1982). Fig. continued.
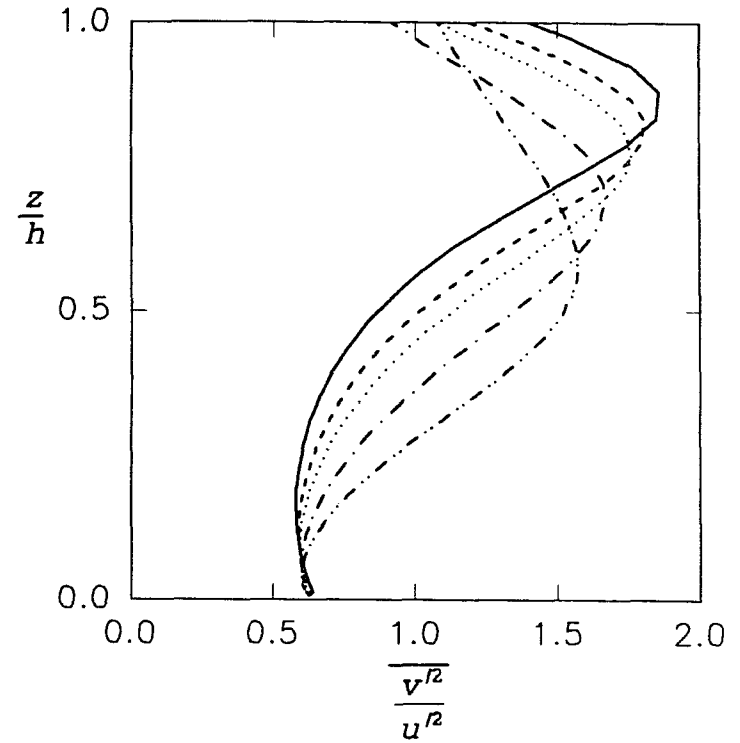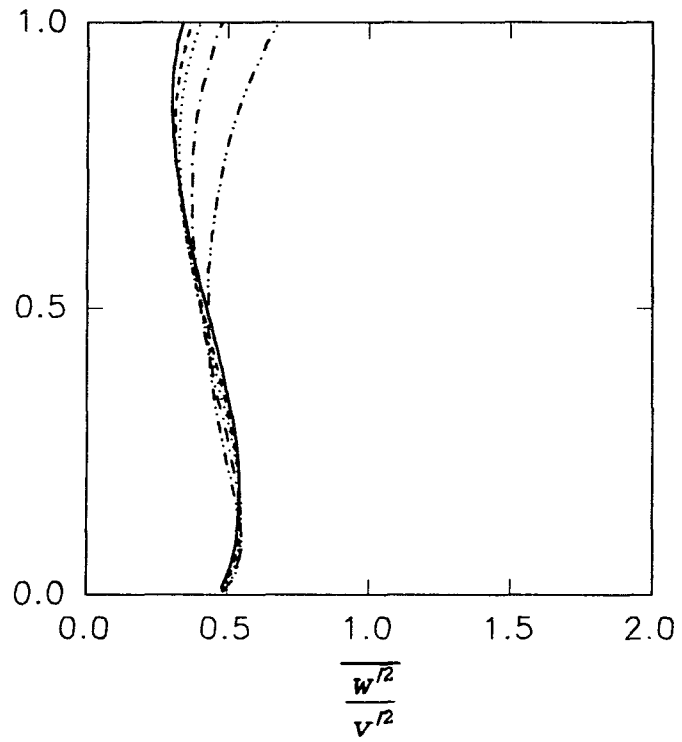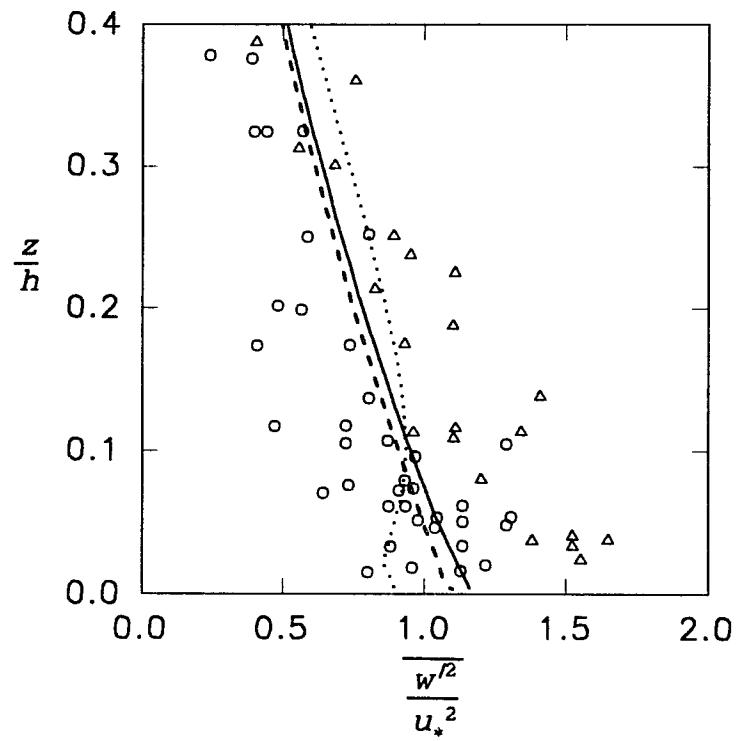
(c)vertical velocity variance
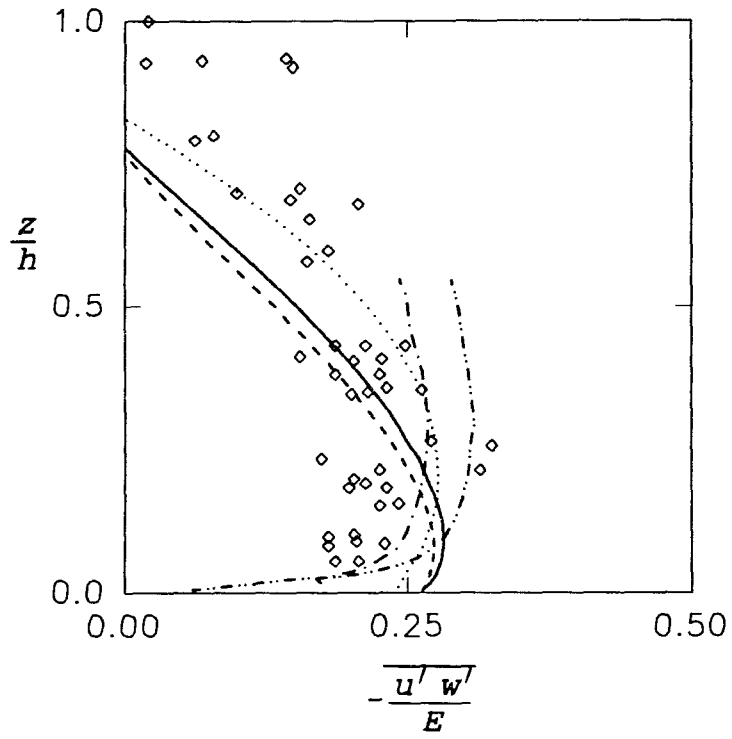
(a) ratio of the shear stress kinetic energy
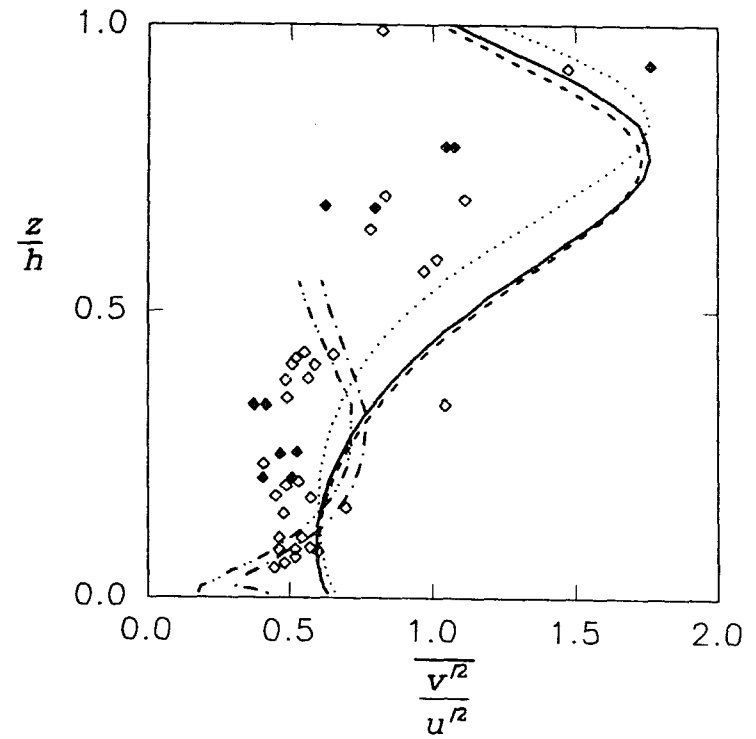
(b) ratio of the lateral and longitudinal velocity variances

Fig.3.10. Turbulence structure in the neutral ABL. Dot-dashed and double dot-dashed lines are from Mason and Thomson large eddy simulation (1987). Dot-dashed lines are for the resolved scale and double dot-dashed line for the total scale. The other lines as in Figure 3.9. Data for filled and blank diamond are from Grant (1992). Fig. continued.
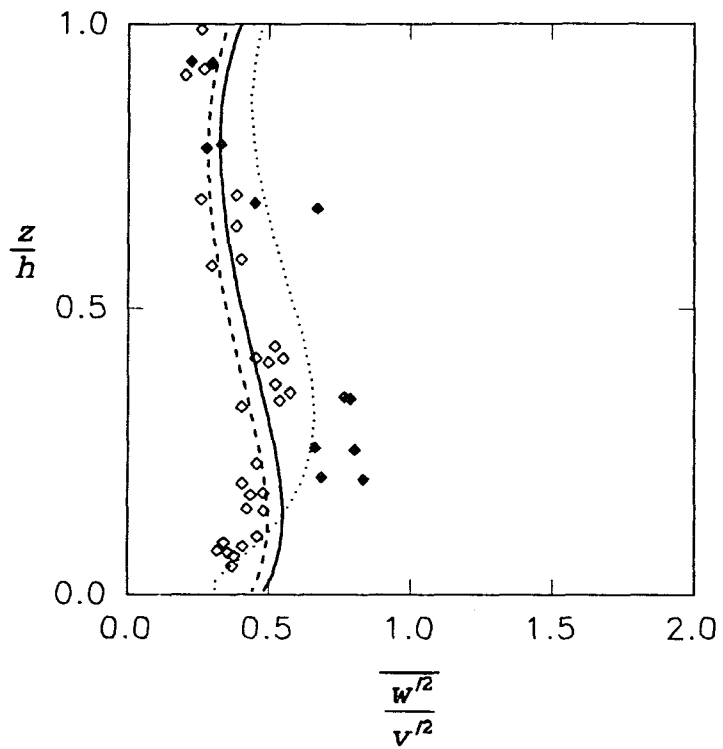
(c)ratio of the vertical and
lateral velocity variances
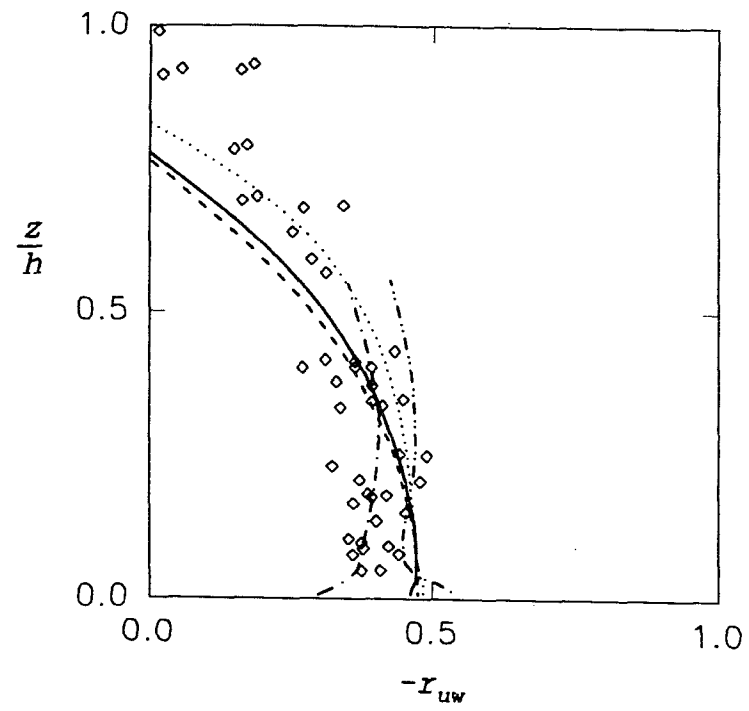
(d)stress correlation coefficient

due to the effects of the low turbulent Reynolds number on the pressure-strain correlations and/or inadequacies in the subgrid parameterization in the large eddy simulation. The calculated kinetic energy budgets are shown in Figure 3.11. In the lower third of the boundary layer, the production and dissipation terms are dominant, and the transport and buoyancy terms are less important.

In order to see the influence of the wall on the turbulence structure, the turbulence structure was calculated with various Kolmogorov constants(c_ϵ) in Equation (A-21). The c_ϵ in this study was 0.13. The wall effect is a significant factor on the ratios of the stress and turbulent kinetic energy and ratios of the vertical and lateral velocity variances as shown in Figure 3.12 (a) and (c). Atmospheric observations suggest that the ratio of the vertical and lateral velocity variances in Figure 3.12(c) is about 0.4 in boundary layers and about 1 in free turbulence (Gibson and Launder, 1978). The calculated ratio for $\overline{w'^2}/\overline{v'^2}$ without the influence of the wall approaches 1 and that with the wall effect included ($c_\epsilon = 0.13$ in Figure 3.8(c)) is about 0.5 near the ground. This supports the validity of the role of the wall function to estimate the influence of the earth's surface on the velocity variances.

3.5. Stable ABL

In order to test the performance of the modified E-ϵ model in the stable ABL, the stable condition was simulated
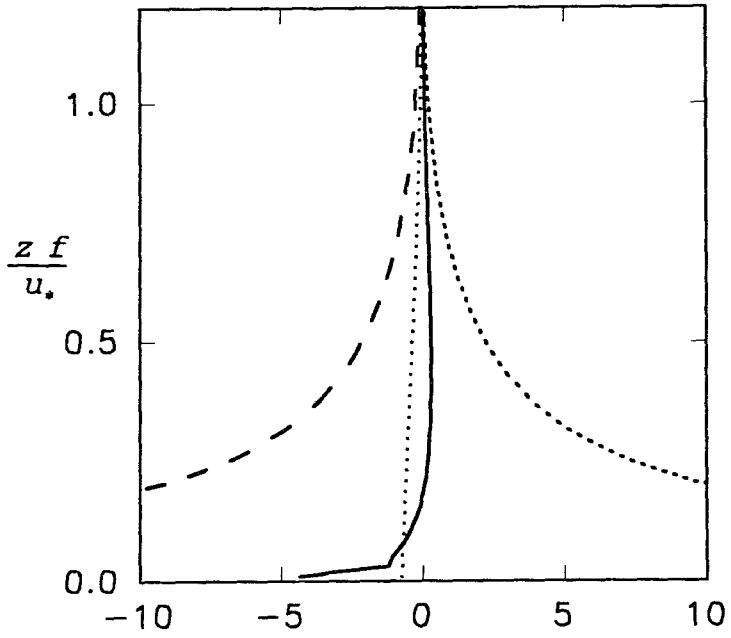
1.0

$\dfrac{z\,f}{u_*}$

0.5

0.0

−10   −5   0   5   10

E-BUDGET(normalized by $\dfrac{u_*^3}{h}$)

(a)standard ϵ-equation

1.0

$\dfrac{z\,f}{u_*}$

0.5

0.0

−10   −5   0   5   10
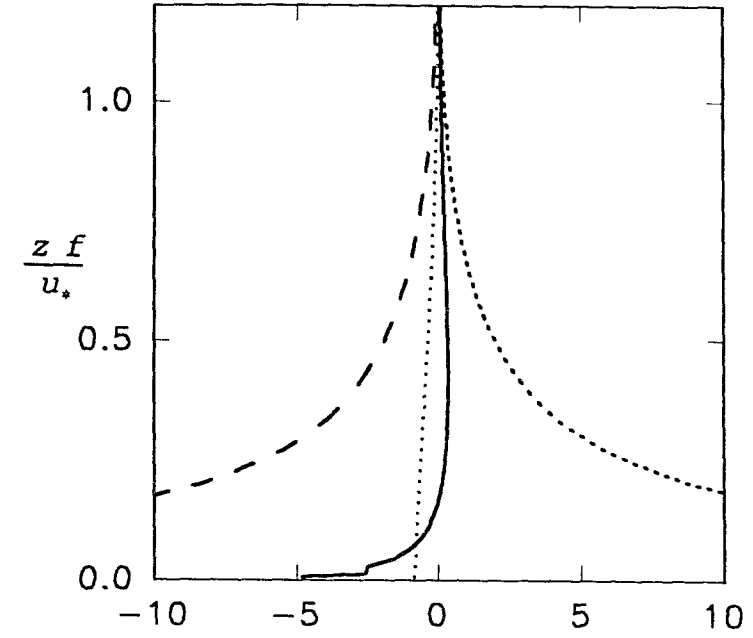
E-BUDGET(normalized by $\dfrac{u_*^3}{h}$)

(b)Duynkerke ϵ-equation

Fig.3.11. Kinetic energy budgets in the neutral ABL. Solid lines
are for transport term, long dashed lines for dissipation rate,
short dashed lines for mean production and dotted lines for
buoyancy. Fig. continued.

$$\frac{z\,f}{u_*}$$

E-BUDGET(normalized by $\frac{u_*^3}{h}$)
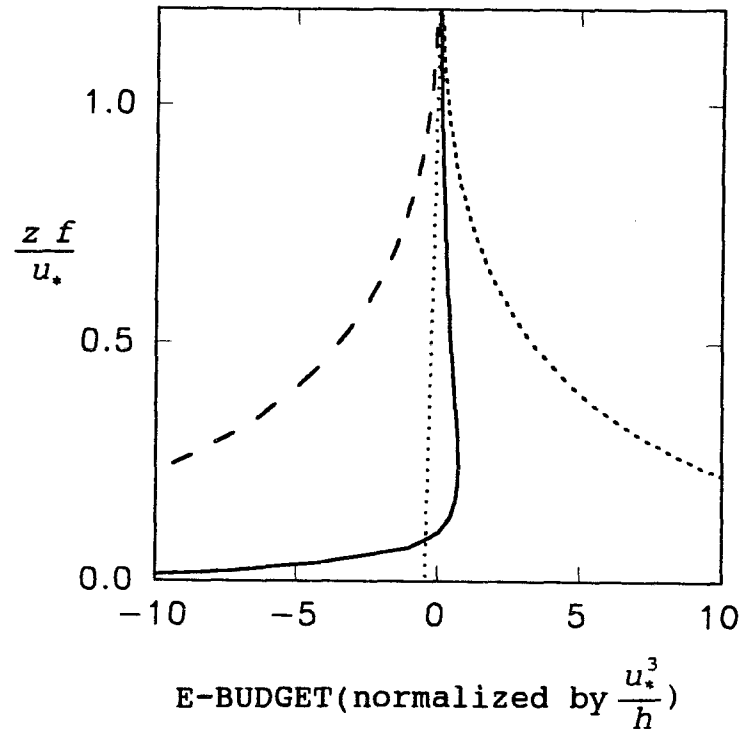
(c)Detering and Etling ϵ-equation
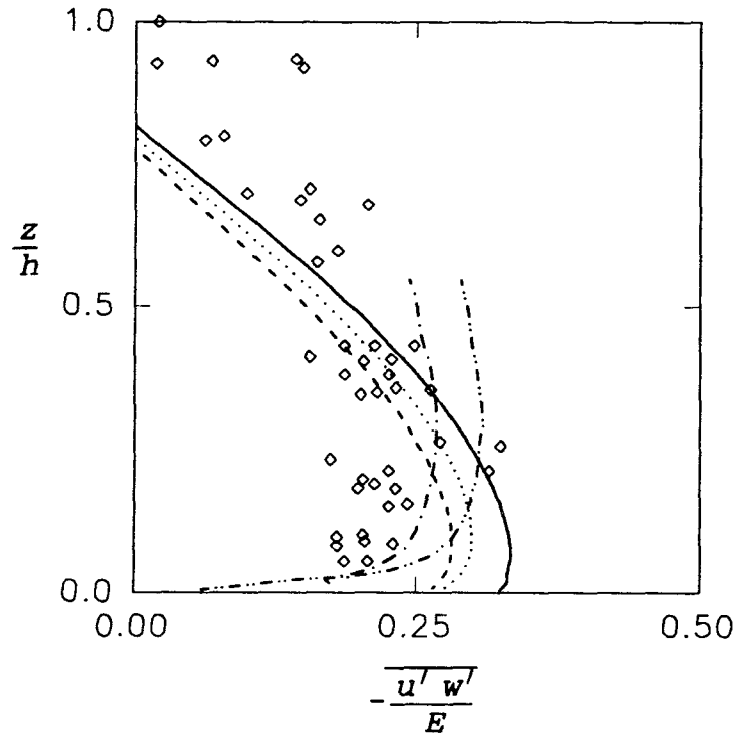
(a)ratio of the shear stress kinetic energy
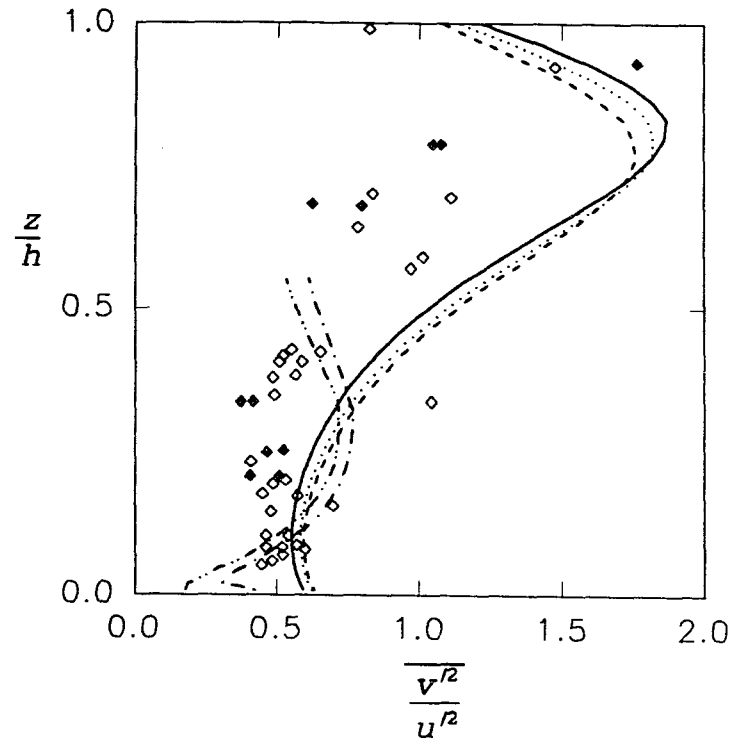
(b)ratio of the lateral and longitudinal velocity variances

Fig.3.12. Wall proximity effects on turbulence structure in the neutral ABL. Solid lines are no wall effect, dashed lines are c_ϵ = 0.13, dotted lines are c_ϵ = 0.26. Symbols and the other lines as in Figure 3.11. Fig. continued.
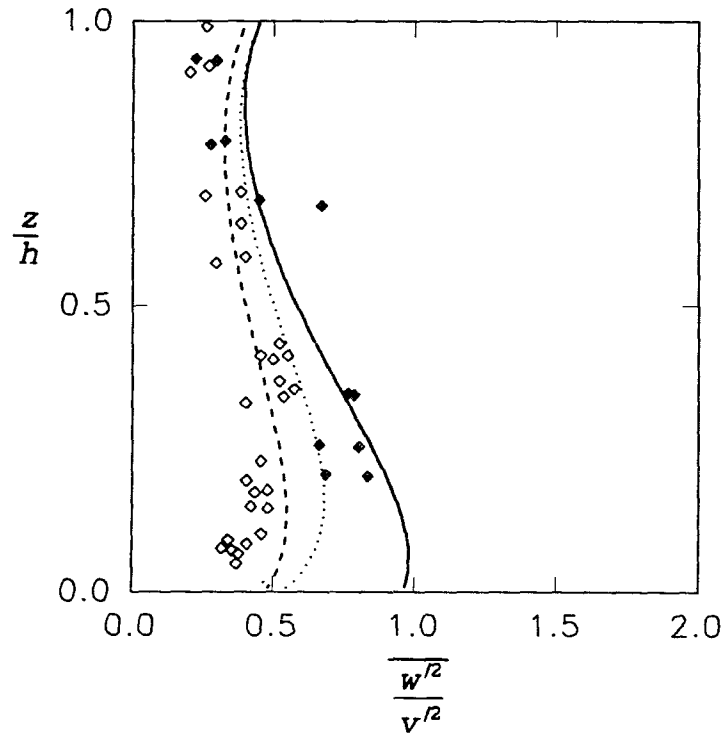
(c)ratio of the vertical and lateral velocity variances
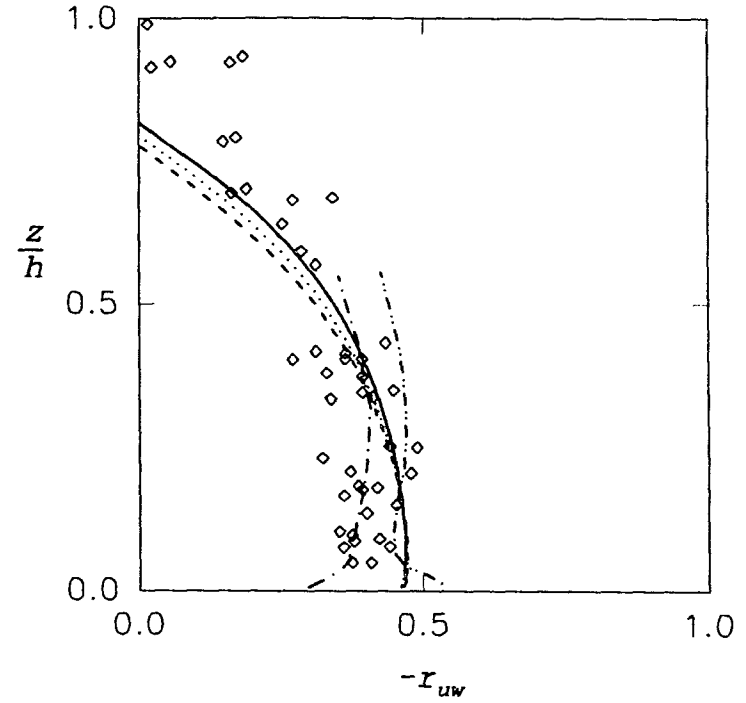
(d)stress correlation coefficient

by decreasing the surface temperature at a rate of 1 K/hr.
After 15 hr of simulated time, the results reached a quasi-
steady state. The conditions for the geostrophic winds and
roughness length were the same as the neutral case. The
height of model was 500m.

The calculated parameters in the stable ABL are in Table
3.3. Wyngaard (1975) integrated a full Reynolds Stress Model
and found that the boundary layer height (h), the height at
which the stress is 5% of its surface value, obeyed
Zilitinkevich's similarity relation (1967).

$$h = d \left(\frac{u_* L}{f}\right)^{\frac{1}{2}} \tag{3.19}$$

Later Brost and Wyngaard (1978, 1979) used a higher order
closure model and showed that the value of d varied from
0.37 to 0.51 for cooling rates from 0.2 to 6 K/hr.

Table 3.3.   Calculated surface layer parameters with
modified E-ϵ model in the stable ABL.

ϵ-equation	u_* (ms^{-1})	$-Q_s$ (Kms^{-1})	h (m)	d (m)	L (m)	α (deg)
standard	0.237	0.028	137.7	0.48	35.4	37.5
Duynkerke	0.215	0.025	105.8	0.42	29.9	40.6
Detering & Etling	0.295	0.060	227.3	0.74	32.2	33.21

The modified model with Duynkerke and standard ϵ-
equations in Table 3.3 shows similar ranges of the selected
parameters. The Detering and Etling equation shows a deeper

boundary layer and a high surface heat flux. There were numerical difficulties in model calculations with Detering and Etling equation, therefore, the constant value of c_m = 0.026 was used.

The normalized profiles for the stable ABL were compared with measurements from Caughey et al. (1979) and Nieuwstadt (1984) and the calculation from Brost and Wyngaard (1978) and Duynkerke (1988) in Figure 3.13. The eddy viscosity profiles of the modified model with the standard and Duynkerke equations show similar patterns to those of the higher order calculation by Brost and Wyngaard (1978). Duynkerke's calculation (1988) with constant c_m = 0.033 (double dot-dashed line in Figure 13(a)) and standard model with c_m = 0.09 (long dashed line in Figure 13(a)) show high eddy viscosity at the maximum value. Modified model with Duynkerke ϵ-equation (dashed line in Figure 3.13(a)) is much closer to that calculated by higher order closure model of Brost and Wyngaard (1978, dot-dashed line in Figure 3.13(a)). The heat flux (Figure 3.13 (b)), momentum flux (Figure 3.13(c)) and wind spiral (Figure 3.13(d)) show typical patterns compared with the calculations from Wyngaard (1975), Brost and Wyngaard (1978) and Duynkerke (1988). The longitudinal and vertical velocity variances for the standard and Duynkerke constants are shown in Figure 3.13 (e) and (f). Good agreement with the measurements was observed. The results are also similar to those calculated

$$\frac{K_m^z}{\kappa \, u_* \, h}$$
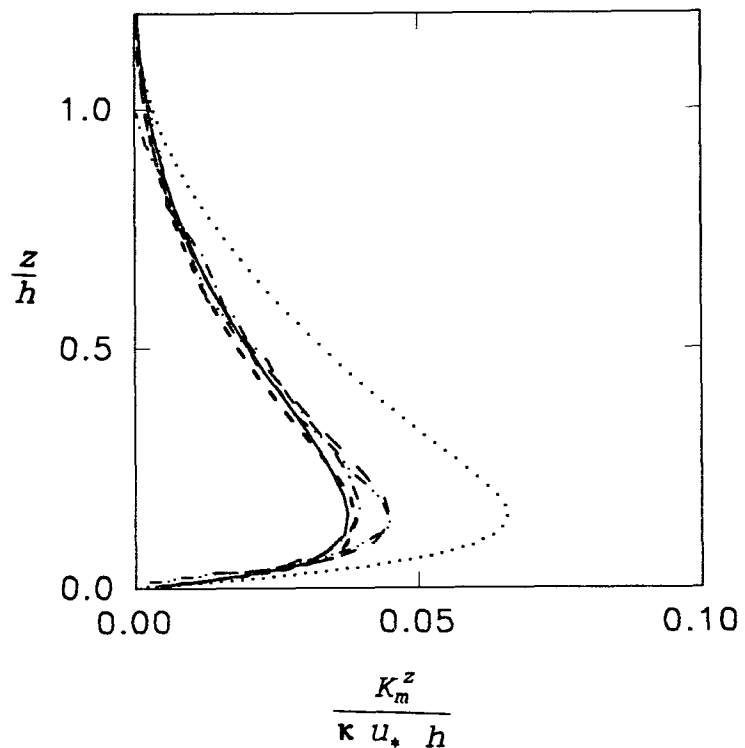
(a)eddy viscosities. Dot-dashed line
the calculated by Brost and Wyngaard
(1978), double dot-dashed line by
Duynkerke (1988), and long dashed
line standard model ($c_m = 0.09$)

$$\frac{\overline{w' \, \theta'}}{\overline{(w' \, \theta')}_s}$$
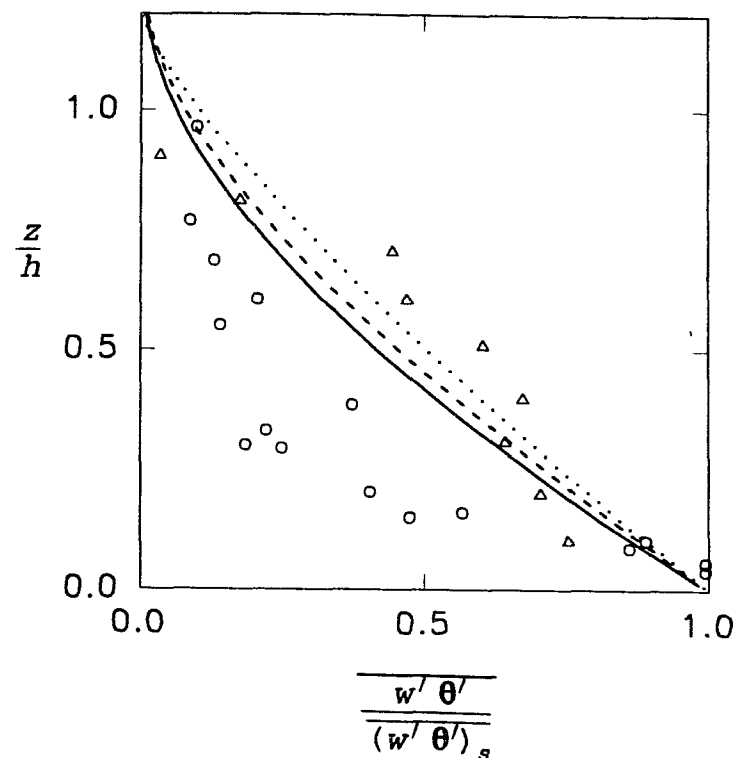
(b)heat flux

Fig.3.13. Normalized profiles for the stable ABL. Solid lines are
the standard ϵ-equation, dashed lines are Duynkerke ϵ-equation and
dotted lines are Detering and Etling ϵ- equation. Circles are data
from Caughey et al. (1979) and triangles from Nieuwstadt (1984).
Fig. continued.
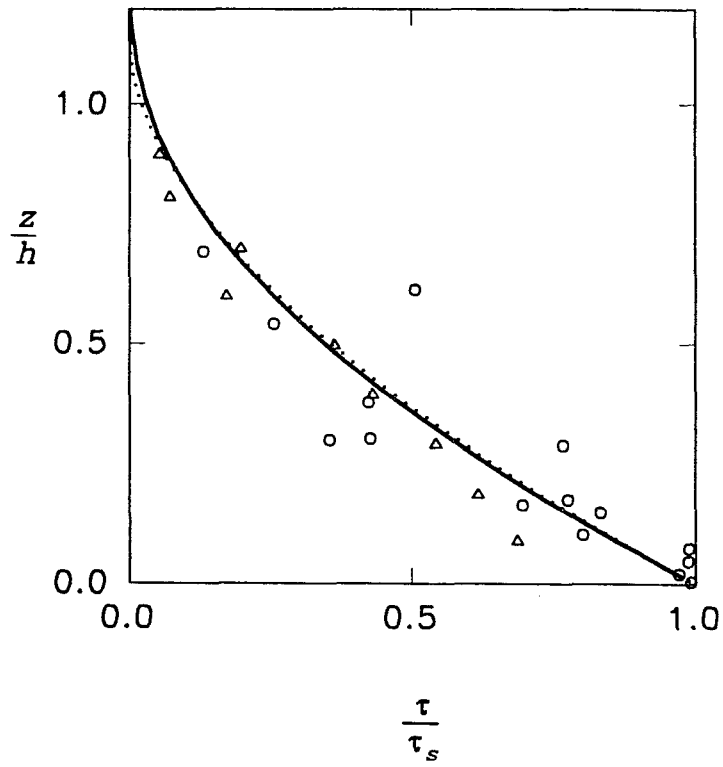
(c) momentum flux
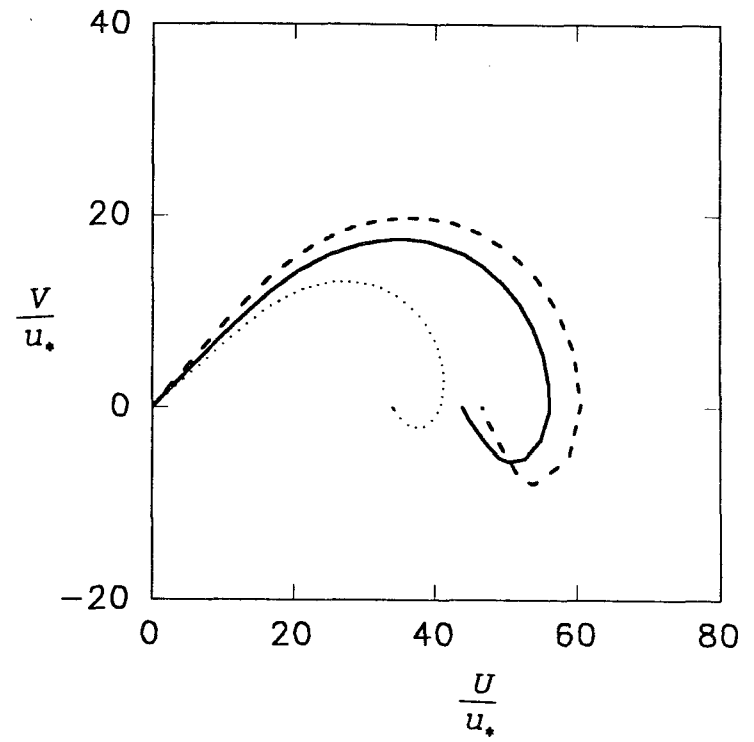
(d) wind spiral

Fig. Continued
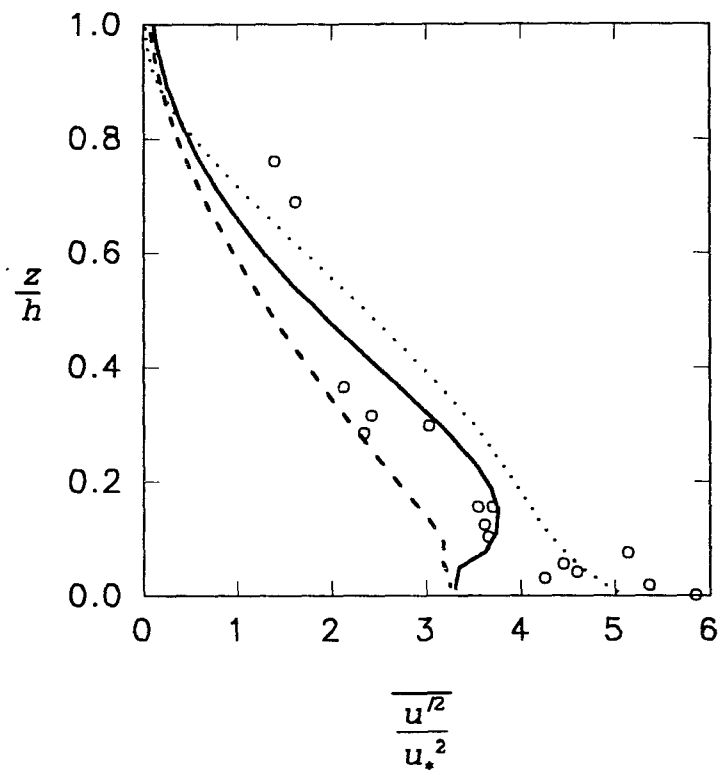
(e)longitudinal velocity variance
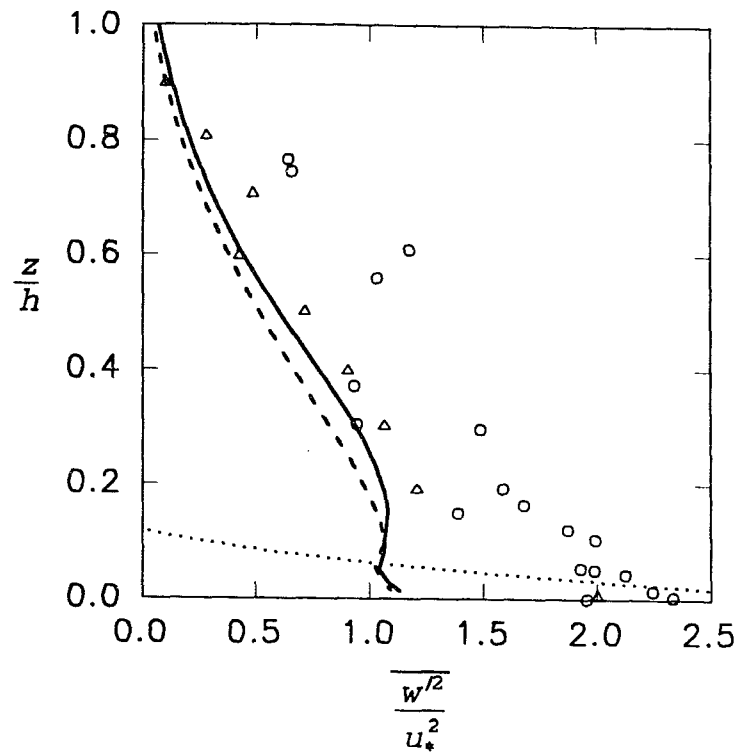
(f)vertical velocity variance
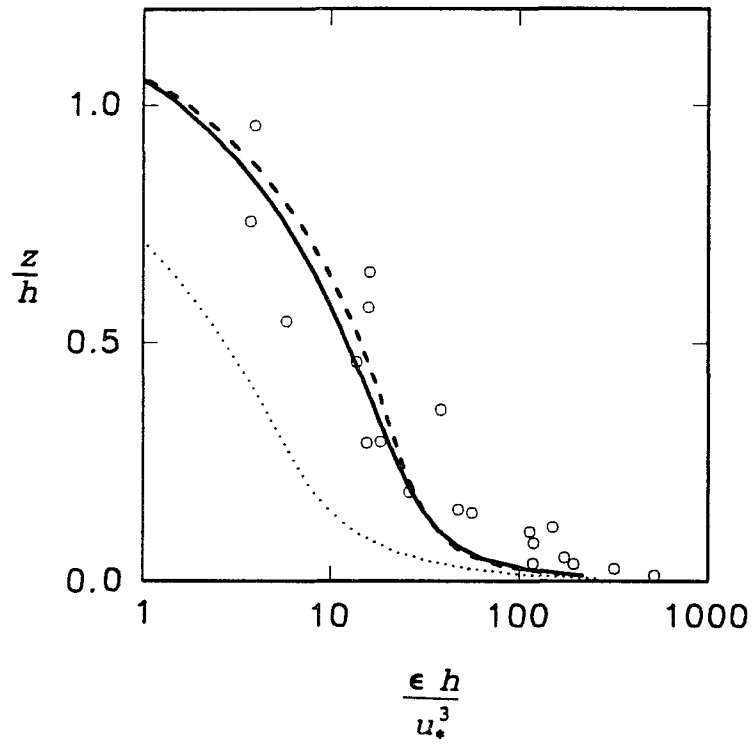
Fig. Continued

(g)dissipation rate
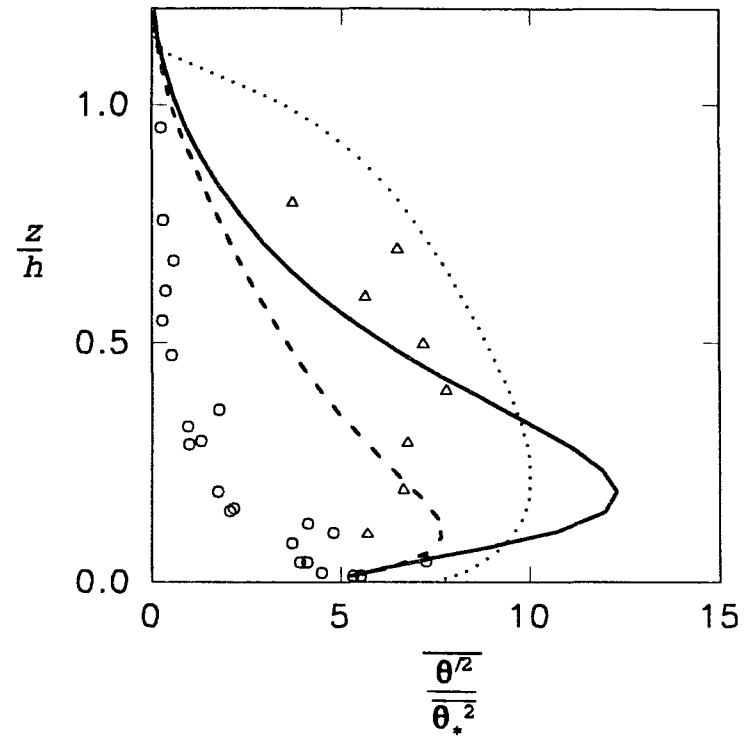
(h)temperature variance

Fig. Continued
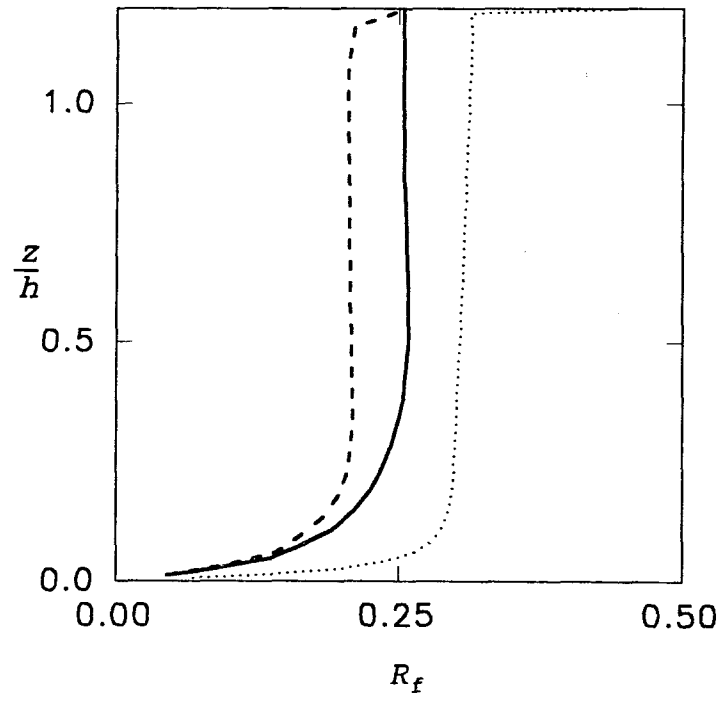
(i) Richardson flux number

by the length scale formulation(Andrén, 1991; not shown in Figure 3.13). The modified E-ϵ model with the Detering and Etling ϵ-equation again shows unrealistic profiles, especially in the vertical velocity variance. The dissipation rate (Figure 3.13(g)) calculated with standard and Duynkerke ϵ-equation show good agreement with the data. But the temperature variances in Figure 3.13(h) are largely scattered in both data and the calculated values. As pointed out by Andrén (1991), this is due to the assumption of the constant ratio between the dissipation time scales in the temperature variance and the turbulent kinetic energy. Figure 3.13(i) shows the flux Richardson number variation with height. The calculated flux Richardson numbers outside of the surface layer can be defined by ratios of the constants in the ϵ-equation.

Figure 3.14 shows the calculated results of the turbulent kinetic energy budgets. The buoyancy term is relatively small compared with the mean production and dissipation terms but is larger than the transport term with the standard and Duynkerke ϵ-equations. The transport term exerts little influence in the kinetic energy budget. This means that there is an equilibrium between the production of the turbulent kinetic energy by mean production and buoyancy and the dissipation. The additional diffusion terms in Equations (A-22) and (A-23) have no effect on the vertical velocity and temperature variances because they
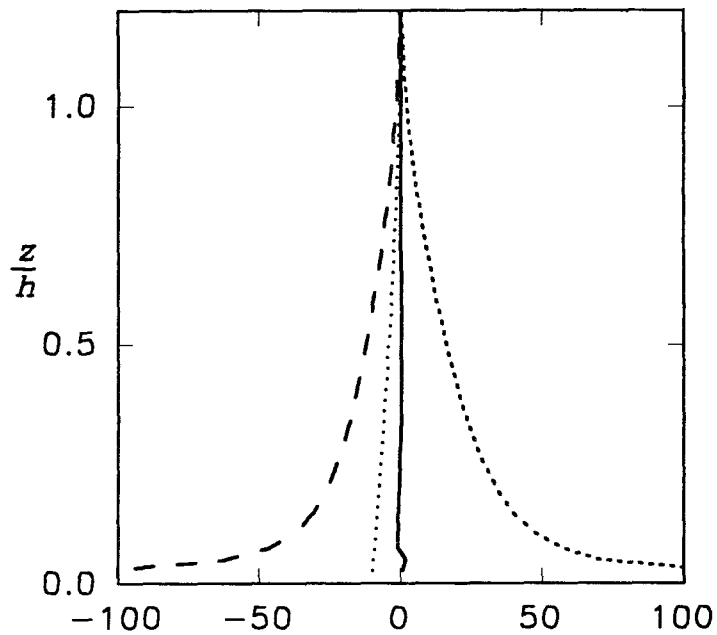
E-BUDGET(normalized by $\frac{u_*^3}{h}$)

(a)standard ϵ-equation
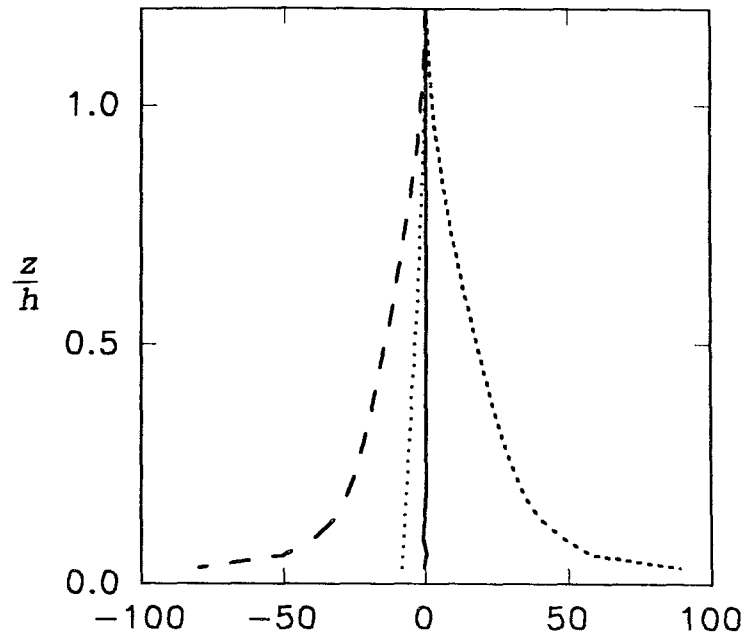
E-BUDGET(normalized by $\frac{u_*^3}{h}$)

(b)Duynkerke ϵ-equation

Fig.3.14. Kinetic energy budgets in the stable ABL. Solid lines are for transport term, long dashed lines for dissipation rate, short dashed lines for mean production and dotted lines for buoyancy. Fig. continued.

$$\frac{z}{h}$$
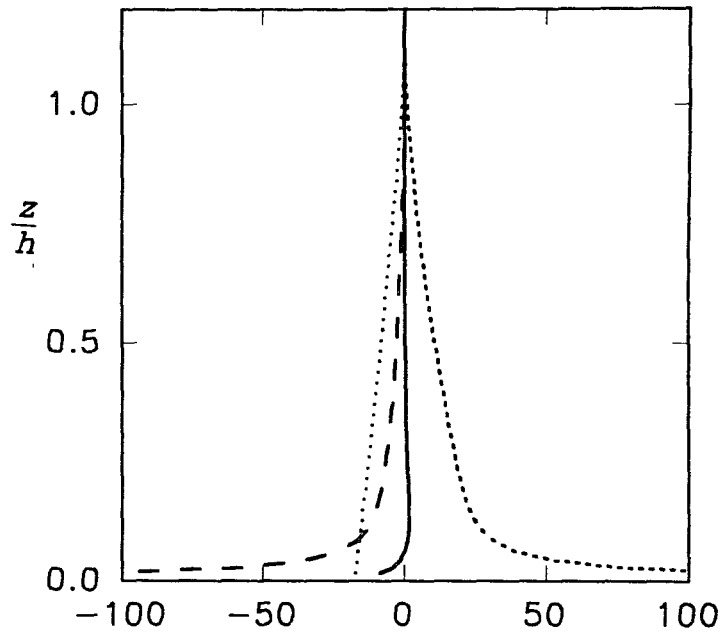
E-BUDGET(normalized by $\dfrac{u_*^3}{h}$)

(c)Detering and Etling ϵ-equation

approach zero. This supports our discussion in Chapter 2 in which the additional diffusion terms were neglected. The kinetic energy budget profiles with the standard and Duynkerke ϵ-equations are included in Figure 3.14 and show good agreement with the calculated results in the nocturnal rural boundary layer (Uno et al., 1989). The model with Detering and Etling ϵ-equation shows a different profile. The buoyancy by Detering and Etling's ϵ-equation is larger than the dissipation term because the high surface heat flux shown in Table 3.3.

3.6. Convective ABL

According to the studies of Deardorff (1973, 1974a, b) and Caughey (1982), the vertical profiles of heat flux and velocity variances normalized by the convective velocity scale (w_*) and temperature variance normalized by the convective temperature scale (T_*) are independent of initial conditions at quasi-steady state. The scale parameters for the convective ABL are;

$$w_* = (\frac{z_i \, g \, \overline{(w' \, \theta')}_s}{\Theta})^{\frac{1}{3}}$$
(3.20)

$$T_* = \frac{\overline{(w' \, \theta')}_s}{w_*}$$
(3.21)

where z_i is the height of inversion layer which is taken as the level of the maximum negative heat flux (Willis and Deardorff, 1974).

In order to run the convective case, the initial
conditions were set as $U = U_g = 5$ m/s and $V = V_g = 0$. The
potential temperature was set as a constant up to 100m and
then an overlying stable layer was imposed by a potential
temperature gradient of 0.005 K/m to the model top. The
height of the model was 2500m and roughness parameter was
0.05. After running 15 hr without a heat flux at the
surface, the potential temperature at the surface was
sinusoidally increased by 14 K during 7 hr and then the data
were analyzed. The period in the sine curve was 24 hr and
the surface temperature reached maximum after 6 hr
calculation.

Table 3.4. Calculated surface layer parameters with
modified E-ϵ model in the convective ABL.

ϵ-equation	u_* (ms^{-1})	w_* (ms^{-1})	T_* (K)	z_i (m)	L (m)	α (deg)
standard	0.388	2.69	0.189	1132	-8.6	15.3
Duynkerke	0.390	2.68	0.195	1107	-8.5	15.6
Detering & Etling	0.391	2.67	0.177	1210	-9.4	17.9

The surface layer parameters and height of the inversion
layer are shown in Table 3.4. The parameters with the
standard and Duynkerke ϵ-equations display similar values
but the inversion height and the cross isobaric angle of
Detering and Etling ϵ-equation again differ and show higher
values.

Normalized profiles for the convective ABL are shown in Figure 3.15. Eddy viscosities with standard and Duynkerke ϵ-equation show high values comparing to Detering and Etling ϵ-equation. The maximum value of the eddy viscosity with standard ϵ-equation is about 0.11 $w_* z_i$ in the middle of the boundary layer. The maximum eddy viscosity of Yamada and Mellor (1975) was about $0.02 w_* z_i$ and that of Wyngaard (1983) was $0.05 w_* z_i$ in the mid-boundary layer. The eddy viscosity of the large eddy simulation by Moeng and Wyngaard (1989) however was $1.0 w_* z_i$. As they pointed out, the eddy viscosity from the large eddy simulation seems to be very large. Comparisons of the turbulent kinetic energy with the large eddy simulation (Moeng and Wyngaard, 1989) and Yamada and Mellor (1975) are shown in Figure 3.15(b).

The kinetic energy profiles with the standard and Duynkerke ϵ-equations show relatively large values and they are close to the profile of the large eddy simulation. The potential temperature and mean velocities in the longitudinal and lateral directions show typical convective boundary layer profiles. The dissipation rates in Figure 3.15(f) show good agreement with measurements in the lower boundary layer but there are discrepancies near the inversion layer. The vertical and horizontal velocity variances with the standard and Duynkerke ϵ-equations in Figure 3.15 (g) and (h) also show good agreement with data except near the inversion layer. The discrepancies near the
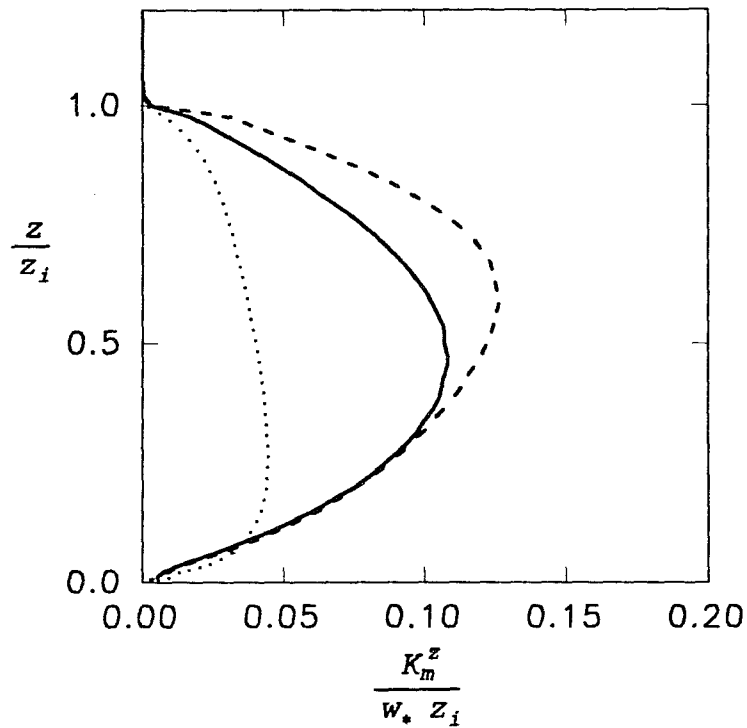
(a)eddy viscosity
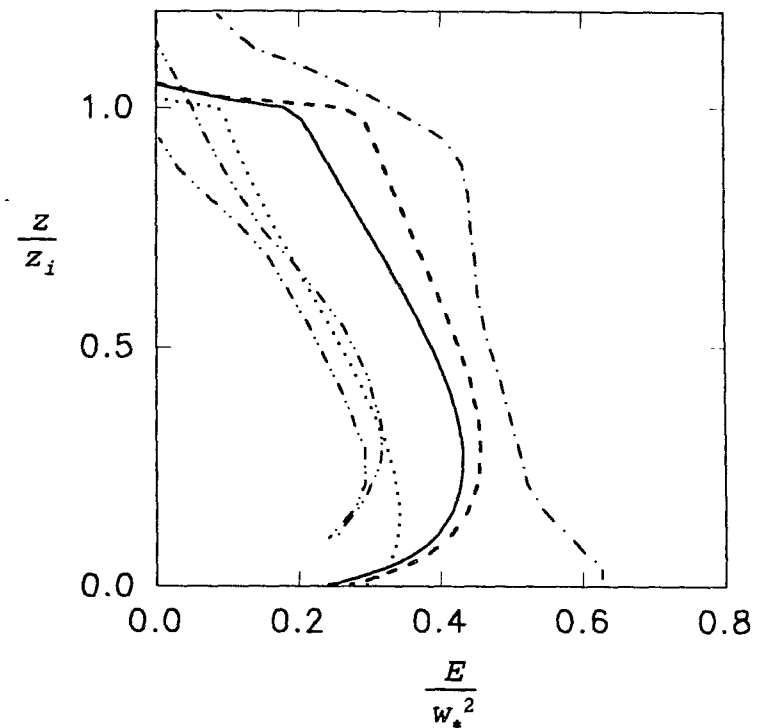
(b)turbulent kinetic energy. Dot-dashed line the calculated values by Moeng and Wyngaard(1989) and double dot-dashed line by Yamada and Mellor(1975).

Fig.3.15. Normalized profiles in the convective ABL. Solid lines are the standard ϵ-equation, dashed lines Duynkerke ϵ-equation, dotted line Detering and Etling ϵ-equation. Circles are data from Caughey and Palmer (1979) and triangles from Minnesota and Ashchurch data. Fig. continued.
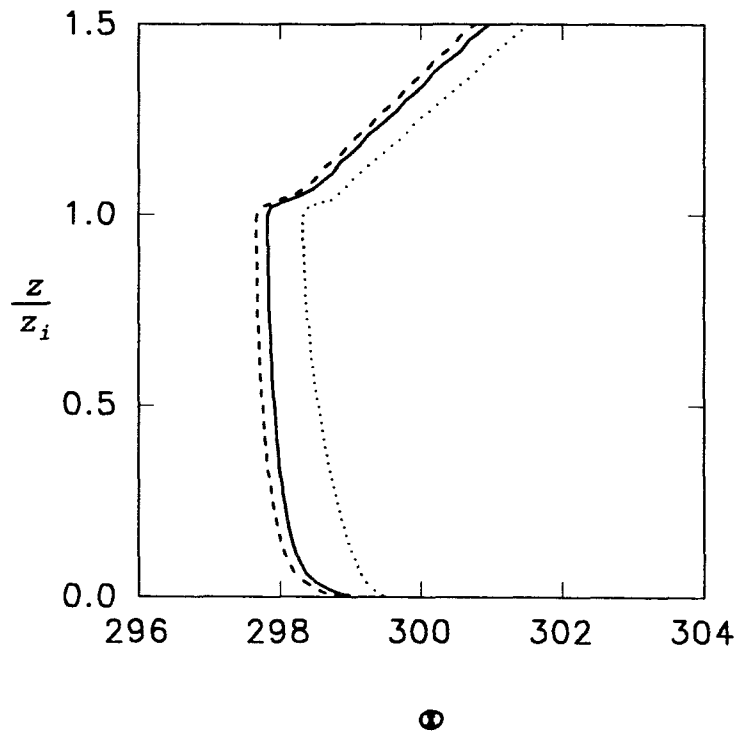
(c)temperature
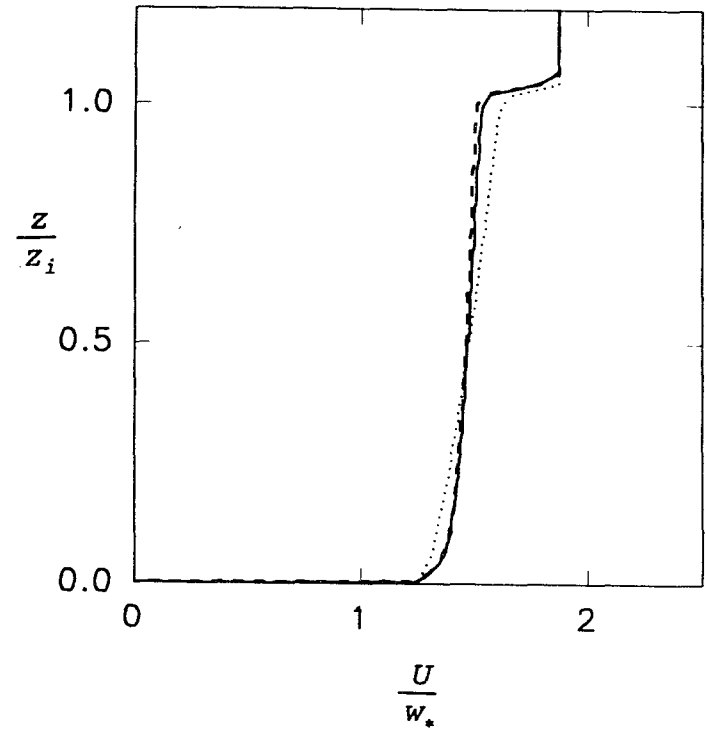
(d)mean velocity in the
longitudinal direction

Fig. Continued
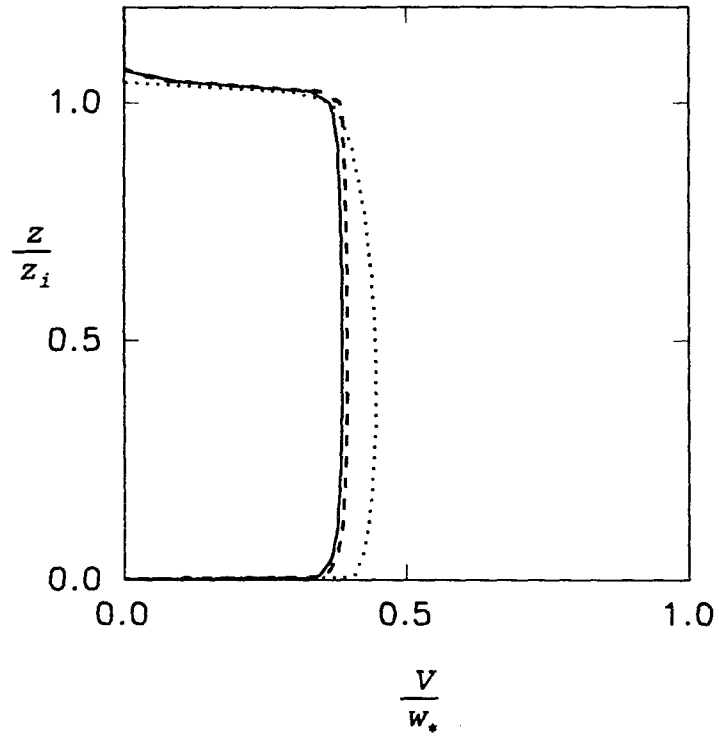
(e)mean velocity in the lateral direction
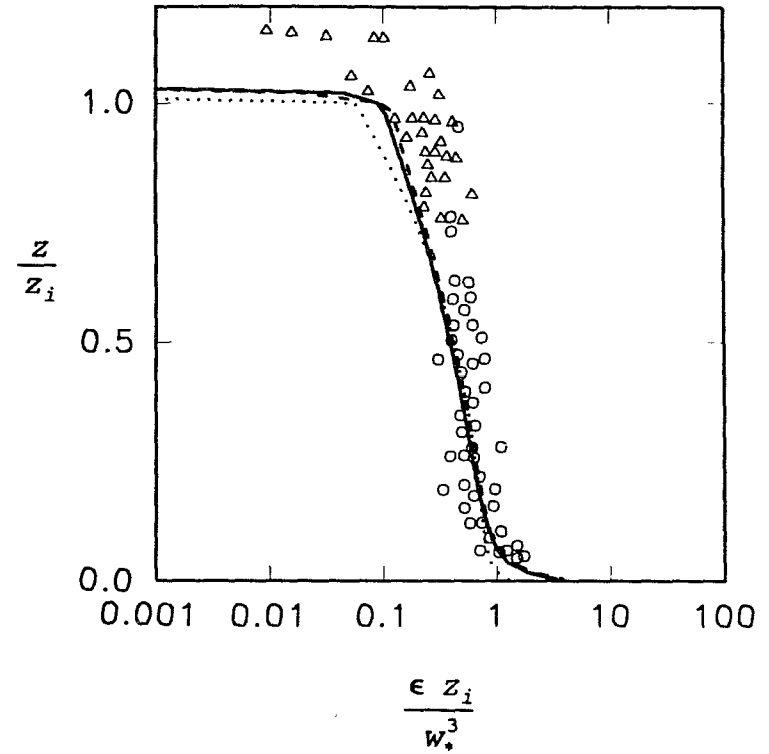
(f)dissipation rate

Fig.   Continued
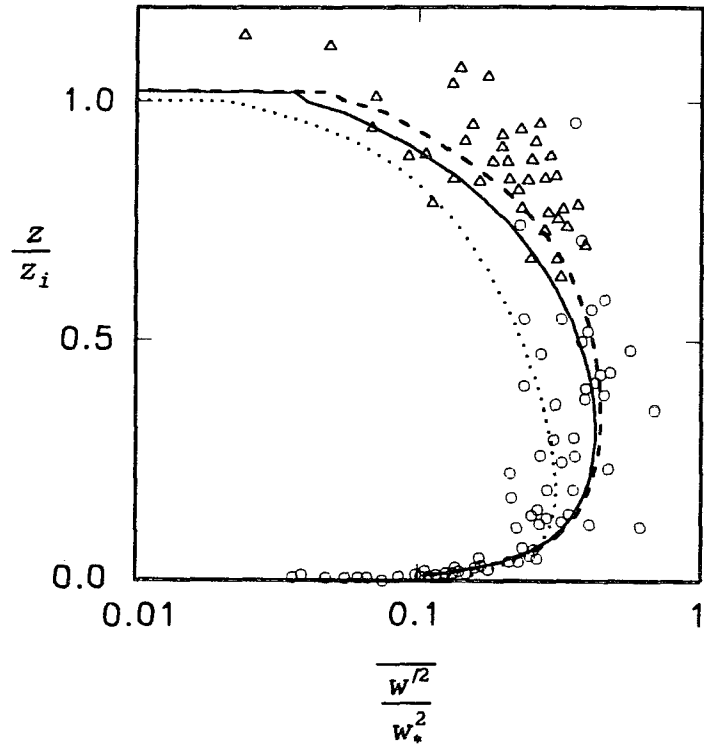
(g) vertical velocity variance
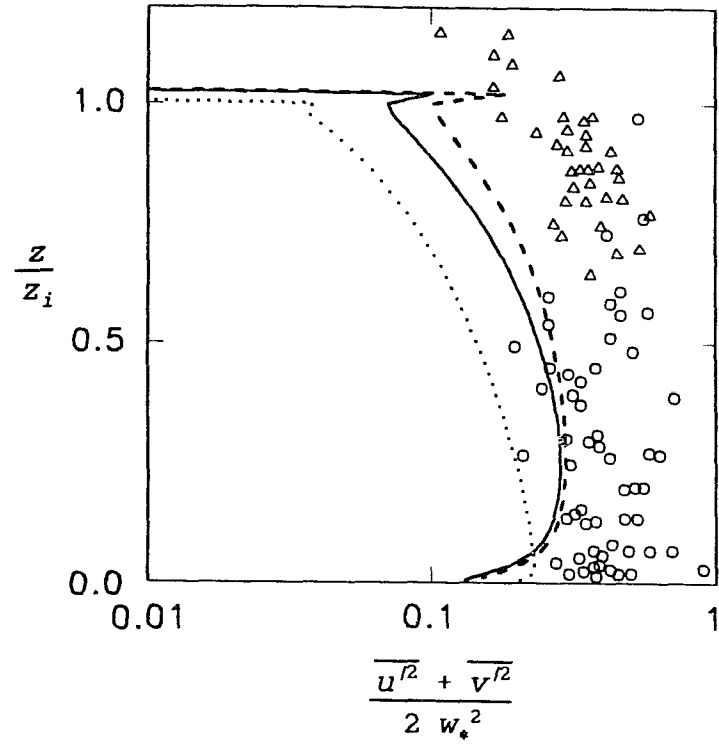
(h) horizontal velocity variance

Fig. Continued
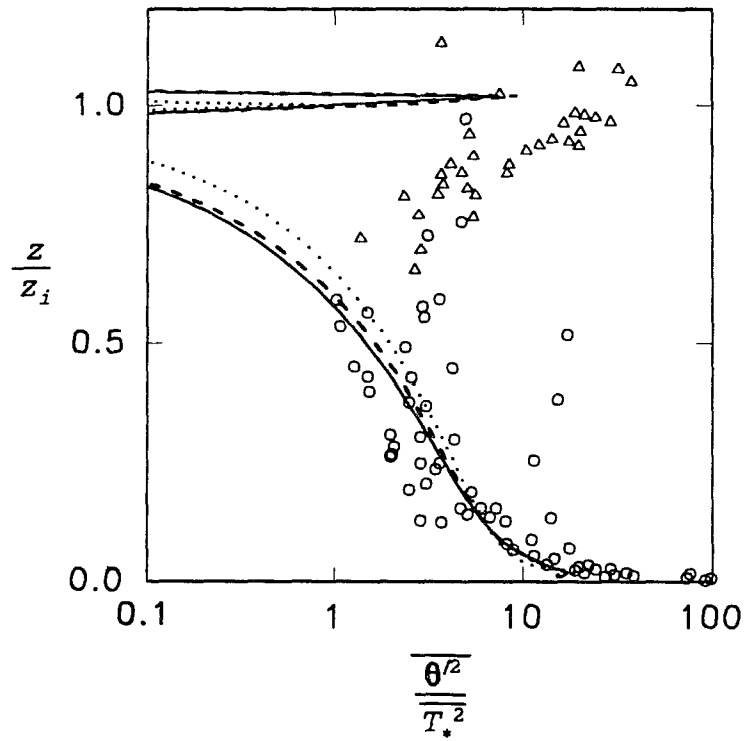
(i)temperature variance
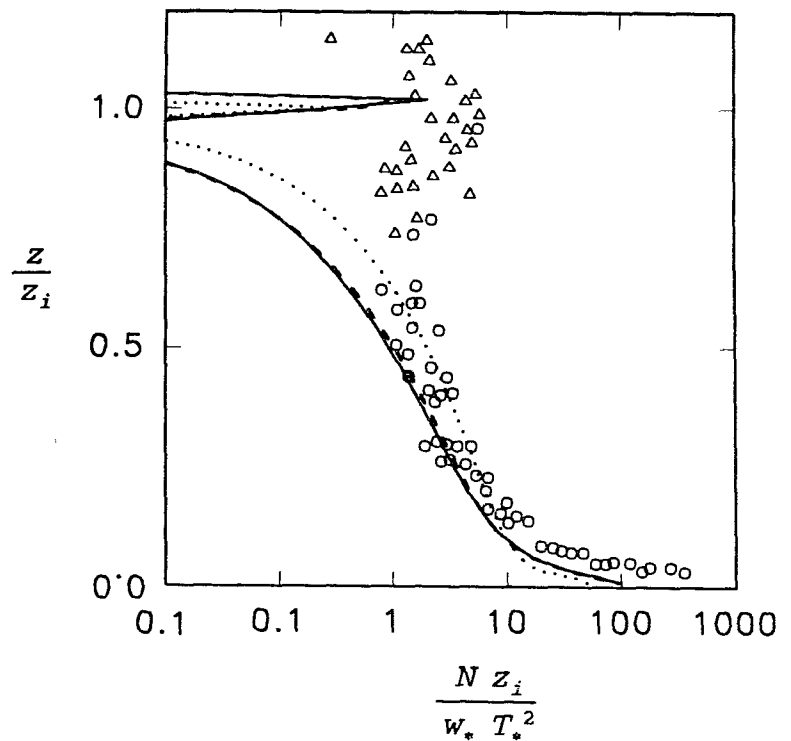
(j)dissipation of the half
temperature variance

inversion layer especially above the zone of 0.6 z/z_i are significant in the profiles of potential temperature variance and dissipation rate of the half temperature variance in Figure 3.15 (i) and (j).

These discrepancies in the turbulent statistics are due to the diffusion effects in the turbulent fluxes and Reynolds stresses which are neglected during the simplification to the modified model. Moeng and Wyngaard (1989) analyzed the effect of the gradient diffusion parameterization on the turbulent transport using the large eddy simulation. They suggested several methods for diffusion parameterizations. In order to simulate the convective ABL more accurately, higher order closure models such as a level 3 and 4 model in Mellor and Yamada's terminology (1982) have to be considered with well defined diffusion parameterizations. That means the simplicity of the modified model would have to be sacrificed. The turbulent kinetic energy budgets are shown in Figure 3.16. The dissipation balances with buoyancy production. The transport terms show the negative values in a large portion of the boundary layer. The profiles of kinetic energy equation terms show good agreement with the calculated results from higher level closure models (Yamada and Mellor, 1975; Sun and Ogura, 1980) and the large eddy simulation (Moeng and Wyngaard, 1989) except the buoyancy terms. The negative heat fluxes near the inversion layer are 2-3% of
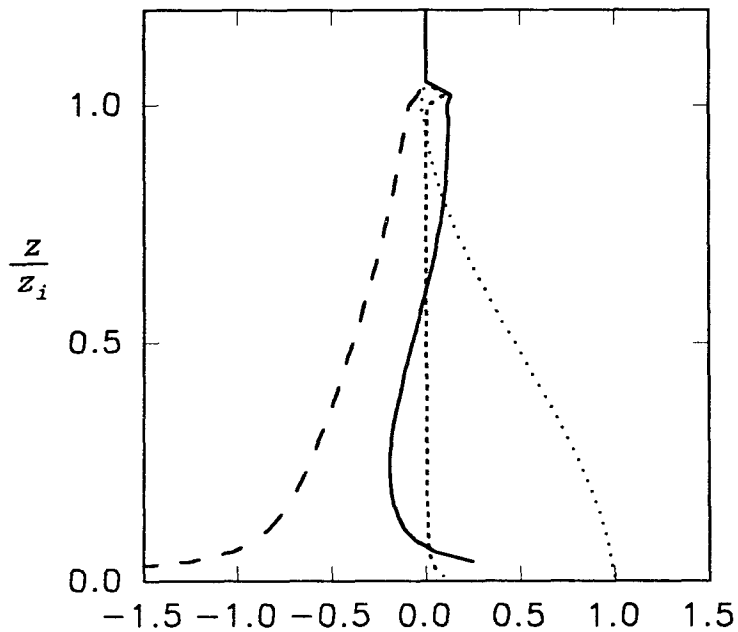
E-BUDGET(normalized by $\dfrac{w_*^3}{z_i}$)

(a)standard ϵ-equation
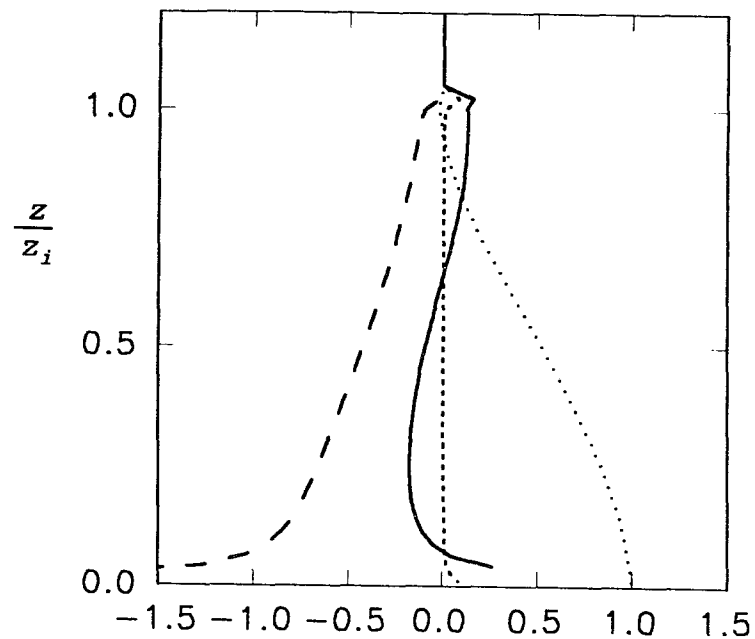
E-BUDGET(normalized by $\dfrac{w_*^3}{z_i}$)

(b)Duynkerke ϵ-equation

Fig.3.16. Kinetic energy budgets in the convective ABL. Solid lines are for transport term, long dashed lines for dissipation rate, short dashed lines for mean production and dotted lines for buoyancy. Fig. continued.
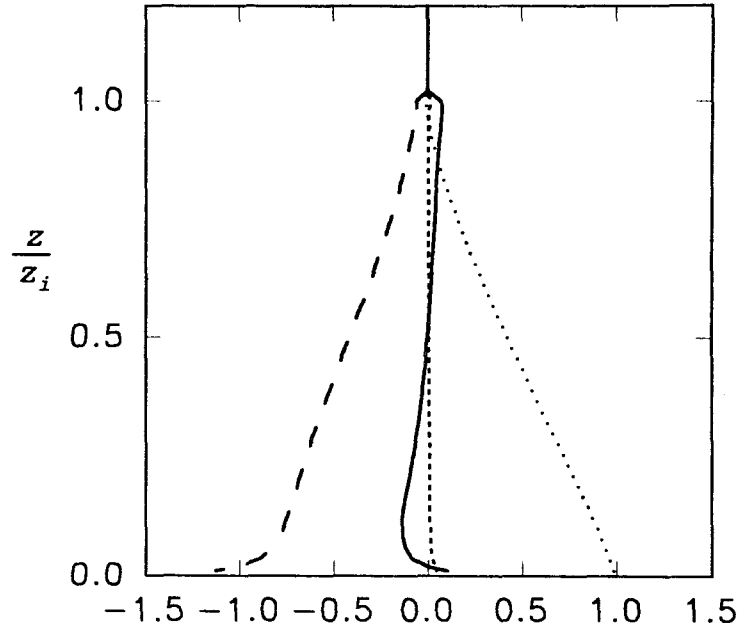
E-BUDGET(normalized by $\dfrac{w_*^3}{z_i}$)

(c)Detering and Etling ϵ-equation

the surface heat flux. The buoyancy profiles with standard and Duynkerke ϵ-equations show an inflection near the surface but that of Detering and Etling ϵ-equation shows straight line. The curvature of the buoyancy line might be related to the mismatch of the surface layer similarity with the ϵ-equation and/or with the effect of the counter-gradient heat flux (Rodi,1985).

3.7. Conclusions

The modified E-ϵ turbulence model was tested in the neutral, stable and convective ABLs. The additional diffusion terms suggested by Rodi (1985) to compensate for the diffusion effects in the vertical velocity and potential temperature variances have no effect in the neutral and stable ABL because the production and the dissipation of the turbulent kinetic energy are approximately balanced. In the convective ABL, the additional diffusion term results in unrealistic predictions. Therefore, Rodi's modification were not incorporated in the final algebraic stress model used herein.

The resulting modified E-ϵ turbulence model was compared with the available data in the neutral, stable and convective ABL. The modified model can largely reproduce the structural characteristics observed in data and in higher order models. There are some discrepancies in the turbulent statistics near the inversion layer under convective condition. These are partially due to the strong

counter gradient transports in the real atmospheric flows which were neglected in the modified model. To more accurately represent the diffusion transport in the strongly convective ABL, a high level model needs to be solved. Such approach would result in a much more complex model and would be impractical to simulate the applications such as a pollutant transport in a land-sea breeze and a thermal fence.

The standard and Duynkerke ϵ-equation approaches show a better prediction of observations than Detering and Etling ϵ-equation approach. The differences between the standard and Duynkerke ϵ-equation approaches are within the ranges of the scattered data. The standard ϵ-equation was selected for the final model.

Chapter 4. Sea Breeze Circulation

4.1. Introduction

A sea breeze circulation develops in coastal areas due to the diurnal surface temperature difference between the sea and the land. In the daytime, the land surface temperature rises as a result of solar radiation whereas the sea surface temperature essentially remains constant. This causes a buoyancy induced flow from the sea to the land. At night, the land cools more rapidly than the sea. The reverse land breeze is developed (Atkinson, 1981; Pielke, 1984). These flows are examples of gravity currents driven by the density difference (Simpson, 1987). Figure 4.1 shows a schematic of sea/land breeze development with local standard time (LST). In midmorning, a convectively unstable boundary layer, i.e., mixed layer, is formed over the land. In late afternoon, offshore winds transport cooler marine air over the land and the sea breeze is fully developed. As the land surface temperature decreases by longwave radiational cooling, the air near the ground becomes denser and tends to sink at early evening. Intensity of the sea breeze becomes weaker and the sea breeze disappears in late evening. In early morning, the situation reverses and the offshore directed land breeze is developed. Depth and intensity of the land breeze are shallower and weaker than those of the sea
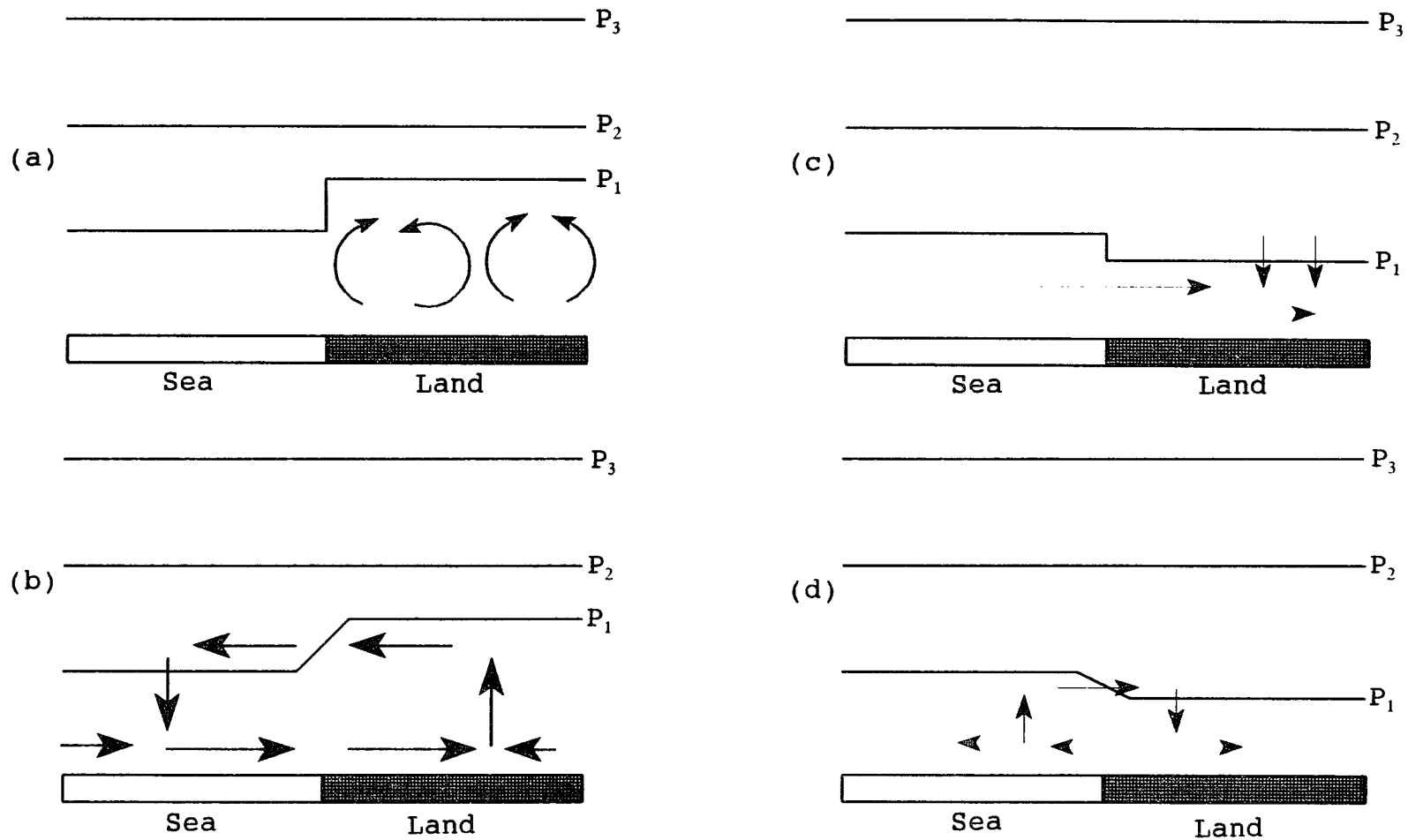
Fig.4.1. Schematic of the diurnal evolution of the sea/land breeze in the absence of geostrophic winds (Pielke, 1984). (a)midmorning (11 LST) (b)late afternoon (16 LST) (c)late evening (22 LST) (d)early morning(4 LST)

breeze because vertical turbulent mixing is weaker due to stable stratification at night.

In order to adequately assess the atmospheric pollution resulting from sea breeze circulation, the transport and dispersion of contaminants in this complex flow are essential. Conventional atmospheric dispersion and air quality models assume that the wind field is a known quantity. This approach is often unsatisfactory in a coastal complex sea breeze flow because the traditionally sparse wind monitoring network typically exists only over land, essentially limiting the known wind field to half of the domain of interest. In addition, the sea breeze is exceedingly complex with a sharply defined internal boundary layer that varies significantly with both time and position. To overcome the difficulty of the poor resolution of the recorded winds, it becomes necessary to mathematically predict the flow field in addition to the contaminant transport and dispersion in the sea breeze circulation (Novitsky et al., 1991).

There are several meteorological factors affecting the sea/land breeze phenomena such as an ambient background stratification, onshore / offshore geostrophic winds, and temperature difference between the land and the sea (Physick, 1980; Bechtold et al., 1991; Arritt, 1991,1993).

Stable stratification suppresses the development and movement of the sea breeze. The vertical velocity at the

leading edge of the sea breeze deceases remarkably with greater ambient stratification. The horizontal velocity also decreases with increasing stratification, but not as markedly as does the vertical velocity. Stronger stratification generally leads to a weaker sea breeze.

Estoque (1961) found that an ambient wind directed offshore intensified the sea-breeze whereas an onshore ambient wind weakened the circulation. Arritt(1993) performed 31 simulations with geostrophic winds ranging from onshore flow of 15 m/s to offshore flow of 15 m/s with 1 m/s interval. His results indicated that a distinguishable density driven sea breeze was suppressed for onshore flow of a few meters per seconds or more. In contrast, an easily distinguishable density driven sea breeze is produced for an opposing flow as strong as 11 m/s. The offshore flow is generally a favorite condition for a sea breeze circulation except extremely strong offshore flow which completely suppresses the sea breeze.

Physick(1980) showed a significant slowing of the sea breeze advance around midday for the case of lower land heating rate which means lower surface temperature difference between the land and the sea. The low surface temperature difference leads to weaker sea breeze circulation in the early stage.

An interesting aspect of the sea breeze is that there exist different mechanisms for the development of the sea

breeze during a day. At midday, the turbulent mixing above the land due to strong thermal heating is dominant. The sea breeze circulation is limited to near the coastal region and the front velocity is much slower due to mixing induced weakening of the density gradient between sea and land air. In late afternoon, the surface heating induced turbulent mixing over the land weakens. The sea breeze starts to penetrate into the land with a high and nearly constant front speed. In late evening, observation of the inland penetration of the sea breeze front has shown that it can be interpreted as a density current (Garratt and Physick, 1985). The sea breeze may be detached from the rest of the flow and form a cutoff vortex under the nocturnal inversion around midnight (Simpson et al., 1977; Physick, 1980; Sha et al., 1993).

There are several approaches to deal with these different phenomena based on a frontogenesis analysis of the gravity currents. The detailed budget equation for the frontogenesis will be discussed in Section 4.3.2. Reible et al.(1993) proposed a frontogenesis dimensionless number which represents the ratio of the time scale of the turbulent mixing and the front development. Their results showed that the generation of sharp front from general sea breeze circulation results from the competition of two opposing forces. Frontogenesis is produced by convergence in the horizontal wind field and this convergence may be produced

either by density driven flow, or by synoptic winds or a combination of the two. Opposing this tendency toward frontal development is turbulent mixing, associated with the convectively driven turbulence over the land. Arritt(1991, 1993) also showed from numerical simulation that horizontal convergence is an important factor in frontogenesis. Kraus et al.(1990) analyzed the detailed budgets in the frontogenesis forcing terms in the equation of the frontogenesis with high quality field data of the sea breeze in South Australia. From their studies on the frontogenesis, we can expect that the different mechanisms in a day may be analyzed on the basis of the balance between the horizontal convergence and the turbulent mixing. High-resolution numerical simulation has the potential to examine the mechanism of sea breeze frontogenesis in detail (Reible et al., 1993).

The sea breeze plays an important role in the transport of air pollutants emitted from industrial sites or mineral resource development in a coastal area. The circulation of the sea breeze and interaction between the surface flow and the return flow aloft can potentially limit the net ventilation of an air basin by recycling pollutants (Ozoe et al, 1983; Pielke et al., 1983; Kitada and Kitagawa, 1990; Novitsky et al, 1991; Schlünzen and Pahl, 1992). This often can result in the high concentration of pollutants near the coastal area. Shair et al. (1982) and McRae (1981)

investigated the transport and dispersion of plumes released into the land breeze circulation system. In their experiments, the elevated plumes were released above the base of the night time inversion from a coastal power plant stack. The plumes were transported out over the ocean, fumigated and downmixed to the sea surface by the convective layer which was formed above the sea during the land breeze. All of the tracer was essentially observed to return to the shore during the subsequent afternoon sea breeze. Reible et al. (1983) studied the interaction of the plume between the surface mixing layer and the residual air aloft. They showed that the characteristic exchange rate between the air aloft and the surface mixing layer is large enough that the residual plume aloft should be considered when describing long range transport or the multi-day impacts of pollutants such as the sea/land breeze.

The fumigation of elevated coastal plumes along a thermal internal boundary layer (TIBL) can also adversely affect air quality in the coastal area. Fumigation is the process of downmixing by the incorporation of pollutants into the convectively mixed layer. Figure 4.2 shows typical TIBL and fumigation at midday under the sea breeze. The TIBL is formed with distance inland from the shore as the stable cold air over the sea or the lake is advected over warmer land. Plumes emitted from an elevated line source near the shore travel inland with little dispersion in the stable
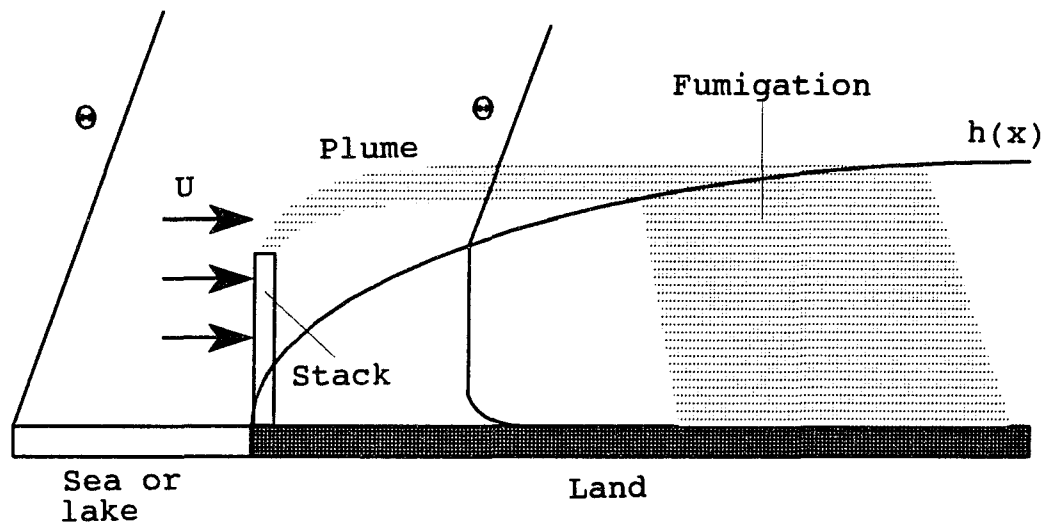
Fig.4.2. Thermal internal boundary layer (TIBL) and fumigation.

flow aloft until they intersect the TIBL where the convective turbulence of the underlying unstable air fumigates the plumes to the ground. It results in high ground level concentrations (Lyons and Cole, 1973; Misra, 1980; Kerman, 1982; Hoff, et al., 1982).

In order to improve the resolution of the prediction and develop a more general model of the sea breeze circulation, the modified E-ε model with a full nonhydrostatic equations was applied to the sea breeze circulation, frontal development of the sea breeze, and TIBL and fumigation in TIBL. Attempts to simulate the pollutant transports and the interaction of the sea breeze with the residual pollutants aloft were included.

4.2. Model Formulation

4.2.1. Governing Equations

Assuming two dimensional incompressible flow with a nonhydrostatic assumption, the governing equations are;

$$\frac{\partial U}{\partial x} + \frac{\partial W}{\partial z} = 0 \tag{4.1}$$

$$\frac{\partial U}{\partial t} + U \frac{\partial U}{\partial x} + W \frac{\partial U}{\partial z} = -\frac{1}{\rho} \frac{\partial P}{\partial x} + \frac{\partial}{\partial x}(K_m^x \frac{\partial U}{\partial x}) + \frac{\partial}{\partial z}(K_m^z \frac{\partial U}{\partial z}) + f(V - V_g) \tag{4.2}$$

$$\frac{\partial V}{\partial t} + U \frac{\partial V}{\partial x} + W \frac{\partial V}{\partial z} = \frac{\partial}{\partial x}(K_m^x \frac{\partial V}{\partial x}) + \frac{\partial}{\partial z}(K_m^z \frac{\partial V}{\partial z}) + f(U_g - U) \tag{4.3}$$

$$\frac{\partial W}{\partial t} + U \frac{\partial W}{\partial x} + W \frac{\partial W}{\partial z} = -\frac{1}{\rho}\frac{\partial P}{\partial z} + \frac{\partial}{\partial x}(K_m^x \frac{\partial W}{\partial x}) + \frac{\partial}{\partial z}(K_m^z \frac{\partial W}{\partial z}) + g \frac{\Theta'}{\Theta_m} \quad (4.4)$$

$$\frac{\partial \Theta}{\partial t} + U \frac{\partial \Theta}{\partial x} + W \frac{\partial \Theta}{\partial z} = \frac{\partial}{\partial x}(K_h^x \frac{\partial \Theta}{\partial x}) + \frac{\partial}{\partial z}(K_h^z \frac{\partial \Theta}{\partial z}) \quad (4.5)$$

$$\frac{\partial C}{\partial t} + U \frac{\partial C}{\partial x} + W \frac{\partial C}{\partial z} = \frac{\partial}{\partial x}(K_h^x \frac{\partial C}{\partial x}) + \frac{\partial}{\partial z}(K_h^z \frac{\partial C}{\partial z}) \quad (4.6)$$

where U, V and W are corresponding mean velocity components in the x, y and z directions, respectively. The x-axis is assumed to be directed perpendicular to the shore in the onshore direction while z is the vertical direction. U_g and V_g are geostrophic wind components in the x and y direction which represent geostrophic pressure gradients in each direction. P is a mesoscale perturbation pressure from the background geostrophic pressure and f is a Coriolis parameter (10^{-4} sec^{-1}). Θ' is a mean temperature deviation from the background initial mean temperature.

Various formulae of the eddy diffusivity for the sea breeze are available from first order turbulence models (Pielke, 1974a, 1974b, 1984; Mahrer and Pielke, 1977; Physick, 1980; Novitsky et al., 1991), conventional E-ϵ model (Kitada 1987; Sha et al., 1991, 1993), Yamada and Mellor's level 2.5 model (Huang and Raman, 1991) to the second order closure (Briere, 1987). The first order closure model lacks universality in the complex flow

situation because this model neglects transport history effects of the turbulence and it is difficult to prescribe the mixing length distribution required to estimate the eddy diffusivity in a situation other than simple shear layer flow. The standard E-ε model cannot describe the anisotropy of transport in a vertically stratified atmosphere. The use of the second order closure is restricted by the high computational cost. The modified E-ε model, which corresponds to the algebraic stress model and at the same time maintains the simplicity of the formulation, is expected to be a feasible solution. Each of these models were described in Chapter 2. To determine the vertical turbulent eddy and thermal diffusivity, the modified E-ε model was used.

The horizontal thermal and eddy diffusivities were estimated via (for example, Pielke, 1974; Mahrer and Pielke, 1977; Physick, 1980; Sha et al., 1991)

$$K_m^x = K_h^x = c \ (\Delta x)^2 \ [\ \frac{1}{2}(\frac{\partial V}{\partial x})^2 + (\frac{\partial U}{\partial x})^2 \ ] \tag{4.7}$$

The constant c can be determined computationally such that the simulation minimizes propagation of numerical noise without excess smoothing of the horizontal variation of the temperature and concentration. The reported range of the constant c was from 0.36 to 3. The constant values might be dependent on the numerical method and the eddy formulation.

In our study, c=2.0 showed the smooth and stable numerical solution.

According to the study of Avissar et al. (1990), model dynamics and physics in the atmospheric flows are closely related to the choice of the governing equations, the grid resolution and the domain size. Figure 4.3 shows the operating range and the choice of governing equations for the sea/land breeze. The important aspect of model dynamics is the treatment of vertical motion in Equation (4.4). The hydrostatic model refers to the model which neglects the acceleration of the vertical motion. In the hydrostatic model, the perturbation pressure is statically balanced with the perturbation temperature. Pielke (1984) with his scaling analysis suggested that the hydrostatic assumption can be used if the horizontal scale of interest is of the same order or greater than 8 km. In the case of the sea breeze simulation, the majority of numerical simulations have adapted the hydrostatic assumption. Avissar et al. (1990) set the narrow restriction for the sea breeze simulation that the hydrostatic assumption should not be made for a horizontal grid smaller than 2 km due to shallow vertical depth of the sea breeze circulation. Martin and Pielke (1983)'s study concluded that the nonhydrostatic model should be used for the simulation of the sea breeze front because the sea breeze front often has an intense, narrow updraft flow near the convergence zone of the front.
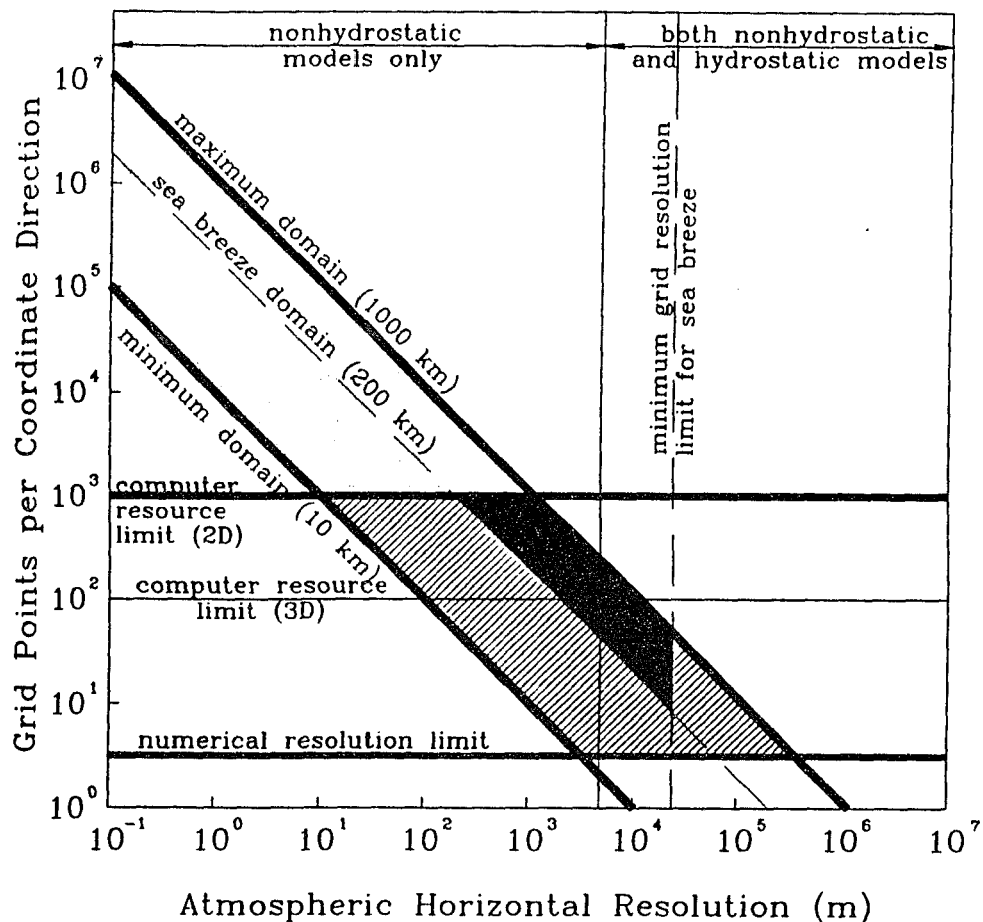
Fig.4.3. The operating range(OR) of mesoscale numerical models for the sea/land breeze simulations. The stippled area denotes the potential OR for mesoscale numerical models in a homogeneous synoptic environment given more powerful computer. The hatched and blacked areas indicate the current mesoscale model OR. The blackened area denotes the current OR for sea/land breeze simulation (Avissar et al., 1990).

The nonhydrostatic model with 2 km horizontal grid resolution was used to investigate the detailed structure of sea breeze.

4.2.2. Boundary Conditions

In order to calculate friction velocity and surface heat flux, an analytic method instead of the Monin-Obukhov similarity described in Section 3.2.2 was used because the Monin-Obukhov similarity often fails to predict in the strong convective condition, especially free convective condition. The friction velocity and surface heat flux can be calculated from the following analytic relationships (Louis, 1979).

$$u_*^2 = a^2 \ U^2(z) \ F_m$$
$$u_* \ \theta_* = \frac{a^2}{0.74} \ U(z) \ \Delta\Theta \ F_h$$

$$(4.8)$$

where

$$a^2 = \frac{\kappa}{(\ln\frac{z}{z_o})^2}$$

a is a drag coefficient in the neutral condition and F_m and F_h are functions of a roughness length and bulk Richardson number for momentum and heat fluxes, respectively. F_m and F_h are determined from the dimensionless analysis in the free convective condition and the Monin-Obukhov similarity. For unstable conditions:

$$F_{m,h} = 1 - \frac{b\ Ri_B}{1 - c|Ri_B|^{1/2}} \qquad (4.9)$$

where $\quad c = C^* a^2 b\ (\frac{z}{z_o})^{1/2}, \quad Ri_B = \frac{g\ z\ \Delta\Theta}{\Theta\ U^2}$

b is 9.4 and C^* is 7.4 for F_m and 5.3 for F_h.

For stable conditions:

$$F_{m,h} = \frac{1}{(1 + 4.7\ Ri_B)^2} \qquad (4.10)$$

The sea surface temperature was set as a constant(288K) and the land surface temperature was varied as:

$$T_{land} = T_{sea} + 8.0\ \sin(\frac{2\pi t}{24\times3600}) \qquad (4.11)$$

$$T_{land} = T_{sea} + 2.8(10+\frac{x}{10})\sin(\frac{2\pi t}{24\times3600}+6) + 3.4\sin(\frac{4\pi t}{24\times3600}+310) \qquad (4.12)$$

The time(t) is local standard time (LST). The land surface temperature variations with time are shown in Figure 4.4. The maximum temperature difference between the land and the sea is 8 K for Equation (4.11) and 18 K for Equation (4.12). The variation of the land surface temperature with time in Equation (4.12) was obtained by Neumann and Mahrer (1971) based on the observation. The case with low temperature difference (Equation 4.11) is herein called Case L and the case with high temperature difference (Equation 4.12) called Case H.
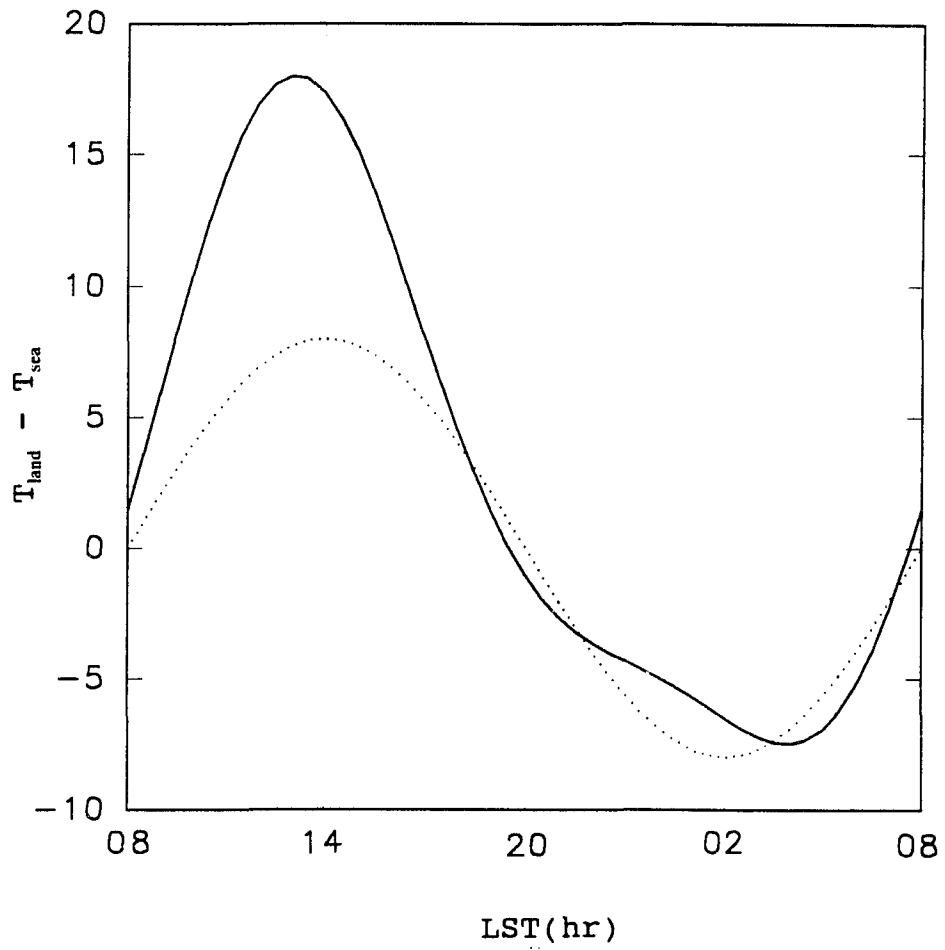
Fig. 4.4. Surface temperature difference between the land and the sea with time. Dotted line is for Case L and solid line for Case H.

The ambient background stratification was 3.3K/Km (Arritt, 1993). Roughness length (z_o) was 0.05m over the land. z_o over the sea was calculated by $z_o = 0.032 \, u_*^2/g$ assuming that z_o is greater than 1.5×10^{-5}m. Lateral boundary conditions were assumed to be homogeneous with respect to x direction for all variables. At the top, the initial values were retained throughout the simulation. The initial velocities were calculated from Ekman layer equations with a geostrophic wind. The same initial conditions were used by Arritt (1991, 1993). Integration of the sea breeze started at 18 LST and continued for 32 hours.

4.2.3. Numerical Methods

In order to enhance the accuracy and convergence in each time step, an implicit finite difference method with a control volume approach and a staggered grid system were used to discretize the governing equations. This method had been suggested by Patankar (1980) and used largely in engineering flow field. Sha et al. (1991) and Kitada (1987) used the same method in the application of a conventional E-ϵ model to the sea breeze. Figure 4.5 shows typical control volume and grid point for the variables.

SIMPLE (Semi-Implicit Method for Pressure-Linked Equation) method was applied to solve the discretized equations (Patankar , 1980; Anderson et al., 1984). The procedure is based on a cyclic series of guess and
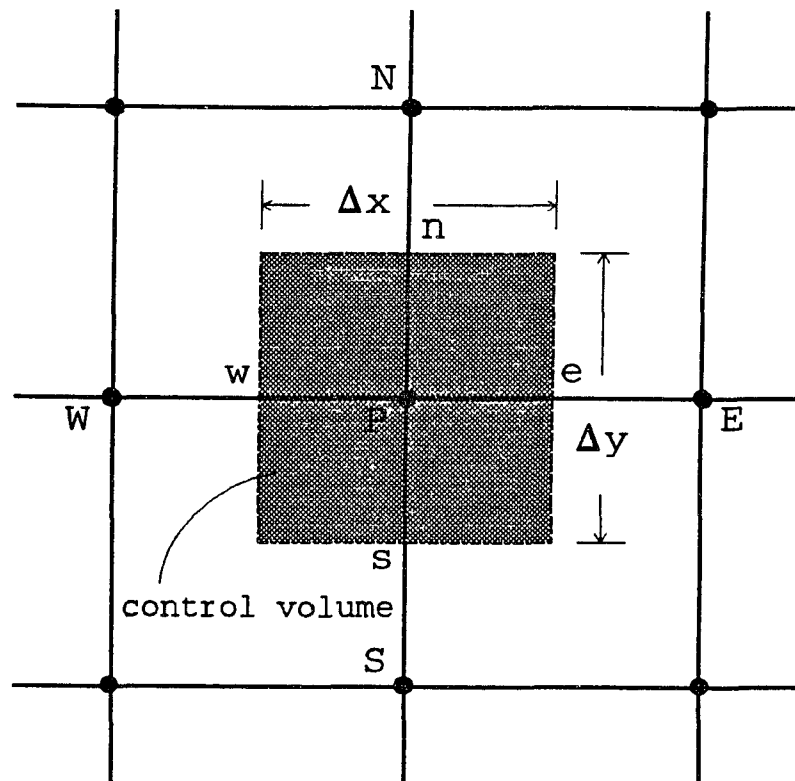
Fig.4.5.Control volume and grid points for a sea breeze.
P, S, N, E, and W grid points are for Θ, C, E, ϵ and V
velocity. w and e grid points for U velocity, n and e
grid points for W velocity.

correction operations to solve the equations. The velocity components are first calculated from the momentum equations using a guessed pressure field. And the guessed pressure is corrected so as to satisfy the continuity equation via the corrected pressure. The process continues until the solution converges in each time step.

In this procedure, the mesoscale perturbation pressure P is written as:

$$P = P^* + P'$$ (4.13)

where the superscript * means the guessed value and a prime represents the corrected value. In the same manner, the velocity components are written as:

$$U = U^* + U'$$ (4.14)

$$W = W^* + W'$$

The pressure corrections are related to the velocity corrections by approximate forms of the momentum equations:

$$\rho \frac{\partial U'}{\partial z} = - \frac{\partial P'}{\partial x}$$ (4.15)

$$\rho \frac{\partial W'}{\partial t} = - \frac{\partial P'}{\partial z}$$

Since the velocity corrections can be assumed to be zero at the previous iteration step, the above equation can be written as:

$$U' = -A \frac{\partial P'}{\partial x} \qquad (4.16)$$

$$W' = -A \frac{\partial P'}{\partial z}$$

where A is a time increment divided by the density. After combining the above equations and substituting the result into the continuity equation, a Poisson equation for the corrected pressure can be obtained:

$$\frac{\partial^2 P'}{\partial x^2} + \frac{\partial^2 P'}{\partial z^2} = \frac{1}{A} \left(\frac{\partial U_*}{\partial x} + \frac{\partial W_*}{\partial z} \right) \qquad (4.17)$$

This Poisson equation is solved for the pressure correction. If the estimated velocities satisfy continuity equation at each grid point, then the pressure correction is zero.

The SIMPLE procedure applied in each time step can be summarized by the following steps:

1) Guess the pressure field P^*.

2) Solve the momentum equations to find the estimated velocities(U^* and W^*).

3) Solve the pressure correction Equation(4.17) to find P'.

4) Correct the pressure and velocities using Equations (4.13) and (4.14).

5) Replace the previous guessed pressure and estimated velocities with the new calculated ones and return to step

2 until the continuity equation at each control volume satisfied with 5×10^{-4}.

The time step used in this study was 20 sec. 60 uniform grids in the x-direction with 2km horizontal grid resolution were used for the Case L. The domain of calculation was 120 km in horizontal dimension which consisted of 40 km over the sea and 80km over the land and 2.5 km for vertical dimension. For case H, non-uniform grid in the x-direction with 2km near the shore and 4 km at the lateral boundary. The domain size for the simulation was 240 km in the horizontal direction (50km in the sea side) and 5km in the vertical direction. In both cases, a logarithmically varied non-uniform vertical grid was used. The lowest grid point was 3.4m from the surface and the highest was 161m at the top of the domain.

The numerical details such as convergence test as well as effects of grid resolution and horizontal domain size on the sea breeze are in Appendix C.

4.3. Results and Discussions

4.3.1. Sea Breeze Development

In order to understand the influences of meteorological conditions on the sea breeze development, simulations of Case L and H surface temperature differences have been carried out with various offshore geostrophic winds. The geostrophic wind was fixed as – 1 m/sec in Case L and was

varied from 0 m/sec to -3 m/sec in Case H. The velocity profiles and temperature and kinetic distributions from 12 LST to 24 LST with Case L are shown in Figures 4.6 - 4.12. The velocity and temperature distributions of Case H with U_g = 0, -1, -3m/sec are shown in Figures 4.13 - 4.18. The negative values in U_g represent an offshore directed geostrophic wind. Inland penetrations of the sea breeze with various geostrophic winds and different surface temperature differences are compared with observations in Figure 4.19. The inland penetration is very sensitive to the surface temperature differences between the land and the sea and scale of geostrophic wind. The low heat flux from the land which means low surface temperature difference leads to weaker sea breeze and results in low inland penetration (Physick, 1980). The calculated inland penetrations with time show good agreement in respect of their shapes but some discrepancies. In order to be compatible with the observation, detailed meteorological data such as land surface temperature based on a energy balance at the land surface, geostrophic wind, and initial temperature profile should be considered in the simulation. The key features of the sea breeze, however, can be obtained from the idealized meteorological system.

The calculated front velocities and depths of mixed layer with various conditions are in Table 4.1. The mixed layer

Fig.4.6. A sea breeze at 12 LST for Case L and U_g = -1 m/sec. (a)velocity (b)temperature (c)kinetic energy(m^2/sec^2).

Fig.4.7. A sea breeze at 14 LST for Case L and U_g = -1
m/sec.   (a)velocity   (b)temperature   (c)kinetic
energy(m^2/sec^2).
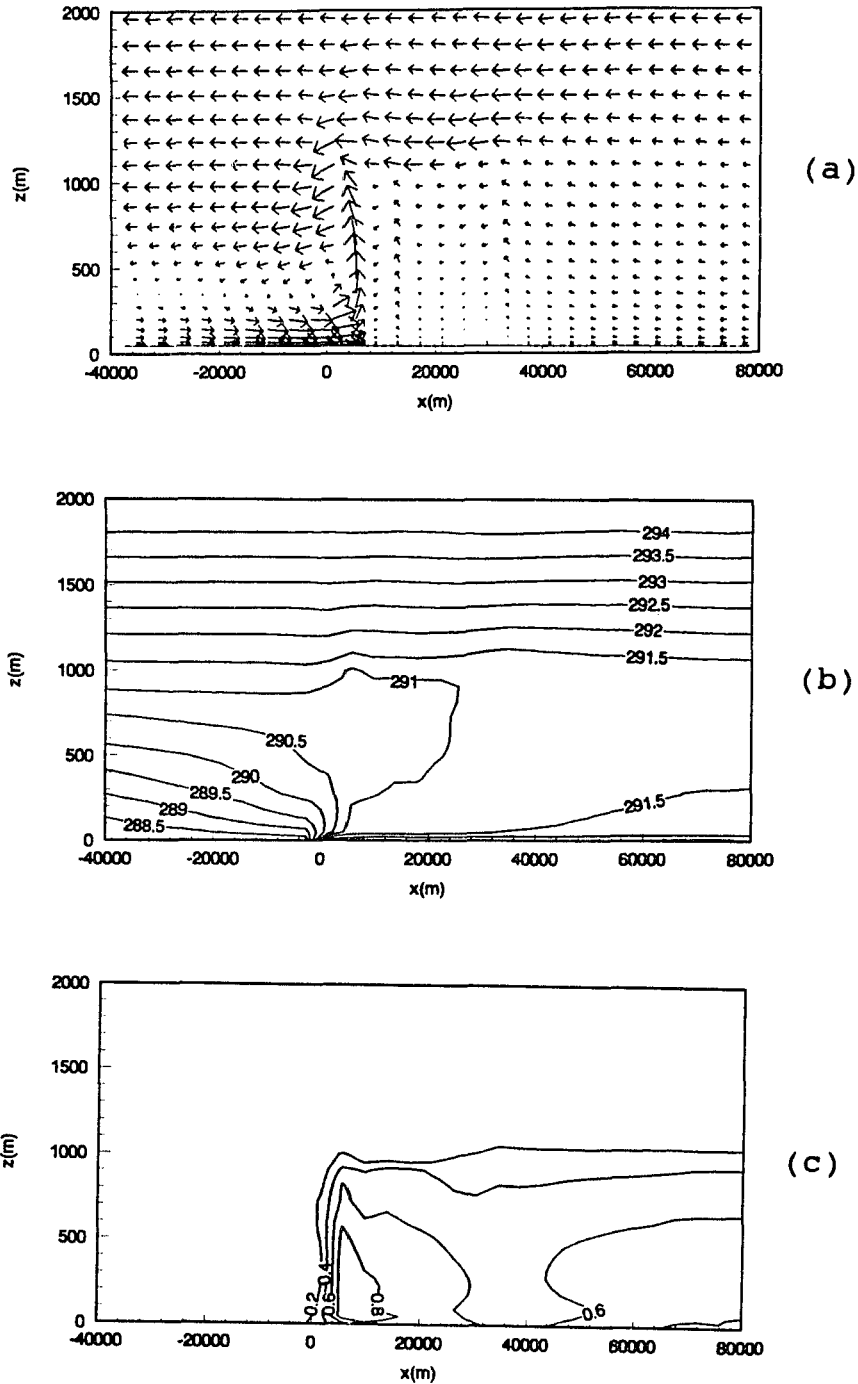
Fig.4.8. A sea breeze at 16 LST for Case L and U_g = -1 m/sec. (a)velocity (b)temperature (c)kinetic energy(m^2/sec^2).
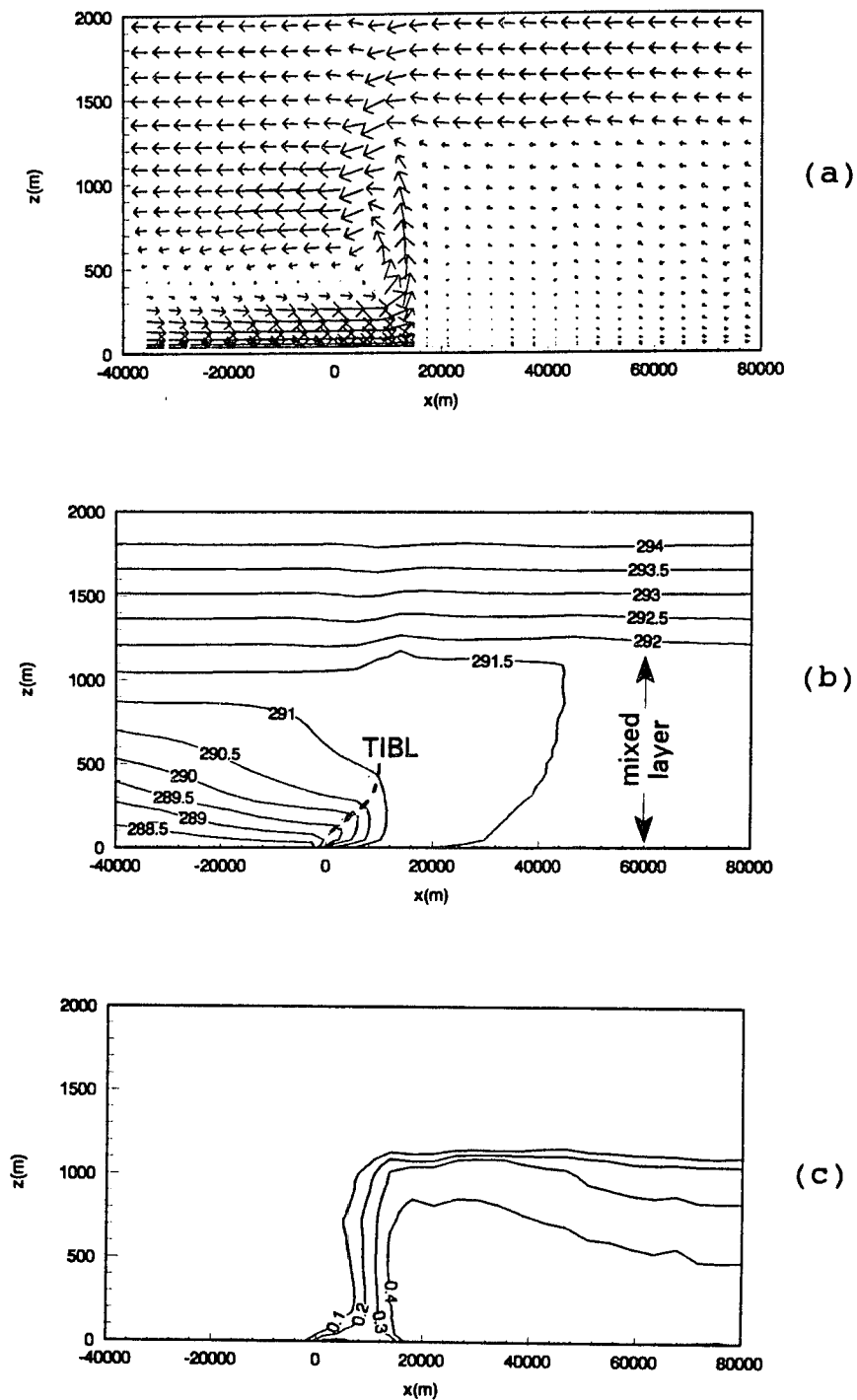
Fig.4.9. A sea breeze at 18 LST for Case L and U_g = -1 m/sec. (a)velocity (b)temperature (c)kinetic energy(m^2/sec^2).
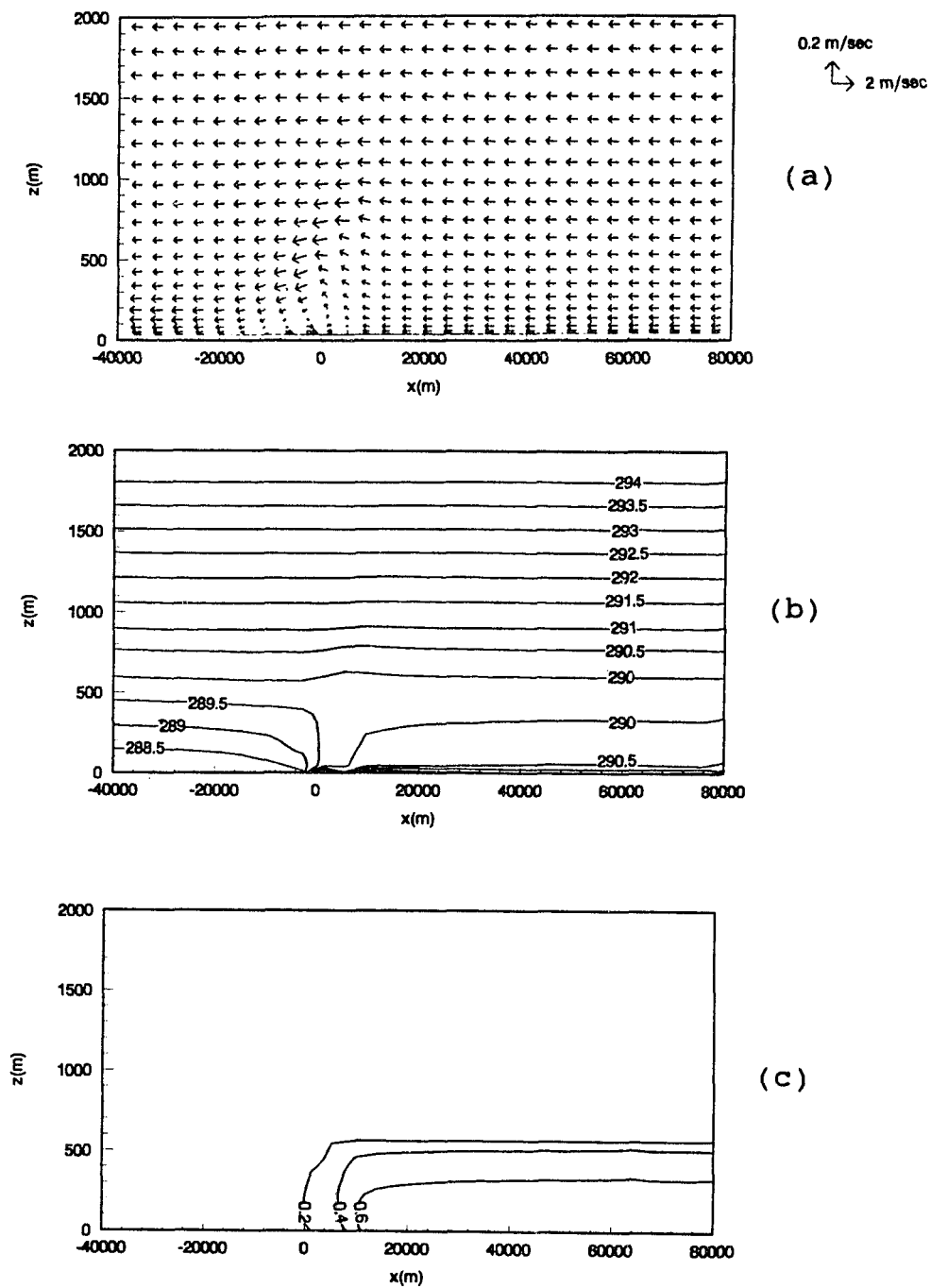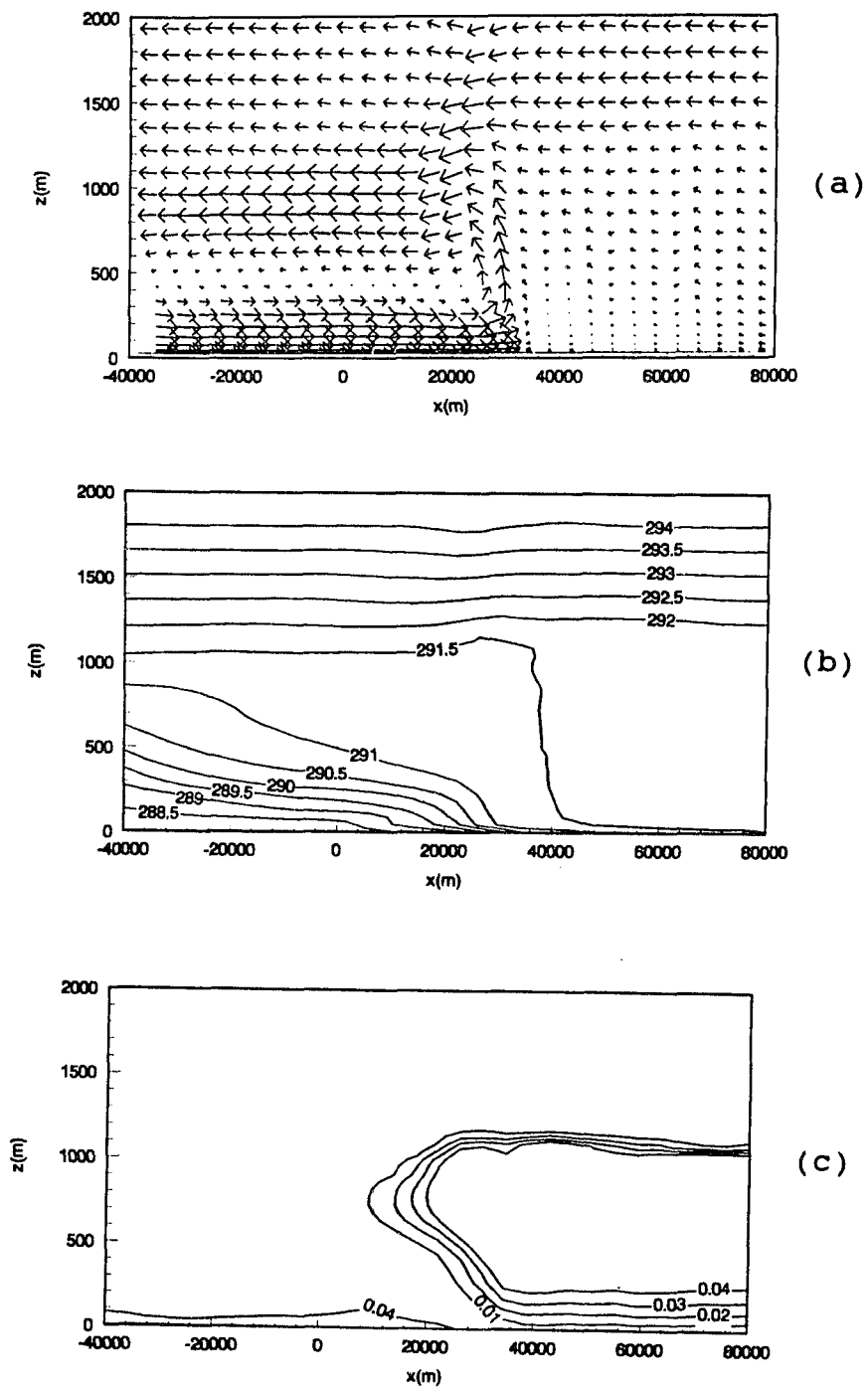
Fig.4.10. A sea breeze at 20 LST for Case L and U_g = -1 m/sec.   (a)velocity   (b)temperature   (c)kinetic energy(m^2/sec^2).

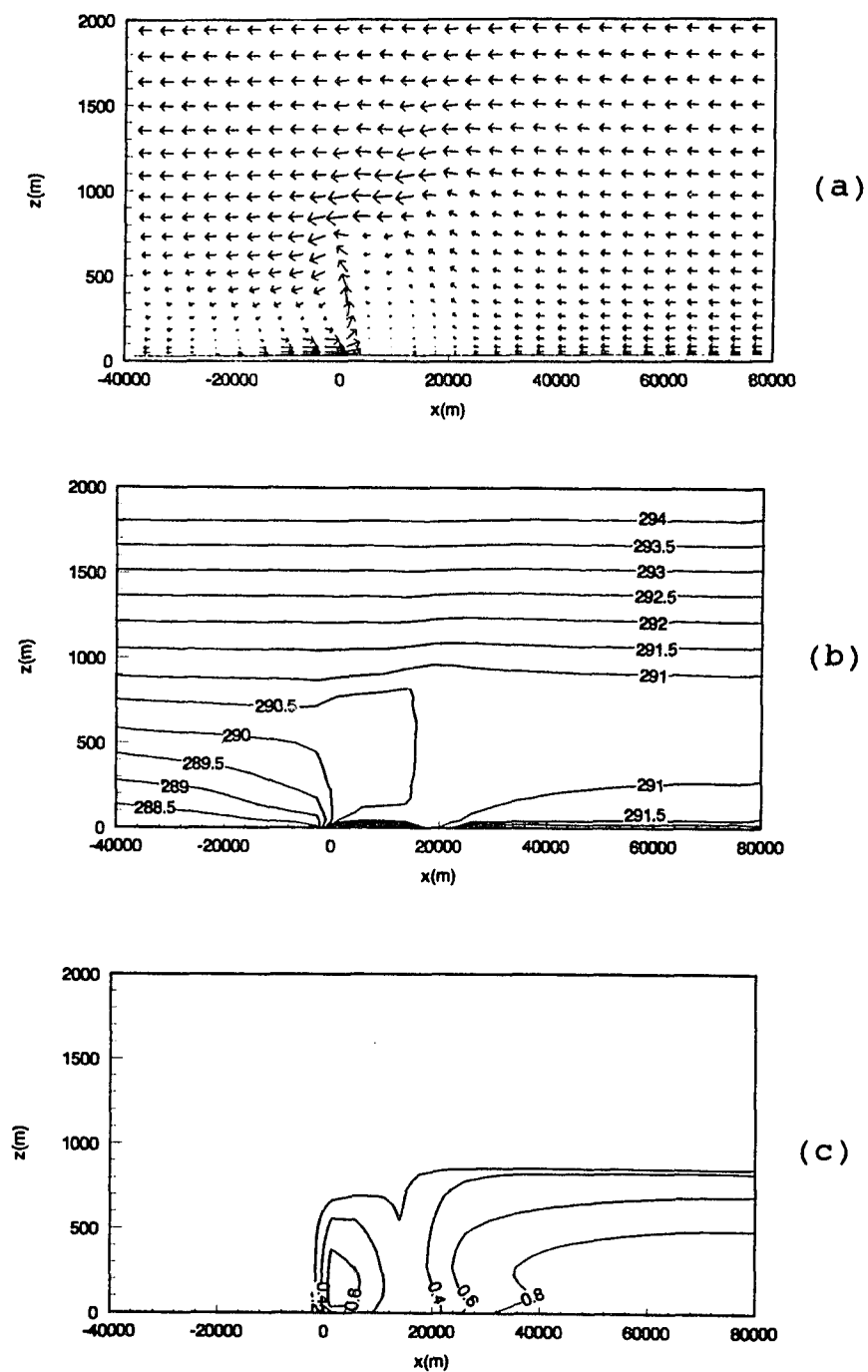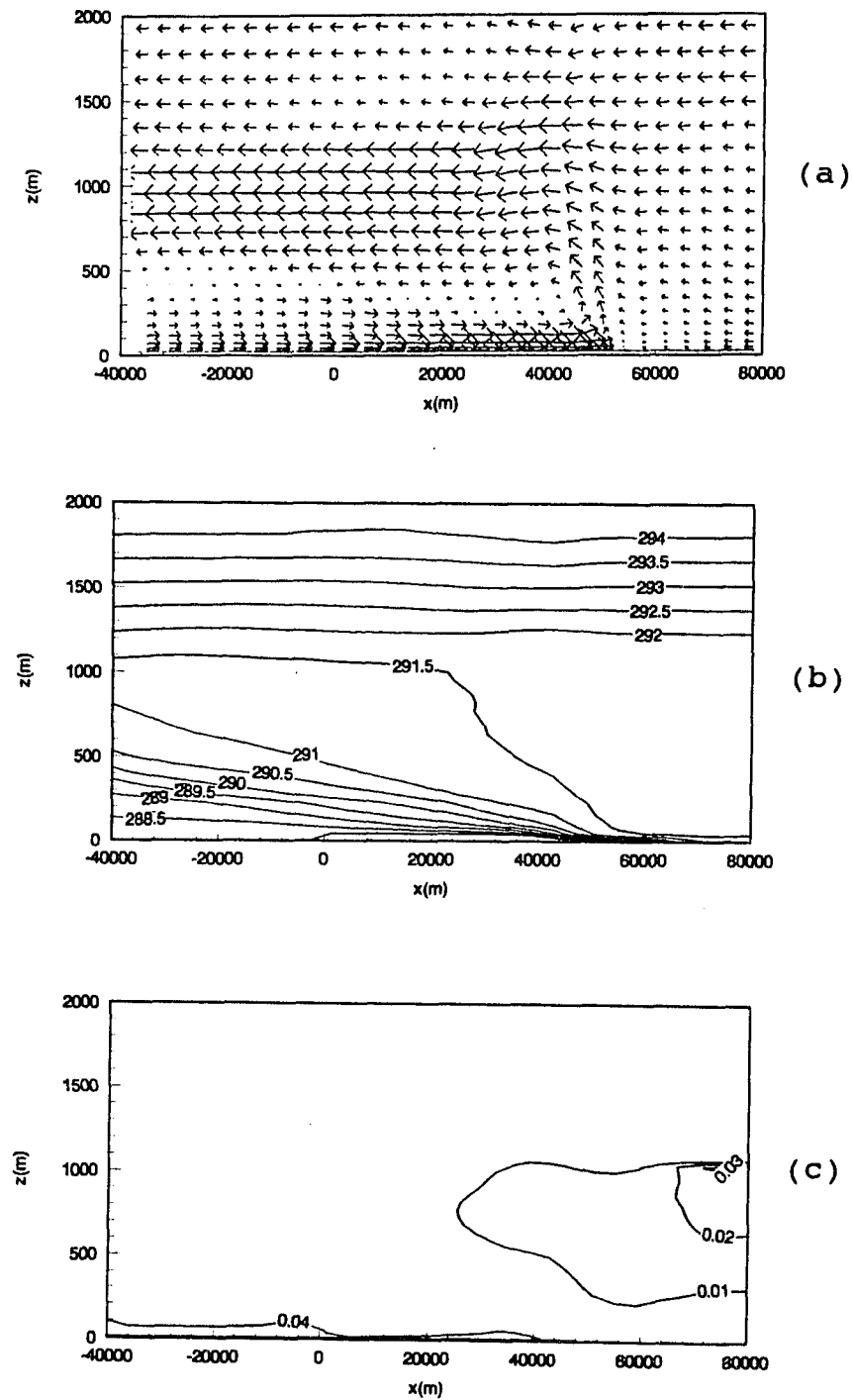Fig.4.11. A sea breeze at 22 LST for Case L and U_g = -1 m/sec. (a)velocity (b)temperature (c)kinetic energy(m^2/sec^2).
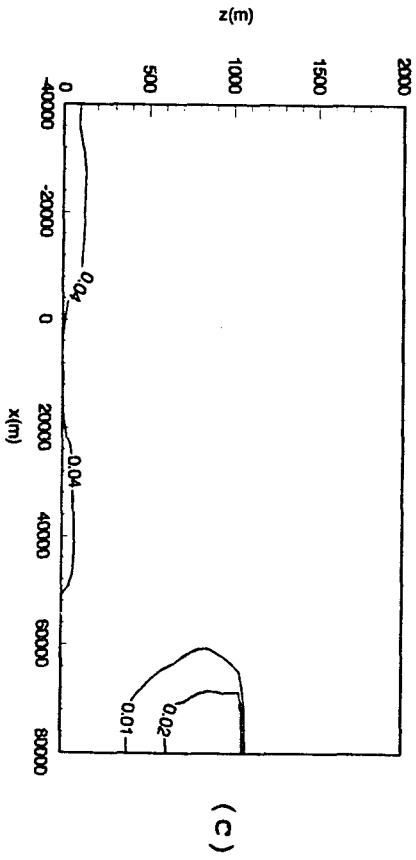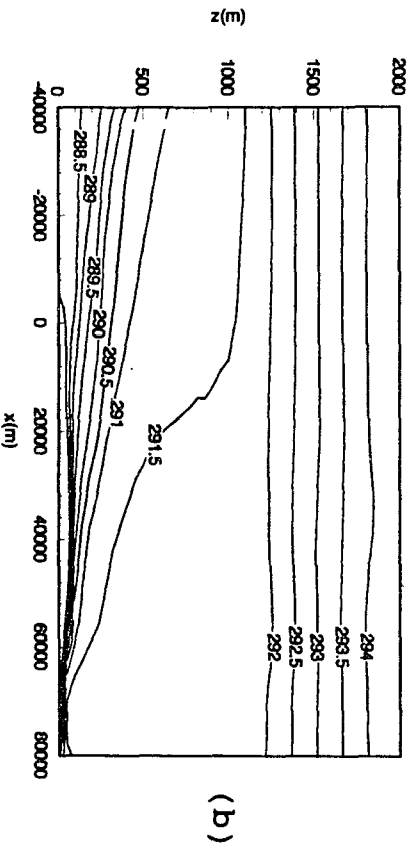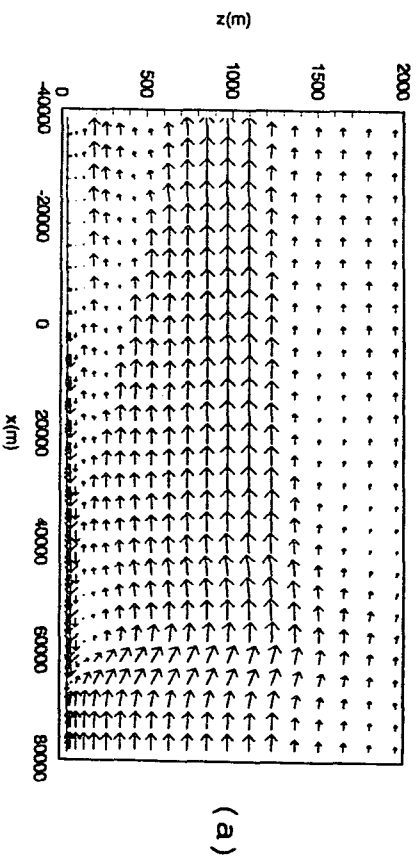
Fig.4.12. A sea breeze at 24 LST for Case L and $U_g = -1$ m/sec. (a)velocity (b)temperature (c)kinetic energy(m^2/sec^2).
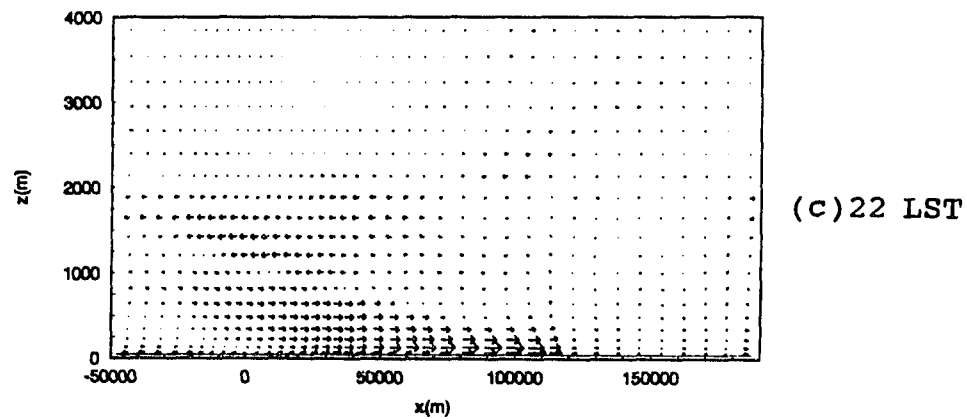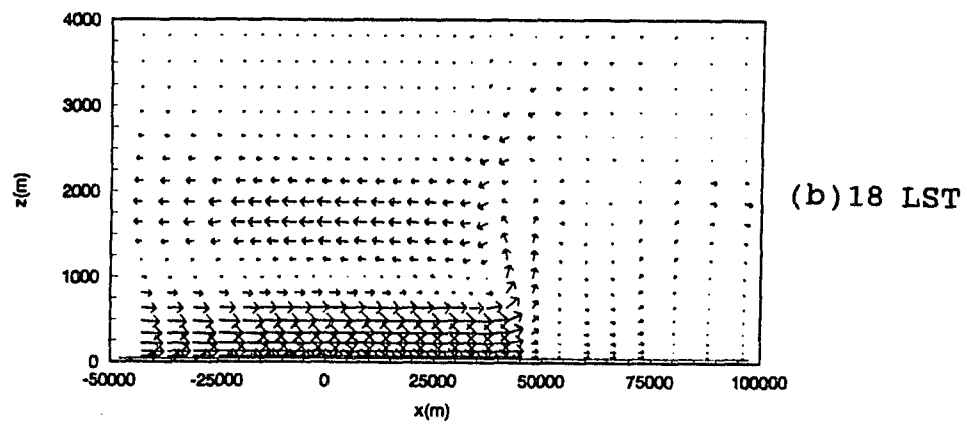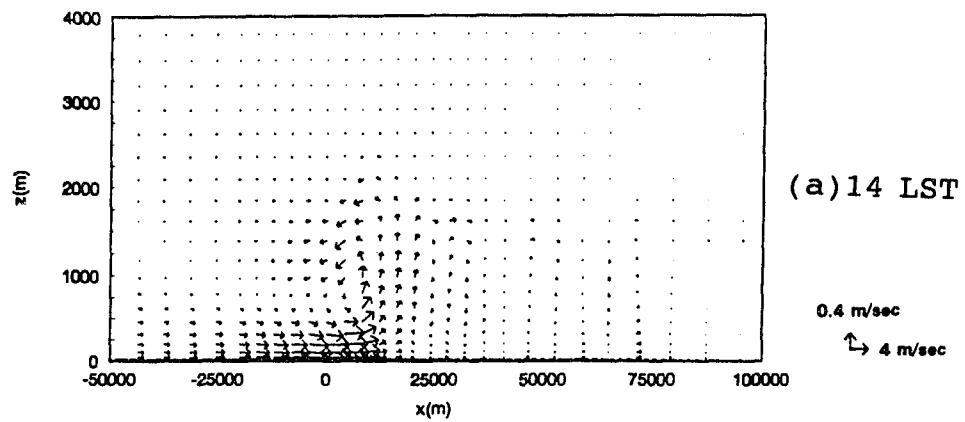
Fig.4.13. Velocity profiles of $U_g = 0$ m/sec for Case H. Note x-scale change in (c).
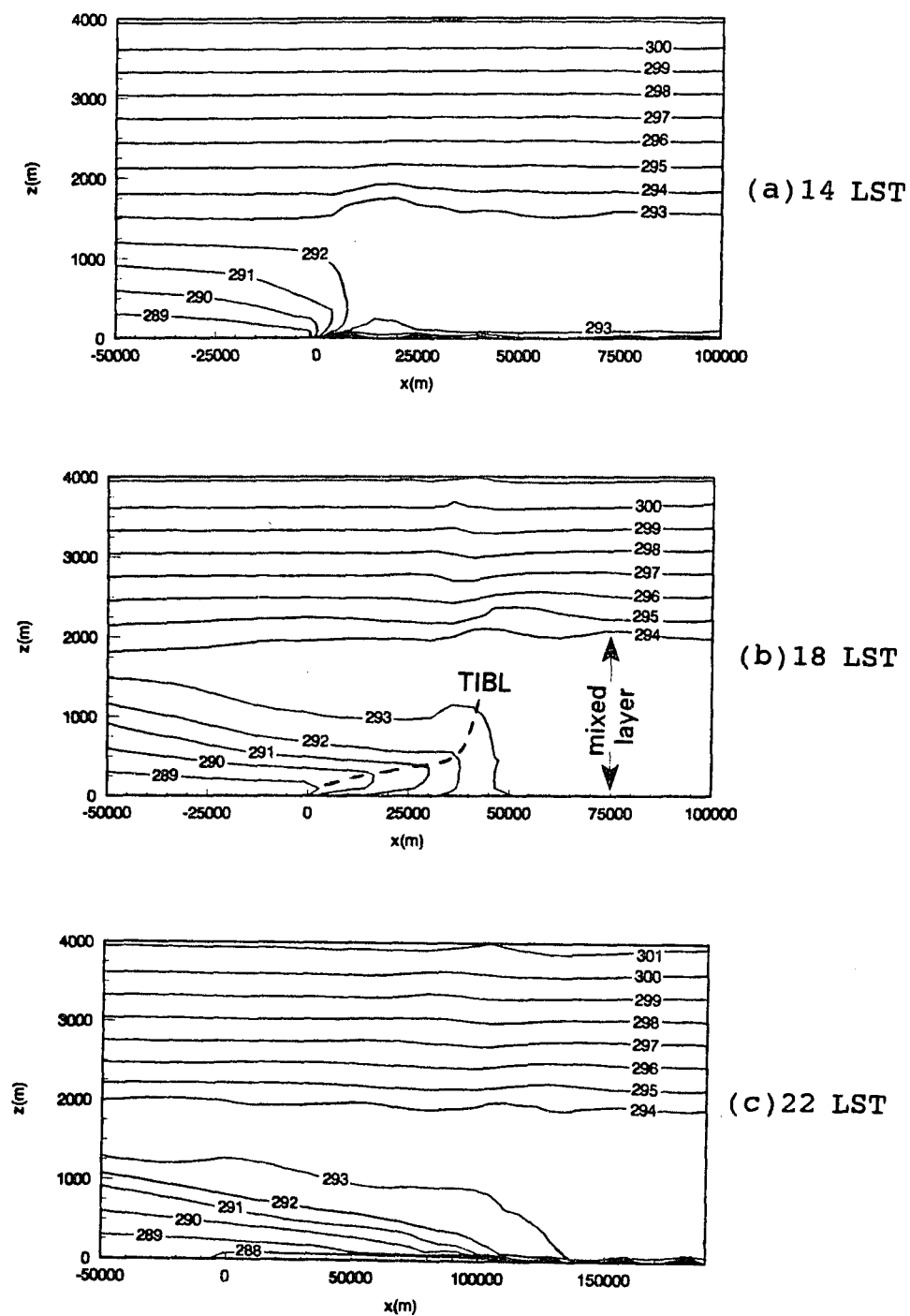
Fig.4.14. Temperature profiles of U_g = 0 m/sec for Case H. Note x-scale change in (c).
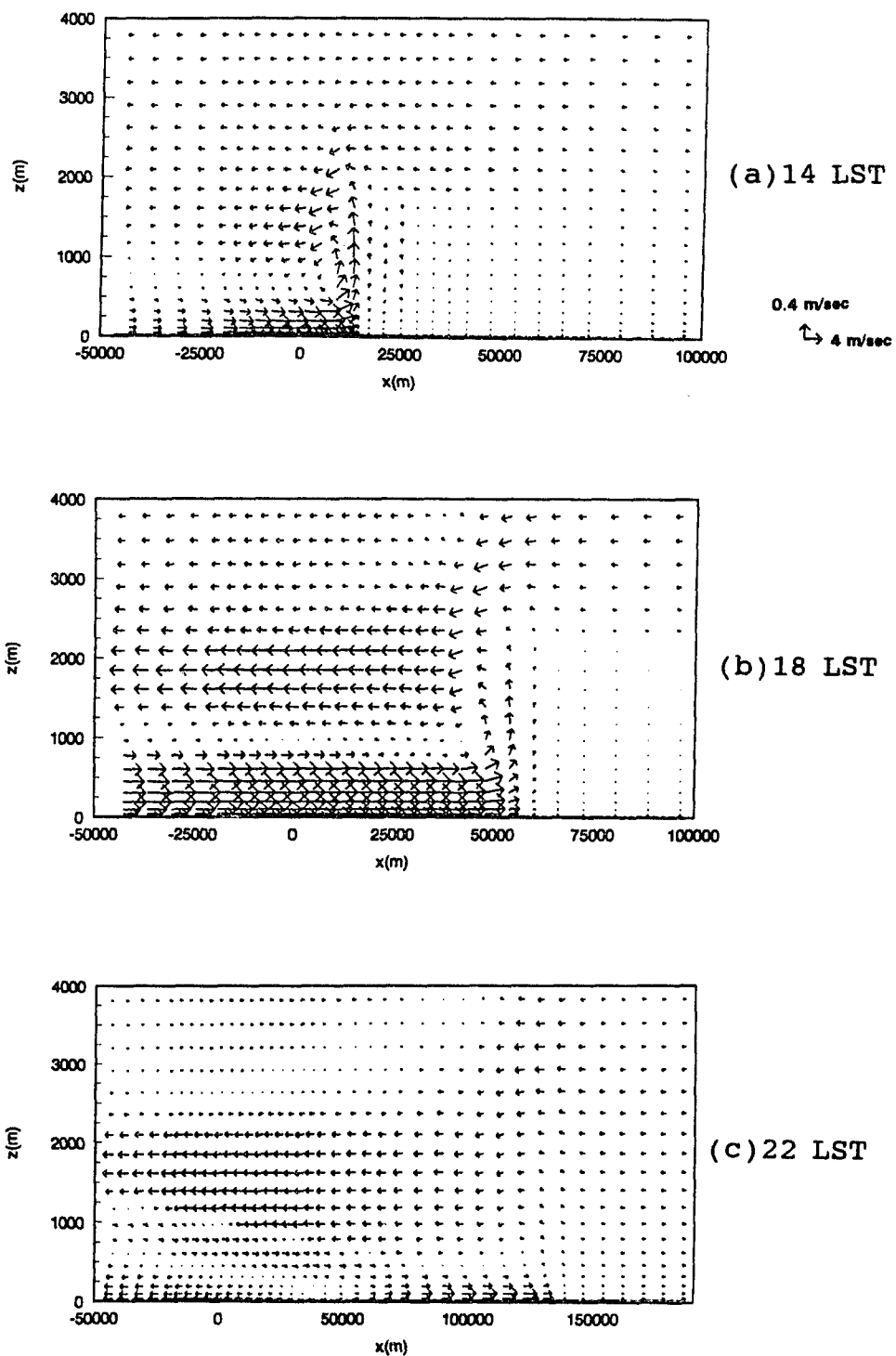
Fig.4.15. Velocity profiles of U_g = -1 m/sec for Case H.
Note x-scale change in (c).
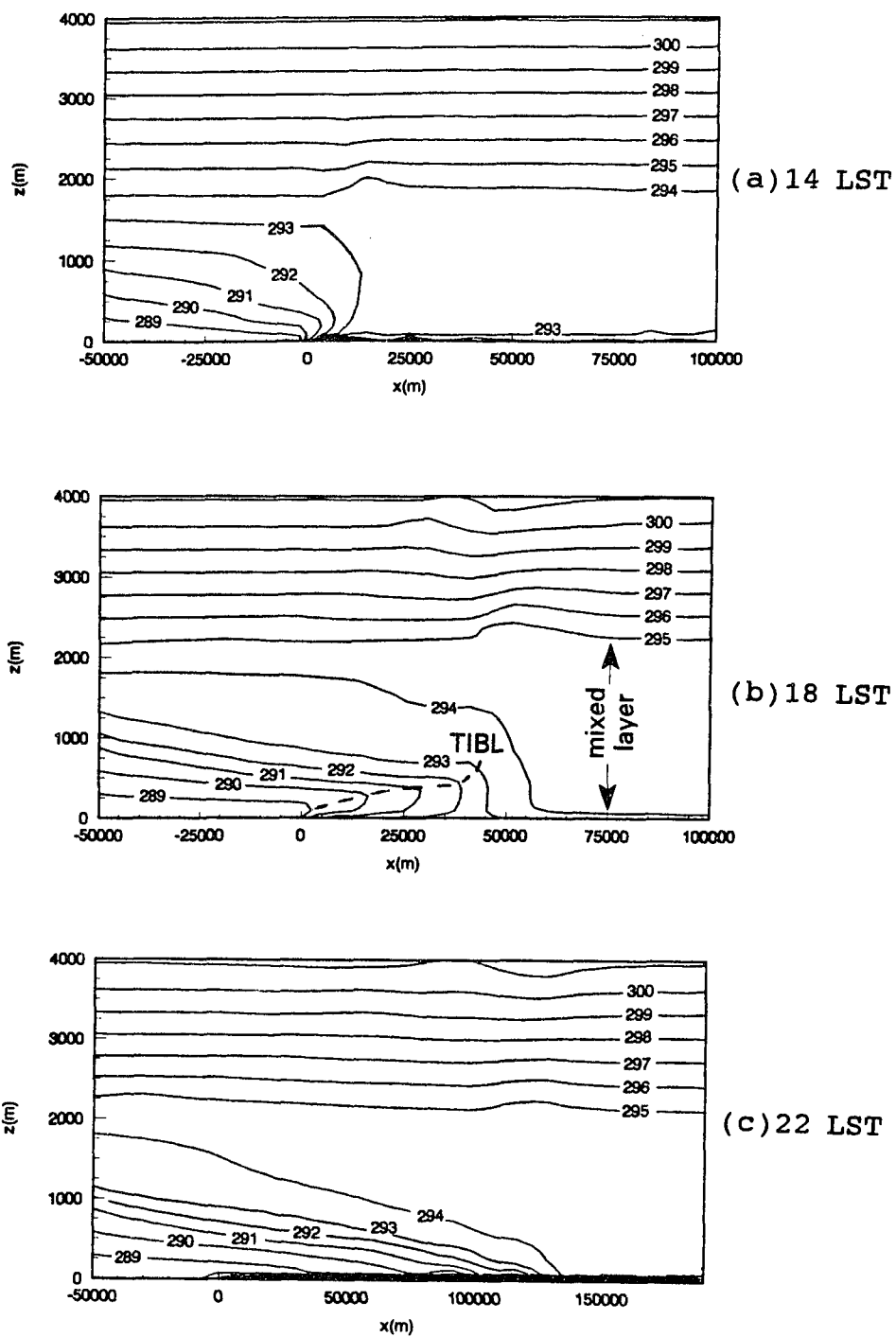
Fig.4.16. Temperature profiles of U_g = -1 m/sec for Case H. Note x-scale change in (c).
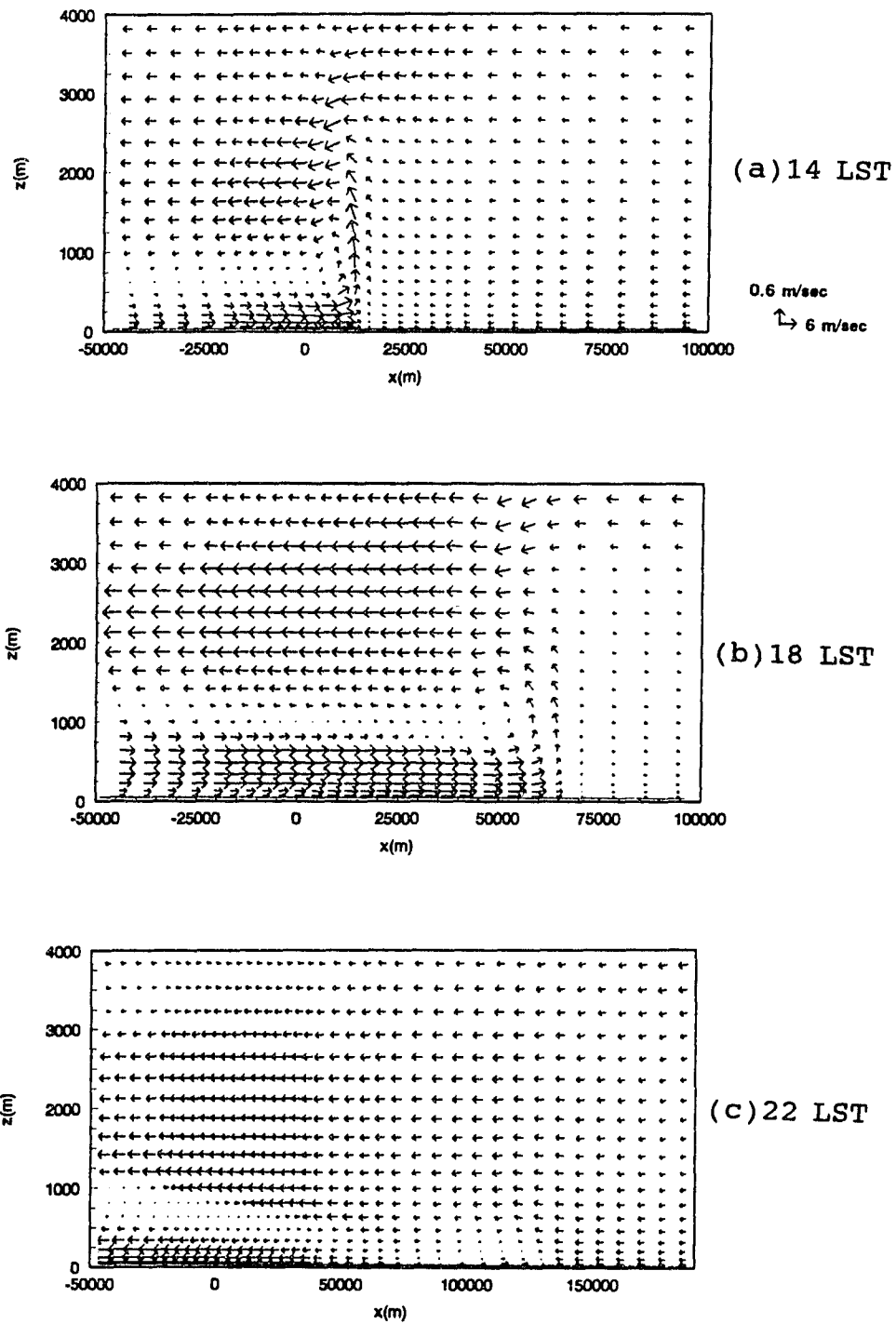
Fig.4.17. Velocity profiles of U_g = -3 m/sec for Case H.
Note x-scale change in (c).
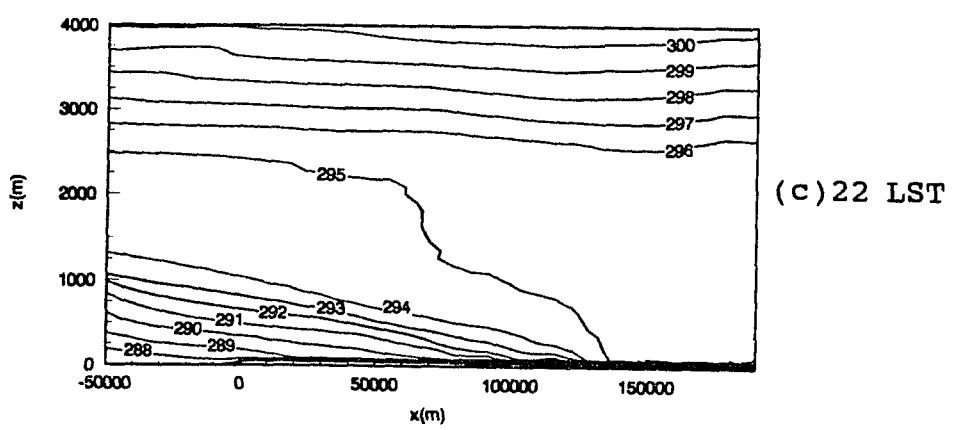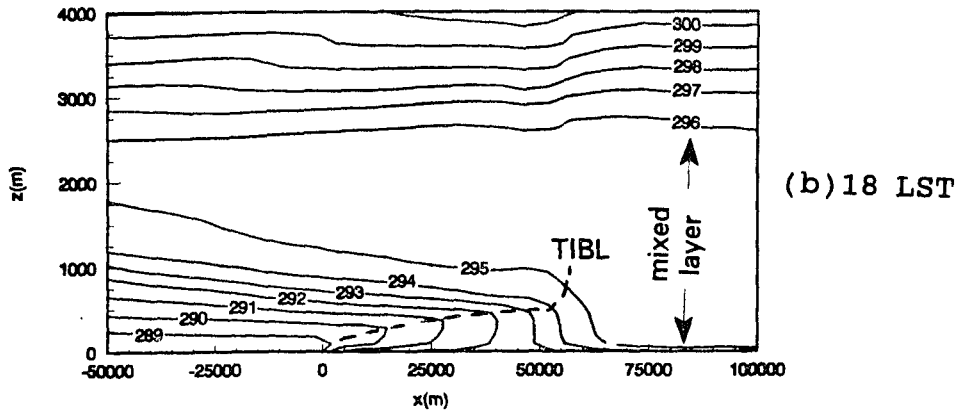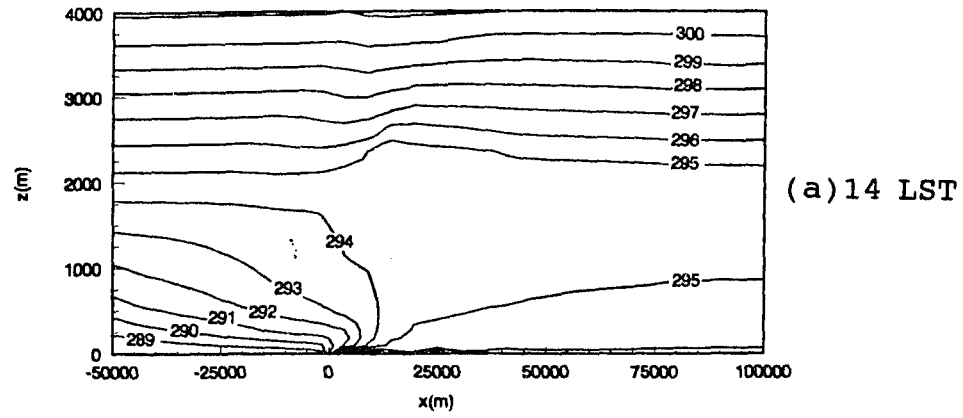
Fig.4.18. Temperature profiles of U_g = -3 m/sec for Case H. Note x-scale change in (c).
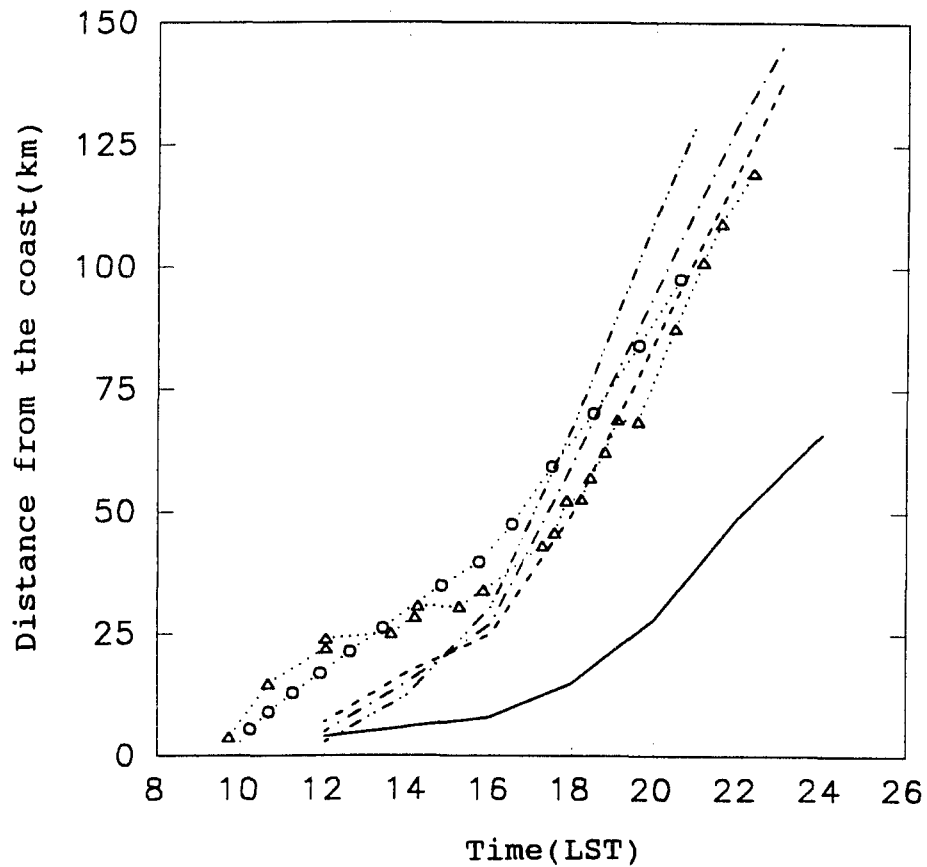
Fig.4.19. Inland penetration of the sea breeze front. Triangles are for a observed penetration by Simpson et al. (1977), circles for the observed average in southern England for 11 years (Physick, 1980). Solid line for Case L, dashed line for Case H and U_g = 0 m/sec, dot-dashed line for Case H and U_g = -1 m/sec, double dot-dashed line for Case H and U_g = -3 m/sec.

herein are referred to the convective layer over the land where the front of the sea breeze has not yet reached.

Table 4.1. Calculated front velocity (U_f) and depths of the mixed layer (z_i).

surface temp. difference		Case L	Case H		
U_g(m/s)		-1	0	-1	-3
U_f (m/s)	before 16 LST	0.27	1.39	1.37	1.32
	after 16 LST	2.36	4.46	4.76	5.53
z_i(m) at 18LST		1210	2010	2250	2610

A sea breeze is fully developed in late afternoon (about 18 LST). The leading edge of sea breeze reached 2050 m, about twice the height of the following flows (1010m) in Case H at 18 LST (Figure 4.15 (b)). The speed of following flow of the sea breeze is much faster than the speed of front. The maximum horizontal velocity in the following flow is 8.19 m/sec but the front speed is 4.76m/sec at 18 LST with Case H and U_g = -1 m/sec. Observations have also showed that the velocity in the following flow is about two times of the front velocity (Simpson et al., 1977). The faster following flow results in convergence and air flow upward at the front.

As the following flow with cool sea air moves toward the land, the temperature gradually increases and the TIBL is formed with distance from the shore (Figures 9 (b), 14(b), 16(b) and 18(b)). The detailed structure of the TIBL and

fumigation will be discussed later. When the following flow reaches to the front, convergence results in a rapid updraft flow. It then becomes a return flow moving back toward the sea just above the following flow. The sharp horizontal gradients in both temperature and wind velocity are formed near the front. The key features of the sea breeze development and circulation pattern show a good agreement with laboratory experiments and observations.

The two distinct stages of the sea breeze can be seen from Figure 4.19 and Table 4.1.

First, the initial stage is that an onshore directed sea breeze is limited to the region near the shore and the front moving velocity is relatively slow before 16 LST in Figure 4.19. The sea breeze circulation continues to grow in the vertical direction with time until 16 LST and a mixed layer with strong mixing is formed over the land. The uniform temperature and maximum kinetic energy in the middle of the boundary layer over the land show typical mixed layer. The depth of mixed layer increases as the offshore geostrophic wind and surface temperature difference increase. Figure 4.20 shows the turbulent characteristics at 14 LST with Case L. The dissipation rate is more intense near the ground and the leading head of the sea breeze. The eddy viscosity gives a typical profile in the convective mixed layer, i.e., maximum value near the middle of boundary layer. The horizontal and vertical velocity variances shown in Figure
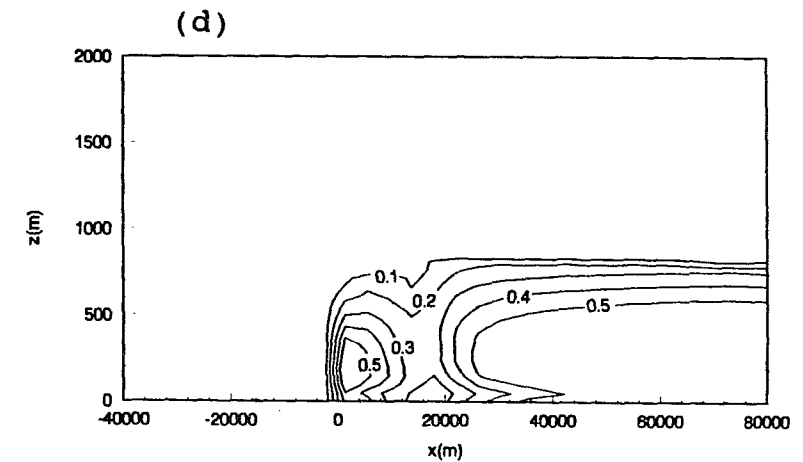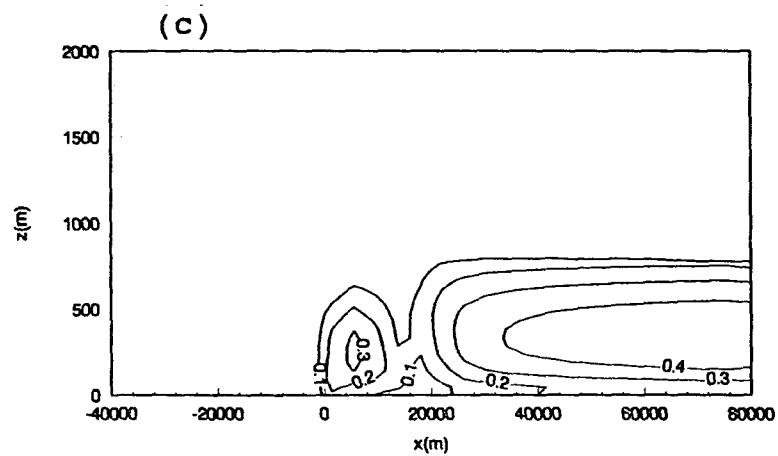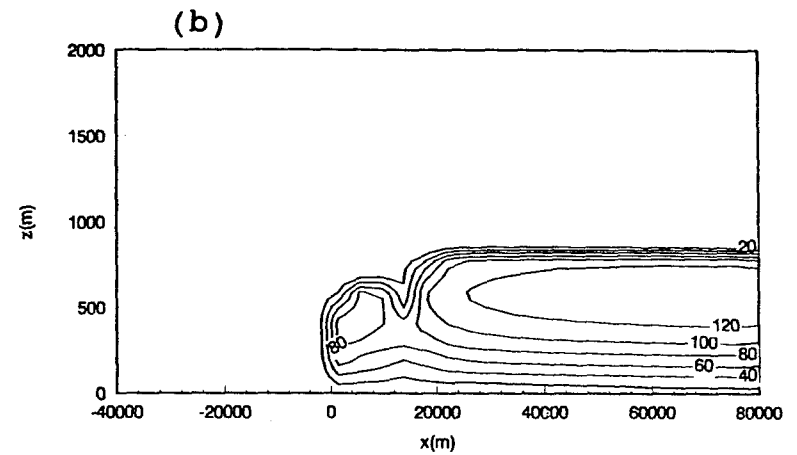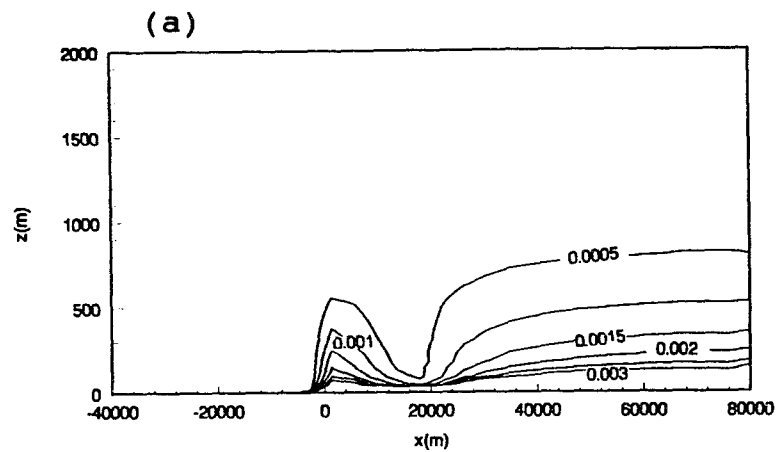
Fig.4.20. Turbulence characteristics at 14 LST for Case L and U_g = -1 m/sec. (a)Dissipation rate (m^2/sec^3), (b)vertical eddy viscosity (m^2/sec^2), (c)vertical velocity variance (m^2/sec^2), (d)horizontal velocity variances (m^2/sec^2)

4.20 (c) and (d) show similar profiles to those calculated by the second order closure of Briere (1987). The strength of sea breeze during this time is insufficient to overcome the turbulent mixing.

The sea breeze starts to accelerate from 16 LST. The front velocity before 16 LST is 0.27 m/sec and it is 2.36 m/sec at 16 LST with Case L. The velocity after 16 LST remains essentially constant. The trend of the front speed is the same for Case H with various geostrophic wind velocities. The sea breeze in both cases enters into a fully developed stage from 16 LST. The front moves faster than that of the initial stage and maintains nearly constant speed. This stage continues until 24 LST. This is consistent with the behavior observed by Reible et al. (1993).

A maximum level of the kinetic energy of the mixed layer over the land decreases rapidly with time, i.e., from 0.6 m^2/sec^2 at 16 LST to 0.02 m^2/sec^2 at 24 LST for Case L. The kinetic energy inside the following flow of the sea breeze, however, continues to increase due to the higher turbulent motion of the following flow. Estoque (1961) explained these phenomena based on the vertical heat transfer mechanism. There are two driving forces for the vertical heat transfer at all points over the land, free convection and turbulent shear mixing. The free convection ceases at early evening and the only wind shear mixing therefore

accounts for the vertical mixing. This means that in the inland region, where the front has not reached and wind strength is weaker, there is very little turbulent heat flux to the ground. Wind intensity behind the front, however, is much greater and thus larger turbulent mixing, i.e., larger kinetic energy. It implies that the turbulence over the land gradually decreases due to the decrease of surface heat flux over the land in late afternoon whereas the mixing within following flow of the sea breeze continues to grow. The acceleration of the front in late afternoon was observed by Simpson et al. (1977) at the south coast of England and calculated by Physick (1980). In the developed stage, the sea breeze penetrates into the land with high and nearly constant speed. The turbulent mixing over the land gradually decreases whereas the turbulent mixing by the following flow continues to grow.

The sea breeze penetrates deeply into the land in early evening. The sea breeze is detached from the feeding flow near the shoreline as shown in Figures 4.12(a) and 4.15(c). When the sea breeze penetrates far inland, the local density difference is a governing factor for the sea breeze movement (Simpson et al., 1977) and the observed sea breeze front can be interpreted as a density current (Garratt and Physick, 1985). Figure 4.21 shows the gravity current at 23.5 and 24 LST with Case L. The height of gravity current head is about two times the depth of the gravity current.
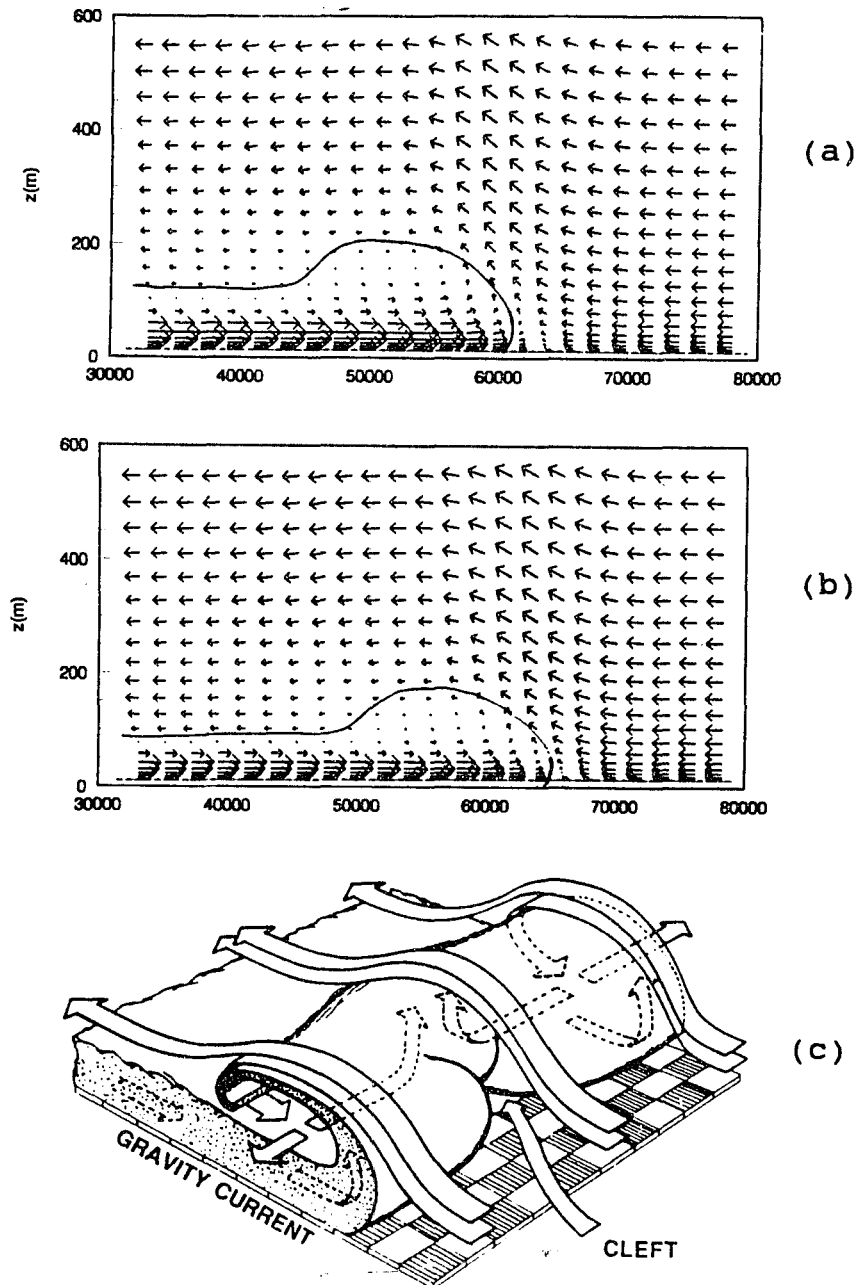
Fig.4.21. Detailed flow structures of the head of the gravity currents for Case L and U_g = -1 m/sec. (a)23.5 LST (b)24 LST (c)three dimensional gravity current from Simpson et al.(1977).

4.3.2. Frontogenesis Analysis

The pronounced differences of the front penetration between the initial stage and the developed stage may be explained from a frontogenesis analysis. The equation for frontogenesis can be obtained by taking the partial derivative with respect to x of Equation (4.5).

$$\frac{\partial}{\partial t}(\frac{\partial \Theta}{\partial x}) + U\frac{\partial}{\partial x}(\frac{\partial \Theta}{\partial x}) + W\frac{\partial}{\partial x}(\frac{\partial \Theta}{\partial z}) = -\frac{\partial U}{\partial x}\frac{\partial \Theta}{\partial x} - \frac{\partial W}{\partial x}\frac{\partial \Theta}{\partial z}$$
$$+ \frac{\partial^2}{\partial x \partial z}(K_m^z\frac{\partial \Theta}{\partial z})$$

$$(4.18)$$

The first term on the left hand side (LHS) is the local change of the horizontal temperature gradient and the other two terms are the horizontal and vertical advection terms. The whole term of LHS can be rewritten as the substantial derivative of the horizontal temperature gradient. The first term of the right hand side (RHS) represents the frontogenesis by convergence of the horizontal wind. The second term on RHS represents the rotation of the vertical temperature gradient into a horizontal gradient. The third RHS term represents the frontogensis due to the horizontal gradient in the vertical turbulent heat flux, i.e., turbulent mixing. In a developing front, the vertical property variations tend to be small and horizontal shear in the vertical velocity is unlikely to be the major factor driving frontogenesis (Reible et al., 1993). Therefore, both

horizonal convergence and turbulent mixing largely define the frontal development.

Balance between the turbulence and convergence in a developing front is expected to control the inland penetration of the front. Figures 4.22 to 4.28 show the frontogenesis and frontolysis (weakening of the front, negative values) of the horizontal convergence and the turbulent mixing for Case L. The convergence builds strongly up as the time increases in the initial stage from 12 LST to 16 LST. The convergence clearly shows the position of the front. The front and the leading edge of the sea breeze front are positioned in the center of the horizontal convergence. The turbulent mixing is distributed across the convergence. It also increases with time in the initial stage. These results are in general agreement with the observations of Kraus et al.(1990) and the calculations of Arritt(1991). The strong turbulence in front of the horizontal convergence is likely to prevent the inland penetration of the front during this time. By 18 LST, convergence is strongest around 10 km inland (Figure 4.25) while turbulence is strongest at 5 km inland. This separation indicates that the front has passed through the region of greatest turbulent mixing as the front develops and the front velocity increases. There are no turbulent mixings after 18 LST ahead of the front. At this time, the developed stage starts and the only prevailing term in the

(a)

(b)

Fig.4.22. Frontogenesis of (a)horizontal convergence and (b)horizontal gradients of the vertical turbulent flux at 12 LST for Case L. Contour interval is 2×10^{-8} K/m/sec. Solid line is for a positive value and dashed line for the negative.

(a)

(b)
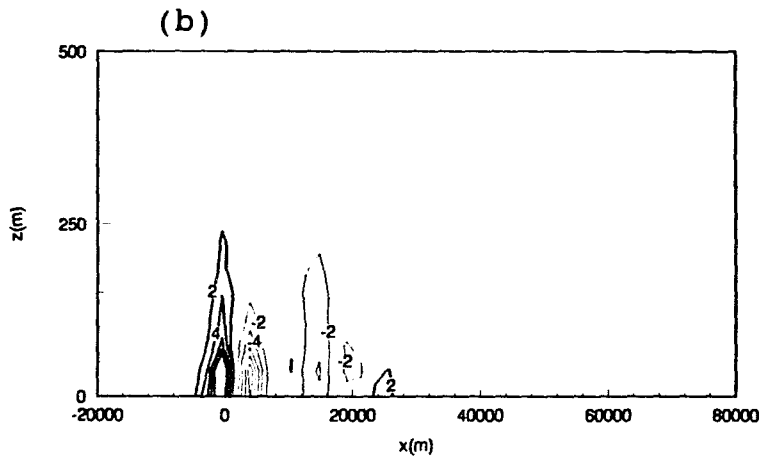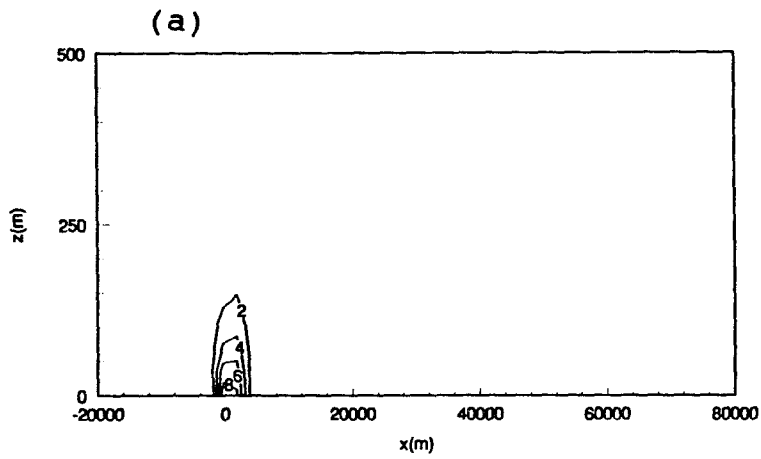
Fig.4.23.Same as Fig.4.22 except
at 14 LST.

(a)

(b)

Fig.4.24.Same as Fig.4.22 except
at 16 LST.

(a)

(b)
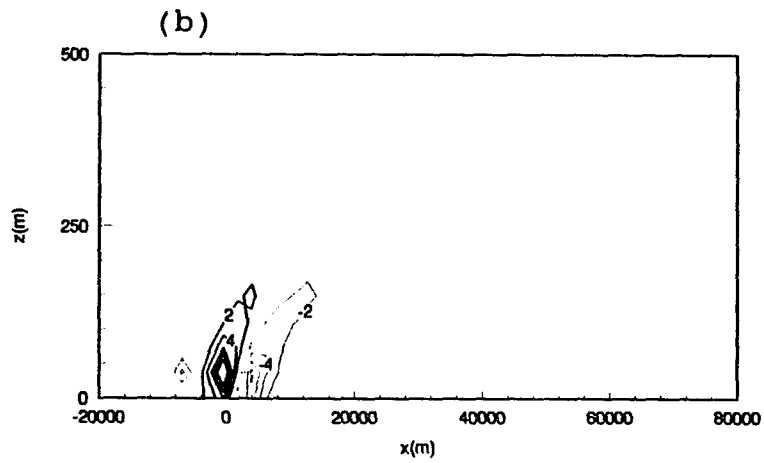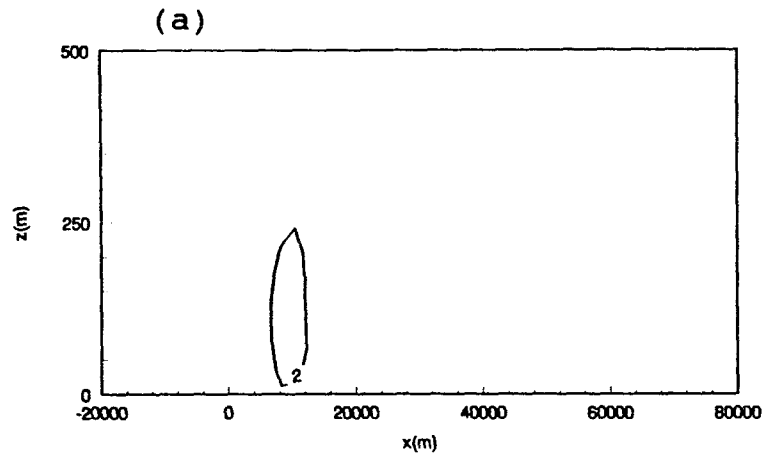
Fig.4.25.Same as Fig.4.22 except at 18 LST.

(a)

(b)
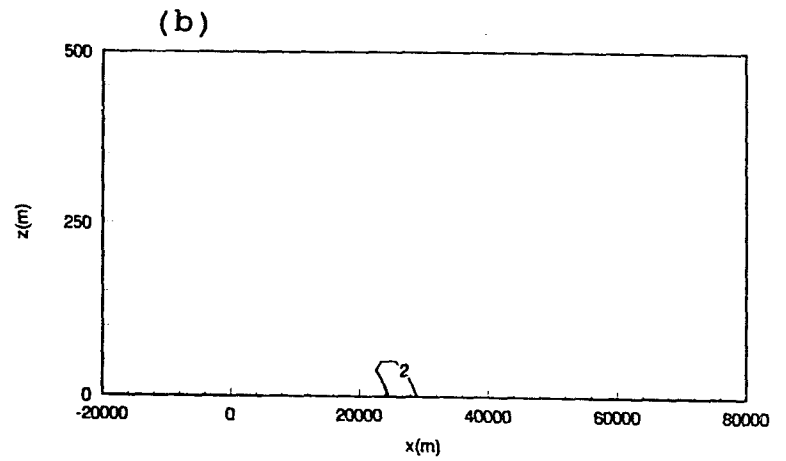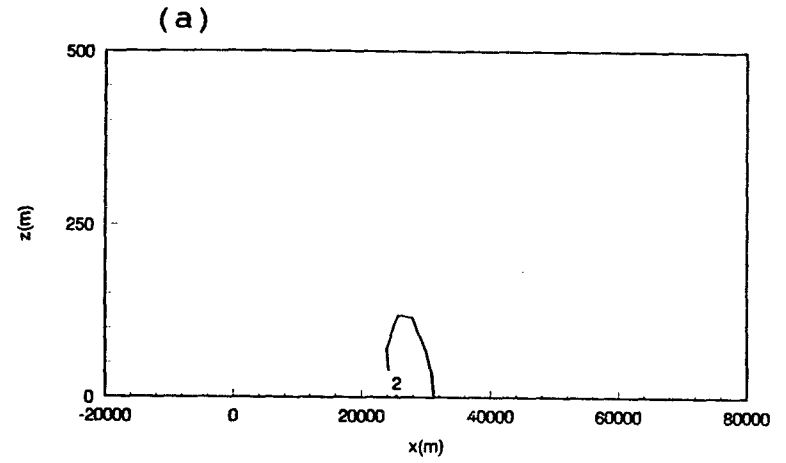
Fig.4.26.Same as Fig.4.22 except at 20 LST.

(a)

(b)
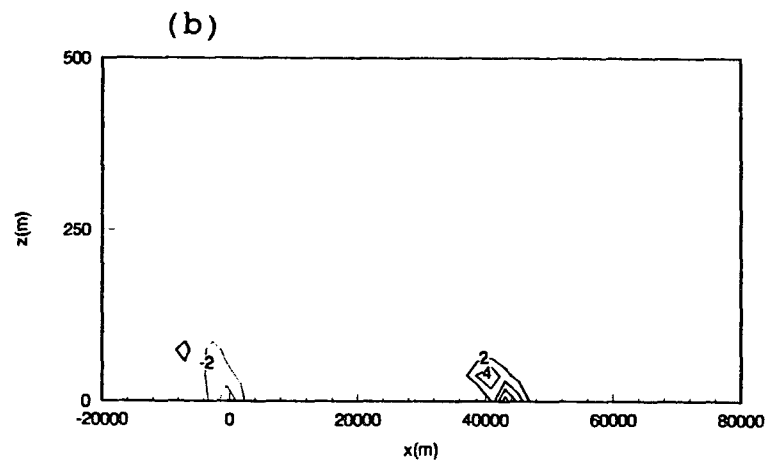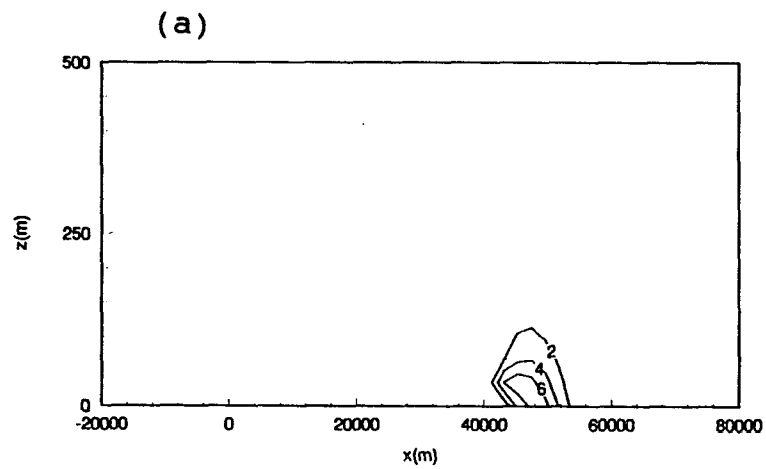
Fig.4.27.Same as Fig.4.22 except at 22 LST.

(a)

(b)
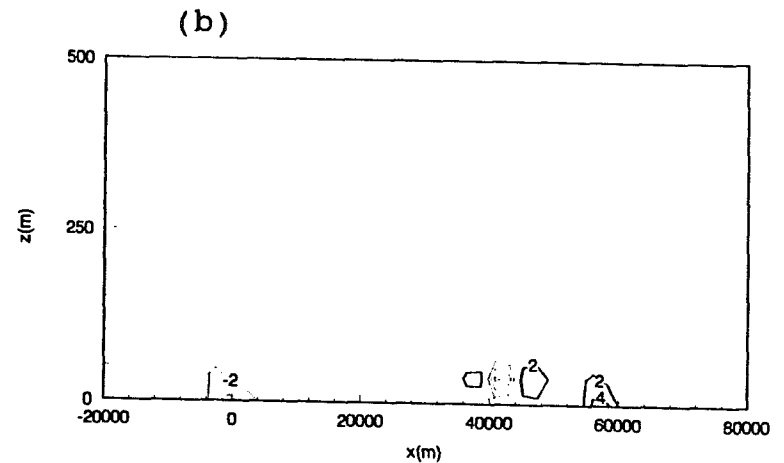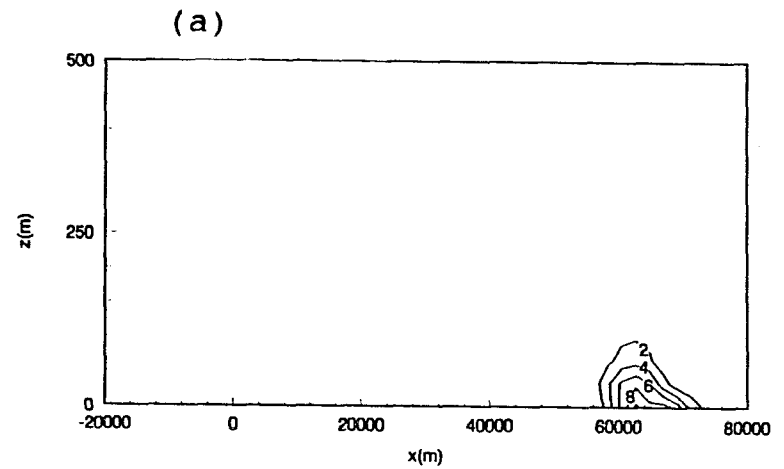
Fig.4.28.Same as Fig.4.22 except at 24 LST.

frontogenesis is the horizontal convergence. This process is also demonstrated in Figures 4.29, 4.31 and 4.33 showing the convergence and turbulent mixing at 12 LST with U_g = 0, -1, and -3 m/sec, respectively. At this time, the front velocities are relatively low and the sea breezes are limited near the shore region, i.e., the initial stage.

After passing the region of the turbulence after 16 LST, the front starts to accelerate and move with higher and constant speed (Figures 4.30, 4.32 and 4.34).

The turbulent mixing lasts until 20 LST near the coastal region. This turbulence barrier near the shoreline might be the result of the boundary layer transition between land and sea. Both the heating of the land surface and the surface roughness changes at the coastline. The boundary layer over the sea is shallower and smoother than that over the land. Velocity variances and vertical eddy viscosity in Figure 4.20 also support the concept of weaker boundary layer mixing over the sea. The sudden expansion of the boundary layer and the large increase in vertical turbulent mixing near the shoreline might result in the strong turbulent mixing just inside of the shoreline that arrests the penetration of the sea breeze.

In late evening, the convergence frontogenesis shown in Figures 4.27 and 4.28 increases due to sharp horizontal gradient of the temperature and velocity. It may be the
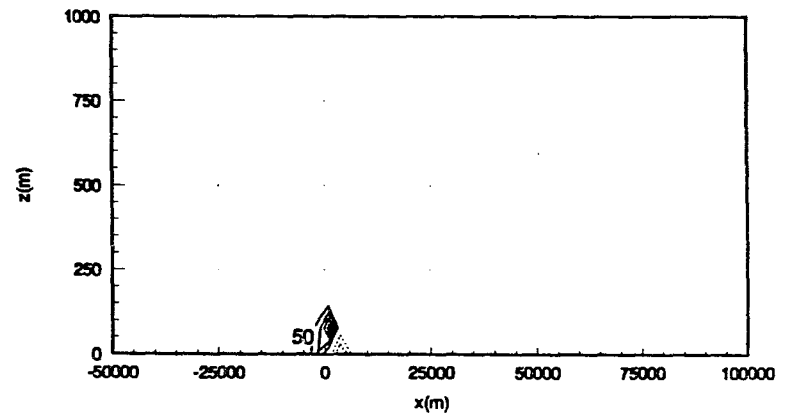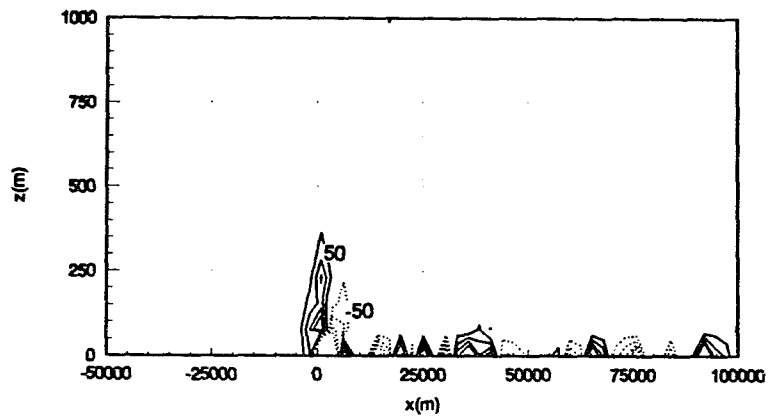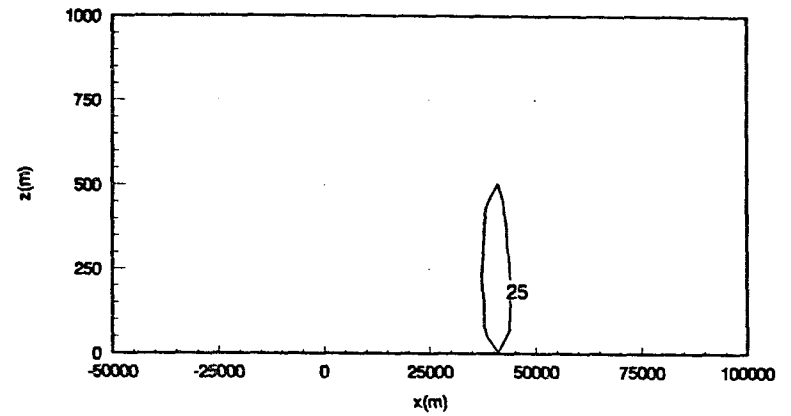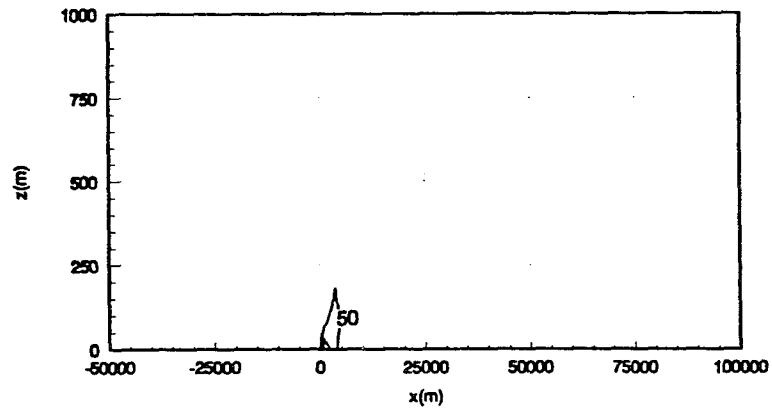
Fig.4.29. Frontogenesis of (a)horizontal convergence and (b)horizontal gradients of the vertical turbulent flux at 12 LST for Case H and U_g = 0 m/sec. Contour interval is 5×10^{-7} K/m/sec. Solid line is for a positive value and dashed line for the negative.

Fig.4.30.Same as Fig.4.29 except at 18 LST.
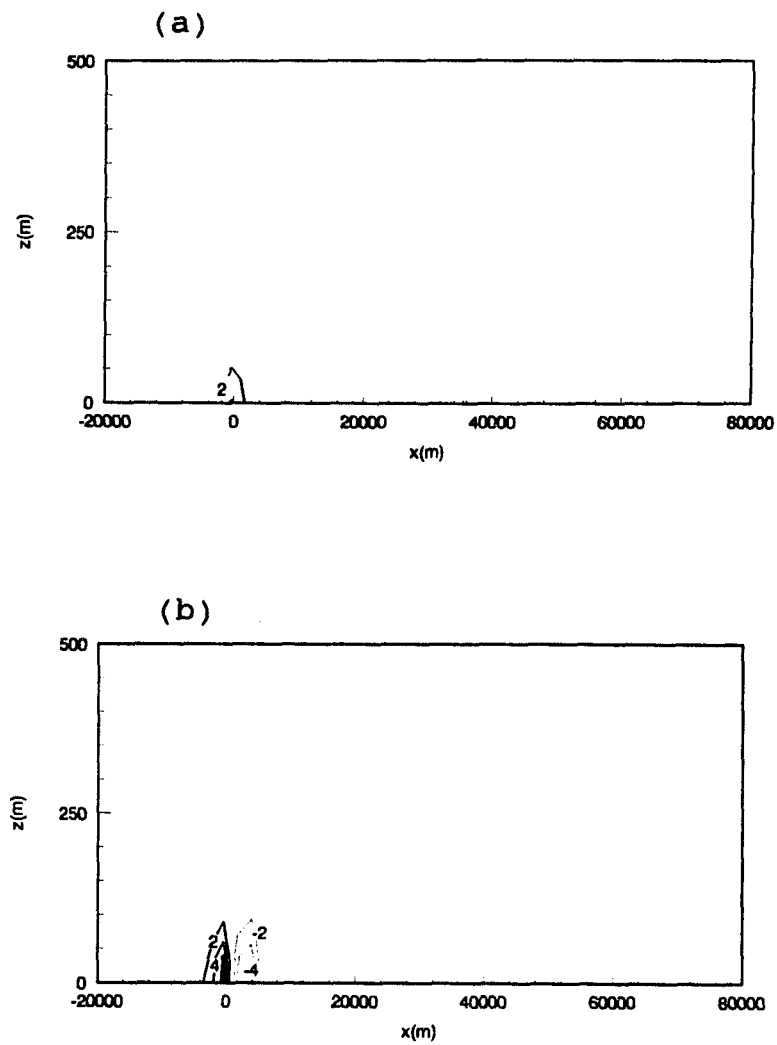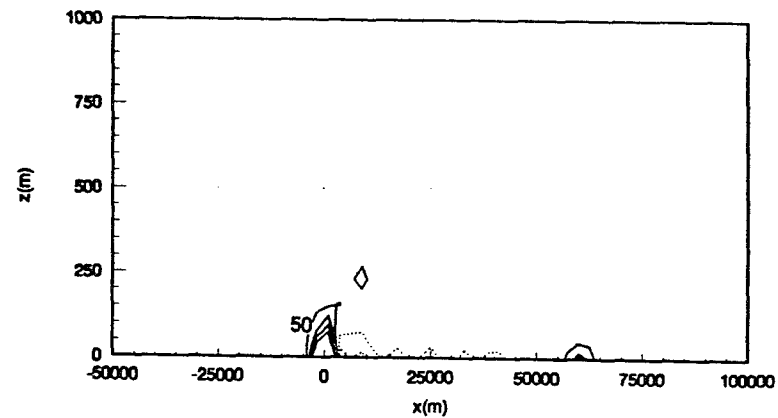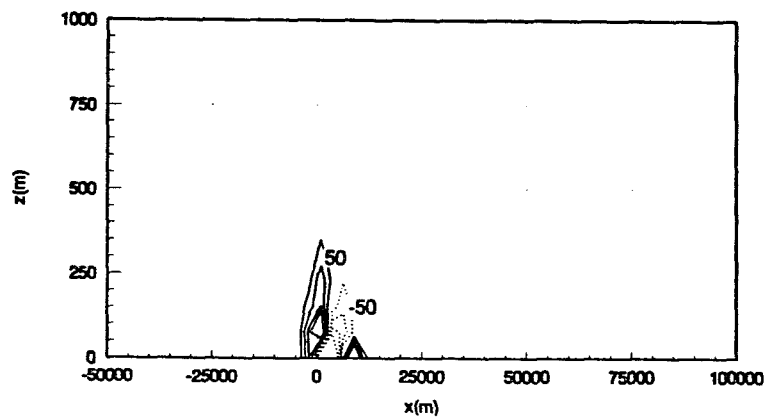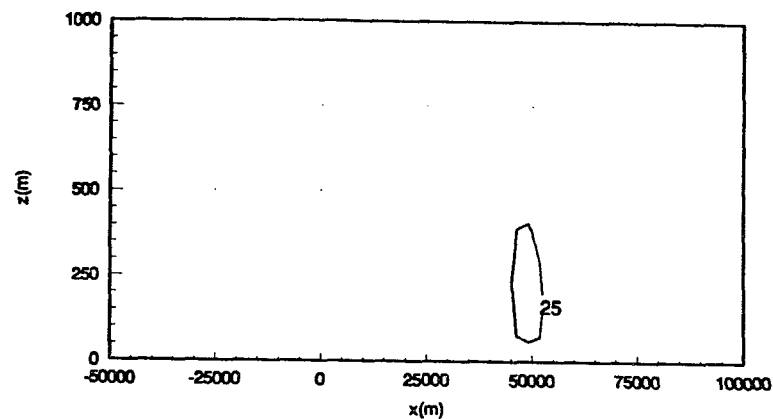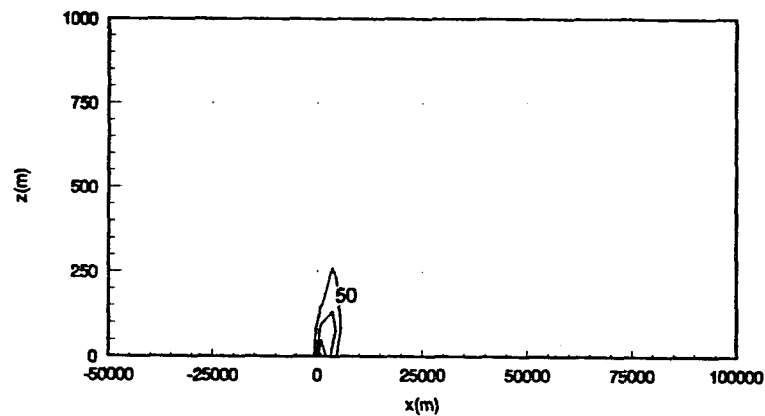
Fig.4.31. Frontogenesis of (a)horizontal convergence and (b)horizontal gradients of the vertical turbulent flux at 12 LST for Case H and $U_g = 1$ m/sec. Contour interval is 5×10^{-7} K/m/sec. Solid line is for a positive value and dashed line for the negative.

Fig.4.32.Same as Fig.4.31 except at 18 LST.
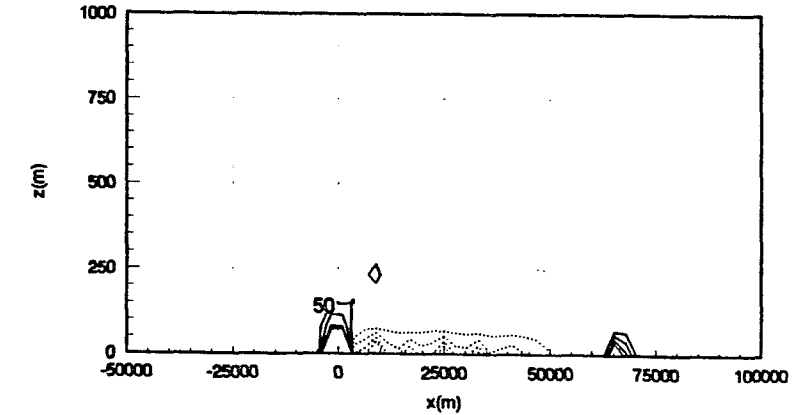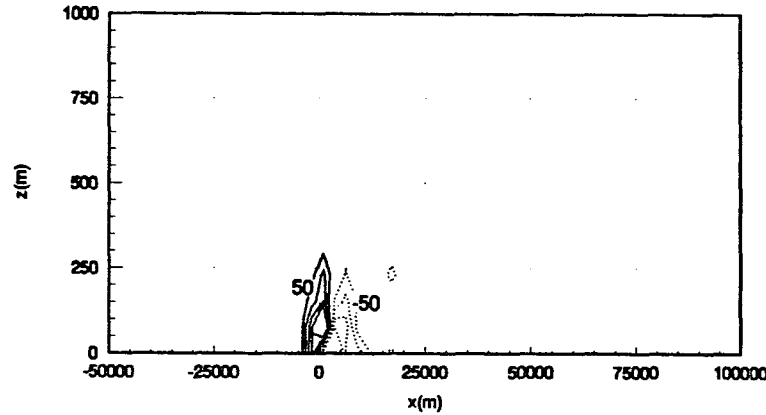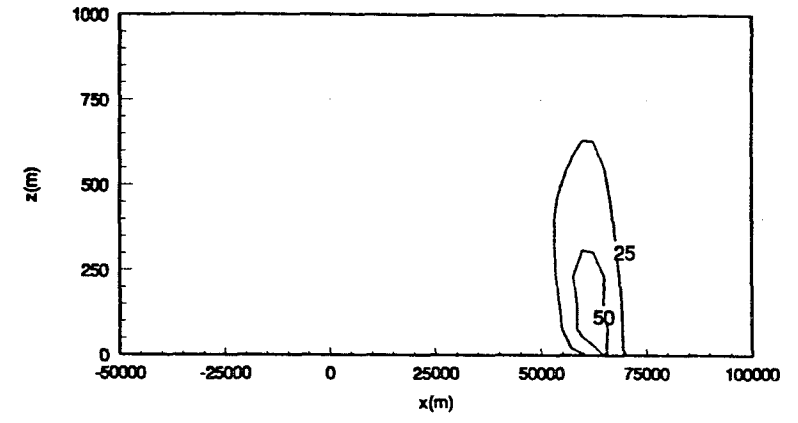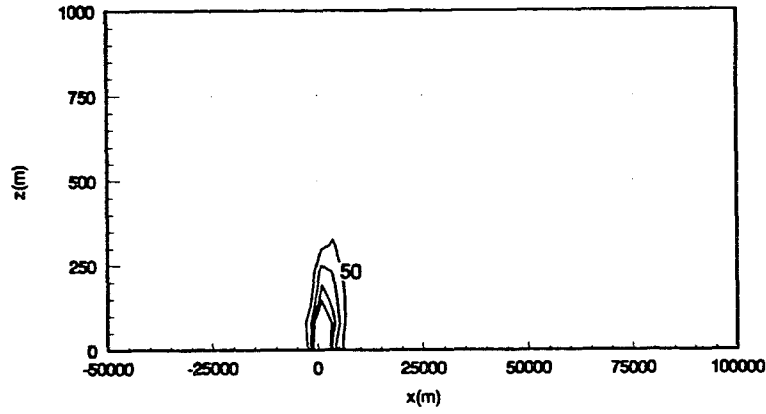
Fig.4.33. Frontogenesis of (a)horizontal convergence and (b)horizontal gradients of the vertical turbulent flux at 12 LST for Case H and U_g = 3 m/sec. Contour interval is 5×10^{-7} K/m/sec. Solid line is for a positive value and dashed line for the negative.

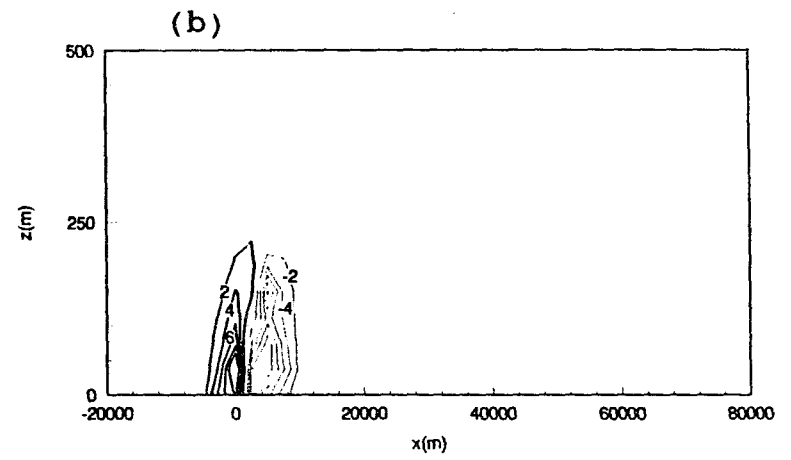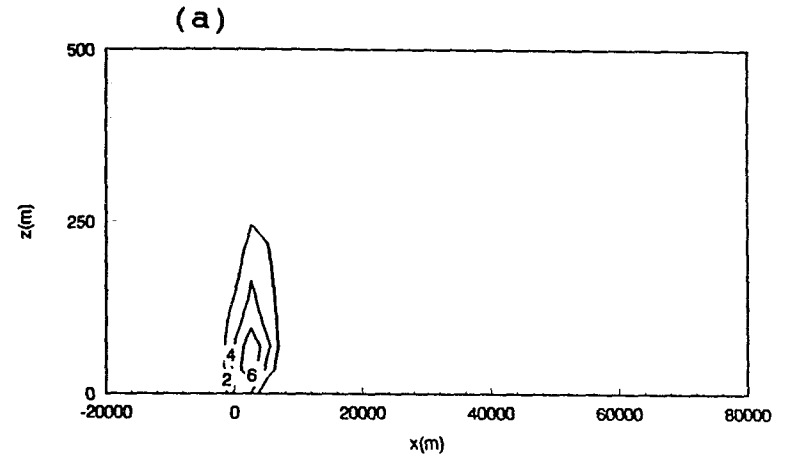Fig.4.34. Same as Fig.4.33 except at 18 LST.

driving force to form the gravity current shown in Figure 4.21.

4.3.3. Pollutant Transport

In order to understand the mechanism of pollutant transport near the coastal region, two cases have been simulated. One is from the residual pollutants above the sea and the other is from the plumes emitted from an elevated line source at night.

Reible et al. (1983) developed a two-layer air pollution model to investigate the inter-layer mixing between the surface mixed layer and the residual plume aloft. They concluded that the exchange rate between the air aloft and the surface mixing layer is large enough that the pollutants aloft should be considered when describing the multi-day impacts of pollutants. In the coastal area, the mixed layer is normally developed in the daytime and the height of the mixed layer over the land is much higher than the height of the boundary layer over the sea. The ground based pollutants are well mixed within the mixed layer. As the land surface cools down in the evening, the mixed layer quickly turns into stable boundary layer and the depth of mixing is much shallower and limited to near the ground. The residual pollutant plumes aloft however remain unmixed. The residual plume is often expected to move toward the sea by the nighttime offshore winds. In order to describe this residual plume above the sea, the residual plume was placed

from the height of 413m to 1055 m over the sea at 08 LST with dimensionless concentration 1.

Figure 4.35 shows the movement of the residual plume as the daytime sea breeze develops. The meteorological conditions for the sea breeze was U_g = -1m/sec and Case H. The residual plume starts to move downward as the sea breeze develops near the shore at 12 LST. The following flow of the sea breeze carries the residual plume to the land and then to the front around 14 LST (Figure 4.35 (b)). The pollutants can move back toward the sea with the return flow in the late afternoon and evening. These pollutant plumes might be another residual plume in the following day.

A further investigation of contaminant transport was undertaken by considering elevated stack pollutants at night. The plume emitted from the stack was assumed to be emitted from an elevated line source which was homogeneously mixed within one grid. The location of the grid which contained the stack was 313 m < z < 448 and 0 < x < 2000 m. The pollutants were emitted from 24 LST to 6 LST. The emission rate of pollutants was 2.7 mg/sec. Figure 4.36 shows the transport of pollutants with time. All pollutants were transported to the sea and they formed narrow band of pollutant zone over sea in Figure 4.36 (a). It shows that the pollutants dispersed very little and moved out to the sea under the stably stratified night time condition. The calculation indicated little mixing over sea even if there

(a)12 LST

(b)14 LST

(c)16 LST
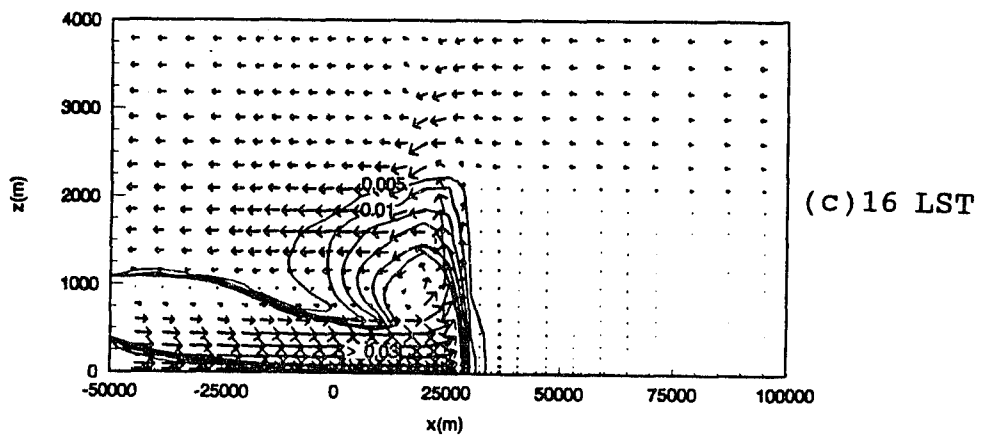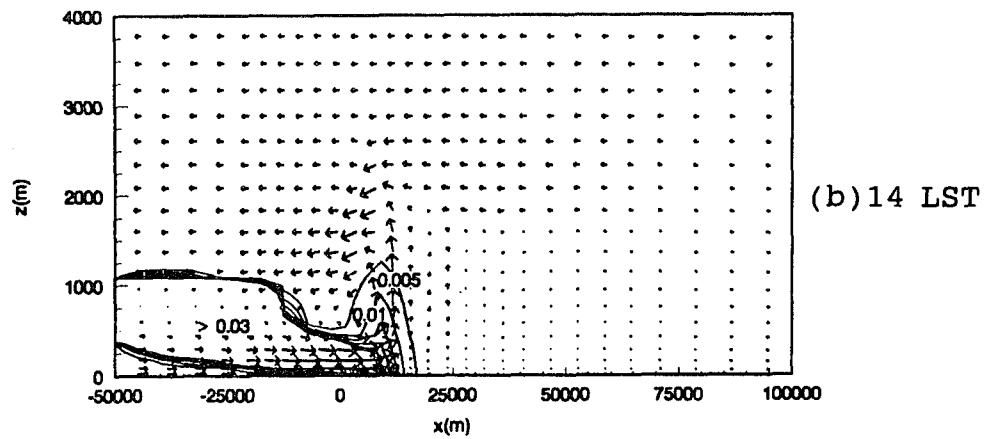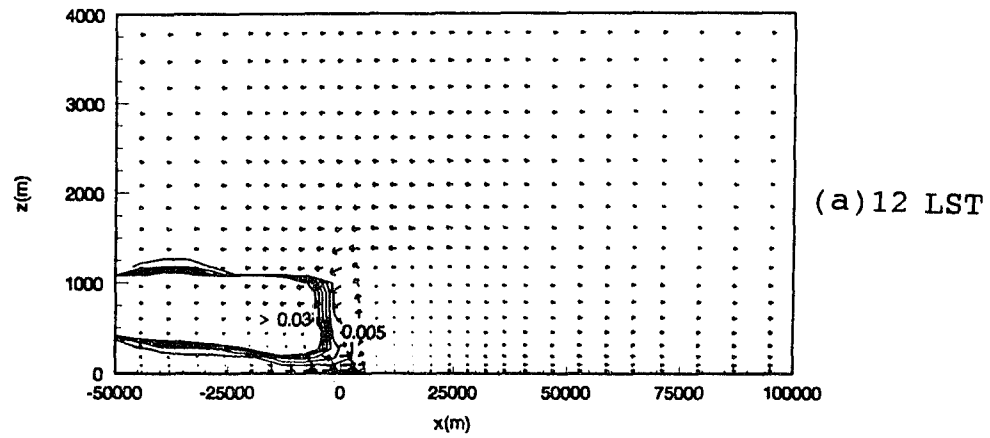
Fig.4.35. Variations of concentration of residual pollutants aloft with time. Fig. continued.

(d) 18 LST

(e) 20 LST

(f) 22 LST
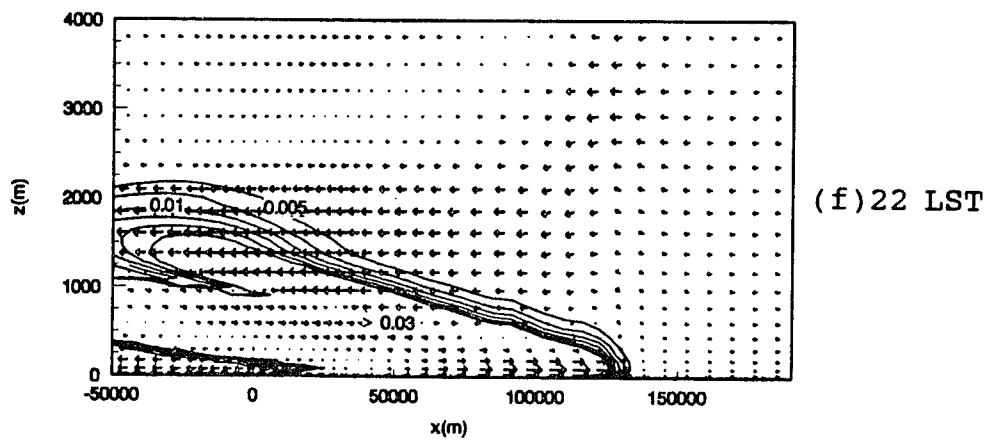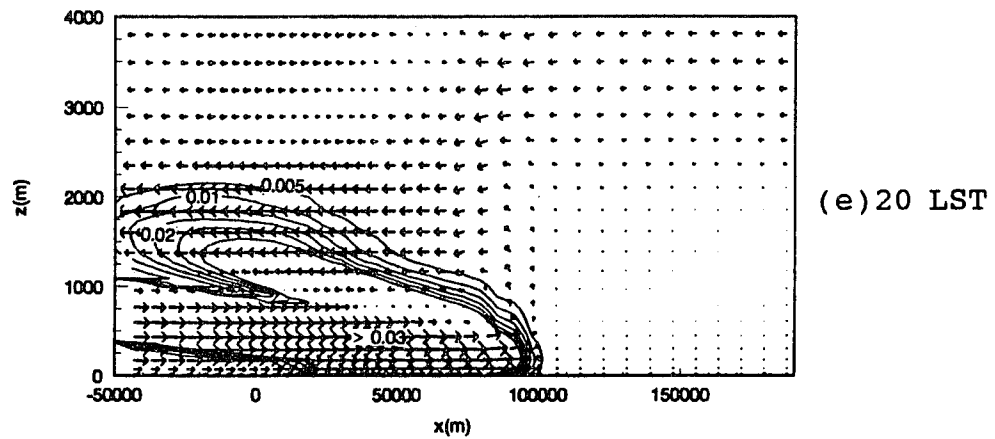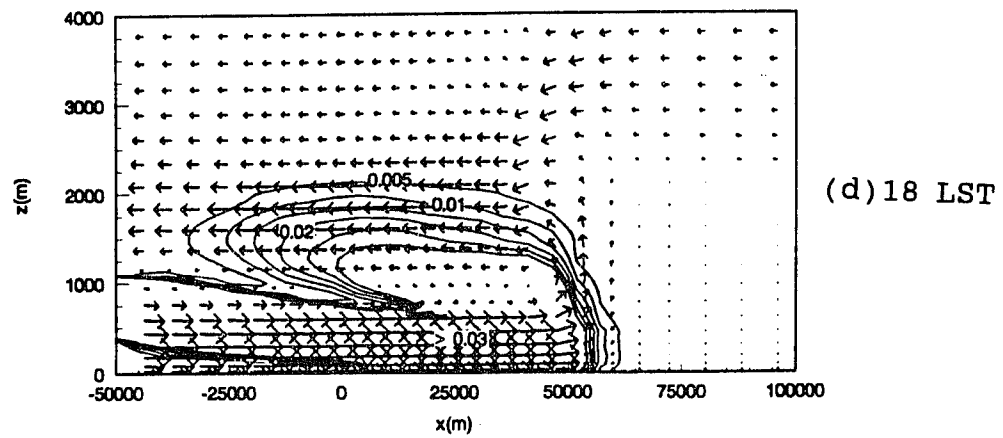
Fig. Continued. Note x-scale changes in (e) and (f).

Fig.4.36. Variations of pollutant concentration emitted from an elevated line source at night with time. Fig. continued.

(d)16 LST

(e)18 LST

(f)20 LST
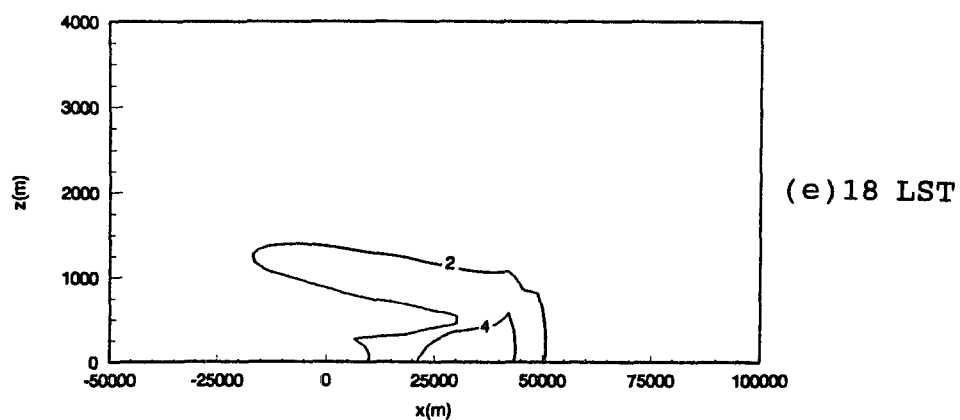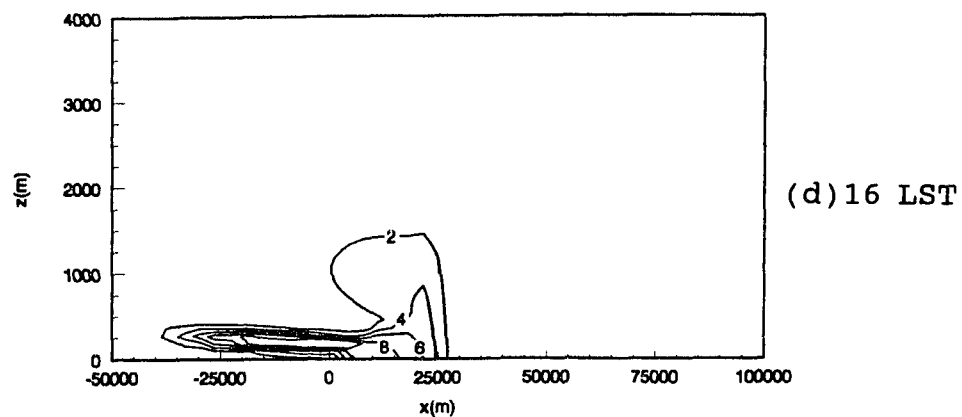
Fig. Continued. Note x- and contour scale changes in (f).

was a land breeze at nighttime. The calculated depth of mixing layer by the land breeze was below 100m. The plume emitted from the elevated line source did not reach to the sea. Shair et al. (1982) and McRae (1981), however, showed that the large portion of the plume emitted from the stack during the night time fumigated and downmixed to the sea level by the connectively mixed layer. Meteorological conditions favorable for the strong land breeze should be incorporated to simulate the fumigation over the sea under the land breeze.

The emitted plume was transported back to the land with the following day sea breeze. The elevated plume by the front also moves back to the sea by the return flow. Consistent with the experiment of Shair et al. (1982), all the pollutants emitted from the nighttime according to the calculation pass the shoreline by 18 LST.

4.3.4. TIBL and Fumigation

As discussed in the previous section, the TIBL is formed as the sea breeze carries cooler sea air into the warm land. The typical TIBL is shown in Figures 4.9(b), 4.14(b), 4.16(b) and 4.18(b) with the temperature profile over the whole calculation domain. In order to understand the vertical temperature profile with height, the vertical temperature profiles with various distances from the shoreline are plotted in Figure 4.37. The conditions for the sea breeze was U_g = -1 m/sec and Case H. The temperature
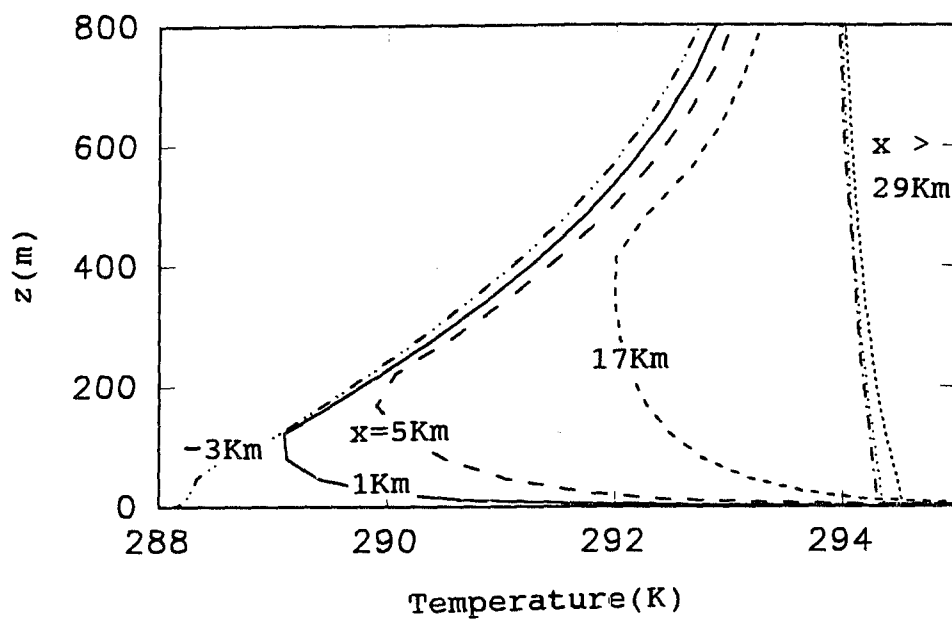
(a)16 LST
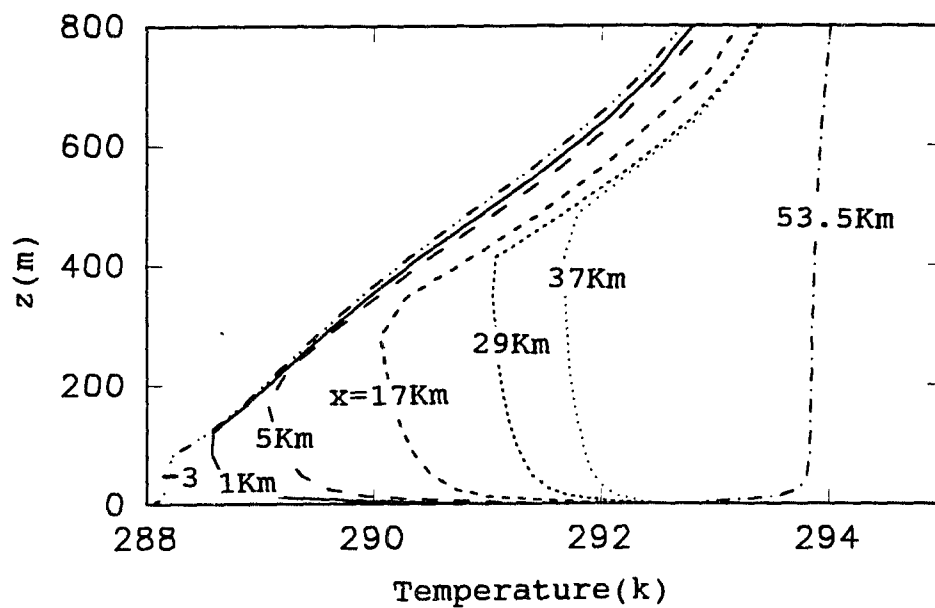
(b)18 LST

Fig.4.37. Vertical profiles of temperatures at various distances from the shoreline(x).

profiles show strong unstable condition near the ground and relatively constant value in the TIBL and stable layer over the TIBL. The height of TIBL was calculated from the height which the vertical temperature gradient (temperature lapse rate) was greater than 3.3 K/km. The TIBL was formed to x=17km at 16 LST and to x=37 km at 18 LST. The height of TIBL is plotted against the fetch $x^{0.5}$ in Figure 4.38. According to summary study of Stunder and Sethuraman (1985), the general relations between the height and the fetch is z_i = A $x^{0.5}$. A is a proportionality constant representing meteorological conditions. The calculated A is 2.47 at 18 LST. Hsu (1986) evaluated A value from the available data from various observations and set the range of A value from 1.15 to 2.67 with 95 confidence limit. The calculated value is within the range.

The velocity variances are compared with typical convective ABL in Figure 4.39 and the calculated surface layer parameters are in Table 4.2.

Table 4.2. Calculated surface layer parameters in the TIBL.

x(Km)	z_i(m)	u_*(ms^{-1})	Q_s(Kms^{-1})	w_*(ms^{-1})
5	200	1.11	0.095	0.86
17	319	1.11	0.066	0.89
29	418	1.08	0.033	0.78

The velocity variances show a good agreement with observations in the convective ABL. It means that TIBL is
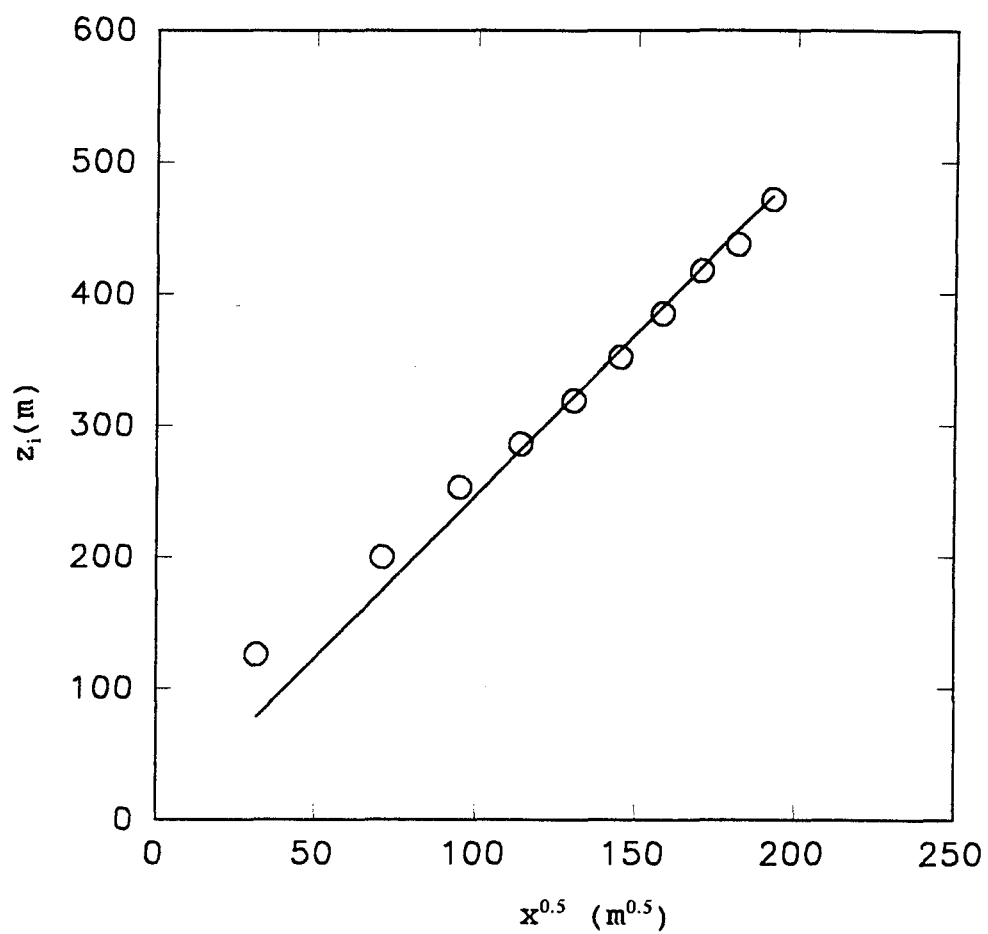
Fig.4.38. Height of TIBL(z_i) along $x^{0.5}$. Circles are for the calculated and solid line for $z_i = 2.47\ x^{0.5}$.

$$\dfrac{z}{z_i}$$

$$\dfrac{\overline{w'^2}}{w_*^2}$$
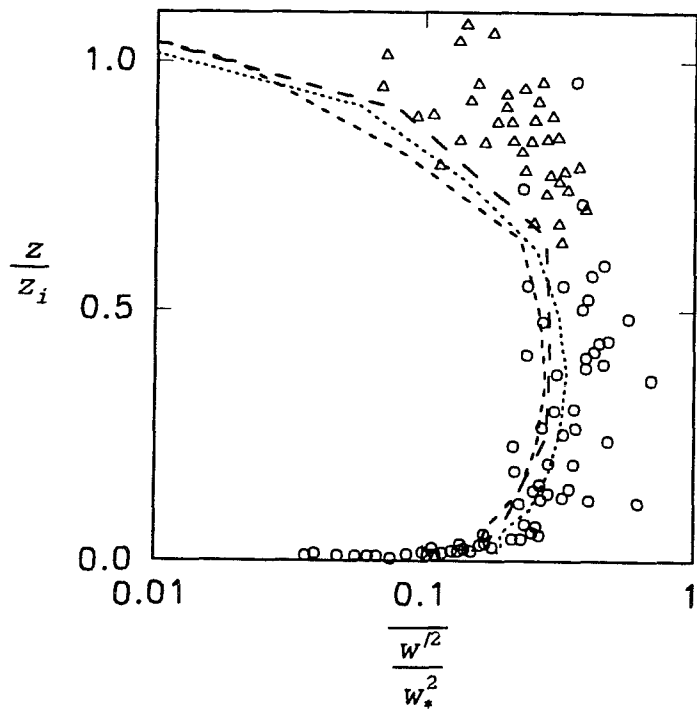
(a) Vertical velocity variance

$$\dfrac{(\overline{u'^2} + \overline{v'^2})}{2\,w_*^2}$$
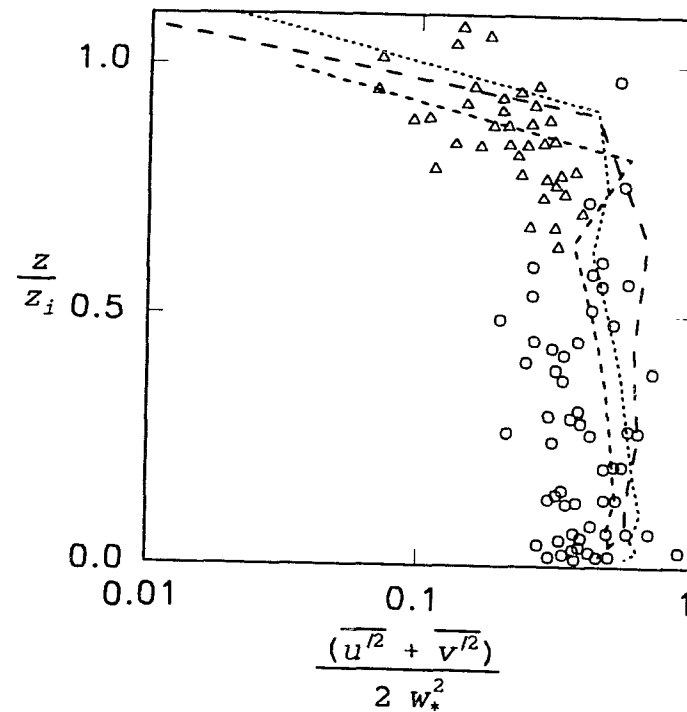
(b) Horizontal velocity variance

Fig.4.39. Velocity variances in the TIBL at various distances from the shoreline. Long dashed line is for x=5Km, medium dashed for x=17Km, and short dashed for x=29Km. Circles are data from Caughey and Palmer (1979) and triangles from Minnesota and Ashchurch data.

well developed convective mixed layer. The velocity variances also show good agreement with the observation of Durand et al. (1989) (not shown in Figure 4.39). They observed the velocity variances in wide range of x distance, i.e., up to 40 km from the shoreline. The range of x is similar to that of this calculation. Measurements of Ohara and Ogawa (1985) and Ogawa et al. (1986) , however, showed smaller values of velocity variances in the TIBL than those in the convective ABL and had difficulties in normalization of the velocity variances by convective velocity scale (w_*). Their observation sites were limited to within 3km from the shoreline. As shown in Figure 4.37, the temperature profiles at x=-3km and x= 1km show the initial height of TIBL. As shown in Figure 4.38, the initial height of TIBL deviates from the expected square root dependence near the shore. This means that the temperature of the following flow was increased by the subsidence of the return flow. It might partially contribute to difficulties of the analysis of Ohara and Ogawa (1985) and Ogawa et al. (1986).

In order to simulate the fumigation in the TIBL, the pollutants were assumed to be emitted from an elevated stack, i.e., elevated line source. The location of the source and emission rate were the same as described previous section. The emission started from 08 LST. Figure 4.40 shows the pollutant transport with time. The plumes emitted from the elevated line source are widely diffused near the
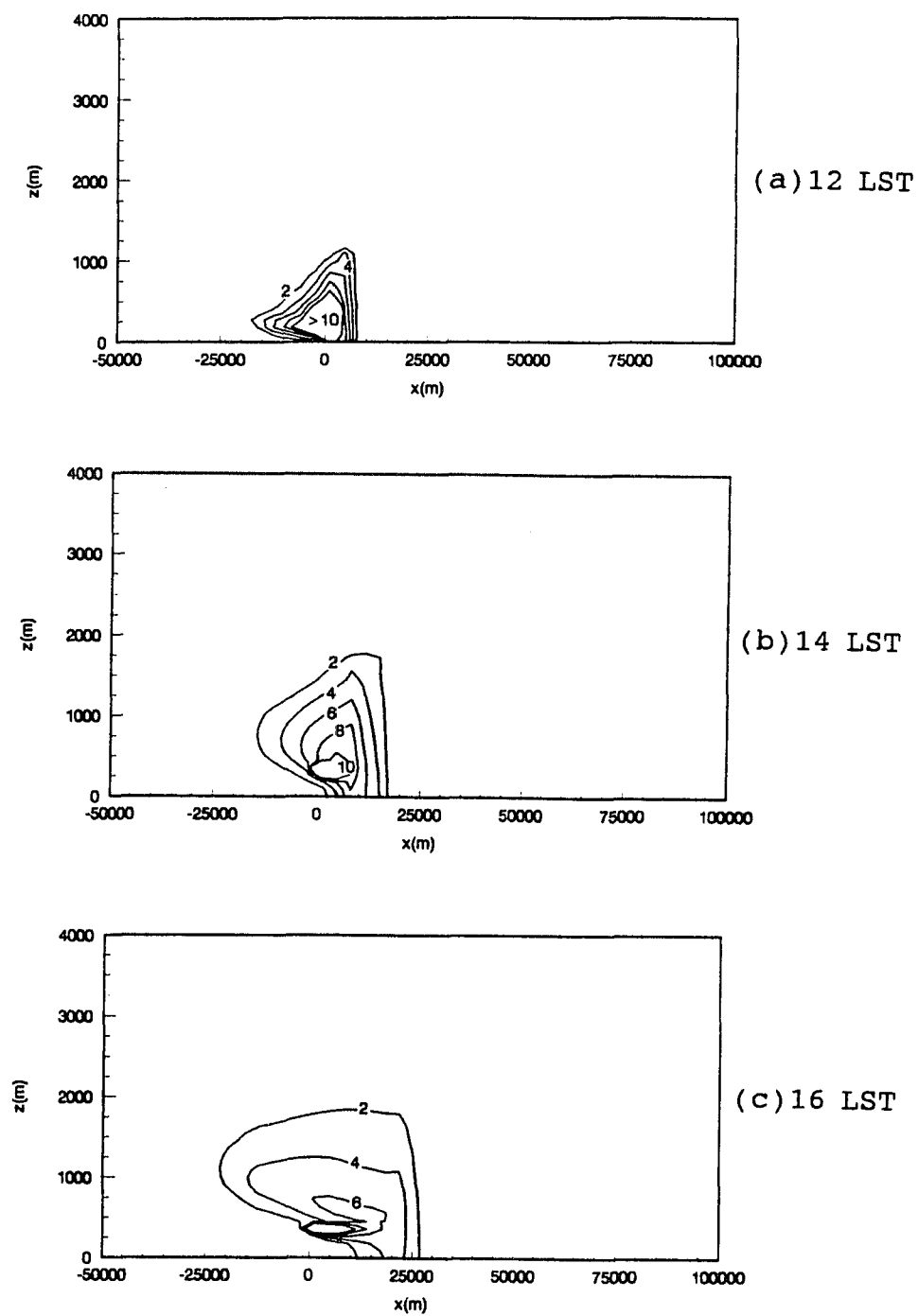
Fig.4.40. Variations of pollutant concentration emitted
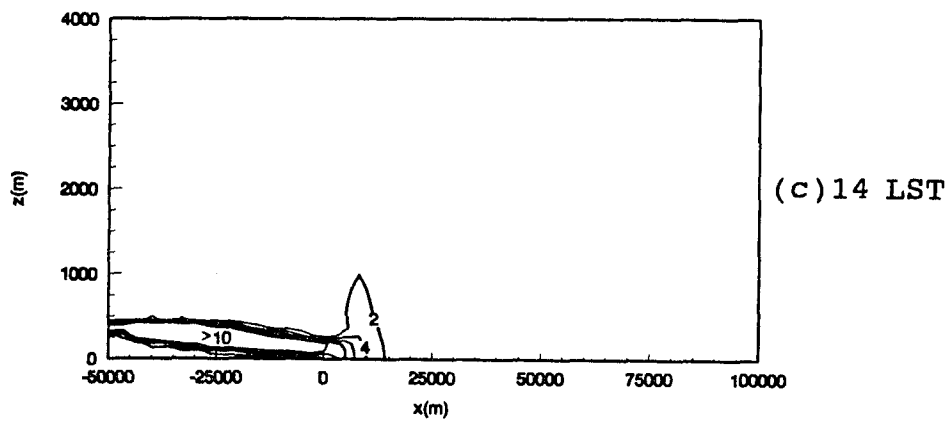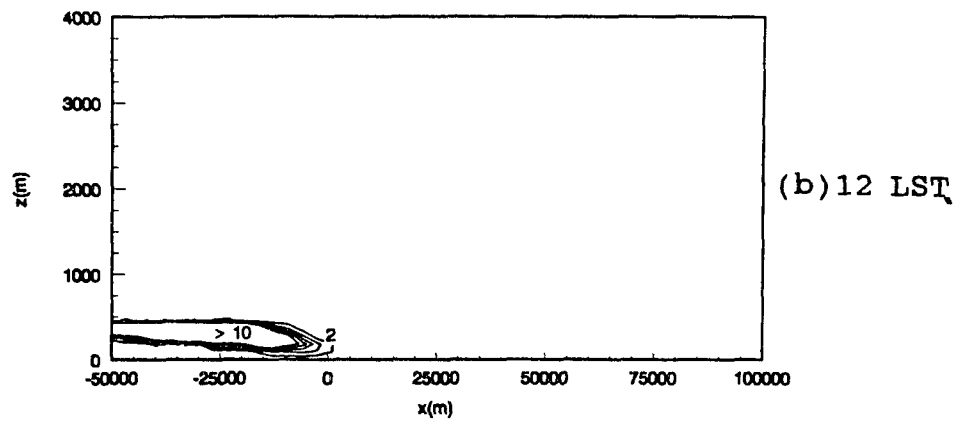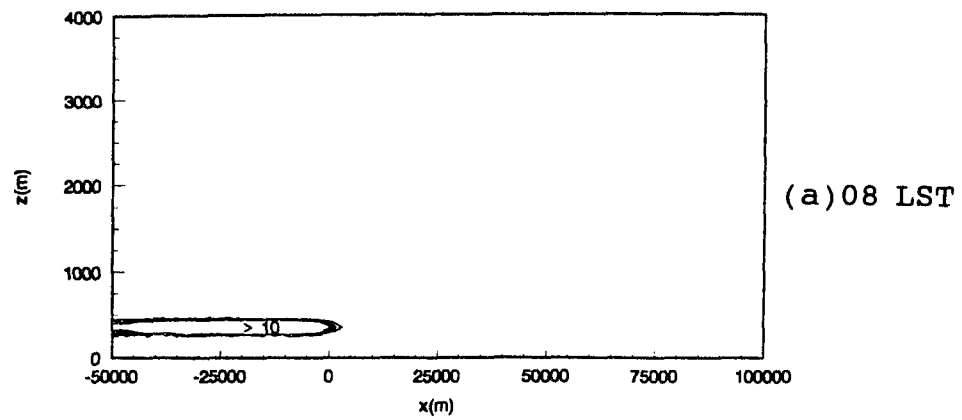from an elevated line source during a day with time.
Fig. continued.
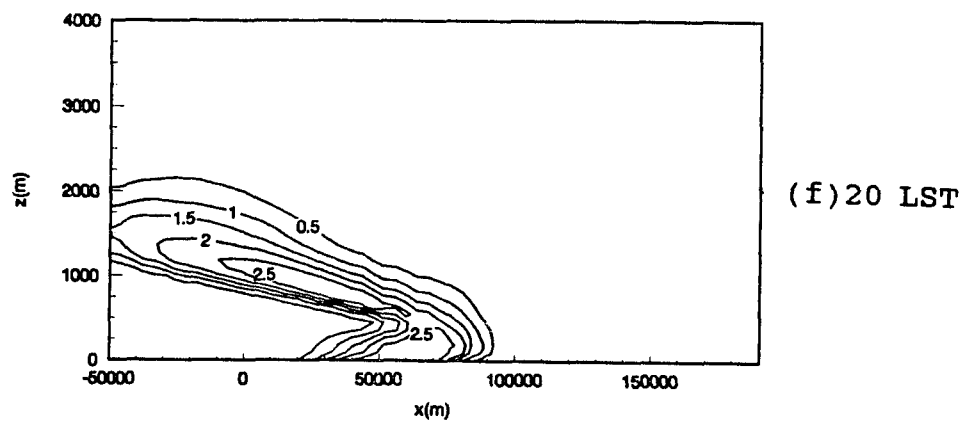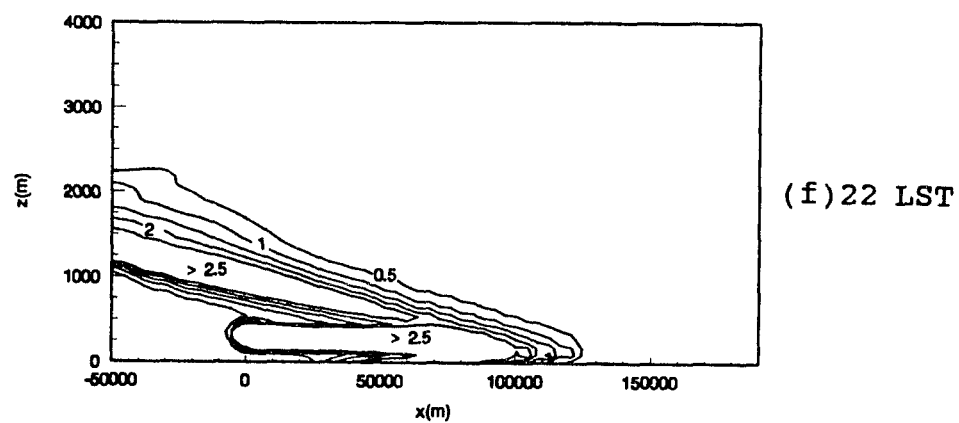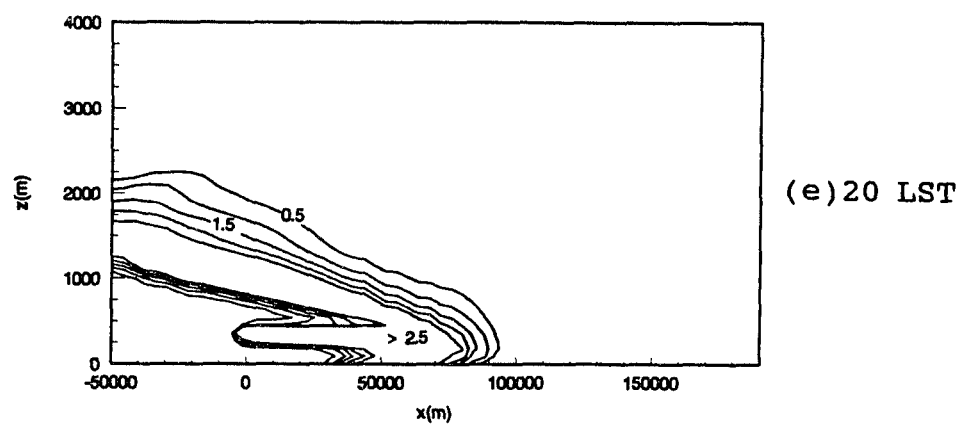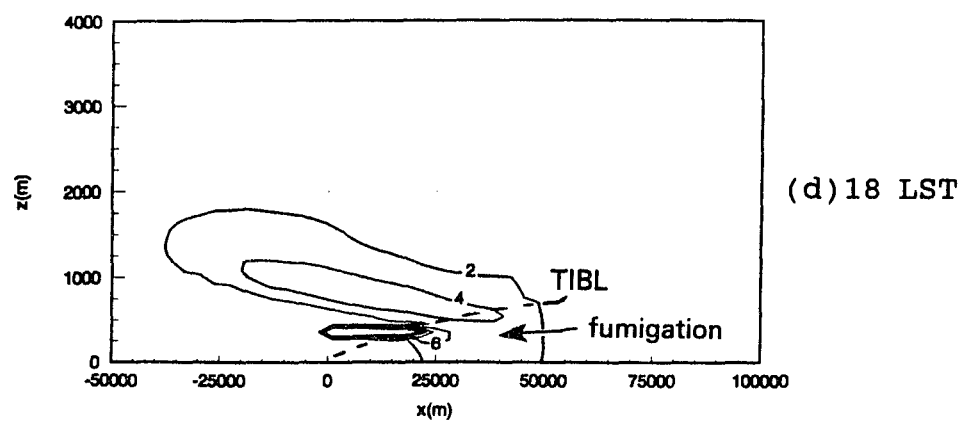
Fig. Continued. Note x- and contour scale changes in (e) and (f).

shoreline at the initial stage of the sea breeze. As the front moves toward the land, the pollutants follow the movement of the sea breeze. A large portion of the pollutants also moves back toward the sea by the return flow. Ultimately, the elevated pollutants fumigate as shown in Figure 4.40 (d) at 18 LST. The vertical profiles of the concentration with various distances from the shore are shown in Figure 4.41. The heights of TIBL based on the vertical concentration profile (solid circle in Figure 4.41) correspond to those calculated from the vertical temperature profile. The low height of incoming plume in the stable layer is 313 m. x value corresponding to z_i = 313 m can be calculated from Figure 4.38 and it is 16 km. The incoming plume is expected to intersect with the TIBL at x=16 km. The vertical concentration profiles at x=29 and 37 km show uniform values in the TIBL. It also supports that the TIBL is well-mixed convective layer. Figure 4.42 shows the ground level concentrations with time. The x position of maximum ground level concentration at 18 LST is 37km whereas the x position of intersection of plume with the TIBL is 16 km. The profiles of ground level concentration along the distance from the shoreline and the location of the maximum ground concentration are similar to the observations of Nanticoke experiment and similarity model (Misra and Onlock, 1982; Kerman, 1982).
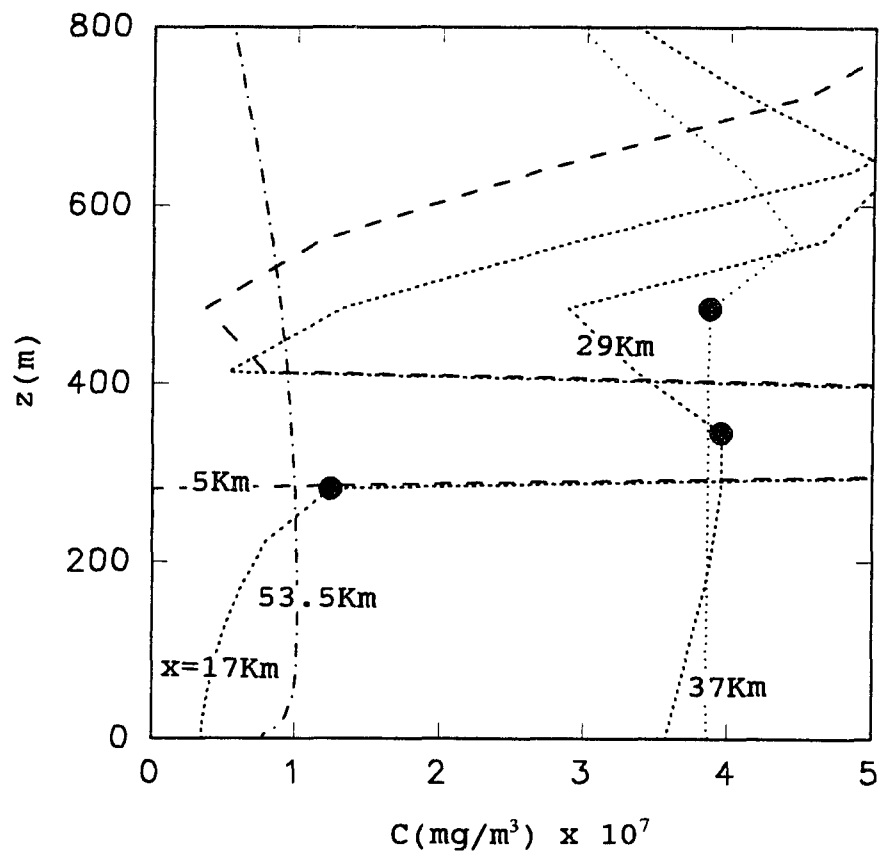
Fig.4.41· Concentration profiles along the height at various distances from the shoreline. Solid circles indicate positions of TIBL.
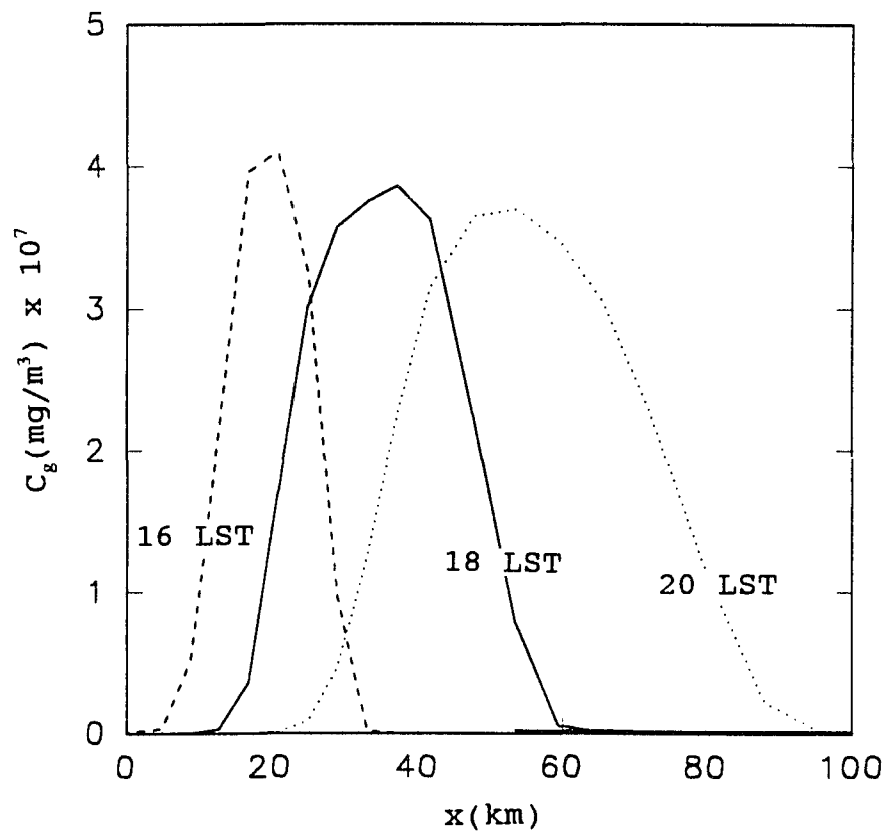
Fig.4.42. Ground level concentrations (C_g) with time.

4.4. Conclusions

The modified E-ϵ model with full nonhydrostatic equations was applied to the sea breeze circulation. The detailed structures of the sea breeze, such as the initial stage observed in early afternoon, the developed stage in late afternoon, the gravity current in late evening can be reproduced. The frontogenesis analysis with time of day shows that the turbulent mixing which is formed in the shore region deters the inland penetration of the front in the initial stage. Once the region of convergence passes through or overcomes the mixed region, the front starts to accelerate and penetrate far inland.

The flow model was also used to simulate pollutant transport by considering the previous day's residual contaminants remaining over the sea at the start of the sea breeze and by considering fumigation from an elevated line source. The residual plume over the sea has great impact on the ground level concentration in the following day sea breeze and it should be considered in the pollutant transport near the coastal region. All the plumes emitted from the elevated line source during the nighttime return inland with the subsequent afternoon sea breeze. Velocity variances, temperature, concentration profile with height in the TIBL show typical convective ABL profiles. The fumigation in the TIBL is reproduced and it shows a good agreement with observations and similarity theory.

Chapter 5. Manipulation of the Atmospheric Boundary Layer by a Thermal Fence

5.1. Introduction

Due to limited dispersion under the nighttime stable condition, odors and pollutants from ground based pollutant sources such as landfills are often detected at nearby residences (Figure 5.1(a)). If the boundary layer is expanded or the dispersion of pollutants increases, effects of the pollutants on the residences may be reduced. In order to enhance the dispersion or to expand the boundary layer, forming a thermal fence has been proposed as a possible means to manipulate the ABL as shown in Figure 5.1(b). The thermal fence could serve to destroy the stable stratification occurring under the nighttime stable condition and result in greater vertical mixing of the pollutants and odors. The model developed herein is capable of modeling flow and transport in stable anisotropic and neutral conditions and therefore should be applicable to describing the behavior under these conditions.

A solid obstacle has been used to reduce pollutant concentration at the flow downstream in a neutral atmospheric flow and its application is quite successful (Suttan et al., 1986; Mouzakis et al., 1991). They used the standard E-ϵ model for the simulation of the neutral boundary layer flow and did not consider geostrophic wind

Boundary layer

Pollutants

Residential area

Landfill

(a) No control case

Thermal fence

Residential area
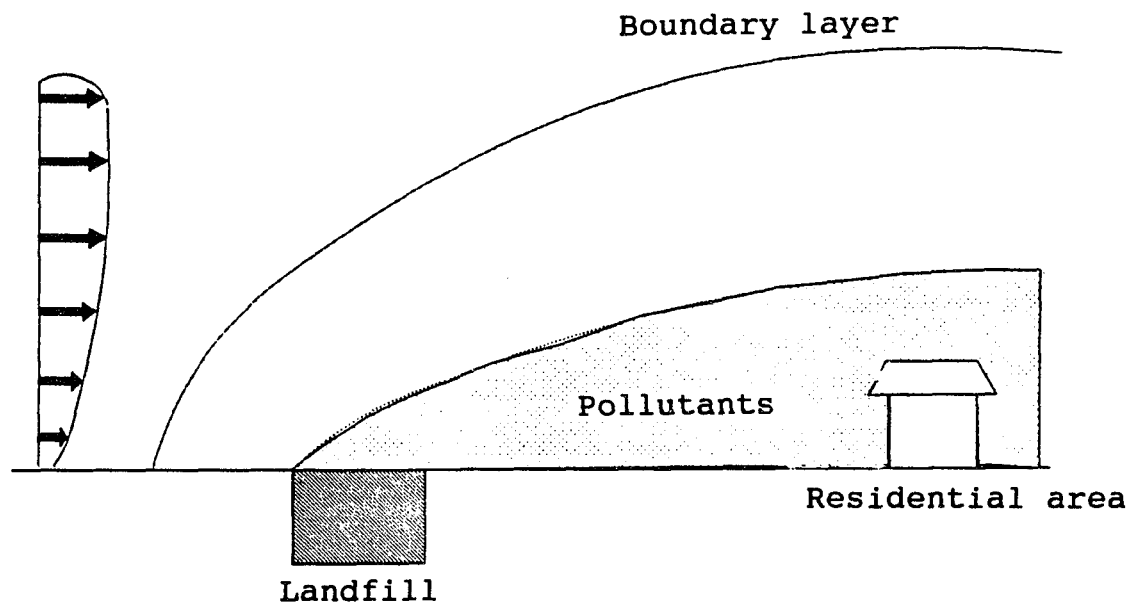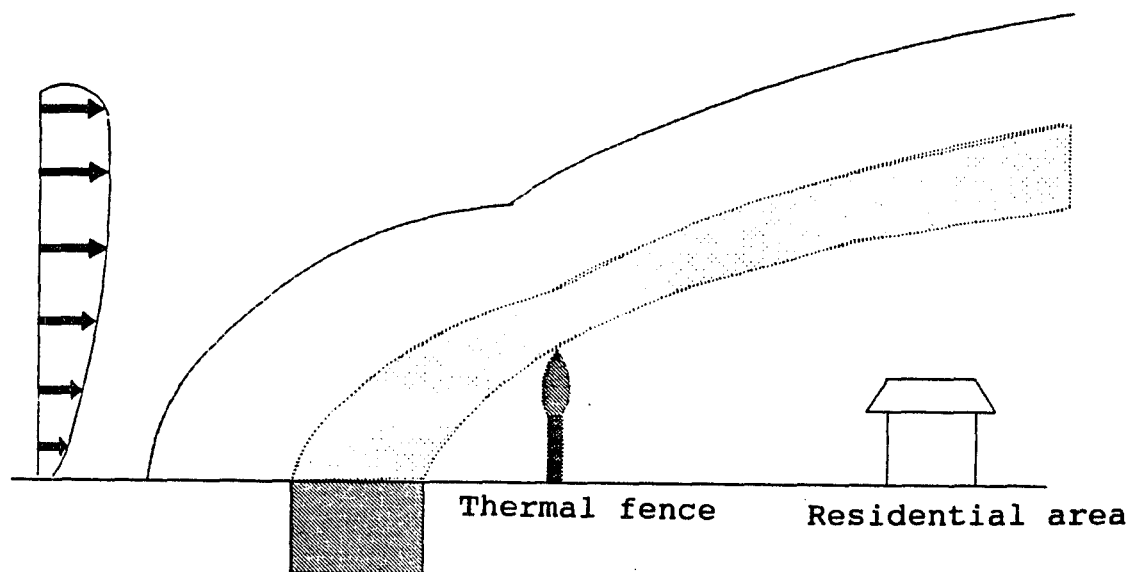
(b) Expanded ABL

Fig.5.1. Schematic representation of the manipulation of ABL by a thermal fence.

effects on the pollutant transport because the domain of interest was within the surface layer of the ABL.

In the case of the thermal fence, the flow situation is quite different from that of the obstacle because the buoyancy force plays an important role. A related topic is the forest fire (Albini,1984; Beer, 1991; Kondo and Kuwagata, 1992; Luti, 1980). Luti (1980) applied the standard E-ϵ model to study a transient atmospheric flow development with a fire. According to his study, there is strong mixing and circulation induced by the heat source of the fire. Strong mixing behind the heat source is expected to homogenize the stable stratification and enhance the dispersion.

In order to understand the interaction of the thermal fence with the environmental atmospheric flow and its effect on the dispersion of the pollutants, the modified E-ϵ model was applied to the thermal fence. The neutral and stable ABLs were considered as the case study.

5.2. Descriptions of Model Calculation

The governing equations and the numerical method are the same as the equations for the sea breeze circulation described in Chapter 4 except the assumption that density change is mainly due to temperature variation. The density was evaluated using the ideal gas equation.

$$\rho = \rho_o \frac{\Theta_o}{\Theta} \qquad (5.1)$$

The subscript o refers to an initial condition.

The horizontal eddy viscosity and diffusivity were assumed to be the same as the vertical values because the domain of interest was relatively small compared with the sea breeze circulation (Luti, 1980).

A schematic of model domain and locations of the pollutants and thermal fence are in Figure 5.2. Detailed dimensions for the neutral and stable ABLs are in Table 5.1. The thermal fence is placed in the middle of the calculation domain and the pollutant source for describing the landfills is located upwind the thermal fence.

Table 5.1. Detailed dimensions for model calculation in the neutral and stable ABL.

	Neutral	Stable
L(m)	4000	2000
H(m)	2000	500
x_f(m)	1997.5	997.5
d_f(m)	5	5
x_c(m)	1440	740
d_c(m)	60	60

The initial conditions for velocities, temperature and turbulent properties were calculated using the one dimensional atmospheric flow model which was described in
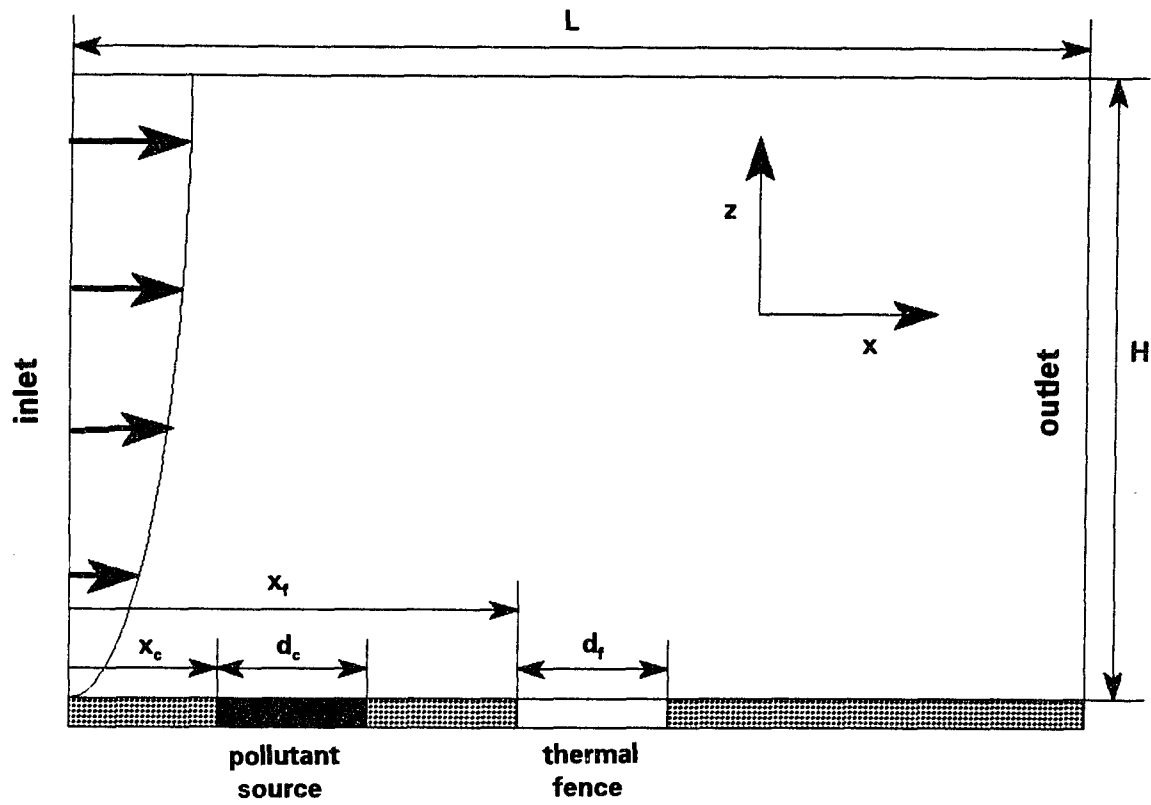
Fig.5.2. Schematic diagram for a model domain and locations of the heat and pollutant sources. Detailed dimensions are in Table 5.1.

Chapter 3. Inlet conditions remained unchanged through the calculation. The initial conditions for the neutral case were chosen to be the nearly neutral case with a background stratification of 10^{-6} K/km and a surface cooling rate of $(d\Theta/dt)_s = -0.003$ K/hr (Case C3 of Table 3.1 in Chapter 3). For the stable ABL, the background stratification was 3.3 K/km and the surface cooling rate was varied from -0.5 K/hr to -1 K/hr. A typical example of the initial conditions for the stable ABL is shown in Figure 5.3. The boundary conditions at the top of the domain were fixed. The initial conditions and the boundary conditions at the ground were the same as those used in the one dimensional flow model in Chapter 3. An impermeable ground condition was used for concentration. At the outlet of the flow, the fluxes for all variables were set to zero. A non-uniform grid was used with 70 grids in the x and z directions. The grid size in the x direction near the thermal fence was 5m and the rest was 60m. The grid size in the z-direction was varied with a logarithmic scale.

5.3. Results and Discussions

5.3.1. Comparisons with an Analytic Solution

In order to verify the accuracy of the dispersion model calculation, it was first used to calculate dispersion under conditions for which an analytic solution exists. The

Fig.5.3. Typical example of initial conditions used for the stable ABL (U_g = 5 m/sec, $(d\Theta/dt)_s$ = -0.5 K/hr).
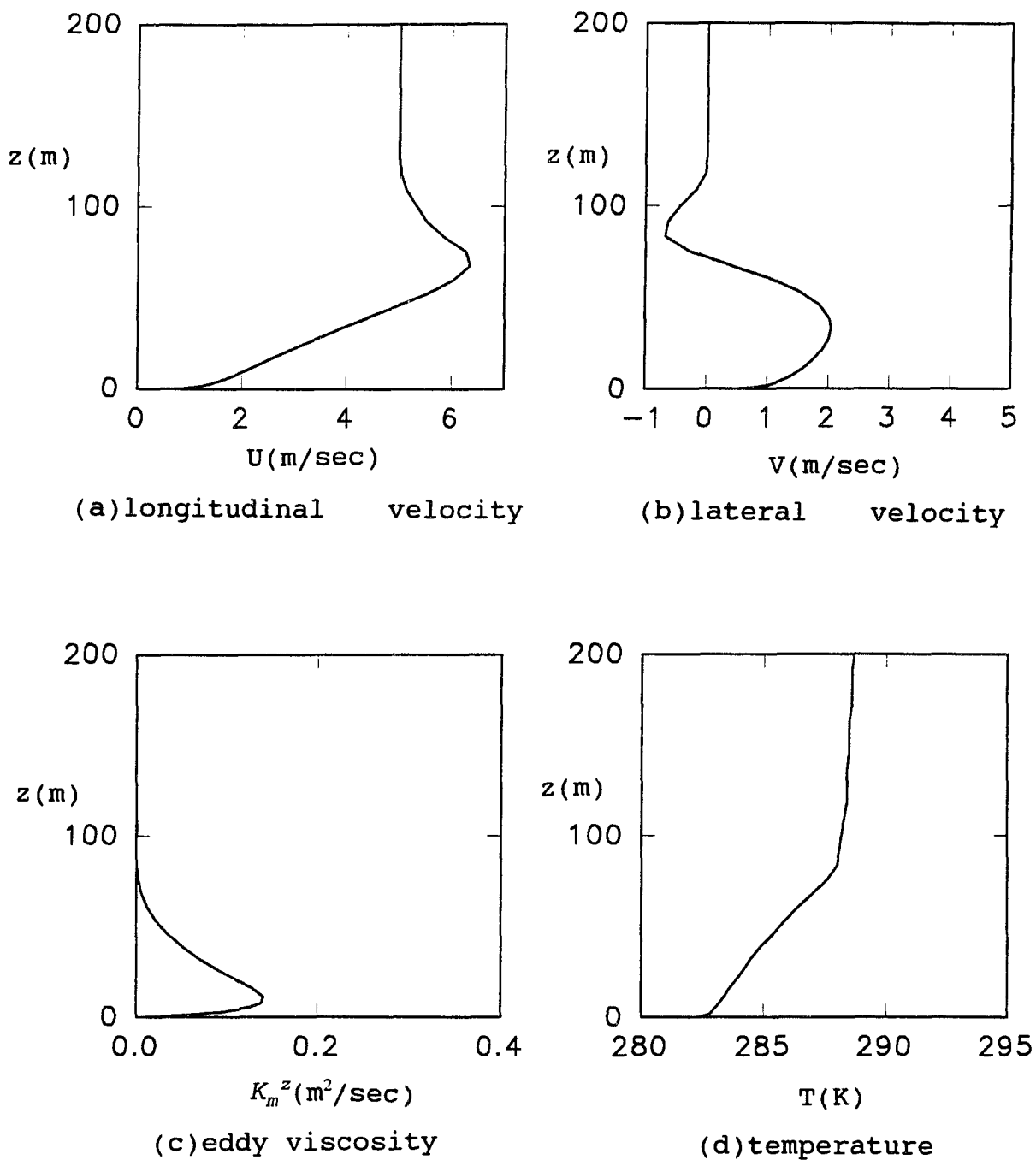
Fig.5.3. Typical example of initial conditions used for the stable ABL (U_g = 5 m/sec, $(d\Theta/dt)_s$ = -0.5 K/hr).

analytic solution of a continuous crosswind line source is given by Pasquill and Smith (1983) and van Ulden (1978) as:

$$C\ (x\ ,\ z)\ =\ \frac{Q_c}{A(s)\ U_p\ \sigma_z}\ \exp\ (\ -\ (\frac{z}{B(s)\ \sigma_z})^s)$$ (5.2)

where Q_c is the emission rate per the unit length of the source line. σ_z is a standard deviation of the concentration distribution in the vertical direction. U_p is a wind velocity in the pollutant plume zone. s is a parameter related with indexes in the power law forms of wind velocity and eddy diffusivity. The range of s values depends on the stability and the roughness height in the atmosphere. In the neutral stability, it varies from 1.14(smooth ground) to 1.3(rough ground) (Panofsky and Dutton, 1984). In the model calculation, the roughness height(z_o) was 0.01m. The s value with z_o =0.01m is expected to be between 1.0 and 1.25 in the neutral ABL. For the stable ABL, Monin-Obukhov length (L) was used as a reference parameter for comparison between the model prediction and the analytic solution. L was 25 for E stability class and 9.3 for F stability class (Chitgokekar, 1988). By varying the geostrophic wind and surface cooling rate in the one dimensional flow model, the corresponding L values to E and F stability classes were found in the model calculation. Parameters used for the analytic solution are listed in Table 5.2.

The comparison of the concentrations with Q_c = 1200 g/sec-m are shown in Figures 5.4 and 5.5 for the neutral and stable ABLs, respectively. The error of the ground concentration ((concentration by analytic solution - concentration by the model) divided by (concentration by the model)) is less than 15% in the neutral case. In case of E and F stability classes, the errors are 6% and 20%, respectively. The calculated concentration profiles with height show good agreement with the analytic solutions.

Table 5.2. Parameters for analytic solution

stability class	Neutral ABL[*]		Stable ABL [**]	
	D		E	F
L	∞		25	9.3
s	1.0	1.5	1.97	2.17
A(s)	0.707	0.902	1.24	1.30
B(s)	0.707	0.968	1.40	1.47
a[***]	0.029		0.017	0.009
b[***]	0.81		0.78	0.72

[*] Pasquill and Smith, 1981
[**] Chitgokekar, 1988
[***] $\sigma_z = a\ x^b$

5.3.2. Transient Thermal Fence

A transient thermal fence was studied to understand thermal fence interactions with the atmospheric flow. If the buoyancy force resulting from the thermal fence is so strong
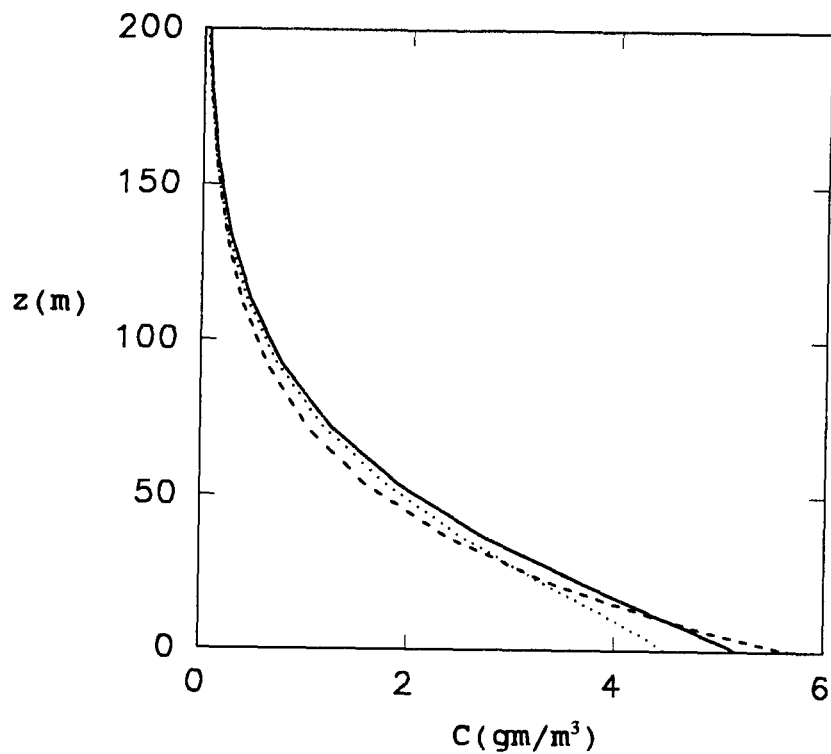
Fig.5.4. Comparisons of calculated concentrations with analytic solutions in the neutral ABL. Solid line is for model calculation, dashed line for analytic solution with s=1.0 and dotted line for analytic solution with s=1.25.
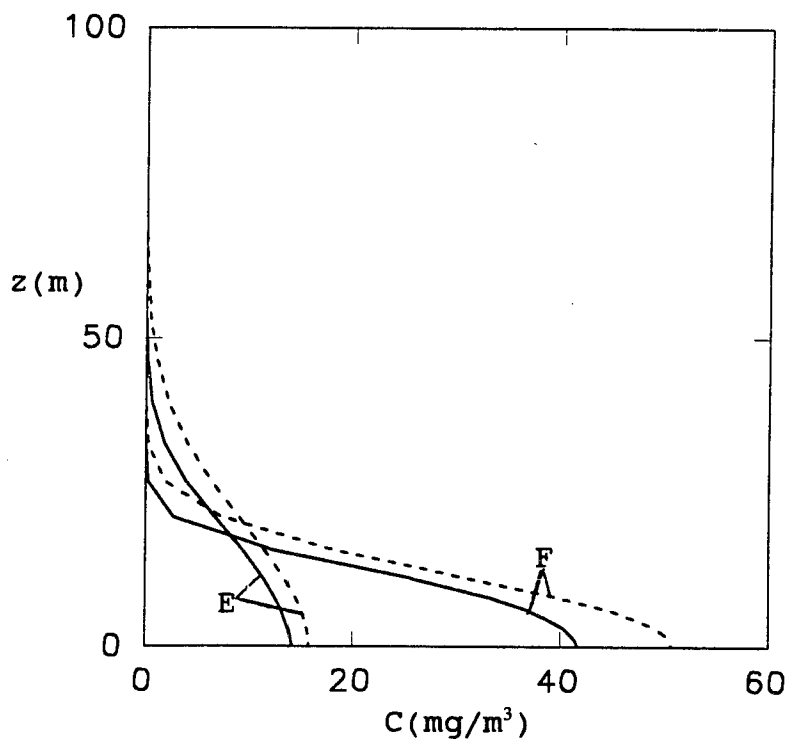
Fig.5.5. Comparisons of calculated concentrations with analytic solutions in the stable ABL. Solid line is for model calculation, dashed lines for analytic solution. E is for E stability class and F for F stability class in Table 5.2.

that it modifies the atmospheric flow, it is difficult to obtain the steady state solution with a limited calculation domain. The calculations were then limited to a relatively short time transient behavior.

Figures 5.6 to 5.8 show velocity, temperature and turbulent kinetic energy profile developments with time, respectively. The geostrophic wind velocity was 1.5 m/sec and a rate of heat(Q_f) was 10^7 w/m^2. The initial thermal plume at time 3 min shows that comparatively small recirculation loop is developed behind the thermal fence. As the time elapses, the thermal plume and the recirculation loop continue to grow. The temperature and the level of the turbulent energy behind the thermal fence also continue to increase. The thermal plume by the thermal fence at time 8 min reaches to the top of the boundary layer and begins to modify the environmental flow. The hot air of the thermal plume continues to rise and acts as a barrier to the passage of the incoming wind from the upstream. No air can thus propagate through the thermal fence. The calculated flow pattern shows typical two dimensional flow development of the wildfire (Nelson, 1986; Grishin, 1984) although there are some controversies in the two dimensional nature of the wildfire (Beer, 1991).

In order to understand the effect of strong thermal heating, a larger calculation domain is required. Our interest, however, is limited in the relatively short

(a) t=3min

(b) t=5min

(c) t=8min
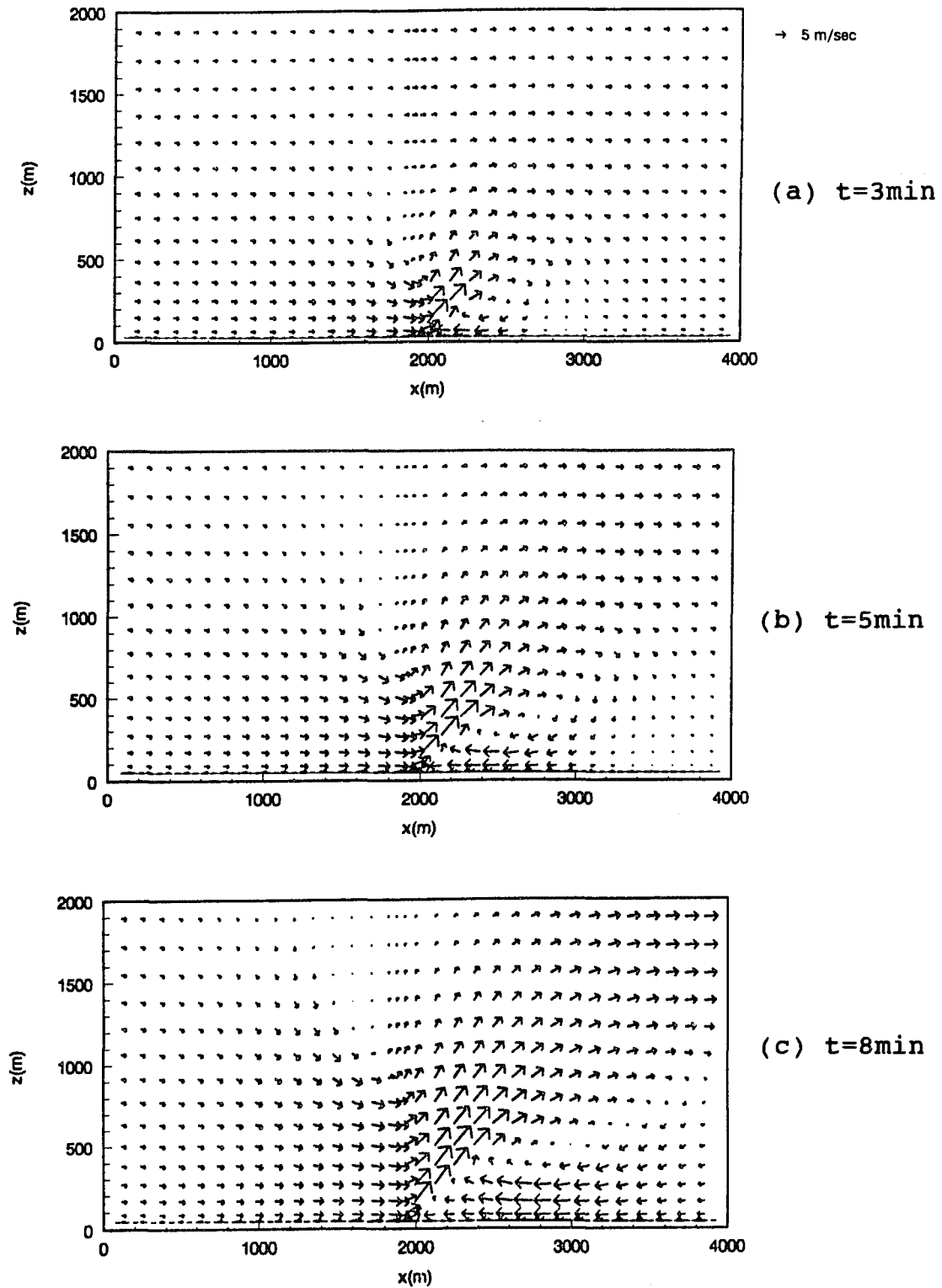
Fig.5.6. Velocity profiles with time in the neutral ABL ($Q_f = 10^7$ W/m^2, $U_g = 1.5$ m/sec).
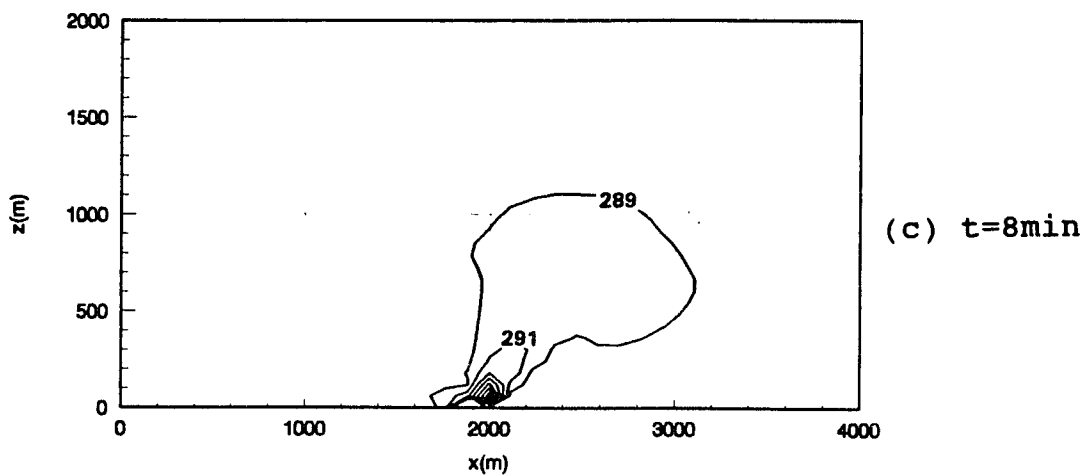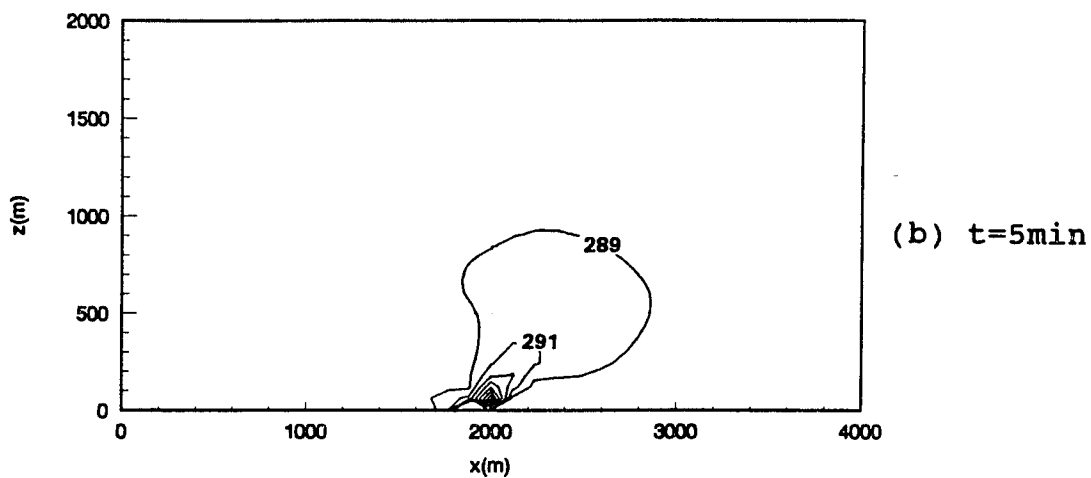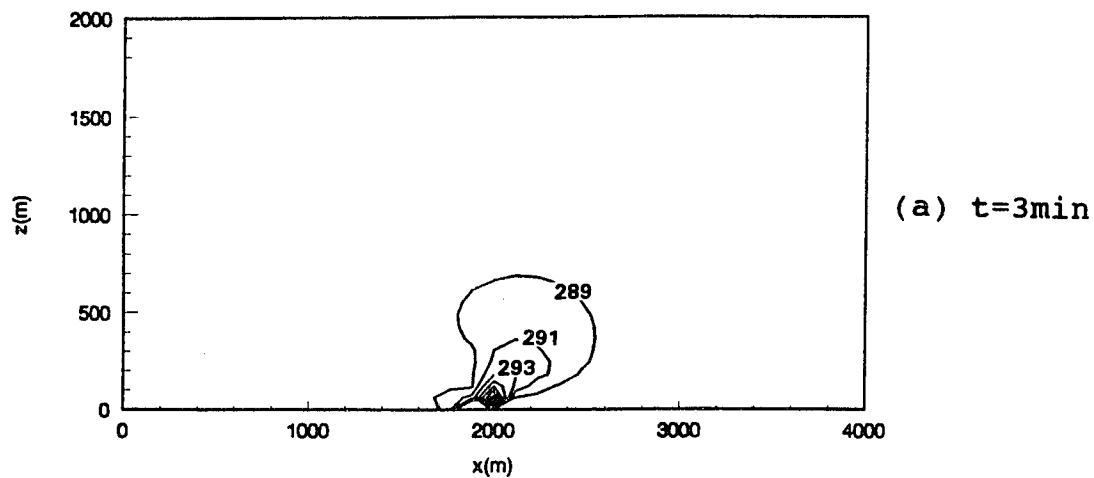
Fig.5.7. Temperature(K) distribution with time in the neutral ABL ($Q_f = 10^7$ W/m^2, $U_g = 1.5$ m/sec).
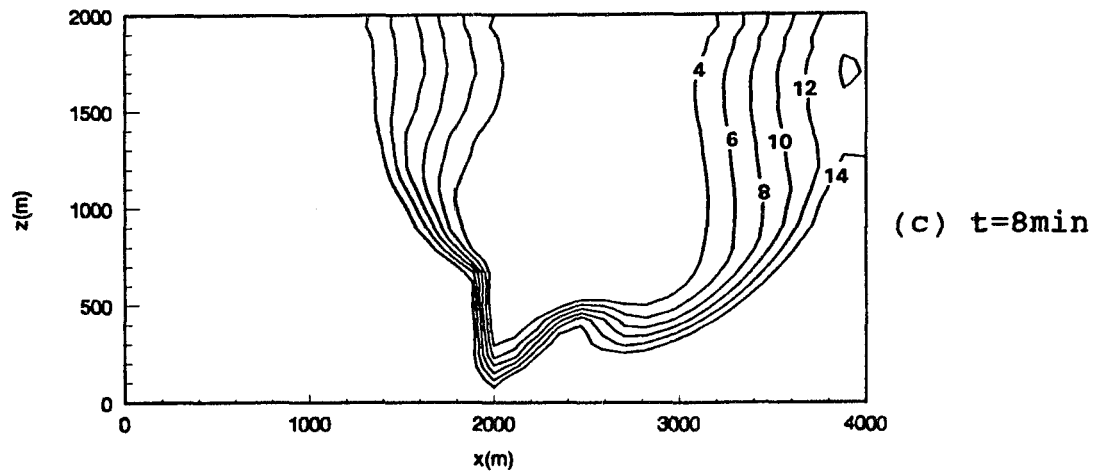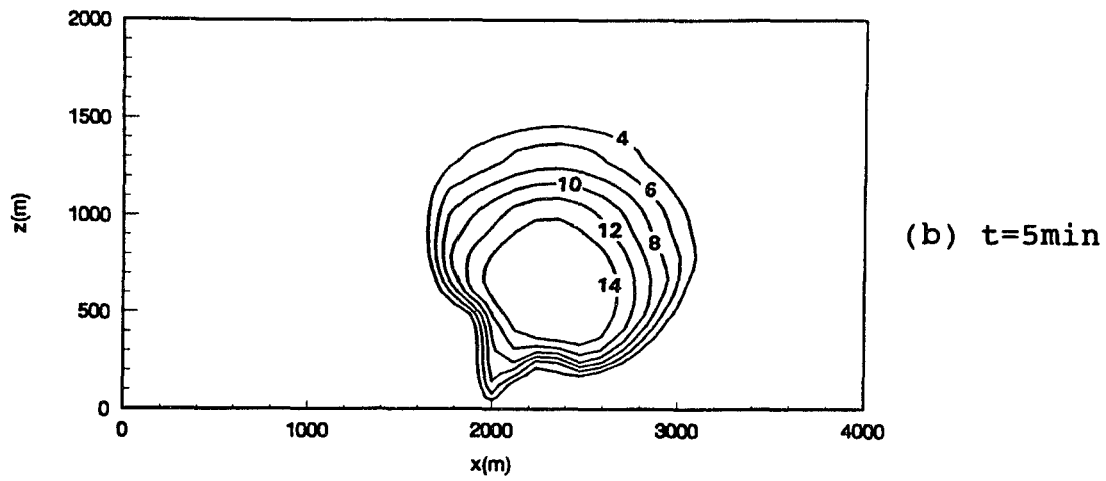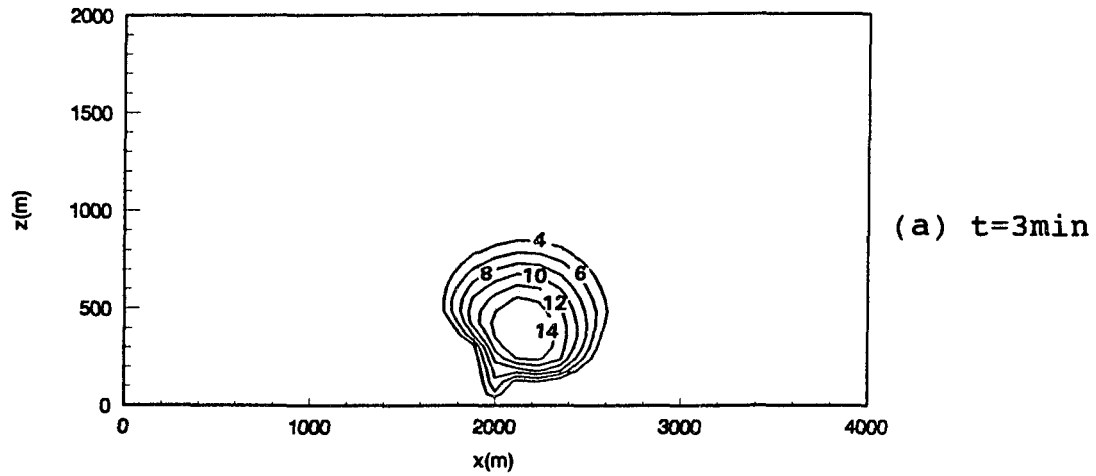
Fig.5.8. Turbulent kinetic energy(m^2/sec^2) distribution with time $(Q_f = 10^7 \ W/m^2, \ U_g = 1.5 \ m/sec)$.

distance (1-2km) dispersion of the pollutants. Within the limited domain of interest, either the wind velocity was increased or the rate of heat was decreased to obtain the state steady.

5.3.3. Steady State Thermal Fence

<u>Neutral ABL</u>

By increasing the wind velcocity from 1.5 m/sec to 5 m/sec with fixed heat flux ($Q_f = 10^7$ W/m^2), the steady state was obtained after 3 hour calculation. Figure 5.9 shows the velocity, turbulent energy, temperature and concentration profiles. The velocity and temperature increase behind the thermal fence. The turbulent kinetic energy also shows higher value behind the thermal fence. It might cause the additional dispersion of the pollutants. Figure 5.10 shows the effects of the heating rate on the vertical concentration profiles at the outlet. As the heating rate increases, the concentration with height becomes uniform due to the vertical mixing of the pollutants. This mixing results from the increase of eddy diffusivity behind the thermal fence. The effects on the ground concentration with the various heating rates are shown in Figure 5.11. The ground concentration at the outlet decreases rapidly as the heating rate increases. The ground concentration is reduced by 38% with 10^4 W/m^2 heating rate.

<u>Stable ABL</u>
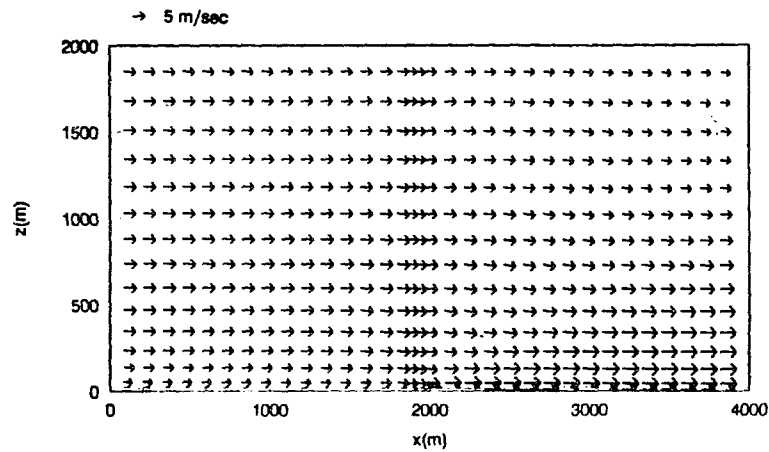
(a) velocity
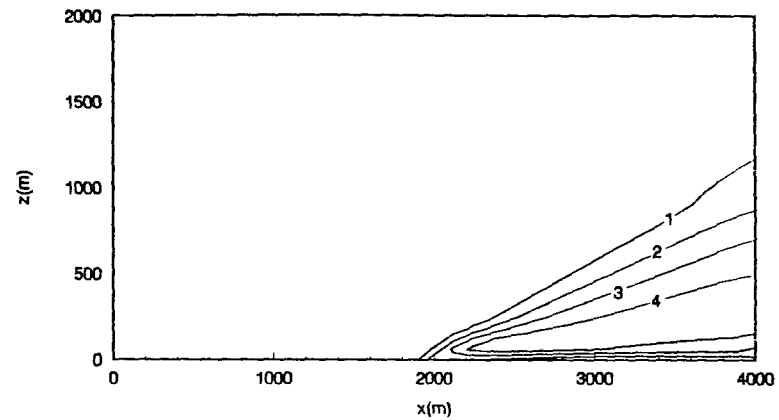
(b) kinetic energy(m^2/sec^2)
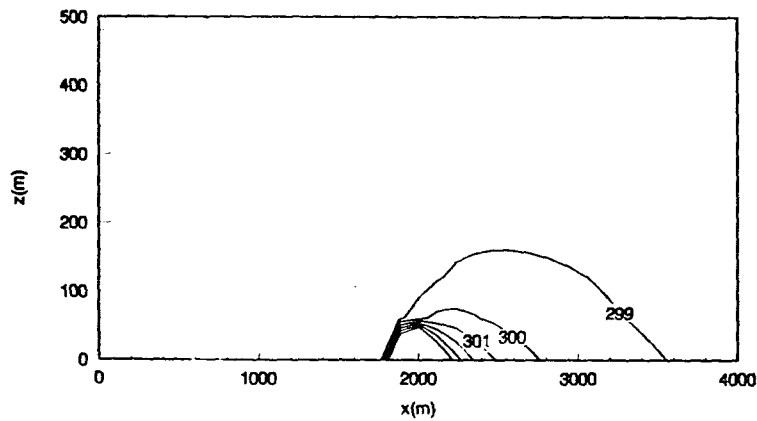
(c) temperature(K)
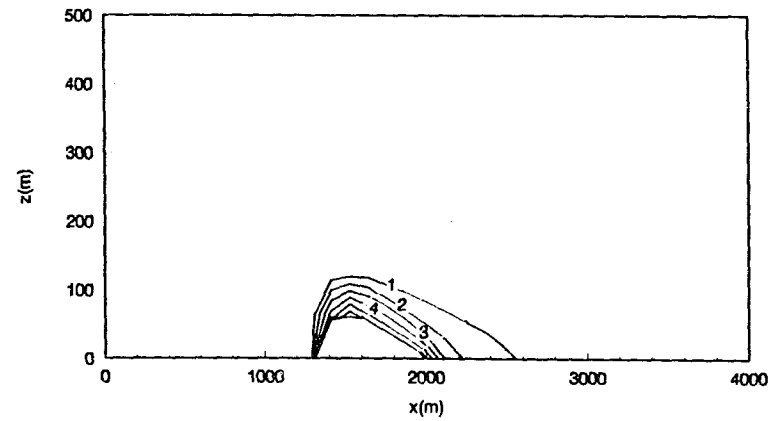
(d) concentration(gm/m^3)

Fig.5.9. Calculated flow characteristics at steady state in the neutral ABL (U_g =5 m/sec, Q_f =10^7 W/m^2).
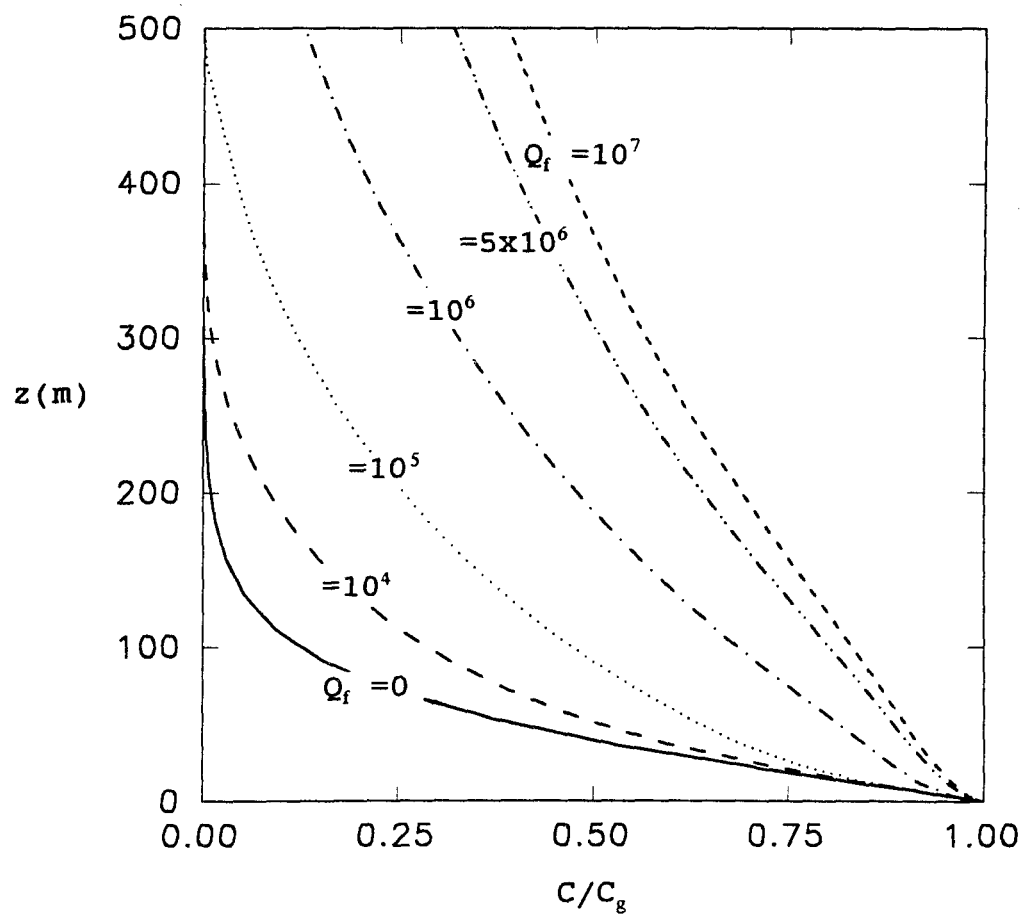
Fig.5.10. Effect of the thermal fence heating on normalized concentration(C/C_g) with height in the neutral ABL. C_g is a ground concentration.
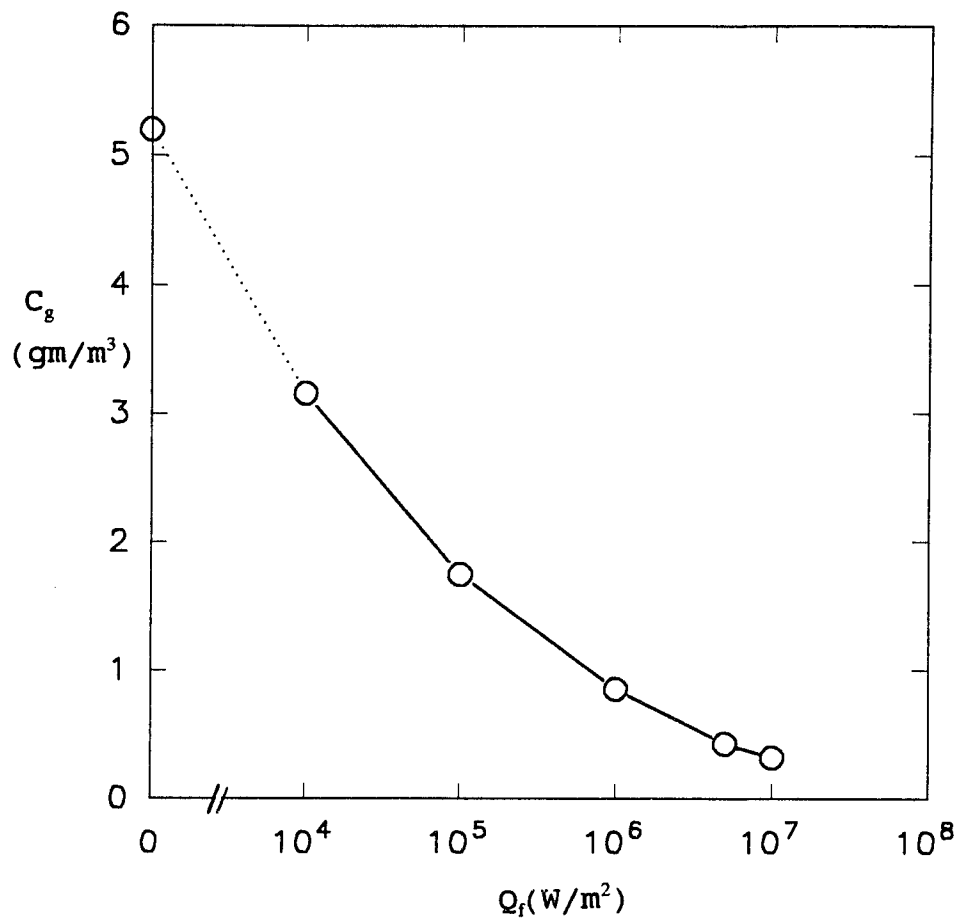
Fig.5.11. Effect of the thermal fence heating on a ground concentration in the neutral ABL.

Figure 5.12 shows a typical example of thermal fence flow in the stable ABL. The velocity and temperature also rise behind the thermal fence and the turbulent kinetic energy increases. The effect of heating to the boundary layer is much shallower than the neutral case due to the strong stable stratification aloft. Figure 5.13 shows effects of the thermal fence on the vertical concentration profile at the outlet. Figure 5.14 shows the ground concentration at the outlet with various heating rates. As compared with the neutral case, a larger heating rate is required to enhance the vertical mixing. With 10^5 W/m^2 cooling rate, the ground concentration is reduced by 23%. There is little mixing effect with 10^4 W/m^2 heating rate (not shown in Figure 5.14).

In order to understand the effect of thermal heating on the flow structure, the flow characteristics at the inlet and outlet are compared in Figure 5.15. The profiles at the inlet are equivalent to those of the initial conditions. The wind velocity near the surface increases and temperature at the outlet show mixed layer in the middle of the boundary layer. This mixed layer results in the higher eddy viscosity at the outlet which enhances the vertical mixing of pollutants.

The surface cooling rate was changed to understand its effect on the flow and dispersion of pollutants with the thermal fence (Figures 5.16 and 5.17). The effects of the thermal heating on the flow and dispersion show the same
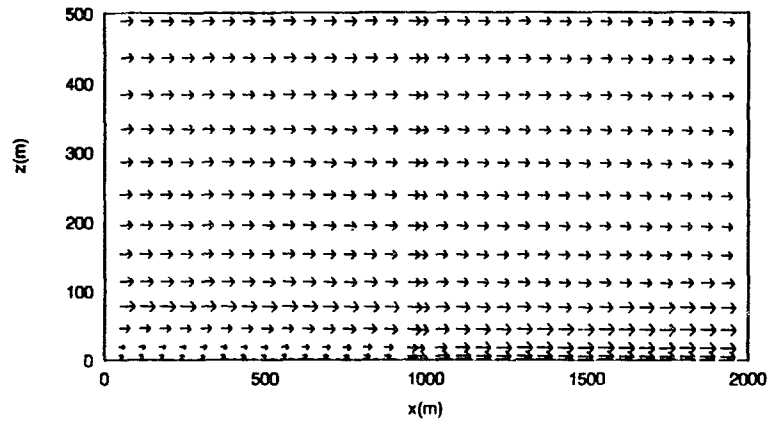
(a) velocity
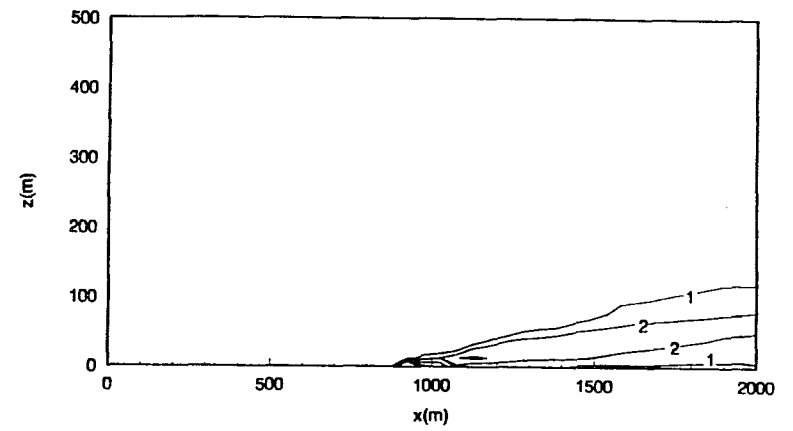
(b) kinetic energy(m^2/sec^2)
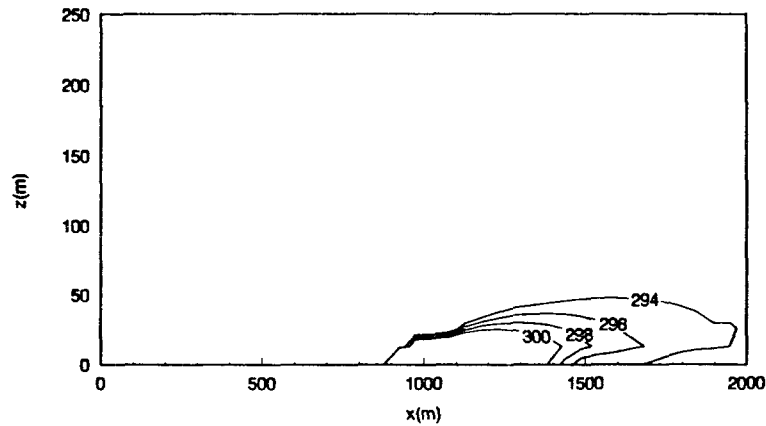
(c) temperature(K)
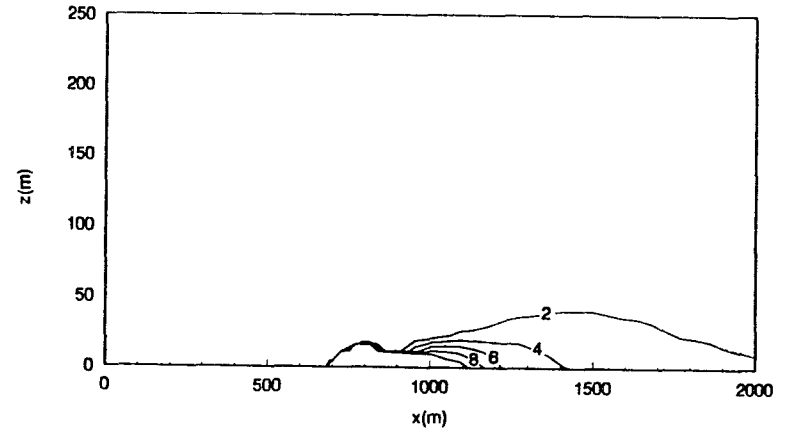
(d) concentration(gm/m^3)

Fig.5.12. Calculated flow characteristics at steady state in the stable ABL (U_g = 5 m/sec, $(d\Theta/dt)_s$ = -0.5 K/hr, Q_f =10^7 W/m^2).
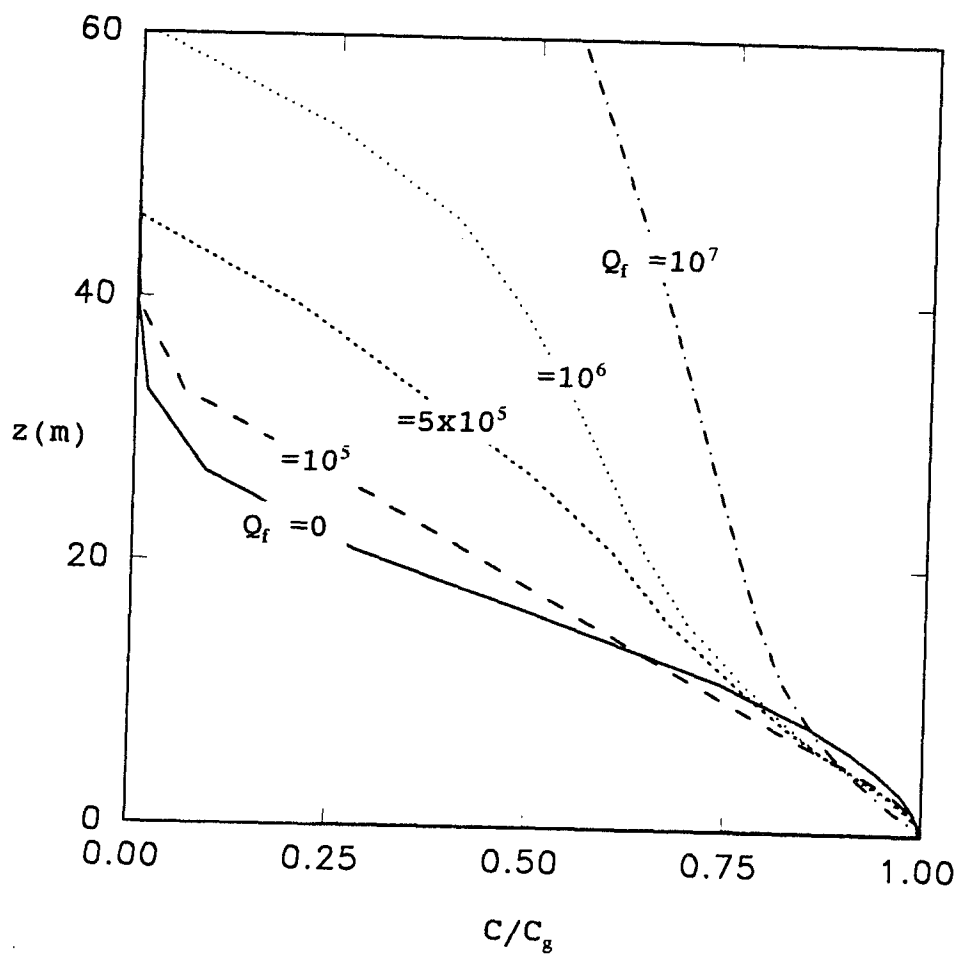
Fig.5.13. Effect of the thermal fence heating on normalized concentration(C/C_g) with height in the stable ABL. C_g is a ground concentration.
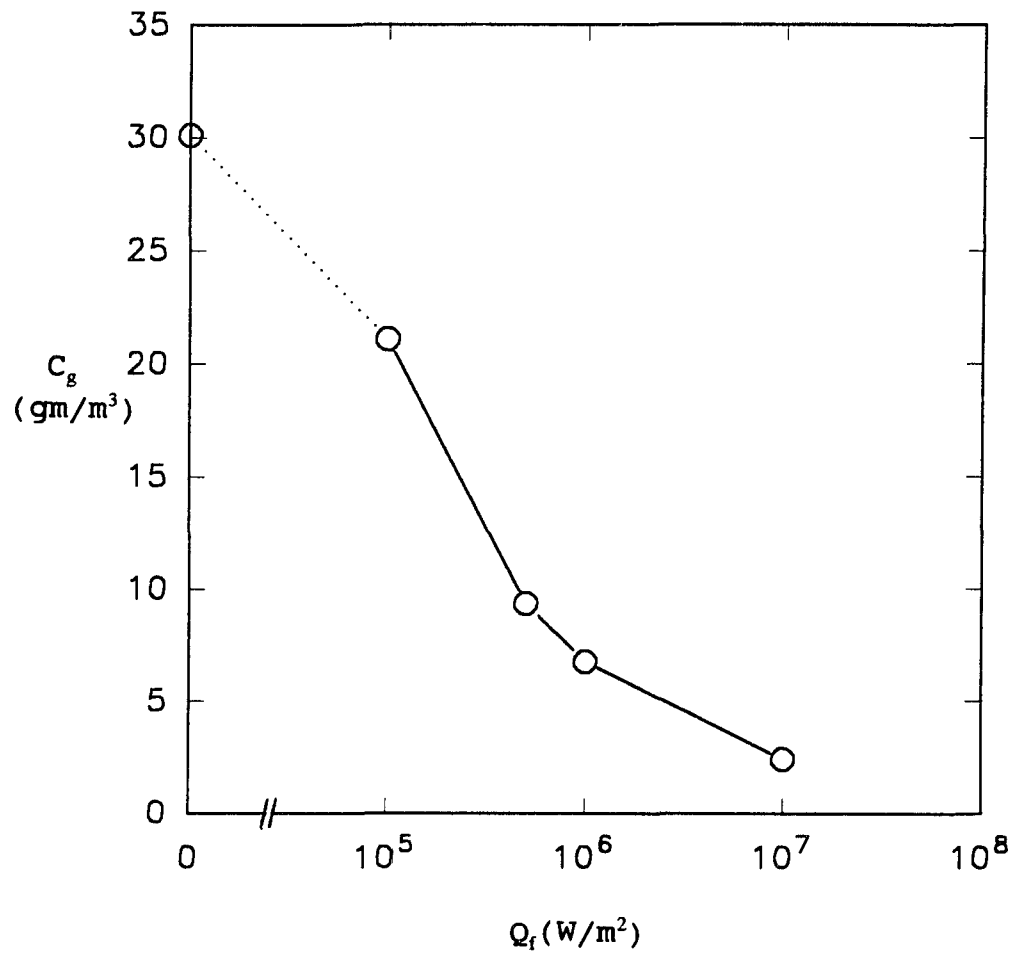
Fig.5.14. Effect of the thermal fence heating on a ground concentration in the stable ABL.
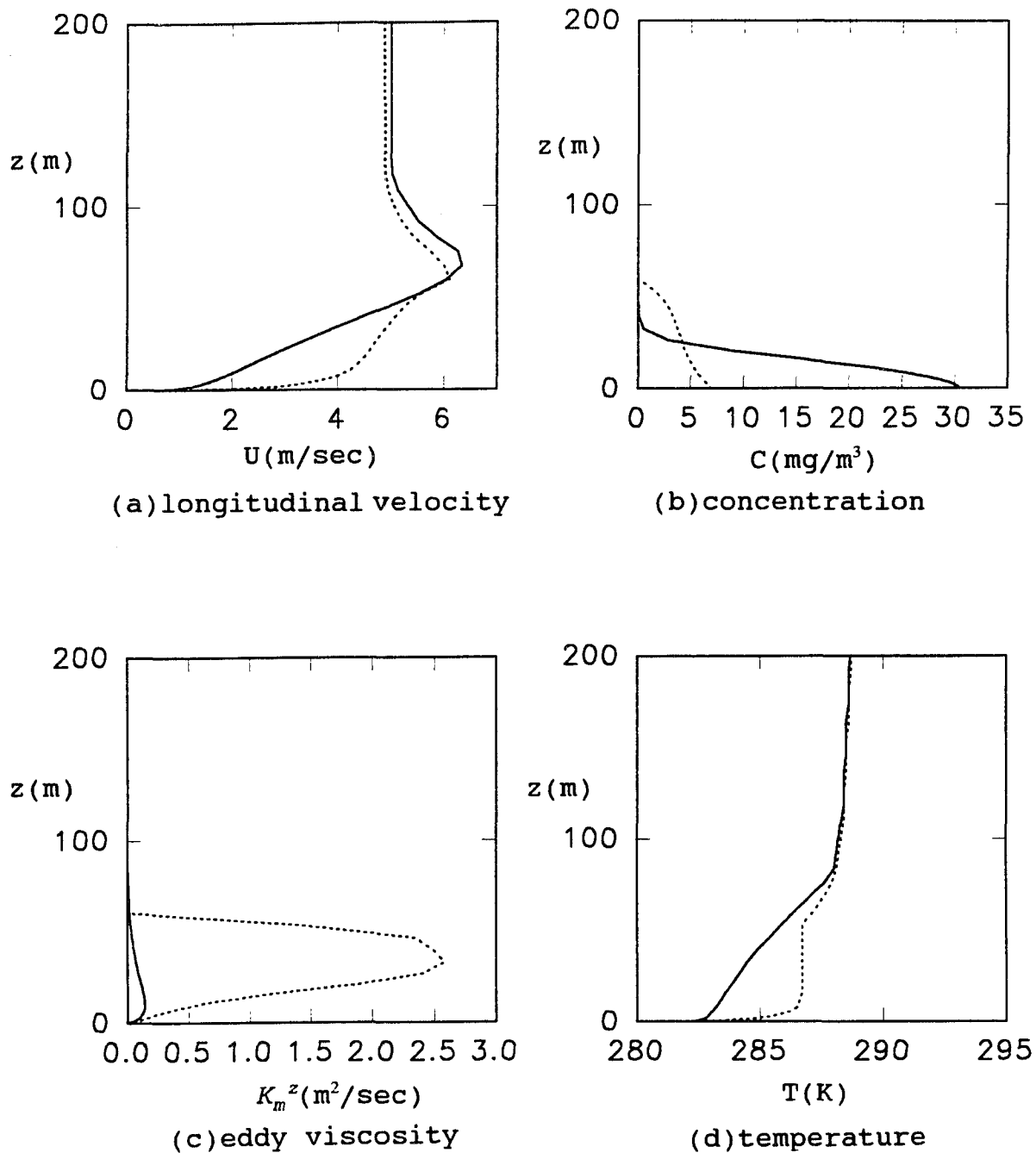
Fig.5.15. Effect of thermal fence on the flow and dispersion in the stable ABL (U_g = 5 m/sec, $(d\Theta/dt)_s$ = - 0.5 K/hr, Q_f = 10^6 W/m^2). Solid lines for profiles at the inlet and dotted lines for profiles at the outlet.
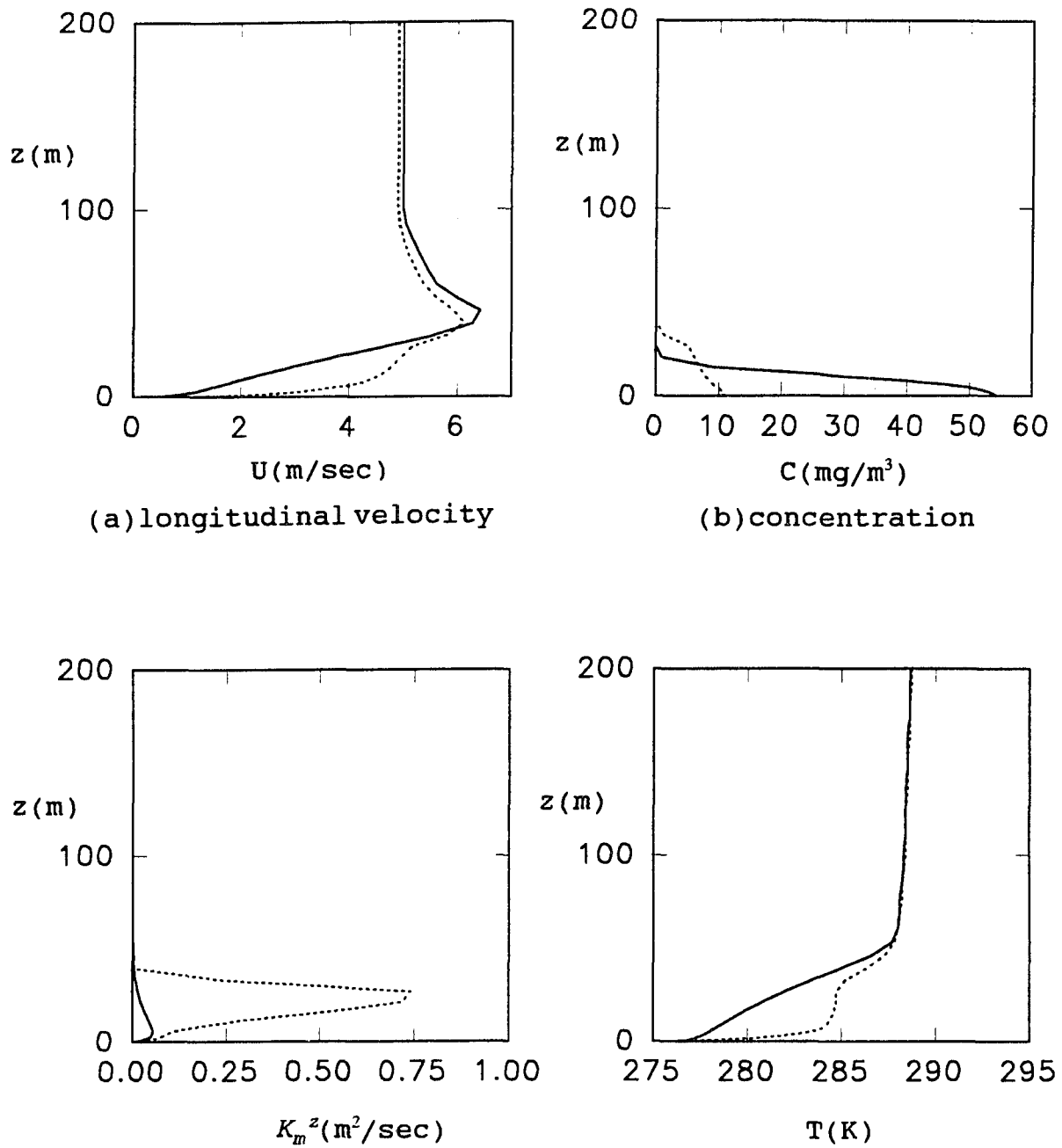
Fig.5.16. Effect of thermal fence on the flow and dispersion in the stable ABL (U_g = 5 m/sec, $(d\Theta/dt)_s$ = - 1 K/hr, Q_f = 10^6 W/m^2). Lines are the same as in Fig.5.15.
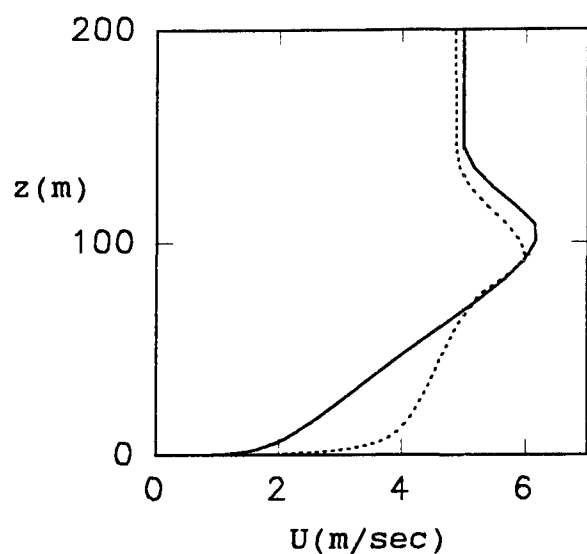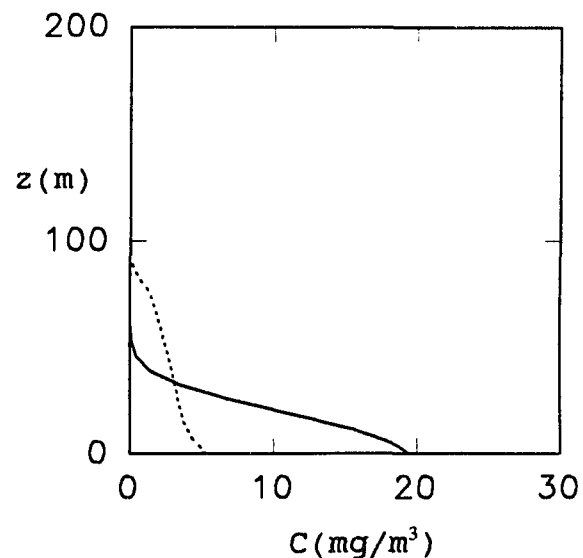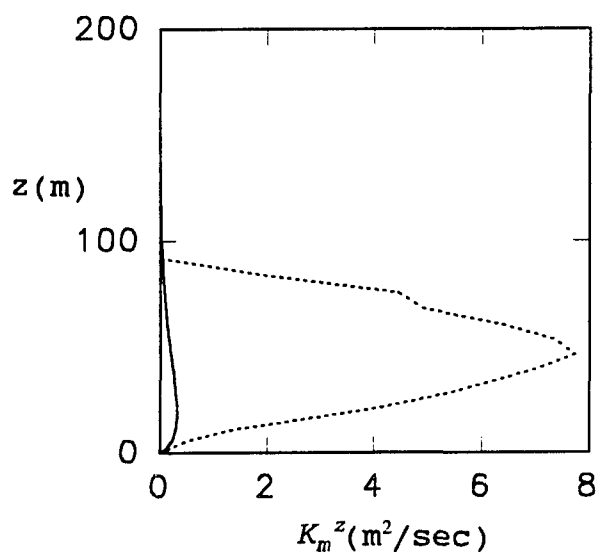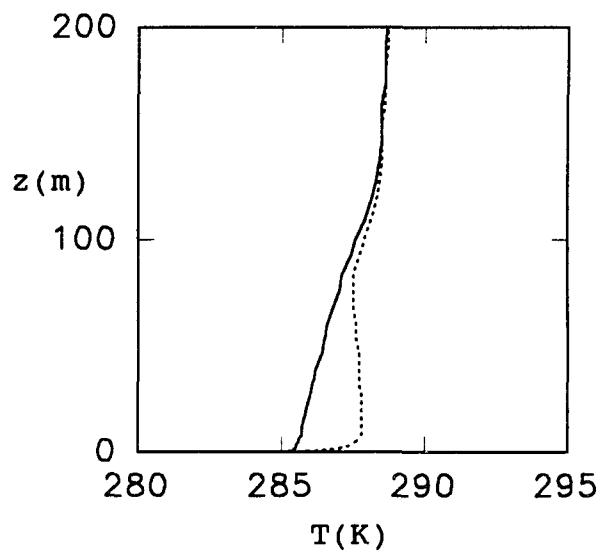
Fig.5.17. Effect of thermal fence on the flow and dispersion in the stable ABL (U_g = 5 m/sec, $(d\Theta/dt)_s$ = - 0.25 K/hr, $Q_f = 10^6$ W/m²). Lines are the same as in Fig.5.15

trends under the conditions considered here. Larger heating rate leads to greater vertical mixing at the flow downstream.

5.4 Conclusions

In order to understand the interactions of the thermal fence with the neutral and stable atmosphere boundary layers, the modified $E-\epsilon$ model was applied to the thermal fence.

It was proved that the thermal fence is an effective means to enhance dispersion of the pollutants under the neutral and stable conditions. The thermal fence induces the mixed layer at the flow downstream. This leads to a higher eddy viscosity and an enhanced mixing of the pollutants. For the neutral ABL, the ground concentration at the outlet is reduced by 38 % with 10^4 W/m^2 heating rate. For the stable ABL, a larger heating rate is required to control pollutant dispersion. The ground concentration is reduced by 23 % with 10^5 W/m^2 heating rate.

Chapter 6. Recommendations for Further Studies

6.1. Turbulence Model

In order to consider the strong diffusions in the convective ABL, two approaches are recommended:

1) A higher order closure model with inclusions of the counter gradient diffusions in the prognostic equations of Reynolds stresses and turbulent fluxes.

2) Modified E-ϵ turbulence model with additional parameters to compensate the counter gradient diffusions in the Boussinesq's approximation.

The Modified E-ϵ turbulence model needs to be confirmed in the water tank experiments such as heated horizontal surface and inclined surface to extend its applicability to two dimensional engineering flows. In this case, expressions for c_m and c_h should be re-derived because the water flows in the tank are nearly two dimensional case and there are no lateral shear stresses and turbulent heat fluxes.

6.2. Sea Breeze Circulation

In order to develop two and three dimensional mesoscale flow models for general purpose, the following is recommended:

1) Incorporation of the surface energy balance to compute the land surface temperature.

2) Development of numerical methods to reduce the computational time.

3) Hydrostatic model for three dimensional flows and comparison with non-hydrostatic model.

4) Check effects of level of turbulence closure on the sea breeze circulation. If possible, a lower level closure would be preferred.

5) The model should be modified to include the topography coordinates to simulate complex terrain flows.

6) Finally, comparison of the model calculation with a set of field experiments to fully confirm the model simulation.

Further phenomena of interest in the sea/land breeze are:

1) Simulation of the land breeze and fumigation at nighttime stable condition over the sea.

2) Full analysis of frontogenesis with inclusion of all terms in Equation (4.18).

3) Simulation with fine grid size to understand the detailed flow structure.

References

Albini,f.:1984, 'Wildland Fires', **American Scientist**, *72*, 590-597.

Anderson, D.A., J.C. Tannehill and R.H. Pletcher:1984, 'Computational Fluid Mechanics and Heat Transfer', McGraw-Hill Co.

André, J.C., G. Demoor, P. Lacarrere, G. Therry and R. du Vachat:1979, 'The Clipping Approximation and Inhomogeneous Turbulence Simulations, **Turbulent Shear Flow I**, F. Durst, B.E. Launder, F. W. Schmidt and J. H. Whitelaw, Eds., Springer-Verlag, 307-318.

Andrén, A.:1990, 'Evaluation of a Turbulence Closure Scheme Suitable for Air-Pollution Applications', **J. of Appl. Meteor.**, *29*, 224-239.

Andrén, A.:1991, 'A TKE-Dissipation Model for the Atmospheric Boundary Layer', **Bound. Layer Meteor.**, *56*, 207-221.

Arritt, R.W.:1993, 'Effects of the Large-Scale Flow on Characteristic Features of the Sea Breeze', **J. Appl. Meteor.**, *32*, 116-125.

Arritt, R.W.:1991, 'A Numerical Study of Sea Breeze Frontogenesis', **Fifth Conference on Meteorology and Oceanography of the Coastal Zone, American Meteorological Society**, May 6-10.

Atkinson, B.W.:1981, 'Meso-scale Atmospheric Circulation', Academic Press.

Avissar, A., M.D. Moran, G. Wu, R.N. Meroney, and R.A. Pielke: 1990, ' Operating Ranges of Mesoscale Numerical Models and Meteorological Wind Tunnels for the Simulation of Sea and Land Breezes', **Bound. Layer Meteor.**, *50*, 227-275.

Bechtold,P., J.P. Pinty and P. Mascart:1991, 'A Numerical Investigation of the Influence of Large-Scale Winds on Sea-Breeze and Inland-Breeze Type Circulations', **J. Appl. Meteor.**, *30*, 1268-1278.

Beer, T.:1991, 'The Interaction of Wind and Fire', **Bound. Layer Meteor.**, *54*, 287-308.

Beljaar, A.G.M., P. Schotanus and F.T.M. Nieuwstadt:1983, 'Surface Layer Similarity under Nonuniform Fetch Conditions', **J. Climate Appl. Meteor**, *22*, 1800-1810.

Blackadar, A.K.:1962, 'The Vertical Distribution of Wind and Turbulent Exchange in a Neutral Atmosphere', **J. Geophys. Res.**, *67*, 3095-3102.

Briere,S.:1987,'Energetics of Daytime Sea Breeze Circulation as Determined from a Two-Dimensional, Third-Order Turbulence Closure Model', **J. Atmos. Sci.**, *44*, 1455-1474.

Brost, R. and J.C. Wyngaard:1978, 'A Model Study of the Stably Stratified Planetary Boundary Layer', *J. Atmos. Sci.*, **35**, 1427-1440.

Brost, R.A. and J.C.Wyngaard:1979, 'Reply', **Bound. Layer Meteor.**, *36*, 1821-1822.

Brost, R.A., Wyngaard, J.C. and Lenshow, H.:1982, 'Marine Stratocumulus Layers, Part II: Turbulence Budgets', **J. Atmos. Sci.**, *39*, 818-836.

Businger, J.A., J.C. Wyngaard, Y. Izumi and E.F. Bradley:1971, 'Flux-Profile Relationships in the Atmospheric Surface Layer', **J. Atmos. Sci.**, *28*, 181-189.

Caughey,S.J., Wyngaard,J.C. and Kaimal,J.C.:1979, 'Turbulence in the Evolving SBL', **J. Atmos. Sci.**, *36*, 1041-1052.

Caughey,S.J. and Wyngaard,J.C.:1979, 'The turbulence Kinetic Energy Budget in Convective Conditions', **Quart. J. R. Met. Soc.**, *105*, 231-239.

Caughey,S.J. and Palmer,S.G.:1979, 'Some Aspects of Turbulence Structure through the Depth of the Convective BL', **Quart. J. R. Met. Soc.**, *105*, 811-827.

Caughey, S.J.:1982,'Observed Characteristics of the Atmospheric Boundary Layer' **Atmospheric Turbulence and Air Pollution Modeling**, F.T.M. Nieuwstadt and H. van Dop, Eds., D. Reidel Publishing Company, 107-158.

Caughey,S.J. and Kaimal,J.C., "Vertical Heat Flux in the Convective Boundary Layer", Notes and Correspondence. pp. 811-815.

Celik, I. and W. Rodi:1984, 'Simulation of Free-Surface Effects in Turbulent Channel Flows', **Physico-Chemical Hydrodynamics J.**, *5*, 217-231.

Chitgopekar, N.:1988, 'Modeling Short Range Air Dispersion from Area Source of Non-Buoyant Toxics', MS Thesis, Louisiana State University.

Deardorff,J.W.:1972, 'Numerical Investigation of Neutral and Unstable Planetary Boundary Layers', **J. Atmos. Sci.**, *29*, 91-115.

Deardorff, J.W.:1973, 'An Explanation of Anomalously Large Reynolds Stresses within the Convective Planetary Boundary Layer', **J. Atmos. Sci.**, *30*, 1070-1076.

Deardorff, J.W.:1974a, 'Three-Dimensional Numerical Study of the Height and Mean Structure of a Heated Planetary Boundary Layer', **Bound. Layer Meteor.**, 7, 82-106.

Deardorff, J.W.:1974b, 'Three-Dimensional Numerical Study of Turbulence in an Entraining Mixing Layer', **Bound. Layer Meteor.**, 7, 199-226.

Detering, H.W. and D. Etling:1985, 'Application of the E-e Turbulence Model to the Atmospheric Boundary Layer', **Bound. Layer Meteor.**, *33*, 113-133.

Durand, P., S. Briére and A. Druihet:1989, 'A sea-Land Transition Observed during the Coast Experiment', **J. Atmos. Sci.**, *46*, 96-116.

Duynkerke, P.G.:1988, 'Application of the E-e Turbulence Closure Model to the Neutral and Stable Atmospheric Boundary Layer', **J. Atmos. Sci.**, *45*, 865-880.

Dutta, S. and S. Acharya:1993, 'Heat Transfer and Flow Past A Backstep with the Nonlinear $k-\epsilon$ Turbulence Model and the Modified $k-\epsilon$ Turbulence Model', **Numerical Heat Transfer Part A**, *23*, 281-301.

Estoque, M.A.:1961, 'The Sea Breeze as a Function of the Prevailing Synoptic Situation', **J. Atmos. Sci.**, *19*, 244-250.

Galperin,B. and Hassid,S.:1986, 'A Modified Turbulent Energy Model for Geophysical Flows: Influence of the Ground Proximity', **Bound.- Layer Meteor.**, *35*, 155-165.

Garratt,J.R. and Physick,W.L.:1985, "The Inland Boundary Layer at Low Latitudes: II Sea-Breeze Influences", **Bound.- Layer Meteor.**, *33*, p.209-231.

Gibson, M.M and B.E. Launder:1978, 'Ground Effects on Pressure Fluctuations in the Atmospheric Boundary Layer', **J. Fluid Mech.**, *86(3)*, 491-511.

Grant,A.L.M.:1986, 'Observations of Boundary Layer Structure Made During the KONTUR Experiment', **Quart. J. R. Met. Soc.**, *112*, 825-841.

Grant, A.L.M.:1992, 'The Structure of Turbulence in the Near-neutral Atmospheric Boundary Layer', **J. Atmos. Sci.**, *49*, 226-239.

Grishin, A.D. and E.E. Gruzina:1984, 'Aerodynamics and Heat Exchange between the Front of a Forest Fire and the Surface Layer of the Atmosphere', **J. Appl. Mech. & Tech. Phys.**, *25*, 889-894.

Guenther, A., B. Lamb and D. Stock:1990, 'Three-Dimensional Numerical Simulation of Plume Downwash with a k-ϵ Turbulence Model', **J. Appl. Meteor.**, *29*, 633-642.
Haines, D. and M.C. Smith:1987, 'Three types of horizontal vortices observed in wildland mass and crown fire', **J. Climate and Appl. Meteor.**, *26*, 1624-1637.

Haroutunian, V. and B.E.Launder:1988, 'Second-Moment Modelling of Free Buoyant Shear Flows: A Comparison of Parabolic and Elliptic Solution', **Stably Stratified Flow and Dense Gas Dispersion**, J.S.Puttock,Clarendon Press, 409-430.

Hassid, S. and B. Galperin:1983, 'A Turbulent Energy Model for geophysical Flows', **Bound. Layer Meteor.**, *26*, 397-412.

Helfand,H.M., and Labraga,J.C.:1988, 'Design of a Nonsingular Level 2.5 Second-Order Closure Model for the Prediction of Atmospheric Turbulence', **J. Atmos. Sci.**, *45*, 113-132.

Hoff, R.M, N.B.A. Trivett, M.M. Millan, P. Fellin, K.G. Ahlauf and H.A. Wiebe:1982, 'The Nanticoke Shoreline Diffusion Experiment, June 1978 - III. Ground-Based Air Quality Measurements', **Atmos. Environ.**, *16*, 439-454.

Hsu, S.A.:1986, 'A Note on Estimating the Height of the Convective Internal Boundary Layer near Shore', **Bound. Layer Meteor.**, *35*, 311-316.

Huang, C.Y., and Raman, S.:1988, 'A Numerical Modeling Study of the Marine Boundary Layer Over the Gulf Stream During Cold Air Advection', **Bound. Layer Meteor.**, *45*, 251-290.

Huang, C.Y., and Raman, S.:1989, 'Application of the E-e Closure Model to Simulations of Mesoscale Topographic Effects', **Bound. Layer Meteor.**, *49*, 169-195.

Huang, C.Y. and Raman, S.:1991a, 'Numerical Simulation of January 28 Cold Air Outbreak during GALE, Part I: The Model and Sensitivity Tests of Turbulence Closures', **Bound. Layer Meteor.**, *55*, 381-407.

Huang, C.Y. and Raman, S.:1991b, 'Numerical Simulation of January 28 Cold Air Outbreak during GALE, Part II: The Mesoscale Circulation and Marine Boundary Layer', **Bound. Layer Meteor.**, *56*, 51-81.

Huang,C.Y. and Raman,S.:1992, 'A Three-Dimensional Numerical Investigation of a Carolina Coastal Front and the Gulf Stream Rainband', **J. of Atmos. Sci.**, *49*, 560-584.

Kerman, B.R.:1982, 'A Similarity Model of Shoreline Fumigation', **Atmos. Environ.**, *16*, 467-477.

Kitada, T.:1987, 'Turbulence Structure of Sea Breeze Front and It's Implication in Air Pollution Transport - Application of k-e Turbulence Model", **Bound. Layer Meteor.**, *41*, 217-339.

Kitada, K. and E. Kitagawa:1990, 'Numerical Analysis of the Role of Sea Breeze Fronts on Air Quality in Coastal and Inland Polluted Areas', **Atmos. Environ.**, *24A*, 1545-1559.

Kondo, J., and Kuwagata, T., " Enhancement of Forest Fires over Northeastern Japan due to Atypical Strong Dry Wind", **American Meteorological Society**, *31*, 1992: pp.386-396.

Kraus, H., J.M. Hacker and J. Hartmann:1990, 'An Observational Aircraft-Based Study of Sea-Breeze Frontogenesis', **Bound. Layer Meteor.**, *53*, 223-265.

Launder, B.E. and D.B.Spalding:1974, 'The Numerical Computation of Turbulent Flow', **Computer Methods in Appl.Mech. and Eng.**, *3*, 269-289.

Lee, H.N. and S.K. Kao:1979, 'Finite-Element Numerical Modeling of Atmospheric Turbulent Boundary Layer', **J. Appl. Meteor.**, *18*, 1287-1295.

Louis, J.-F.:1979, 'A Parametric Model of Vertical Eddy Fluxes in the Atmosphere', **Bound. Layer Meteor.**, *17*, 187-202.

Lyons, W.A. and Lars E. Olsson:1973, 'Detailed Mesometeorological Studies of Air Pollution Dispersion in the Chicago Lake Breeze', **Mon. Wea. Rev.**, *101*, 387-403.

Lyons, W.A. and H.S. Cole:1973, 'Fumigation and Plume Trapping on the Shores of Lake Michigan During Stable Onshore Flow', **J. Appl. Meteor.**, *12*, 494-510.

Luti,F.M.:1980, 'Transient Flow Development Due to a Strong Heat Source in the Atmosphere PartI: Uniform Temperature Source', **Combustion Science and Technology**, *23*, 163-175.

Ly,L.N.:1991, 'An Application of the E-ϵ Turbulence Model for Studying Coupled Air-Sea Boundary-Layer Structure', **Bound. Layer Meteor.**, *54*, 327-346.

Mahrer, Y. and R.A. Pielke:1977, 'The Effects of Topography on Sea and Land Breezes in a Two-Dimensional Numerical Model', **Mon. Wea. Rev.**, *105*, 1151-1162.

Mason, P.J. and R.I. Sykes:1980, 'A Two-Dimensional Numerical Study of Horizontal Roll Vortices in the Neutral Atmospheric Boundary Layer', **Quart. J. R. Met. Soc.**, *106*, 351-366 (1980).

Mason,P.J. and Thomson,D.J.:1987, 'Large-Eddy Simulations of the Neutral-Static-Stability PBL', **Quart. J. R. Met. Soc.**, *113*, 413-443.

McRae, G.J.:1981, 'Mathematical Modeling of Photochemical Air Pollution', Ph.D. Dissertation, California Institute Technology.

Mellor, G.L. and T. Yamada:1982, 'Development of a Turbulence Closure Model for Geophysical Fluid Problems', **Reviews of Geophysics and Space Physics**, *20(4)*, 851-875.

Mellor, G.L. and T. Yamada:1974, 'A Hierarchy of Turbulence Closure Models for Planetary Boundary Layers", **J. Atmos. Sci.**, *31*, 1791-1806.

Misra, P.K.:1980, 'Dispersion from Tall Stacks into a Shore Line Environment', **Atmos. Environ.**, *14*, 397-400

Misra, P.K. and S. Onlock:1982, 'Modelling Continuous Fumigation of Nanticoke Generation Station Plume', **Atmos. Environ.**, *16*, 479-489.

Moeng,C.H., and Wyngaard,J.C.:1989, 'Evaluation of Turbulent Transport and Dissipation Closures in Second-Order Modeling', **J. Atmos. Sci.**, *46.*, 2311-2330.

Mouzakis,F.N., and Bergeles,G.:1991, 'Pollutant Dispersion Over a Triangular Ridge: A Numerical Study', **Atmos. Environ.**, *25a. No.2.*, 371-379.

Neumann, J. and Y. Mahrer:1971, 'A Theoretical Study of the Land and Sea Breeze Circulation', **J. Atmos. Sci.**, *32*, 532-542.

Nelson, R.M. and C.M. Adkins:1986, 'Flame Characteristics of Wind-Driven Surface Fires', **Can. J. For. Res.**, *16*, 1292-1300.

Nieuwstadt, F.T.M. and H. von. Dop:1982, 'Atmospheric Turbulence and Air Pollution Modelling', D. Reidel Publishing Co.

Nieuwstadt,F.T.M.:1984,'The Turbulence Structure of the Stable Boundary Layer', **J. Atmos. Sci.**, *41*, 2202-2216.

Novitsky, M., D.D. Reible and B.M. Corripio:1991, 'Modeling the Dynamics of the Land-Sea Breeze Circulation for Air Quality Modeling', **Bound. Layer Meteor.**,?????.

Ogawa, T., T. Ohara, S. Wakamatsu, P.G. Diosey and I. Uno:1986, ' Observation of Lake Breeze Penetration and Subsequent Development of the Thermal Internal Boundary Layer for the Nanticoke II Shoreline Diffusion Experiment', **Bound. Layer Meteor.**, *35*, 207-230.

Ohara, T. and Y. Ogawa:1985, 'The Turbulent Structure of the Internal Boundary Layer near the Shore', **Bound. Layer Meteor.**, *32*, 39-56.

Ozoe, H., T. Shibata and H. Sayama:1983, 'Characteristics of Air Pollution in the Presence of Land and Sea Breeze-A numerical Simulation', **Atmos. Environ.**, *17*, 35-42.

Panofsky, H.A. and J.A. Dutton:1984, 'Atmospheric Turbulence',Jhon Wiley & Sons.

Pasquill, F. and Smith, F.B.:1983, 'Atmospheric Diffusion', Jhon Wiley & Sons.

Patankar, S.V.:1980, 'Numerical Heat Transfer', McGraw-Hill.

Patankar,S.V.:1981, 'A Calculation Procedure for Two-Dimensional Elliptic Situations', **Num. Heat. Transfer.**, *4*, 409-425.

Physick, W.L.:1980, 'Numerical Experiments on the Inland Penetration of the Sea Breeze', **Quart. J. R. Meteor. Soc.**, *106*, 735-746.

Physick, W.:1988, 'Mesoscale Modelling of a Cold Front and its Interaction with a Diurnally Heated Land Mass.', **J. Atmos. Sci.**, *45*, 3169-3187.

Pielke, R.A.:1974, 'A Three-Dimensional Numerical Model of the Sea Breezes in the South Florida', **Mon. Wea. Rev.**, *102*, 115-139.

Pielke, R.A. and R.T. McNidar, M. Segal and Y. Mahrer:1983, 'The Use of a Mesoscale Numerical Model for Evaluations of Pollutant Transport and Diffusion in Coastral Regions and

over Irregular Terrain', **Bulletin American Meteor. Soc.**, *64*, 243-249.

Pielke, R.A.:1984, 'Mesoscale Meteorological Modeling', Academic Press.

Rao, K.S., J.C.Wyngaard and O.R.Cote':1974, 'The Structure of the Two Dimensional Internal Boundary Layer over a Sudden Change of Surface Roughness', **J. of Atmos. Sci.**, *31*, 738-746.

Reible, D.D, F.H. Shair and R. Aris:1983, 'A Two-Layer Model of the Atmosphere Indicating the Effects of Mixing between the Surface Layer and the Air aloft', **Atmos. Environ.**, *17*, 25-33.

Reible, D.D., Simpson,J.E., and Linden,P.F.:1993, 'The Sea Breeze and Gravity-Current Frontogenesis', **Quart. J. R. Met. Soc.**, *119*, 1-16.

Riopelle,G. and Stubley,G.D.:1989, 'The Influence of Atmospheric Stability on the 'Leipzig' Boundary-Layer Structure', **Bound. Layer Meteor.**, *46*, 207-227.

Rodi,W.:1982, 'Turbulent Buoyant Jets and Plumes', **The Science and Application of Heat and Mass Transfer**, *6*, Pergamon Press.

Rodi,W.:1985, 'Calculation of Stably Stratified Shear-Layer Flows with a Buoyancy-Extended $k-\epsilon$ Turbulence Model', Turbulence and Diffusion in Stable Environments, J.C.R. Hunt, Clarendon Press, Oxford, 111-143.

Rotta, J.C.:1951, 'Statistische Theorie Nichthomogener Turbulenz', **Zeitschr. fu'r Physik**, *129*, 547-572.

Schlichting, H.: 1979, 'Boundary Layer Theory', Mcgraw-Hill.

Schünzen, K.H. and S. Pahl:1992, 'Modification of Dry Deposition in a Developing Sea-Breeze Circulation-A Numerical Case Study', **Atmos. Environ.**, *26A*, 51-61.

Sha, W., T. Kawamura and Ueda:1993, 'A Numerical Study of Nocturnal Sea Breezes:Prefrontal Gravity Waves in the Compensating Flow and Inland Penetration of the Sea-Breeze Cutoff Vortex', **J. Atmos. Sci.**, *50(8)*, 1076-??.

Sha, W., T. Kawamura, and H. Ueda:1991, 'A Numerical Study on Sea/Land Breezes as a Gravity Current: Kelvin-Helmholtz Billows and Inland Penetration of the Sea-Breeze Front', **J. Atmos. Sci.**, *48(4)*, 1649-1665.

Shair, F.H, E.J. Sasaki, D.E. Carlan, G.R. Cass and W.R. Goodin:1982, 'Transport and Dispersion of Airborne Pollutants Associated with the Land Breeze-Sea Breeze System', **Atmos. Environ.**, *16*, 2042-2053.

Simpson, J.E., D.A. Mansfield, and J.R. Milford:1977, 'Inland Penetration of Sea-breeze Fronts', **Quart. J. R. Met. Soc.**, *103*, 47-76.

Simpson, J.E.: 1987, 'gravity Currents', Jhon Wiley & Sons.

Stubley,G.D. and G. Riopelle:1988, 'The Influence of the Earth's Rotation on PBL Turbulence', **Bound. Layer Meteor.**, *45*, 307-324.

Stubley, G.D. and D.R. Rooney:1986, 'The Sensitivity of $k-\epsilon$ Model Computations of the Neutral Planetary Boundary Layer to Baroclinity', **Bound. Layer Meteor.**, *27*, 53-70.

Stull,R.B.:1988, 'An Introduction to Boundary Layer Meteorology', Kluwer Academic Publishers.

Stunder, M. and S. Sethuraman:1985, 'A Comparative Evaluation of the Coastal Internal Boundary-Layer Height Equations', **Bound. Layer Meteor.**, *32*, 177-204.

Sun, W.Y. and Y. Ogura:1980, 'Modeling the Evolution of the Convective Planetary Boundary Layer', **J. Atmos. Sci.**, *37*, 1558-1572.

Suttan, S.B., H. Brandt and B.R. White:1986, 'Atmospheric Dispersion of A Heavier-Than-Air Gas Near a Two-Dimensional Obstacle', **Bound. Layer Meteor.**, *35*, 125-153.

Uno,I., Ueda,h., and Wakamatsu,S.:1989,'Numerical Modeling of the Nocturnal Urban Boundary Layer', **Bound. Layer. Meteor.**, *49*, 77-98.

van Ulden, A.P.:1978, 'Simple Estimate for Vertical Diffusion from Sources near the Ground', **Atmos. Environ.**, *12*, 2125-2129.

Willis, G.E. and J.W. Deardorff:1974, 'A Laboratory Model of the Unstable Planetary Boundary Layer', **J. Atmos. Sci.**, *31*, 1297-1307.

Wyngaard, J.C.:1975, 'Modeling the Planetary Boundary Layer-Extension to the Stable Case', **Bound. Layer Meteor.**, *9*, 441-460.

Wyngaard, J.C. and O.R. Cote':1974a, 'The Evolution of a Convective Planetary Boundary Layer-a Higher-Order-Closure Model Study', **Bound. Layer Meteor.**, 7, 289-308.

Wyngaard, J.C.:1983, 'The Mean Structure of the Baroclinic, Convective Boundary Layer', **Proceedings of the First Sino-American Workshop on Mountain Meteorology,**

Yamada, T.:1977, 'A Numerical Experiment on Pollutant Dispersion in a Horizontally-Homogeneous Atmospheric Boundary Layer', **Atmos. Environ.**, *11*, 1015-1024.

Yamada, T. and G.L. Mellor:1975, 'A Simulation of the Wangara Atmospheric Boundary LAyer Data', **J. Atmos. Sci.**, *32*, 2309-2329.

Yamada, T.:1982, 'A Numerical Model study of Turbulent Airflow in and Above a Forest Canopy', **J. Meteor. Soc. Japan**, *60(1)*, 439-454.

Zeman, O., and J.L. Lumley:1979, 'Buoyancy Effects in Entraining Turbulent Boundary Layers': A Second Order Closure Study. *Turbulent Shear Flows I*, F.Durst, B.E.Launder, F.W. Schimidt and J.H. Whitelaw, Eds., Springer-Verlag, 295-306.

Zilitinkevich, S.S., Laikhtman, D.L., and Monin, A.S.:1967, 'Dynamics of the Atmospheric Boundary Layer', **Atmos. and Oceanic Phys.**, *3*, 170-191.

Appendix A. Derivation of a Modified E-ϵ Model

The transport equations of the Reynolds stresses and turbulent eddy fluxes are (Gibson and Launder,1978; Mellor and Yamada,1982; Rodi,1985; Haroutunian and Launder,1988):

$$\frac{\partial \overline{u_i'u_j'}}{\partial t} + U_k \frac{\partial \overline{u_i'u_j'}}{\partial x_k} = \frac{\partial}{\partial x_k}(c_s \frac{E}{\epsilon}\overline{u_k'u_l'}\frac{\partial \overline{u_i'u_j'}}{\partial x_l}) + P_{ij} + G_{ij} + \phi_{ij} - \frac{2}{3}\delta_{ij}\epsilon \tag{A-1}$$

$$\frac{\partial \overline{u_i'\theta'}}{\partial t} + U_k \frac{\partial \overline{u_i'\theta'}}{\partial x_k} = \frac{\partial}{\partial x_k}(c_s' \frac{E}{\epsilon}\overline{u_k'u_l'}\frac{\partial \overline{u_i'\theta'}}{\partial x_l}) - \overline{u_i'u_k'}\frac{\partial \Theta}{\partial x_k} + P_{iT} + G_{iT} + \phi_{iT} \tag{A-2}$$

$$\frac{\partial \overline{\theta'^2}}{\partial t} + U_k \frac{\partial \overline{\theta'^2}}{\partial x_k} = \frac{\partial}{\partial x_k}(c_T' \frac{E}{\epsilon}\overline{u_k'u_l'}\frac{\partial \overline{\theta'^2}}{\partial x_l}) - 2\overline{u_k'\theta'}\frac{\partial \Theta'}{\partial x_k} - \frac{1}{R}\frac{\overline{\theta'^2}}{E}\epsilon \tag{A-3}$$

After neglecting time dependent, convective and diffusion transport terms in the above equations, the following algebraic equations for the turbulence fluxes can be obtained (Rodi,1985):

$$P_{ij} + G_{ij} + \phi_{ij} - \frac{2}{3}\delta_{ij}\epsilon = 0 \tag{A-4}$$

$$- \overline{u_i'u_k'}\frac{\partial \Theta}{\partial x_k} + P_{iT} + G_{iT} + \phi_{iT} = 0 \tag{A-5}$$

$$- 2\overline{u_k'\theta'}\frac{\partial \Theta'}{\partial x_k} - \frac{1}{R}\frac{\overline{\theta'^2}}{E}\epsilon = 0 \tag{A-6}$$

The terms P_{ij}, G_{ij}, P_{iT} and G_{iT} represent production of $\overline{u_i'u_j'}$ and $\overline{u_i'\theta'}$ due to mean strain and buoyancy:

$$P_{ij} = -(\overline{u_i'u_k'}\frac{\partial U_j}{\partial x_k} + \overline{u_j'u_k'}\frac{\partial U_i}{\partial x_k}) \tag{A-7}$$

$$G_{ij} = -\beta (g_i\overline{u_j'\theta'} + g_j\overline{u_i'\theta'})$$

191

$$P_{iT} = -\overline{u_k'\theta'}\frac{\partial U_i}{\partial x_k}$$

$$G_{iT} = -\beta\overline{\theta'^2}g_i$$

The ϕ_{ij} and ϕ_{iT} denote the pressure-strain terms. Gibson and Launder (1978) proposed the correction terms for the effects of the wall on the pressure-velocity redistribution terms because there are significant differences of the ratio of the horizontal and vertical velocity variances between near boundary layer and free flows. A theoretical explanation for this difference is due to the influence of the proximity of the wall on the pressure-velocity redistribution:

$$\phi_{ij} = \phi_{ij,1} + \phi_{ij,2} + \phi_{ij,3} + \phi_{ij,1}' + \phi_{ij,2}' + \phi_{ij,3}'$$
$$\phi_{iT} = \phi_{iT,1} + \phi_{iT,2} + \phi_{iT,3} + \phi_{iT,1}' + \phi_{iT,2}' + \phi_{iT,3}'$$

$$(A-8)$$

The Launder and Gibson scheme has terms representing nonlinear turbulence interactions($\phi_{ij,1}, \phi_{iT,1}$), mean shear interaction($\phi_{ij,2}, \phi_{iT,2}$) and buoyancy interactions($\phi_{ij,3}, \phi_{iT,3}$). The prime in each term represents the ground contribution on the pressure redistributions.

$$\phi_{ij,1} = -c_1\frac{\epsilon}{E}(\overline{u_i'u_j'} - \frac{2}{3}\delta_{ij}E) \qquad (A-9)$$

$$\phi_{ij,2} = -c_2(P_{ij} - \frac{2}{3}\delta_{ij}P) \qquad (A-10)$$

$$\phi_{ij,3} = -c_3(G_{ij} - \frac{2}{3}\delta_{ij}G) \qquad (A-11)$$

$$\phi'_{ij,1} = c'_1 \frac{\epsilon}{E} (\overline{u'_k u'_m} n_k n_m \delta_{ij} - \frac{3}{2} \overline{u'_k u'_i} n_k n_j - \frac{3}{2} \overline{u'_k u'_j} n_k n_i) f(\frac{1}{x_i n_i}) \quad \text{(A-12)}$$

$$\phi'_{ij,2} = c'_2 (\phi_{km,2} n_k n_m \delta_{ij} - \frac{3}{2} \phi_{ki,2} n_k n_j - \frac{3}{2} \phi_{kj,2} n_{kn_i}) f(\frac{1}{x_i n_i}) \quad \text{(A-13)}$$

$$\phi'_{ij,3} = c'_3 (\phi_{km,3} n_k n_m \delta_{ij} - \frac{3}{2} \phi_{ki,3} n_k n_j - \frac{3}{2} \phi_{kj,3} n_{kn_i}) f(\frac{1}{x_i n_i}) \quad \text{(A-14)}$$

$$\phi_{iT,1} = -c_{1T} \frac{\epsilon}{k} \overline{u'_i \theta'} \quad \text{(A-15)}$$

$$\phi_{iT,2} = -c_{2T} P_{iT} \quad \text{(A-16)}$$

$$\phi_{iT,3} = -c_{3T} G_{iT} \quad \text{(A-17)}$$

$$\phi'_{iT,1} = -c'_{1T} \frac{\epsilon}{k} \overline{u'_k \theta'} n_i n_k f(\frac{1}{x_i n_i}) \quad \text{(A-18)}$$

$$\phi'_{iT,2} = c'_{2T} c_{2T} P_{kT} n_i n_k f(\frac{1}{x_i n_i}) \quad \text{(A-19)}$$

$$\phi'_{iT,3} = c'_{3T} c_{3T} G_{kT} n_i n_k f(\frac{1}{x_i n_i}) \quad \text{(A-20)}$$

Where $P = 0.5 \; P_{ii}$ and $G = 0.5 \; G_{ii}$. The model constants involved in this model are from Rodi (1985) and are given in Table A.1.

Initial experience using this model indicated that modifications are required to describe pressure fluctuation effects for flows involving a free surface (Celik and Rodi, 1984). This is true even in the case of constant density open-channel flow where a clear additional damping of the transverse normal variance occurs near the free

Table A.1. Constants used in the modified E-ϵ model(Rodi,1985).

c_1	c_2	c_3	c'_1	c'_2	c'_3	c_{1T}	c_{2T}	c_{3T}	c'_{1T}	c'_{2T}	c'_{3T}	R
2.2	0.55	0.55	0.5	0.3	0.0	3.0	0.5	0.5	0.5	0.0	0.0	0.8

surface. It turns out to be equally important in the scalar flux equations. In this expression n_i represents the unit vector normal to the surface. The argument of the function $f(\frac{l}{x_i n_i})$ represents the ratio between the length scale of turbulence and the distance perpendicular to the surface. The role of the function f is to reduce the influence of the corrections away from the immediate vicinity of the surface. It has been usual to choose a linear function normalized in such a way that f takes on a value of unity in the local equilibrium region of the ground and zero near the free surface. The wall effect function(f) is obtained from Gibson and Launder (1978).

$$f = \frac{l}{\kappa \, z} = \frac{c_\epsilon \, E^{3/2}}{\kappa \, z \, \epsilon} \qquad \text{(A-21)}$$

In the above equation, Kolmogorov's hypothesis which relates the dissipation rate with the length scale is used. c_ϵ is determined from the constant values in the ϵ-equation. $c_\epsilon = 0.13$ which is obtained from the standard E-ϵ model and is used in this study.

In the algebraic stress model, diffusion and convection of the velocity variances are neglected. In order to compensate for the neglected diffusion and convection effects, Rodi (1985) and Helfand and Labraga (1988) suggested several methods. According to Rodi's approach, the combined convective and diffusive transport is assumed proportional to the corresponding transport of turbulent

kinetic energy. Rodi (1985) applied this approach to the equations for vertical fluctuating velocity variance and temperature variance.

$$(Conv. - Diff.)_{\overline{w'^2}} = \frac{\overline{w'^2}}{E} (Conv. - Diff.)_E = \overline{w'^2} \frac{\epsilon}{E} (\frac{P + G}{\epsilon} - 1) \quad \text{(A-22)}$$

$$(Conv. - Diff.)_{\overline{\theta'^2}} = \frac{\overline{\theta'^2}}{E} (Conv. - Diff.)_E = \overline{\theta'^2} \frac{\epsilon}{E} (\frac{P + G}{\epsilon} - 1) \quad \text{(A-23)}$$

The algebraic stress equations after applying the horizontal boundary layer approximation to Equations (A-4) and (A-5) are:

$$\overline{u'^2} = \frac{2}{3} \frac{c_1 - 1}{c_1} E + \frac{c_1'}{c_1} f \overline{w'^2} - \frac{E}{c_1 \epsilon} (E_1 \overline{u'w'} \frac{\partial U}{\partial z} + E_2 \overline{v'w'} \frac{\partial V}{\partial z} - E_3 \beta g \overline{w'\theta}) \quad \text{(A-24)}$$

$$\overline{v'^2} = \frac{2}{3} \frac{c_1 - 1}{c_1} E + \frac{c_1'}{c_1} f \overline{w'^2} - \frac{E}{c_1 \epsilon} (E_2 \overline{u'w'} \frac{\partial U}{\partial z} + E_1 \overline{v'w'} \frac{\partial V}{\partial z} - E_3 \beta g \overline{w'\theta}) \quad \text{(A-25)}$$

$$\overline{w'^2} = \frac{2}{3} \frac{c_1 - 1}{E_4} E - \frac{E}{E_4 \epsilon} (E_5 \overline{u'w'} \frac{\partial U}{\partial z} + E_5 \overline{v'w'} \frac{\partial V}{\partial z} - E_6 \beta g \overline{w'\theta}) \quad \text{(A-26)}$$

$$\overline{u'w'} = \frac{E}{\epsilon} (-E_7 \overline{w'^2} \frac{\partial U}{\partial z} + E_8 \beta g \overline{u'\theta'}) \quad \text{(A-27)}$$

$$\overline{v'w'} = \frac{E}{\epsilon} (-E_7 \overline{w'^2} \frac{\partial V}{\partial z} + E_8 \beta g \overline{v'\theta'}) \quad \text{(A-28)}$$

$$\overline{u'v'} = - \frac{E}{\epsilon} \frac{1 - c_2}{c_1} (\overline{u'w'} \frac{\partial V}{\partial z} + \overline{v'w'} \frac{\partial U}{\partial z}) \quad \text{(A-29)}$$

$$\overline{u'\theta'} = - \frac{1}{c_{1T}} \frac{E}{\epsilon} (\overline{u'w'} \frac{\partial \Theta}{\partial z} + (1 - c_{2T}) \overline{w'\theta} \frac{\partial U}{\partial z}) \quad \text{(A-30)}$$

$$\overline{v'\theta'} = - \frac{1}{c_{1T}} \frac{E}{\epsilon} (\overline{v'w'} \frac{\partial \Theta}{\partial z} + (1 - c_{2T}) \overline{w'\theta} \frac{\partial V}{\partial z}) \quad \text{(A-31)}$$

$$\overline{w'\theta'} = - \frac{1}{c_{1T} + c'_{1T}} \frac{E}{\epsilon} \left(\overline{w^2} \frac{\partial \Theta}{\partial z} - E_9 \beta g \overline{\theta'^2} \right) \qquad (A\text{-}32)$$

$$\overline{\theta'^2} = - \frac{2}{E_{10}} \frac{E}{\epsilon} \overline{w'\theta} \frac{\partial \Theta}{\partial z} \qquad (A\text{-}33)$$

where the constants are

$$E_1 = 2 - \frac{4}{3} c_2 + \frac{2}{3} c_2 c'_2 f$$

$$E_2 = \frac{2}{3} c_2 + \frac{2}{3} c_2 c'_2 f$$

$$E_3 = \frac{2}{3} c_3 - \frac{4}{3} c_3 c'_3 f$$

$$E_4 = \frac{(P + G - \epsilon)}{\epsilon} + c_1 + 2 c'_1 f$$

$$E_5 = \frac{2}{3} c_2 - \frac{4}{3} c_2 c'_2 f$$

$$E_6 = 2 - \frac{4}{3} c_3 + \frac{8}{3} c_3 c'_3 f \qquad (A\text{-}34)$$

$$E_7 = \frac{(1 - c_2 + 1.5 c_2 c'_2 f)}{(c_1 + 1.5 c'_1 f)}$$

$$E_8 = \frac{(1 - c_3 + 1.5 c_3 c'_3 f)}{(c_1 + 1.5 c'_1 f)}$$

$$E_9 = 1 - c_{3T} + c_{3T} c'_{3T} f$$

$$E_{10} = \frac{(P + G - \epsilon)}{\epsilon} + \frac{1}{R}$$

In this approximation, the horizontal velocity and temperature gradients are neglected because the order of magnitude of these terms is less than those of the vertical gradients. And the horizontal divergences of the turbulent fluxes are assumed to be negligible. By continuity, the mean vertical velocity is ignored.

All these equations can be reduced to algebraic expressions for the individual turbulent flux. The resulting

expressions for $\overline{u'w'}, \overline{w'\theta'}$ can be written in the turbulent eddy viscosity and thermal diffusivity forms of equations (2-5) and (2-6) with some algebraic manipulations (Yamada, 1977). From these relations, the proportionality coefficients, c_m and c_h, can be expressed as a function of the flow dynamics and the buoyancy. This means that the parameters now depend on stratification and surface damping. The vertical turbulent eddy viscosity($K_m{}^z$) and thermal diffusivity($K_h{}^z$) of the modified E-ϵ model are;

$$K_m^z = c_m \frac{E^2}{\epsilon} \tag{A-35}$$

$$K_h^z = c_h \frac{E^2}{\epsilon} \tag{A-36}$$

and c_m and c_h can be calculated from the following relations;

$$c_m = \frac{2}{3} \frac{(c_1 - 1)(E_7 - A\,G_H)}{E_4 + \dfrac{E_4\,E_8}{C_{1T}}G_H - E_5\,E_7\,G_M + E_5\,A\,G_H\,G_M} \tag{A-37}$$

$$c_h = \frac{\dfrac{2}{3}(C_1 - 1) + E_5\,G_M\,c_m}{(c_{1T} + c_{1T}'\,f)\,E_4 + \left(\dfrac{2\,E_4\,E_9}{E_{10}} + E_6\right)G_H} \tag{A-38}$$

where

$$G_M = \left(\frac{E}{\epsilon}\right)^2 \left[\left(\frac{\partial \overline{U}}{\partial z}\right)^2 + \left(\frac{\partial \overline{V}}{\partial z}\right)^2\right] \tag{A-39}$$

$$G_H = \beta\,g\,\left(\frac{E}{\epsilon}\right)^2 \frac{\partial \theta}{\partial z} \tag{A-40}$$

$$A = \frac{E_6 \, E_7 \, + \, \dfrac{(1 \, - \, c_{2T}) \, E_4 \, E_8}{C_{1T}}}{(c_{1t} \, + \, c_{1T}' \, f) \, E_4 \, + \, (\dfrac{2 \, E_4 \, E_9}{E_{10}} \, + \, E_6) \, G_H} \qquad \text{(A-41)}$$

Appendix B. Derivation of a Level 2.5 Model

The level 2.5 model coupled with a wall function was studied by Galperin and Hassid (1983) and Andrén (1990). They used a length scale approach instead of a dissipation rate model. In order to compare to the ϵ-equation approach used here, level 2.5 model is derived.

The level 2.5 model is derived from the level 4.0 model which is equivalent to Equations (A-1) to (A-3). The systematic simplification based on the analysis of the order of the anisotropy was carried out by Mellor and Yamada (1974,1982). As a result of the simplification, the equations of Reynolds stresses and turbulent fluxes for the level 2.5 model are:

$$P_{ij} + G_{ij} + \phi_{ij} - \frac{2}{3}\delta_{ij}(P + G) = 0 \tag{B-1}$$

$$- \overline{u_i'u_k'}\frac{\partial\Theta}{\partial x_k} + P_{iT} + G_{iT} + \phi_{iT} = 0 \tag{B-2}$$

$$- 2\overline{u_k'\theta'}\frac{\overline{\partial\theta'}}{\partial x_k} - \frac{1}{R}\frac{\overline{\theta'^2}}{k}\epsilon = 0 \tag{B-3}$$

The main difference between the modified E-ϵ and level 2.5 model is that the dissipation rate(ϵ) in Equation (A-4) is replaced by P+G in Equations (B-1). This means that the level 2.5 model implicitly incorporates the local equilibrium assumption. After applying the pressure-strain terms(ϕ_{ij} and ϕ_{iT}) from Equation (A-8) and the horizontal boundary layer approximation to Equations (B-1) - (B-3), the

algebraic equations for the Reynolds stresses and turbulent fluxes are:

$$\overline{u'^2} = \frac{2}{3}E + \frac{c_1'}{c_1}f\,\overline{w'^2} - \frac{E}{c_1\epsilon}\left(\frac{E_1}{3}\overline{u'w'}\frac{\partial U}{\partial z} - \frac{E_2}{3}\overline{v'w'}\frac{\partial V}{\partial z} + \frac{E_3}{3}\beta g\overline{w'\theta}\right) \tag{B-4}$$

$$\overline{v'^2} = \frac{2}{3}E + \frac{c_1'}{c_1}f\,\overline{w'^2} - \frac{E}{c_1\epsilon}\left(-\frac{E_2}{3}\overline{u'w'}\frac{\partial U}{\partial z} + \frac{E_1}{3}\overline{v'w'}\frac{\partial V}{\partial z} + \frac{E_3}{3}\beta g\overline{w'\theta}\right) \tag{B-5}$$

$$\overline{w'^2} = \frac{2}{3}\frac{c_1}{c_1 + 2c_1'f}E + \frac{E}{(c_1 + 2c_1'f)\epsilon}\left(\frac{E_4}{3}\overline{u'w'}\frac{\partial U}{\partial z} + \frac{E_4}{3}\overline{v'w'}\frac{\partial V}{\partial z} + \frac{2E_3}{3}\beta g\overline{w'\theta}\right) \tag{B-6}$$

$$\overline{u'w'} = \frac{E}{\epsilon}\left(-E_5\overline{w^2}\frac{\partial U}{\partial z} + E_6\beta g\overline{u'\theta'}\right) \tag{B-7}$$

$$\overline{v'w'} = \frac{E}{\epsilon}\left(-E_5\overline{w^2}\frac{\partial V}{\partial z} + E_6\beta g\overline{v'\theta'}\right) \tag{B-8}$$

$$\overline{u'v'} = -\frac{E}{\epsilon}\frac{1 - c_2}{c_1}\left(\overline{u'w'}\frac{\partial V}{\partial z} + \overline{v'w'}\frac{\partial U}{\partial z}\right) \tag{B-9}$$

$$\overline{u'\theta'} = -\frac{1}{c_{1T}}\frac{E}{\epsilon}\left(\overline{u'w'}\frac{\partial\Theta}{\partial z} + (1 - c_{2T})\overline{w'\theta}\frac{\partial U}{\partial z}\right) \tag{B-10}$$

$$\overline{v'\theta'} = -\frac{1}{c_{1T}}\frac{E}{\epsilon}\left(\overline{v'w'}\frac{\partial\Theta}{\partial z} + (1 - c_{2T})\overline{w'\theta}\frac{\partial V}{\partial z}\right) \tag{B-11}$$

$$\overline{w'\theta'} = -\frac{1}{c_{1T} + c_{1T}'f}\frac{E}{\epsilon}\left(\overline{w^2}\frac{\partial\Theta}{\partial z} - (1 - c_{3T} + c_{3T}c_{3T}'f)\beta g\overline{\theta'^2}\right) \tag{B-12}$$

$$\overline{\theta'^2} = -2R\frac{E}{\epsilon}\overline{w'\theta}\frac{\partial\Theta}{\partial z} \tag{B-13}$$

where the constants are

$$E_1 = 4 - 4c_2 + 2c_2c_2'f \tag{B-14}$$

$$E_2 = 2 - 2c_2 - 2c_2c_2'f$$

$$E_3 = 2 - 2c_3 + 4c_3 c_3' f$$

$$E_4 = 2 - 2c_2 + 4c_2 c_2' f$$

$$E_5 = \frac{(1 - c_2 + 1.5 c_2 c_2' f)}{(c_1 + 1.5 c_1' f)}$$

$$E_6 = \frac{(1 - c_3 + 1.5 c_3 c_3' f)}{(c_1 + 1.5 c_1' f)}$$

And the parameter c_m and c_h can be obtained from the above equations with some algebraic manipulation as described in Appendix A.

$$c_m = \frac{\dfrac{2\ c_1\ E_5}{c_1 + 2\ c_1'\ f} - 2\ A\ G_H}{3 + \dfrac{E_4\ E_5}{c_1 + 2\ c_1\ f}\ G_M + \dfrac{3\ E_6}{c_{1T}}\ G_H - \dfrac{E_4}{c_1}\ A\ G_H\ G_M} \tag{B-15}$$

$$c_h = \frac{\dfrac{c_1}{3\,(c_1 + 2\ c_1'\ f)}\ \left(2 - \dfrac{E_4}{c_1}\ G_M\ c_m\right)}{c_{1T} + c_{1T}'\ f + \left(\ 2\,(1 - c_{3T} + c_{3T}\ c_{3T}'\ f)\ R + \dfrac{2}{3}\dfrac{E_3}{c_1 + 2\ c_1'\ f}\right)\ G_H} \tag{B-16}$$

where G_M and G_H are the same as the Equations (A-39) and (A-40), and A is:

$$A = \frac{\dfrac{c_1}{c_1 + 2\ c_1'\ f}\ \left(\dfrac{2\ E_3\ E_5}{c_1 + 2\ c_1'\ f} + 3\ E_6\ \dfrac{1 - c_{2T}}{c_{1T}}\right)}{3\,(c_{1T} + c_{1T}'f) + \left(6R(1 - c_{3T} + c_{3T}c_{3T}'f) + \dfrac{2E_3}{c_1 + 2c_1'f}\right)G_H} \tag{B-17}$$

Appendix C. Numerical Details of Sea Breeze Simulation

In order to check the convergence within a given time step, variations of maximum deviation from mass continuity equation in a whole calculation domain (M_{max}), horizontal and vertical velocities, and turbulent kinetic energy at the fixed grid point with number of iteration were monitored in Figure C.1. The monitoring position was chosen as the grid point where the front of the sea breeze was passing at 12:10 LST. The monitoring position was 5km inland and 640m in height. The criterion of the convergence in this calculation was M_{max} = 5 x 10^{-4}. The convergence criterion was satisfied when the number of iteration was over 75. The horizontal and vertical velocities and kinetic energy at the monitoring position, however, converged less than 25 iterations.

The horizontal resolution is expected to be a key parameter in the sea breeze simulation. As pointed out by Avissar et al. (1990), the choice of horizontal resolution is limited by the computer availability and the flow structure of interest. Figure C.2 shows the velocity profile with various horizontal grid sizes (Δx). The position of front is 8km inland with Δx = 4 km and it is 5.0 km with Δx = 2km and Δx = 4km. The maximum vertical velocity near the front with Δx = 1km is higher than those with Δx = 2km and Δx = 4 km. The difference of front position between Δx = 1km and 2 km is not noticeable. The fine grid resolution, however, is expected to give more detailed information of
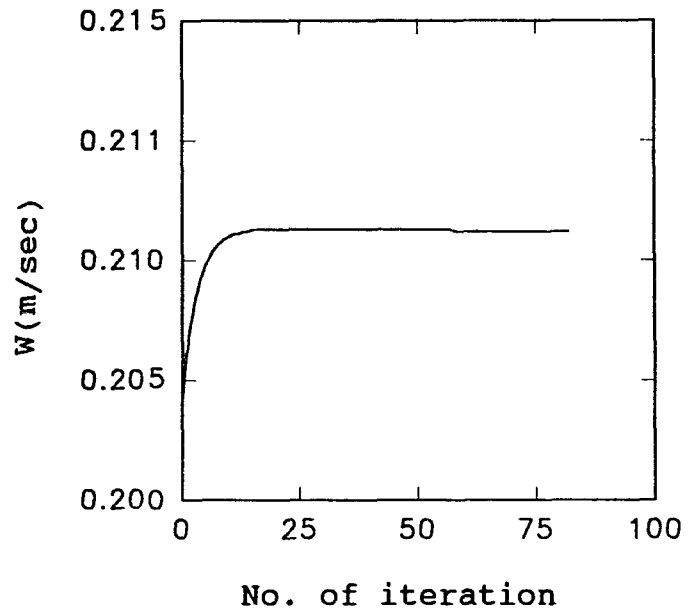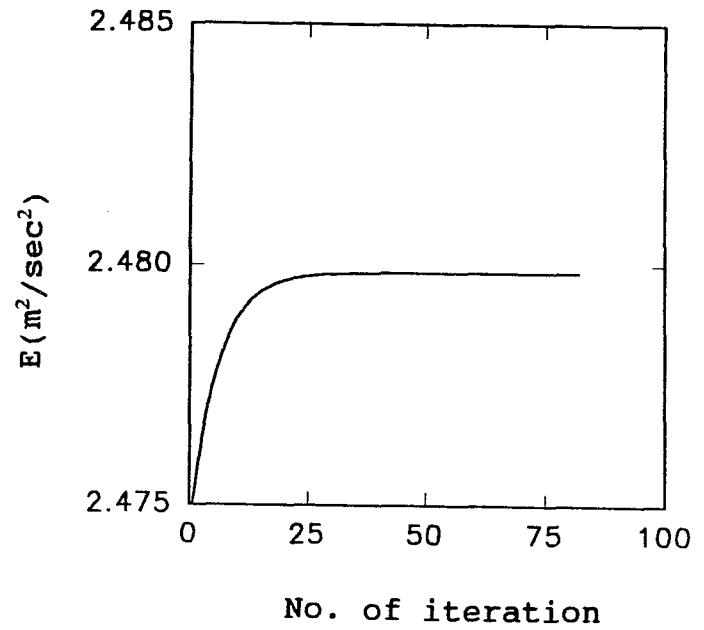
203
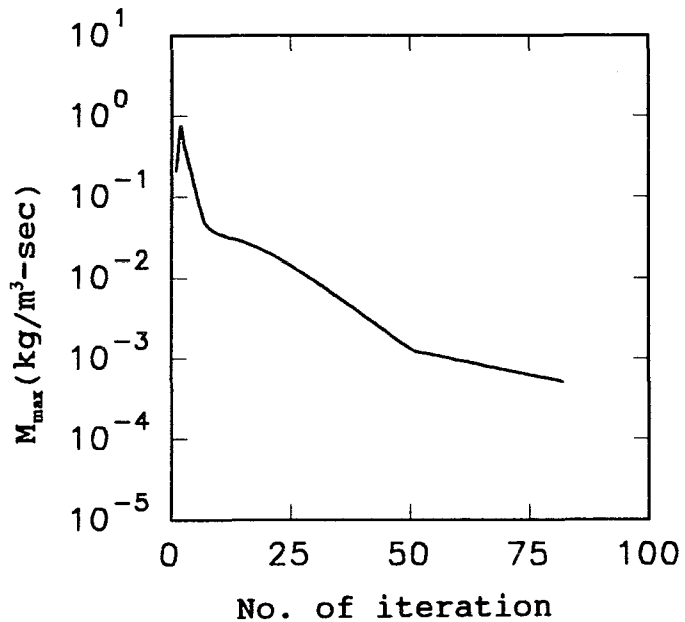
(a)deviation of continuity
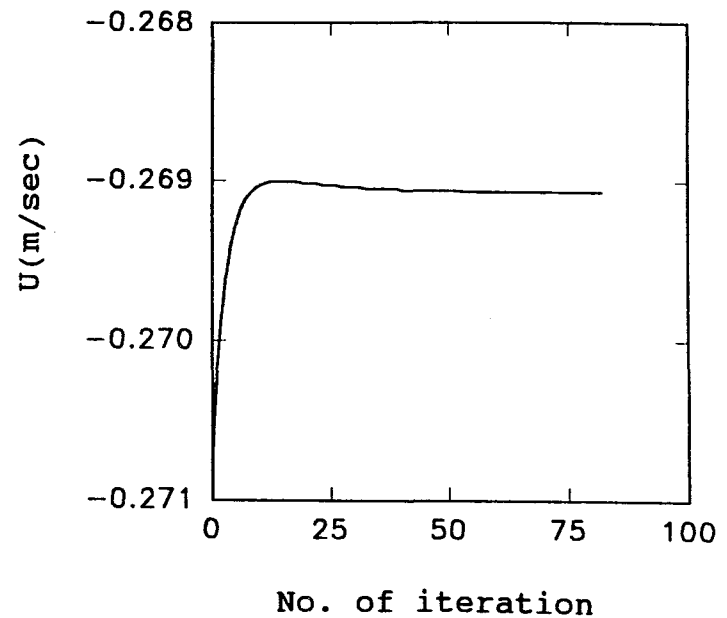
(b)horizontal velocity

Fig.C.1. Example of convergence at 12:10 LST with Case H and U_g = -m/sec. The position of grid is 5km inland and 640m in height. M_{max} is maximum deviation from the continuity equation in the whole calculation domain.

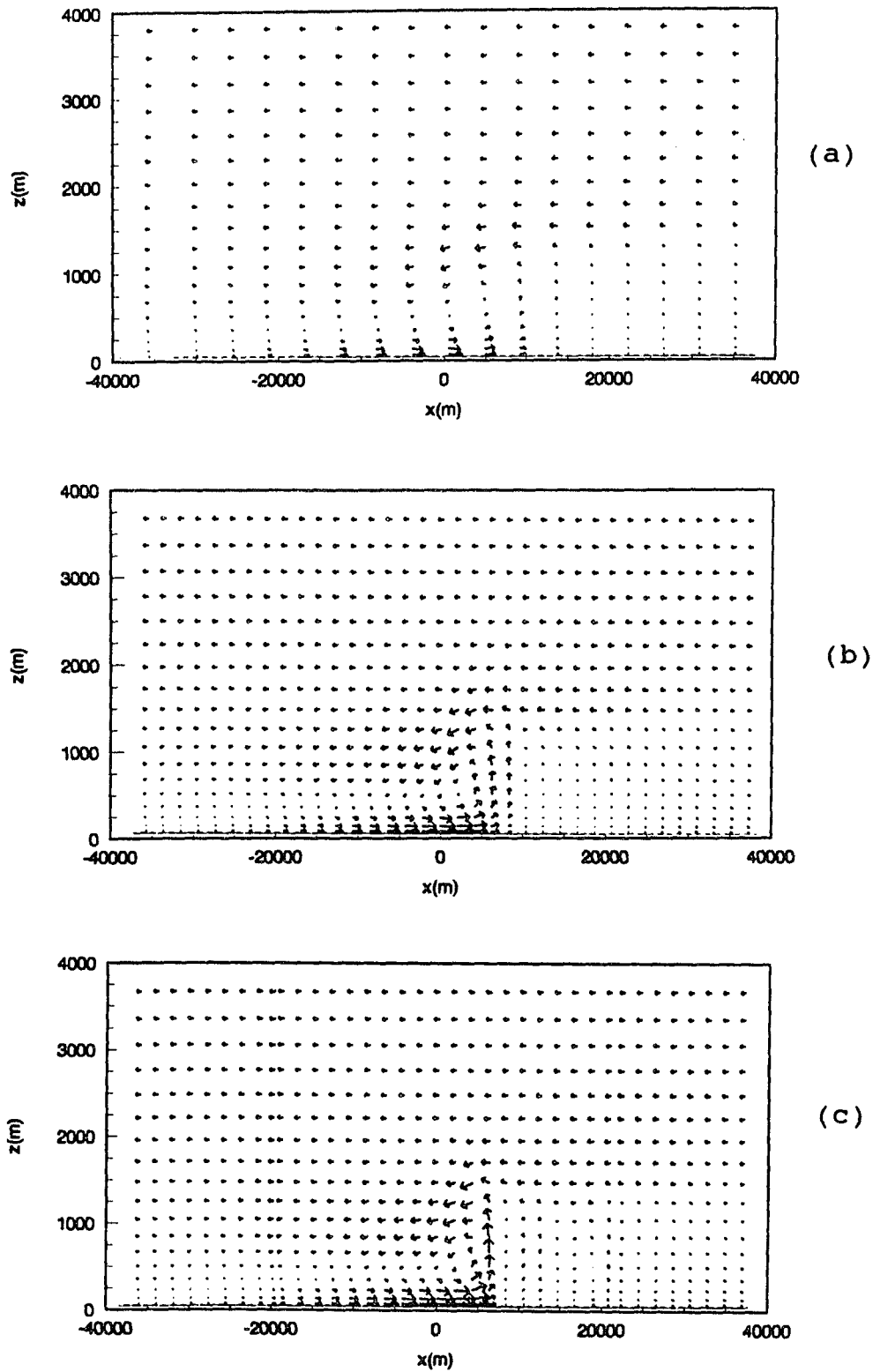(c)vertical velocity

(d)kinetic energy

Fig.C.1. Continued.

Fig.C.2. Effects of horizontal grid size ($\triangle$x) on the velocity profile at 12 LST with Case H and U_g = -1m/sec. (a)$\triangle$x = 4km (b)$\triangle$x = 2km (c)$\triangle$x = 1km.

the flow structure.   Due to the computational time limit, the Δx = 2km was used in this study. It took CPU time of about 3 days in an IBM 3090 to calculate one day cycle of the sea breeze with Case H. The simulation with a fine grid is recommended for further study.

The effects of extent of horizontal domain in the sea side on the sea breeze circulation were investigated by varying the size of the horizontal domain. Figure C.3 shows the velocity profiles obtained by using various sizes of the horizontal domain at 14 LST. The calculated maximum velocity in the following flow (U_{max}) and maximum vertical velocity (W_{max}) near the front are listed in Table C.1.

Table C.1. Calculated maximum velocities with various
          horizontal domain sizes.

horizontal size	U_{max}(m/sec)	W_{max}(m/sec)
−30km < x < 50km	7.5 (3km, 80m)*	0.48 (13km, 898m)
−50km < x < 190km	6.76 (3km, 80m)	0.45 (11km, 898m)
−100km < x < 190km	6.45 (3km, 80m)	0.44 (11km, 898m)

* represents the inland position and height

The small domain (L=80km) shows higher vertical velocity near the front as well as the horizontal velocity in the following flow.   Since the difference of the horizontal domain size between L = 240 km and 290 km was small, the horizonal size with 240km was used in this study.

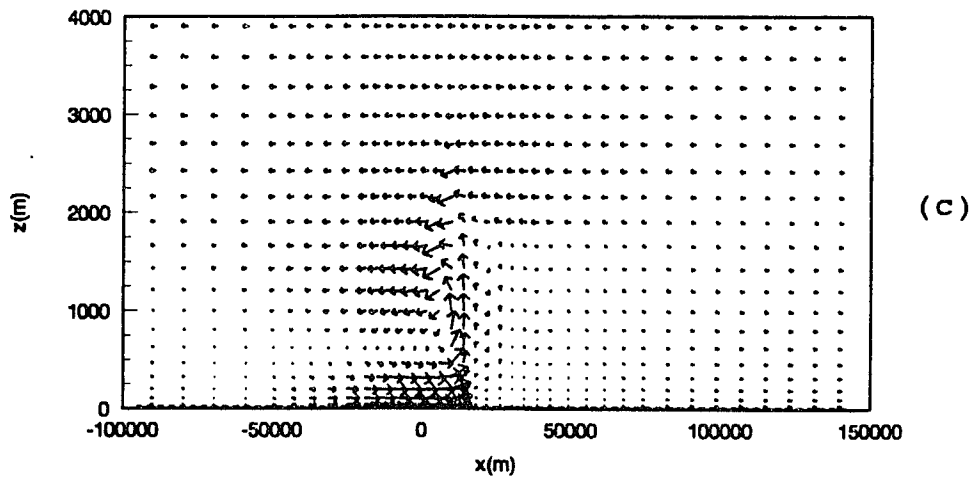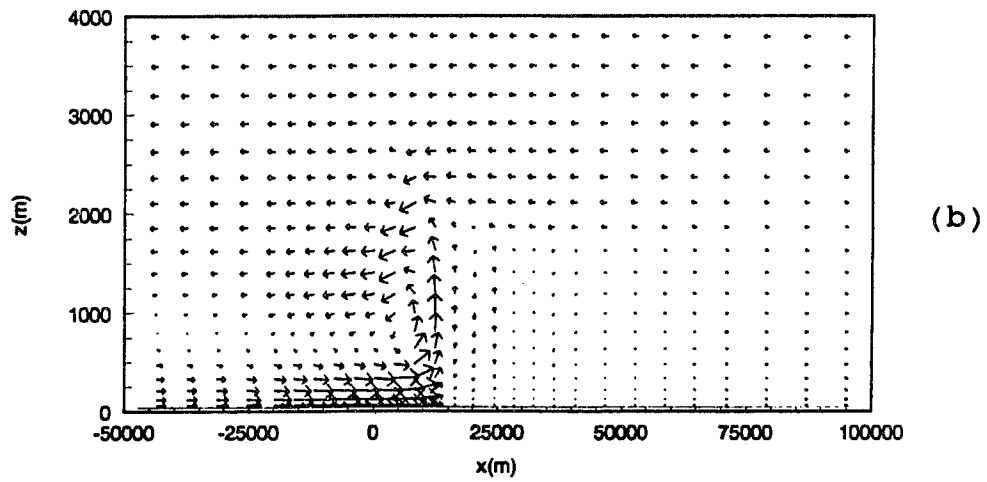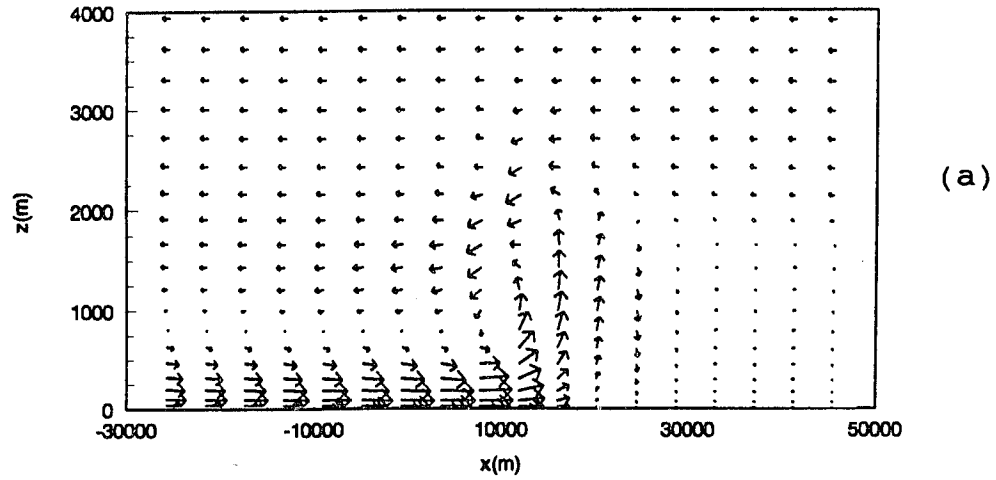Fig.C.3. Effects of horizontal domain size (L) on the velocity profile at 14 LST with Case H and U_g = -1m/sec. (a)L = 80km (b)L = 240km (c)L = 290km.

Vita

The author, Youn-Seo Koo was born in Seoul, Korea on January 7, 1958. In February 1978, he graduated from Wooshin High School in Seoul, Korea. In February 1982, he received a B.S. degree in Chemical Engineering from Seoul City University. He received a M.S. degree in Chemical Engineering from Seoul National University in February 1984. He worked at the Research Institute of Industrial Science and Technology and Pohang Iron & Steel Co. in Pohang, Korea for six and half years. He married Il-Sook Han in November 1984 and has a boy, Ji-Seok Koo. In the fall of 1990, he enrolled in Louisiana State University as a candidate for the degree of Doctor of Philosophy in Chemical Engineering.

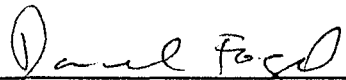# DOCTORAL EXAMINATION AND DISSERTATION REPORT

Candidate: Youn-Seo Koo
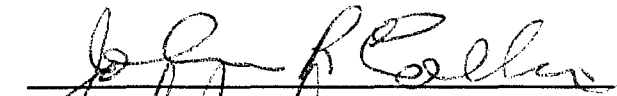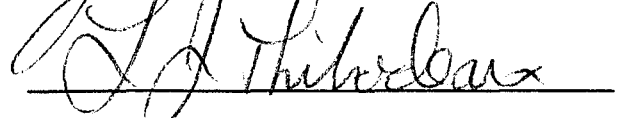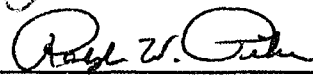
Major Field: Chemical Engineering

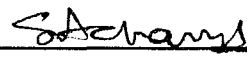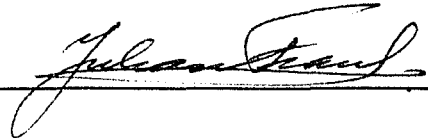**Title of Dissertation:**   Pollutant Transport in Buoyancy Driven
Atmospheric Flows

Approved:

_____
Major Professor and Chairman

_____
Dean of the Graduate School

EXAMINING COMMITTEE:

_____

_____

_____

_____

_____

_____

Date of Examination: _____

November 3, 1993   _____